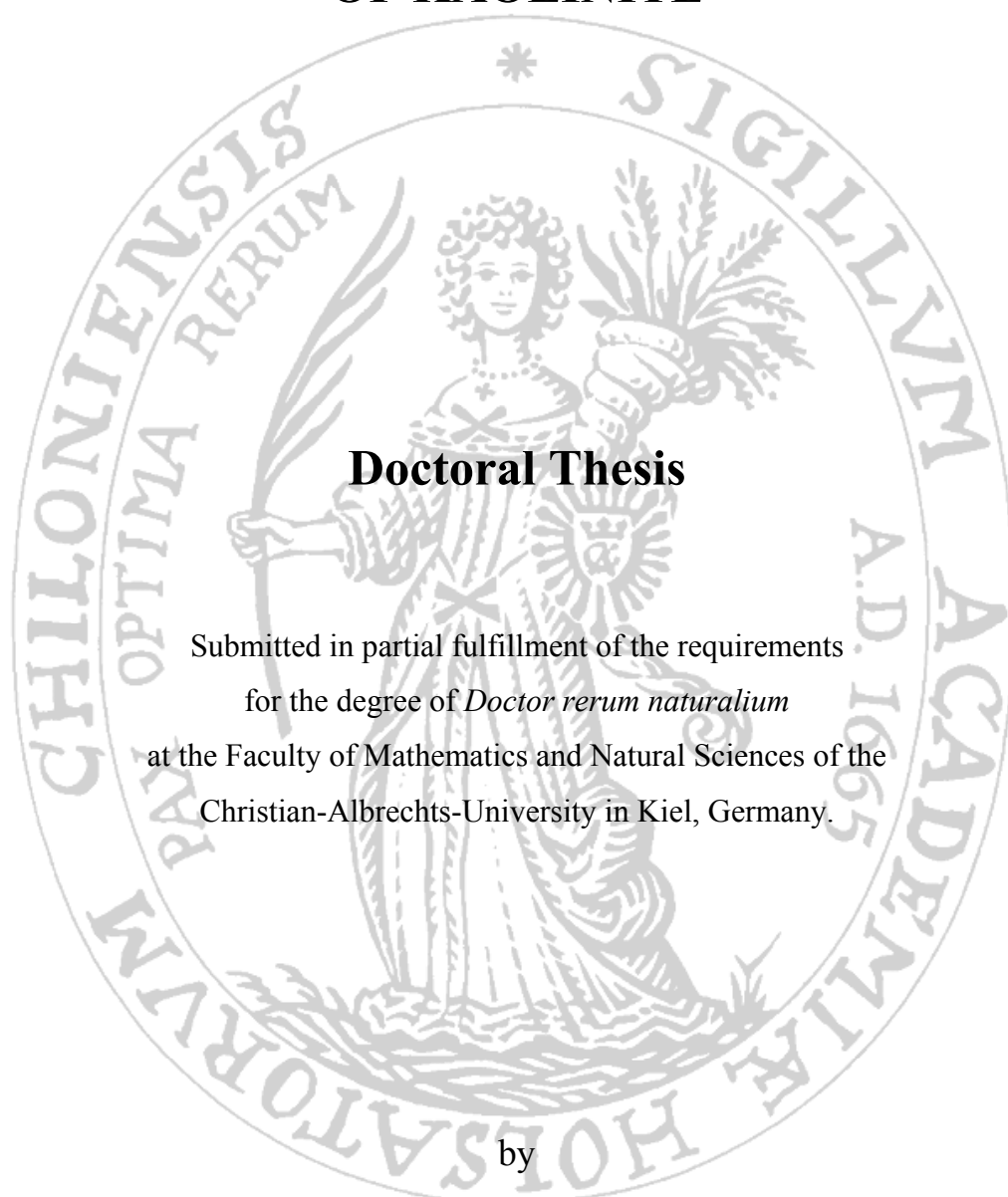


INTERLAYER GRAFTING AND DELAMINATION OF KAOLINITE



Doctoral Thesis

Submitted in partial fulfillment of the requirements
for the degree of *Doctor rerum naturalium*
at the Faculty of Mathematics and Natural Sciences of the
Christian-Albrechts-University in Kiel, Germany.

by

José Eduardo Ferreira da Costa Gardolinski, B.Chem., M.Eng.

Kiel

2005

INTERLAYER GRAFTING AND DELAMINATION OF KAOLINITE

Doctoral Thesis

Submitted in partial fulfillment of the requirements
for the degree of *Doctor rerum naturalium*
at the Faculty of Mathematics and Natural Sciences of the
Christian-Albrechts-University in Kiel, Germany.

by

José Eduardo Ferreira da Costa Gardolinski, B.Chem., M.Eng.

Kiel

2005

Gedruckt mit Unterstützung des Deutschen Akademischen
Austauschdienstes

Referent: Prof. Dr. Dr. h. c. Gerhard Lagaly

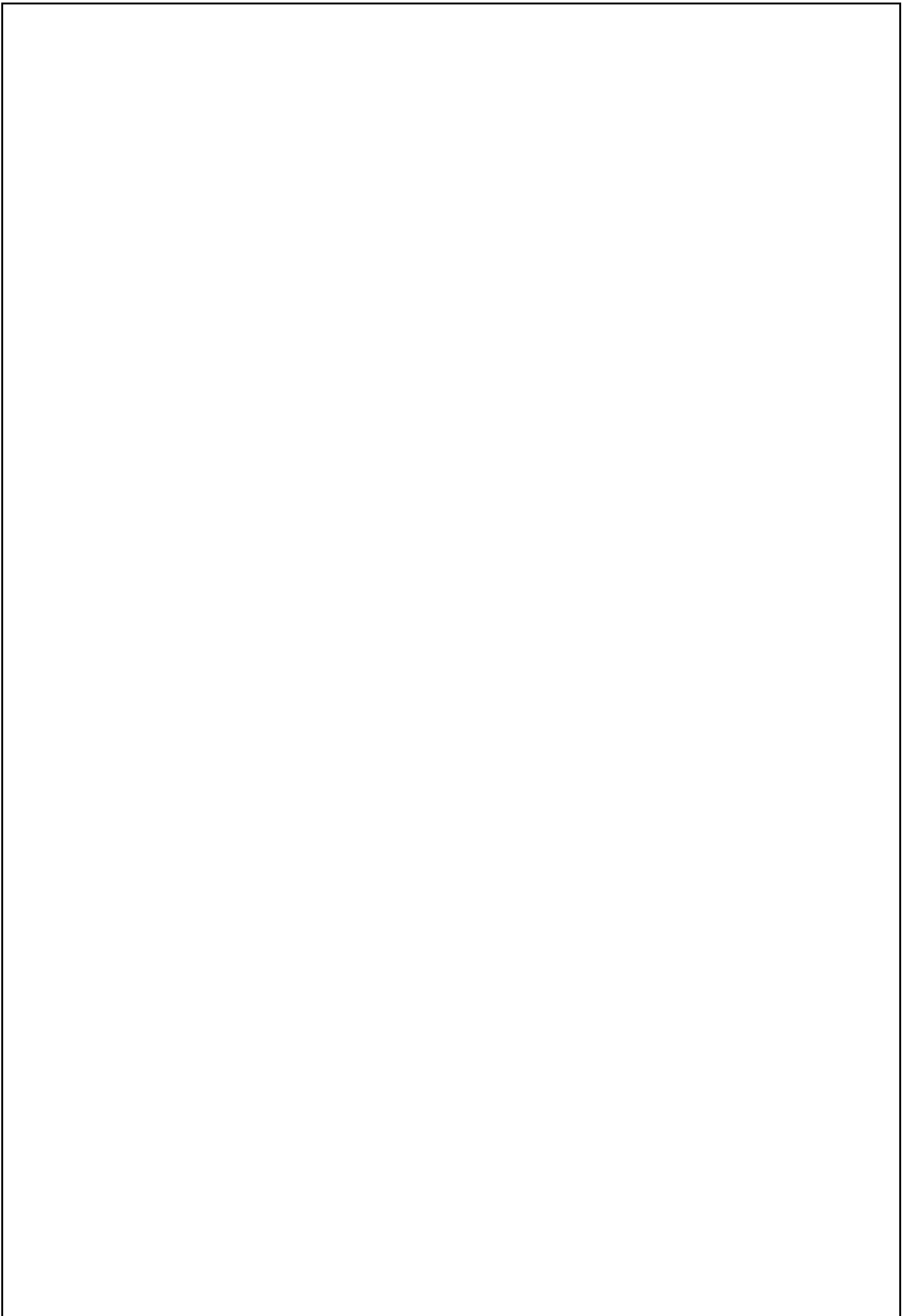
Koreferent: Prof. Dr. Norbert Stock

Tag der mündlichen Prüfung: 8. November 2005

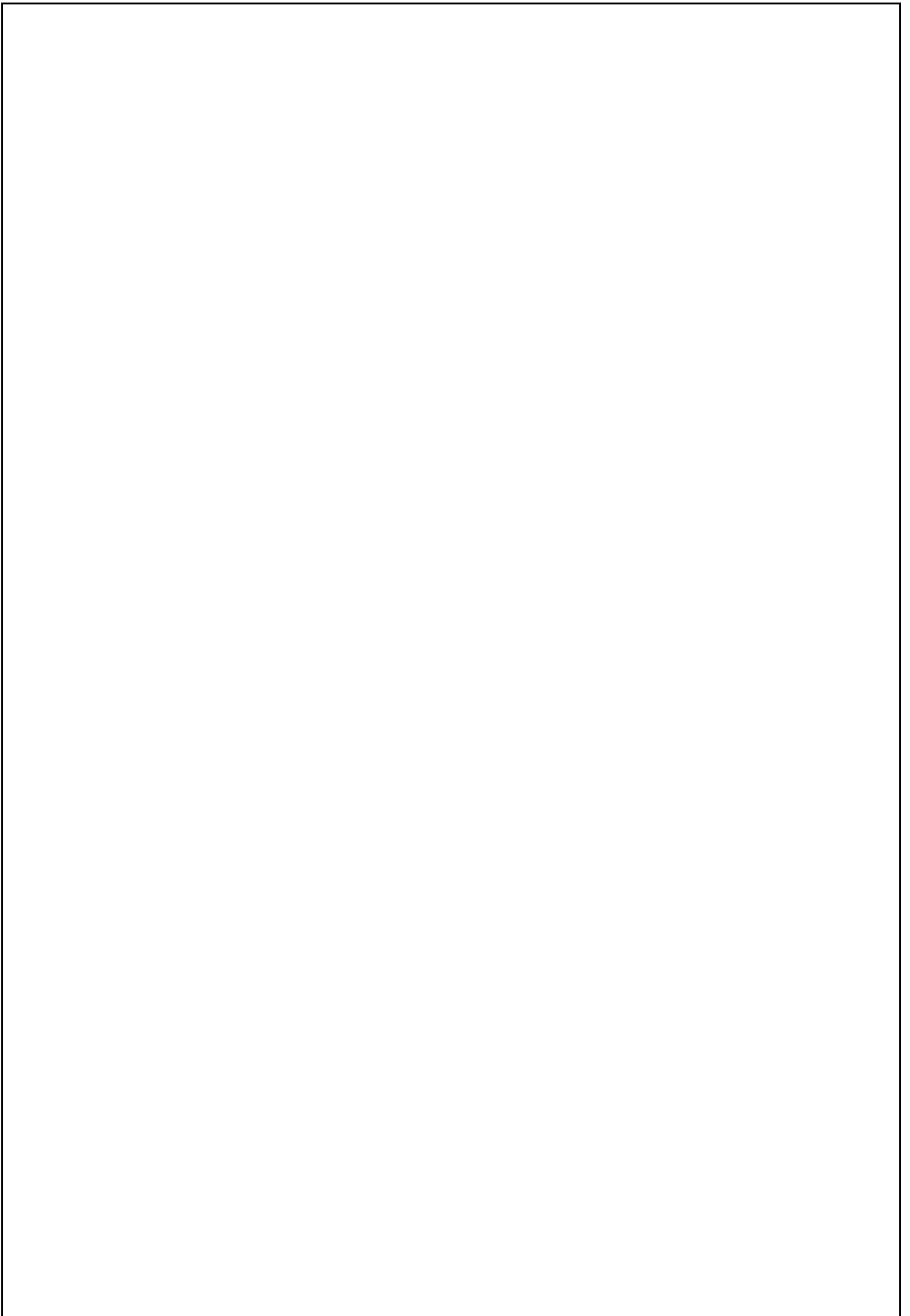
Zum Druck genehmigt: Kiel, den 26. Oktober 2005

.....

Der Dekan



To Helen



ACKNOWLEDGMENTS

First of all, I would like to thank **Herr Prof. Dr. Dr. h. c. Gerhard Lagaly** for many reasons: For so kindly receiving me in Kiel and so openly accepting me to work in his workgroup. For his patience with all the trouble that I caused him with paperwork, emails and bureaucracy in order to get the DAAD Scholarship. For the total liberty he gave me to work on the PhD project (so that I could conduct it as I wished). For the unlimited help and careful guidance during all the research time. For the constant willingness to talk about something else, or to discuss the most amusing topics. For the many interesting “lessons” on Organ Music. For the many CD’s he always so kindly lent me. And for always helping me, whenever necessary.

Thanks to the German Service of Academic Exchange (DAAD) for providing the PhD Scholarship, without which I could never have started dreaming about coming to Germany!

To Klaus Beneke, my thanks for always being there, to help (whenever I needed!), discuss, or just talk. For his insatiable need to teach us some small (but not less important!) piece of the History of Science. For the most enjoyable “Kaffee Pausen”. Ich werde weder Liesegang noch Agnes Pockels wohl je vergessen können!

My thanks to the workgroup Lagaly: Sören, Lars, Nils, Tanja, Heiko and Jörn. Thank you all for making the work in the “Institut” such a pleasant and joyful experience!

Thanks also to Britta Bahn for solving so many problems, for remembering all the birthdays and being such a nice and kind person!

My especial thank to the people of the Institute of Inorganic Chemistry, who helped me with so many analyses: Dr. C. Teske and J. Lichte (TG/DTA), U. Cornelisen and S. Pehlke (FTIR and CHNS). Thanks also to Prof. Dr. W. Bensch for the use of the XRPD equipment and to Prof. Dr. H. Homborg, for lending the cryostat.

To Prof. Dr. Michael Czank (Institute of Geosciences, Dept. of Mineralogy) my most sincere gratitude not only for teaching me how to operate the TEM but also for giving me full freedom with the equipment and for always helping with the interpretation of data. Thank you also for always being so receptive and friendly!

Special thanks to Frau Maria Salgado (my “Godmother” at the DAAD), for solving so many problems and for being so friendly in all occasions!

Thanks also to Prof. Dr. Fernando Wypych (Dept. of Chemistry, Federal University of Paraná, Brazil) for always being in touch, for helping me many times, for providing the

Brazilian Kaolinite sample, for waiting so patiently to publish his own results only after me, and for being a good friend!

Thanks to the friends and colleagues of the time spent in Bremen, who made the very beginning of the time in Germany most amusing and valuable! Especially to the good friend José Dörner-Fernández, who also provided such a good company here in Kiel.

Special thanks also to my parents, who always stood by me, supporting me in any decision I made; who were sadly separated from me by so many thousands of kilometers...and who, ultimately, are the whole cause of my existence! Obrigado Mãe, Obrigado Pai! Amo muito vocês!

Last, but most important of ALL, to my wife, Helen. Thank you for having given up your life as it was in Brazil to be here with me all this time. Thank you for always being there for me, helping me whatever I should need. Thank you for always trying to cheer me up and make me happy in the difficult times. Thank you for loving me so much. Thank you for being my beloved wife! Without you, I would not have achieved all this! Te Amo Muito, sempre, sempre...

CONTENTS

Abstract (En)	xiii
Zusammenfassung (D)	xiv
Resumo (P)	xv
Abbreviations	xvi
Introduction	3
Chapter 1 – The Kaolin Minerals	7
1.1 Introduction: Clay Minerals	9
1.1.1 Clays	9
1.1.2 Clay Minerals	10
1.1.2.1 Definition, structure and classification	10
1.1.2.2 Special characteristics of clay minerals	14
1.1.2.3 Uses and applications of clay minerals	15
1.2 Structure and Morphology of Kaolinite and its Polymorphs	16
1.2.1 The Kaolin Minerals	16
1.2.2 Kaolinite: Structure and Morphology	17
1.2.3 Dickite and Nacrite: Structure and Morphology	23
1.2.3 Halloysite: Structure and Morphology	25
1.3 Genesis and Occurrence	30
1.3.1 The Genesis of Kaolin Minerals	30
1.3.2 Occurrence of Selected Kaolin Deposits	31
1.4 Mining and Production	35
1.4.1 The Mining and Processing of Kaolin Minerals	35
1.4.2 Worldwide Production of Kaolin Minerals	36
1.5 Traditional Uses and Importance	38
1.6 Conclusion	40
Chapter 2 – Kaolinite Chemistry	41
2.1 Introduction	43
2.2 Thermal Behaviour and Dehydration	44
2.3 X-Ray Diffractometry	47
2.4 FTIR Spectroscopy	53
2.5 Surface Reactions and Phenomena	58

2.5.1 Surface Charge and Cation Exchange	58
2.5.2 Adsorption	59
2.5.3 Topotactic Reactions at the External Surfaces (<i>Surface Grafting</i>)	60
2.6 Topotactic Interlayer Reactions	62
2.6.1 Intercalation	62
2.6.1.1 Historic development	62
2.6.1.2 Direct intercalation reactions	66
2.6.1.3 Interlayer forces in kaolinite	66
2.6.1.4 Reaction mechanisms	67
2.6.1.5 Factors affecting the reaction rate	69
2.6.1.6 Displacement reactions	71
2.6.1.7 Hydrated kaolinite	73
2.6.2 Interlayer Grafting	74
2.6.2.1 Definition and peculiarities	74
2.6.2.2 Kaolinite interlayer grafted derivatives	76
2.7 Non-Topotactic Reactions	81
2.8 Exfoliation and Delamination	83
2.9 Rheological Properties of Kaolinite Aqueous Dispersions	86
2.10 Conclusion	90
Chapter 3 – Synthesis and Characterization of Kaolinite Grafted Derivatives	91
3.1 Introduction	93
3.2 Preparation of Precursors	94
3.2.1 Preparation of the Kaolinite-DMSO Intercalation Compound	94
3.2.2 Preparation of the Kaolinite-NMF Intercalation Compound	95
3.3 Grafting of Organic Molecules	96
3.3.1 Reaction with Diols	97
3.3.1.1 Grafting reactions	97
3.3.1.2 Characterization	98
3.3.2 Reactions with Glycol Mono-Ethers	106
3.3.2.1 Grafting reactions	106
3.3.2.2 Characterization	107
3.3.3 Reactions with Alcohols	113
3.3.3.1 Grafting reactions	113

3.3.3.2 Characterization	115
3.3.4 Reaction with Thiols	123
3.4 Conclusion	124
Chapter 4 – Rheological Properties of Dispersions of Grafted Kaolinites	125
4.1 Introduction	127
4.2 Experimental	128
4.2.1 Preparation of the Dispersions	128
4.2.2 Rheological Measurements	128
4.3 Results and Discussion	130
4.4 Conclusion	135
Chapter 5 – Delamination of Amine-Intercalated Kaolinites	137
5.1 Introduction	123
5.2 Intercalation of Primary n-Alkylamines	140
5.2.1 Intercalation on Non-Grafted Kaolinite	140
5.2.1.1 Experimental	140
5.2.1.2 Characterization	140
5.2.2 Intercalation on Grafted Kaolinites	142
5.2.2.1 Experimental	142
5.2.2.1 Characterization	142
5.3 Delamination of Amine-Intercalated Kaolinites	146
5.3.1 Delamination of Non-Grafted Kaolinite	146
5.3.1.1 Experimental	123
5.3.1.2 Characterization	146
5.3.2 Delamination of Grafted Kaolinites	148
5.3.2.1 Experimental	148
5.3.2.2 Characterization	148
5.3.3 Discussion	151
5.4 Conclusion	153
Chapter 6 – The Reaction of Kaolinite with Phenylphosphonic and Similar Acids	155
6.1 Introduction	157
6.2 Preparation of New Compounds	160
6.2.1 Experimental	160
6.2.1.1 Preparation of K-PPA	160

6.2.1.2 Preparation of K-PPiA and K-NPAA	160
6.2.1.3 Preparation of Gi-PPA, Gi-PPiA and Gi-NPAA	160
6.2.2 Characterization	160
6.2.2.1 Kaolinite with PPA, PPiA and NPAA	160
6.2.2.2 Gibbsite with PPA, PPiA and NPAA	168
6.2.3 Discussion	174
6.3 Conclusion	179
Conclusion	181
References	185
Appendix I – Description of materials and analytical methods	203
Appendix II – Particle-size study of kaolinite treated after Lahav (1990) using disc-centrifuge photosedimentometry	211
Appendix III – Investigation of intercalation reactions of kaolinite and some grafted derivatives in liquid ammonia medium	217
Curriculum Vitæ	225

ABSTRACT

This study describes interlayer reactions of the clay mineral kaolinite. After a general introduction to clay minerals, some structural, morphological and geological properties of kaolinite, its mining, processing and industrial importance are described. Some basic chemical aspects of kaolinite are presented, including the most important analytical methods involved in the study of kaolinite and its derivatives. External surface phenomena and reactions are discussed, along with a detailed presentation of the intercalation and interlayer grafting reactions. The theoretical part also contains aspects of non-topotactic reactions of kaolinite, exfoliation and delamination processes and some basic aspects of the rheology of aqueous kaolinite dispersions. The experimental part describes the synthesis of new interlayer-grafted kaolinites. Many new compounds were obtained by the reactions of kaolinite/dimethylsulfoxide with n-alkanols, diols and glycol mono-ethers and characterized by XRPD, FTIR, TG/DTA and TEM. Rheological studies of these compounds show that the flow properties of kaolinite can be changed by grafting. Some of the grafted derivatives were intercalated with long-chain amines. Leaching these compounds with organic solvents efficiently delaminated the clay mineral matrix into kaolinite monolayers. Aluminosilicate nanotubes were obtained with their inner surface tailored by grafting of the kaolinite precursor. It was further shown that grafted derivatives were not obtained by the reaction of kaolinite with phenylphosphonic acid and similar acids. Such reactions destroy the clay mineral structure and new aluminum compounds were obtained. The study of grafting reactions of kaolinite opens many new possibilities for tailoring this clay mineral for use in new types of advanced composite materials.

Keywords: aluminium, amine, clay minerals, delamination, dispersion, exfoliation, flow properties, functionalization, gibbsite, grafting, halloysite, intercalation, kaolinite, nanocomposite, nanotubes, phenylarsonate, phenylphosphinate, phenylphosphonate, rheology.

ZUSAMMENFASSUNG

Diese Arbeit beschreibt neue Zwischenschicht-Reaktionen des Kaolinit. Nach einer allgemeinen Einleitung über Tonminerale werden die strukturellen, morphologischen und geologischen Eigenschaften vom Kaolinit erläutert. Es folgen Angaben über den Abbau, industrielle Aufbereitung und den wichtigsten Anwendungen des Kaolins, sowie über die wichtigsten analytischen Untersuchungsmethoden. Es werden die Oberflächenphänomene und -reaktionen diskutiert sowie eine detaillierte Beschreibung der bisherigen Herstellung von Einlagerungsverbindungen und der Graftreaktionen. Der theoretischen Teil endet mit einer Diskussion über nicht-topotaktische Reaktionen, Exfoliation und Delamination, sowie über Eigenschaften wässriger Kaolinit dispersionen. Im experimentellen Teil wird die Synthese neuer kovalenter (interlamellar grafted) Kaolinit-derivate beschrieben. Es wurden zahlreiche neue Verbindungen durch Reaktionen von Kaolinit-Dimethylsulfoxide mit n-Alkanolen, Diolen und Glykolmonoethern hergestellt und charakterisiert. Rheologische Untersuchungen zeigten, dass die Fließeigenschaften des Kaolins durch Graften gezielt geändert werden können. In einigen kovalente Derivate wurden lankettige Amine eingelagert und dann mit organischen Lösungsmitteln ausgewaschen. Dabei wurden Kaolinitteilchen in Einzelschichten zerlegt (delaminiert). Es entstanden Kaolinit-Nanoröhrchen. Die innere Oberfläche dieser Nanoröhrchen kann gezielt durch Auswahl des Graftreagenzien verändert werden. Weiterhin wurde gezeigt, dass durch Reaktionen von Kaolinit mit Phenylphosphonsäure und verwandten Verbindungen keinen Kaolinit-Derivaten entstehen. Die Tonmineralstruktur wird zerstört. Es bilden sich neue Aluminium-Verbindungen. Die gezielte Derivatisierung von Kaolinit über Graftreaktionen bietet neue Möglichkeiten zum Einsatz von Kaolinen in moderne Werkstoffe.

Schlüsselwörter: Aluminium, Amin, Delamination, Dispersion, Einlagerung, Exfoliation, Fließeigenschaften, Funktionalisierung, Gibbsit, Grafting, Halloysit, Kaolinit, Nanocomposit, Nanoröhrchen, Phenylarsonat, Phenylphosphinat, Phenylphosphonat, Rheologie, Tonminerale.

RESUMO

Este trabalho é dedicado as reações interlamelares do argilomineral caulinita. Após uma introdução geral aos argilominerais, uma descrição sobre algumas das características estruturais, morfológicas e geológicas da caulinita é apresentada. Além disso, a mineração, processamento, importância e usos industriais deste mineral também são abordados. Na seqüência, alguns aspectos químicos básicos deste argilomineral são apresentados, incluindo os mais importantes métodos analíticos utilizados no estudo da caulinita e seus derivados. Fenômenos e reações das superfícies externas são discutidos, é feita também uma apresentação detalhada sobre os compostos de intercalação e funcionalizados interlamelamente (“grafted”). Finalizando a parte teórica, alguns pontos são discutidos sobre reações naotopóticas, sobre os processos de delaminação e esfoliação assim como sobre alguns aspectos básicos da reologia de dispersões aquosas de caulinita. A parte experimental descreve os resultados da síntese de novos derivados da caulinita funcionalizados interlamelamente. Vários novos compostos obtidos das das reações de caulinita-dimetilsulfóxido com n-alcanóis, dióis e mono-éteres de glicóis foram caracterizados. Estudos reológicos destes derivados mostraram que as propriedades de fluxo da caulinita podem ser ordenadamente modificadas pela funcionalização. Alguns destes derivados form intercalados com aminas de cadeia longa e então lixiviados com solventes orgânicos. Este processo delaminou eficientemente a matrix do argilomineral, formando monolamelas de caulinita. Nanotubos de aluminossilicato foram obtidos, os quais puderam ter as características de suas superfícies internas modificadas de acordo com a funcionalização da caulinita precursora. Também foi demonstrado que a reação da caulinita com ácido fenilfosfônico e ácidos similares não gera derivados funcionalizados. Estas reações destroem a estrutura do argilomineral e novos compostos de alumínio são formados. O estudo das reações de funcionalização da caulinita abre muitas novas possibilidades para a utilização de caulins na obtenção de novos tipos de materiais compósitos avançados.

Palavras-Chave: alumínio, amina, argilominerais, caulinita, delaminação, dispersão, esfoliação, fenilarsonato, fenilfosfinato, fenilfosfonato, funcionalização, gibbsita, grafting, haloisita, intercalação, nanocompósito, nanotubos, propriedades de fluxo, reologia.

ABBREVIATIONS

AND SPECIAL SYMBOLS

(This list does not contain symbols for units or chemical elements)

α	intercalation (or reaction) ratio
α, β, γ	unit-cell angles
$\dot{\gamma}$	shear rate
ξ	layer charge
12BD	1,2-butanediol
12PD	1,2-propanediol
13BD	1,3-butanediol
13PD	1,3-propanediol
14BD	1,4-butanediol
16HD	1,6-hexanediol
18OD	1,8-octanediol
22DM13PD	2,2-dimethyl-1,3-propanediol
23BD	2,3-butanediol
a_0	cooperative action length (in the kinetic of intercalation reactions)
a_0, b_0, c_0	unit-cell lengths
AIPEA	International Association for the Study of Clays
CEC	cation(ic) exchange capacity
CIE	Commonwealth of Independent States (former USSR)
CMS	Clay Mineral Society (USA)
d	interplanar distance
d_L	basal spacing
DCP	disc-centrifuge photosedimentometry
DEG2EHE	di(ethylene glycol) 2-ethylhexyl ether
DEGBE	di(ethylene glycol) butyl ether
DEGDE	di(ethylene glycol) decyl ether
DEGHE	di(ethylene glycol) hexyl ether
DEGME	di(ethylene glycol) methyl ether
DM13PD	2,2-dimethyl-1,3-propanediol

DMSO	dimethyl sulfoxide
DRIFT	diffuse reflectance infrared Fourier transform spectroscopy
DTA	differential thermal analysis
EDX	energy dispersive X-ray spectroscopy
EG	ethylene glycol
EGEE	ethylene glycol ethyl ether
EGHDE	ethylene glycol hexadecyl ether
f.u.	formula unit
FTIR	Fourier transform infrared spectroscopy
Gi	gibbsite
H _I	Hinckley crystallinity index for kaolinites
I	relative intensity (in XRPD diffractograms)
K	kaolinite (when used in the name of a compound, the absence of a subscript denotes the SPS sample). Note that K can also denote the chemical element Potassium.
<i>lit</i>	denotes value described in the literature
M	metal
MAS-NMR	solid state nuclear magnetic resonance - magic angle spinning method
MeOH	methanol
MIR	Fourier transform infrared spectroscopy in the “medium region” of the spectrum: from 400 cm ⁻¹ to 4000 cm ⁻¹ .
NMF	N-methyl formamide
NPAA	2-nitrophenol-4-arsonic acid
O	octahedral
PNXET <i>or</i> PnxEt	2-phenoxy-ethanol
PNXPRO <i>or</i> PnxPro	1-phenoxy-2-propanol
PPA	phenylphosphonic acid
PPiA	phenylphosphinic acid
RC <i>or</i> K _{RC}	denotes the kaolinite probe from the Amazon region, Brazil (see Appendix I)
SAED	selected area electron diffraction (diffractometry)
SEM	scanning electron(ic) microscopy
SPF-K	fine particle size fraction from the SPS kaolinite (see Appendix I)

SPS or K _{SPS}	denotes the kaolinite probe from Cornwall, UK (see Appendix I)
T	tetrahedral
TEGHDE	tetra(ethylene glycol) hexadecyl ether
TEM	transmission electron(ic) microscopy
TG	thermogravimetric analysis
TG/DSC	simultaneous thermogravimetric analysis and differential scanning calorimetry
TG/DTA	simultaneous thermogravimetric and differential thermal analysis
TG-EGA	coupled thermogravimetric and evolved gas analysis
TMP	trimethylphosphate
TPGBE	tri(propylene glycol) butyl ether
v/v	volume/volume (in percentages)
VT-DRIFTS	variable temperature diffuse reflectance infrared Fourier transform spectroscopy
w	weight (in percentages)
w/v	weight/volume (in percentages)
w/w	weight/weight (in percentages)
X, Y, Z	crystallographic axes
XRPD	X-ray diffractometry – powder method

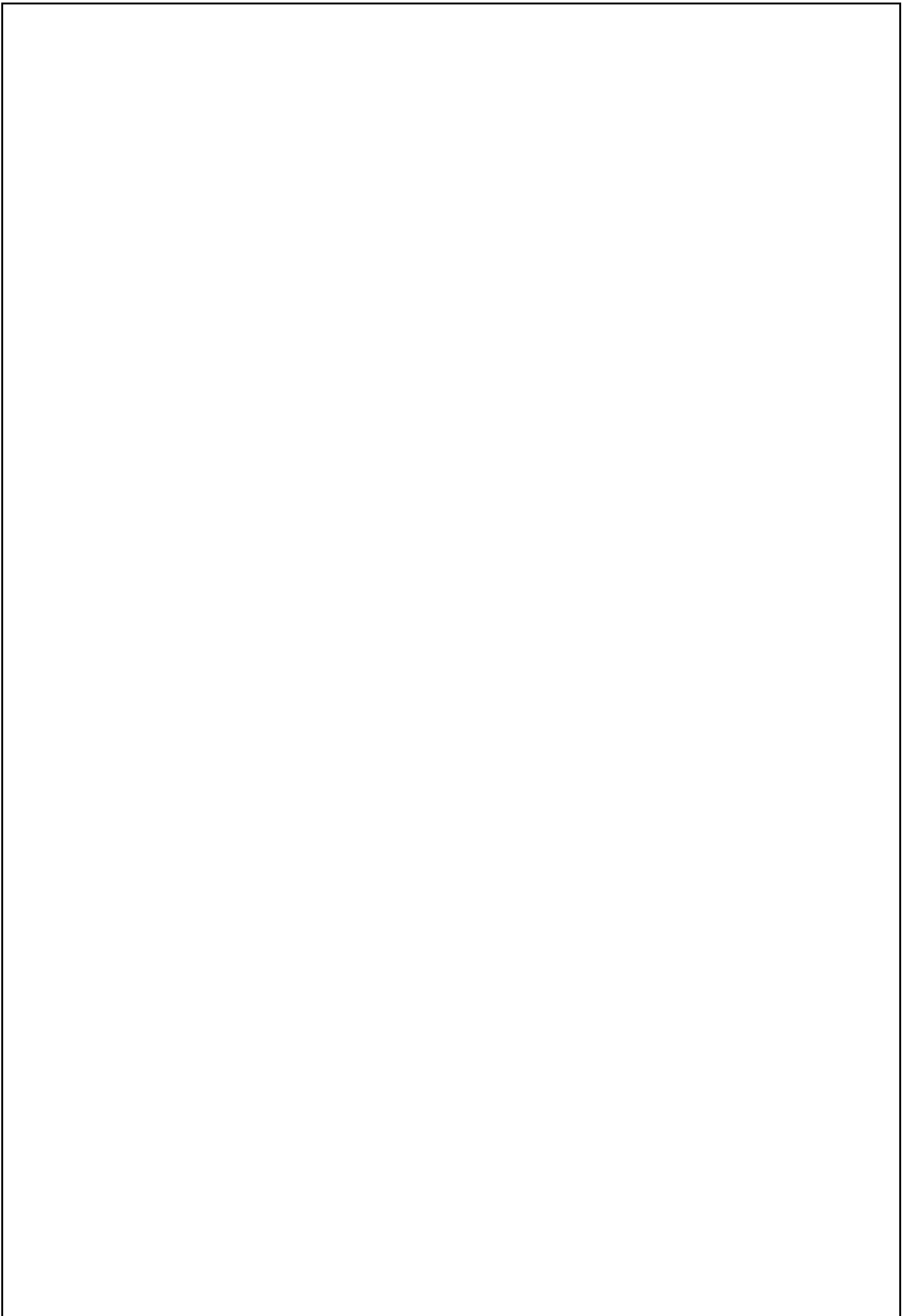
“...Chymicæ studium, ejusque amatores Alchymistas vocant, quibus nihil acceptius, nihil dulcius, suavius nihil & gloriosius, quàm si extreme sordeant, malè mundo audiant, pecuniam cum famâ profundant, venenis palleant, madeant, semper quærant, nihil habeant, omnes interea communes sensus perdunt, planè juxta illud.

Qui pluviam maduistis aquam, fuliginem olentes,

Fumo excæcati, flammis crepitantibus usti,

In hanc verè picam, non nævum modo sed insignem morbum & ego incidi, cui nec aulæ splendor, nec æconomice ratio, nec famæ integritas, nec sanitatis vigor quicquam præ carbonibus, venenis, fuligine, follibus & furnis valere potest, ipso Hercule fortior, cui perpetuum Augiæ stabulum purgandum, forti igne vix non utroque oculo orbatus, periculosis Mercurialibus catarrhis infestatus, totus veneno imbutus alter Mithridates, omni æstimatione & voluptate privatus, mente Cræsus, marsupio Irus at inter hæc omnia incommoda, ita mihi suaviter vivere videor, ut, emoriar, cum Persarum Regis deliciis mutare nolim...”

Johann Joachim Becher (1635 – 1682) at the *Præfatio* of his Mastework: *Actorum Laboratorii Chymici Monacensis, Seu Physicæ Subteraneæ Libri Duo*. Frankfurt, 1667.



Interlayer Grafting and Delamination of Kaolinite

INTRODUCTION

Introduction

Kaolins are present in our every day life, from ceramic materials to medicines, from paper and ink to the catalyst-units in our cars. The figures involved in the production and market of these minerals are overwhelming, more than 45 million tones are mined and beneficiated each year (Jasmund and Lagaly, 1993), in a market that involves more that 4 billion US dollars each year (Gobi, 2002). They are certainly among the most important industrial minerals in our world.

It is easy to see that basic and applied research - which are the cornerstones for new technologies and industrial improvements - on these substances, could be of strategic importance to countries with established tradition in the production of kaolins, in face of such huge international market. The research here presented is a small step in better understanding the chemistry and behavior of kaolin minerals. The possibilities offered by the tailored chemical modification of kaolin minerals are extremely attractive, and every single small step leading into the obtention of improved and “high-tech” materials should be followed.

This work contains the major results of 3.5 years dedicated to the research on the chemical modification of kaolinite. Each chapter describes specific aspects of this clay mineral or presents experimental results on some aspects of kaolinite chemistry.

Chapter 1 presents an introduction to the field of clay science. The definitions of clay and clay minerals are presented followed by the structural and morphological description of the four minerals of the kaolin group (kaolinite, dickite, nacrite and halloysite). A brief introduction in the genesis, occurrence, mining and processing of kaolin minerals is also presented. The chapter closes with a small description of the many uses and applications of the kaolin minerals.

Chapter 2 refers to the chemistry of kaolinite. The characterization of this clay mineral by thermal analysis, infrared spectroscopy and X-ray diffraction is briefly described. Various chemical aspects of kaolinite are discussed in detail, among them surface phenomena and modification, topotactic interlayer reactions (intercalation and interlayer grafting), non-topotactic reactions, exfoliation and delamination, and some aspects of the rheology of aqueous kaolinite dispersions.

Chapter 3 presents experimental results concerning the chemical modification of kaolinite by interlayer grafting of alcohol-like molecules. A large number of different alkanols, diols and glycol mono-ethers were grafted to the interlayer aluminol surfaces of

kaolinite, producing interesting new nanohybrids and enlarging the number of known derivatives of kaolinite.

The next chapter presents the results on the so far first rheological studies of the aqueous dispersions of the modified kaolinites described in chapter 3.

Chapter 5 refers to the question of the delamination of kaolinite. Based on the facts and data exposed on chapter 2, an optimized route to the delamination of kaolinite is presented, culminating with the obtention of rolled single-layers of the mineral. The intercalation behavior of some grafted kaolinites towards alkylamines is also documented.

In chapter 6 the experimental results on the reactions of kaolinite with phenylphosphonic and similar acids are detailed. These interesting results were obtained during the studies of grafting of kaolinite, repeating the results of other groups. It is demonstrated that the product of the reaction of kaolinite with phenylphosphonic acid is an aluminum compound derived from the destruction of the clay mineral structure and not a grafted derivative from a topotactic reaction, as formerly accepted.

In the Appendix I the materials and chemicals used in the experiments are listed, as well as the details of the analytical techniques used. Appendix II describes a particle-size study of kaolinite samples treated by a method that supposedly should delaminate (at least partially) the clay mineral. Appendix III refers to a series of unsuccessful or inconclusive experiments aiming the intercalation of various molecules in kaolinite in liquid ammonia medium.

CHAPTER 1
THE KAOLIN MINERALS

1.1 Introduction: Clay Minerals

1.1.1 Clays

Much confusion still surrounds the term “clay” in the literature. This is not due to the lack of precise definitions but on the contrary, due to the existence of different definitions in almost each application field. Leaving the non-technical definitions aside (which are already many), “clay” is a term used by geologists, soil scientists, civil engineers, material scientists, chemists and others. To each one of these groups, it designates something slightly different. For some of them, the definition is based on the mechanical properties, for others the origin of the material is the factor that matters and, for others, the composition.

Exactly because clays are not simple and uniform substances, but complex mixtures, the exact definition varies from area to area. A general definition, however, is not difficult to establish, and should encompass most of the following aspects:

- natural material;
- earthy texture;
- metamorphic and/or sedimentary origin;
- particles of very small grain size (on the μm scale);
- develops plasticity when mixed with limited amounts of water;
- hardens when dried or fired;
- constituted primarily of one or more clay minerals.

The AIPEA (International Association for the Study of Clays) and the CMS (Clay Mineral Society, USA) presented a formal definition of clay, which encompasses almost all important characteristic above (Guggenheim and Martin, 1995):

*“The term **Clay** refers to a naturally occurring material composed primarily of fine-grained minerals, which is generally plastic at appropriate water contents and will harden when dried or fired. Although clay usually contains phyllosilicates, it may contain other materials that impart plasticity and harden when dried or fired. Associated phases in clay may include materials that do not impart plasticity and organic matter.”*

1.1.2 Clay Minerals

1.1.2.1 Definition, structure and classification

Based on the definitions for clay (see 1.1.1), clay minerals could be defined as *the major constituents of clays, being responsible for their primary characteristics and presenting definite and constant chemical composition and crystalline structures.*

The AIPEA and CMS have also proposed a formal definition of clay mineral:

*“The term **clay mineral** refers to phyllosilicate minerals and to minerals which impart plasticity to clays and which harden upon drying or firing.”* (Guggenheim and Martin, 1995)

In fact, clay minerals are a well-delimited class of minerals, belonging to the phyllosilicates (layer silicates)¹. Clay minerals are extremely abundant substances, it is estimated that the Earth's crust (upper 20 km) is composed of ~ 16 % of clay minerals alone (Schroeder, 2004). From a chemical viewpoint, they are constituted of metal atoms (usually Al, Mg or Fe), silicon, oxygen and hydrogen atoms. Other elements, such as sodium, potassium, calcium, zinc or others may also be present. Silicon is always present in tetrahedral silica-like units. Aluminum, magnesium and other metals are present in octahedral hydroxide-like units (Fig. 1.1). It is the arrangement of these units in sheets and the packing of individual sheets together that makes this class of minerals so large.

When built by combining tetrahedral and octahedral sheets in equal proportions, the minerals are called **1:1 clay minerals**. The sheets are held together by sharing common oxygen atoms, as the apical oxygens of the silica tetrahedra are also octahedrally coordinated to the metal atoms. In the kaolin group minerals, the octahedral sheet is formed by aluminum atoms, in a structure analogue to γ -Al(OH)₃ or *gibbsite*. In the serpentine group minerals, the structure is composed by magnesium atoms instead of aluminum, in a structure analogue to Mg(OH)₂ or *brucite*. In the magnesium sheet all the octahedral sites are occupied by metal atoms, forming the **trioctahedral** structure. In the aluminum sheet only 2/3 of the octahedral sites are occupied by the metal atoms, forming the **dioctahedral** structure (with vacant octahedral sites).

¹ The AIPEA/CMS resolution broadens the definition of “clay mineral” to every substance that can produce plasticity in clays and hardens when dried or fired, even if they are not phyllosilicates, although no such substances have been described so far.

The layers built in this way are electrically neutral, as no excess charge is left unbalanced. As consequence, the layers can superimpose on each other (stacking), being held together by hydrogen bonds between adjacent octahedral hydroxyl groups (basal inner-surface hydroxyls) from one layer and tetrahedral oxygen atoms from the next layer as well as by van-der-Waals forces. A series of stacked layers compose the particles of the clay minerals (Fig. 1.2a).

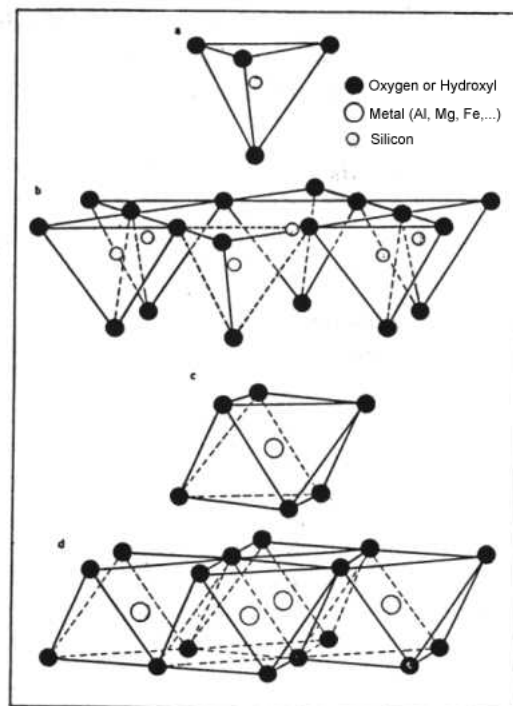


Fig. 1.1: Formation scheme of the tetrahedral sheet (b) from $[\text{SiO}_4]$ tetrahedra (a), and of the octahedral sheet (d) from $[\text{Me}(\text{O},\text{OH})_6]$ octahedra (c) (adapted from Gomes, 1988).

Another possibility to combine individual tetrahedral and octahedral sheets is by adding another tetrahedral sheet to a 1:1 structure. The additional tetrahedral sheet is linked to the octahedral sheet by the oxygens of the former hydroxyl groups in the 1:1 structure. Such structures, composed of two tetrahedral sheets and one octahedral sheet are designated as **2:1 clay minerals**.

The addition of another tetrahedral sheet to the dioctahedral kaolinite layer forms the pyrophyllite structure, while the addition of another tetrahedral sheet to the trioctahedral serpentine layer forms the talk structure. Since both of these 2:1 clay minerals are electrically neutral and there are no basal inner-surface interlayer hydroxyl groups available to build

hydrogen bonds (silica-like surfaces are adjacently stacked), the layers are held together only by van-der-Waals forces.

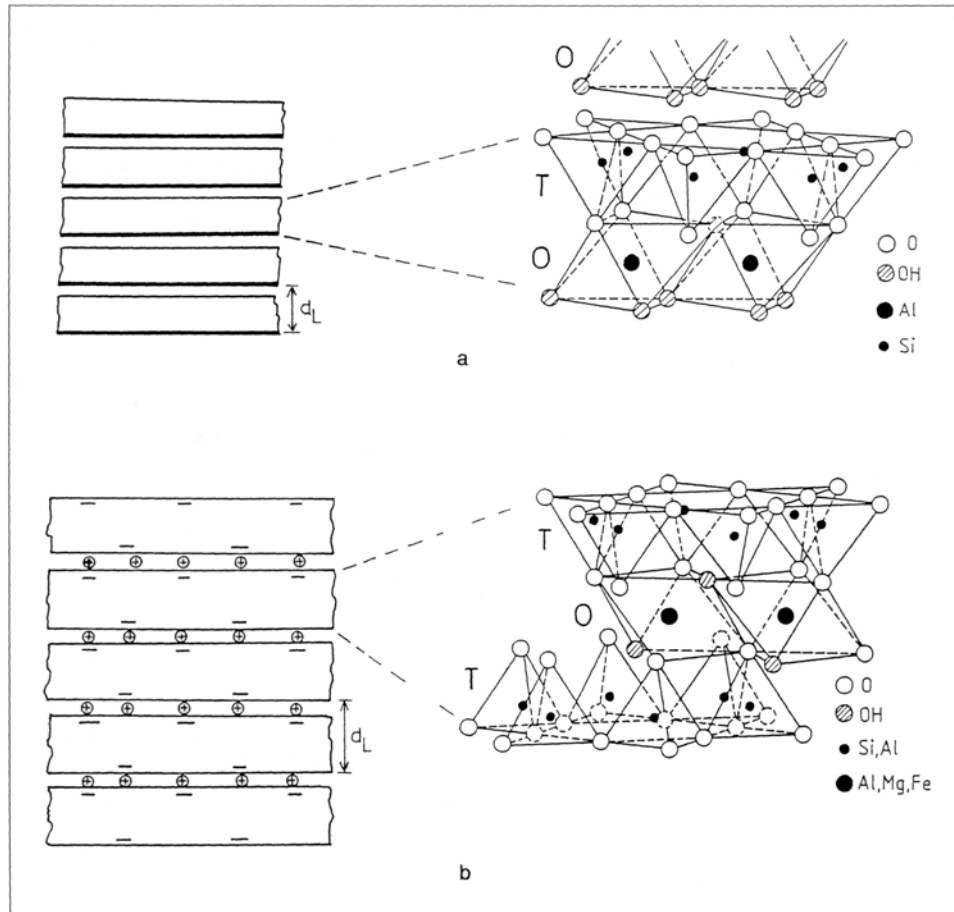


Fig. 1.2: Structure of a 1:1 clay mineral layer (a) and of a 2:1 clay mineral layer (b) (the interlayer cations are depicted on the schematic drawing of the layered structure on the left). T = tetrahedral sheet, O = octahedral sheet. d_L = basal spacing of the crystal. (from Jasmund and Lagaly, 1993)

In the other 2:1 clay minerals the sheets are not electrically neutral, but have an excess of negative charges. In order to obtain an electrically balanced particles, the excess charges must be neutralized by metal cations. These cations (often hydrated) are located between the individual layers. The layers are, therefore, held together by coulombic interactions (Fig. 1.2b).

The charges in these layers are caused by isomorphous substitutions in the sheets. In the tetrahedral sheets, Si^{4+} ions can be substituted by M^{3+} ions (Al^{3+} , as in beidellite or saponite). In the octahedral sheets M^{3+} ions can be substituted by M^{2+} in the dioctahedral structures (Al^{3+} by Mg^{2+} , as in montmorillonite) or M^{2+} by M^+ in the trioctahedral structures (Mg^{2+} by

Li⁺, as in hectorite). The substitutions can occur also in both sheets at the same structure (as in the vermiculites).

The clay mineral group of the chlorites presents charged octahedral gibbsite-like or brucite-like sheets intercalated between the 2:1 sheets.

Table 1.1: General classification of the clay minerals (adapted from Moore and Reynolds, 1989 and Jasmund and Lagaly, 1993).

Structure	Layer Type	Group	Subgroup / Occupation of octahedral sites	Examples
Layered Structure	1:1	Kaolin-serpentine (ξ~0) ^a	Kaolin Dioctahedral	Kaolinite
			Serpentine Trioctahedral	Halloysite
				Antigorite
	2:1	Pyrophyllite-talc (ξ~0)	Pyrophyllite Dioctahedral	Pyrophyllite
			Talc Trioctahedral	Talc
		Smectite (ξ~0.2-0.6)	Dioctahedral smectite	Beidelite
				Montmorillonite
			Trioctahedral smectite	Saponite
				Hectorite
		Vermiculite (ξ~0.6-0.9)	Dioctahedral vermiculite	Dioctahedral-Vermiculite
				Trioctahedral-Vermiculite
			Trioctahedral vermiculite	Muscovite
				Paragonite
		Mica (ξ~1.0)	Dioctahedral mica	Biotite
				Phlogopite
Trioctahedral mica	Margarite			
	Clintonite			
Brittle mica (ξ~2.0)	Dioctahedral brittle mica	Cookeite		
		Sudoite		
	Trioctahedral brittle mica	Clinochlore		
		Nimite		
2:1 + hydroxide sheet	Chlorite (ξ variable)	Dioctahedral chlorite	Donbassite	
		Trioctahedral chlorite	Clinochlore	
		Di,Trioctahedral chlorites	Nimite	
Fibrous Structure	(2:1)	Sepiolite-palygorskite		Palygorskite
				Sepiolite

^a) ξ = Layer charge = Charge / Formula Unit {(M³⁺, M²⁺, M⁺)₂₋₃[(Si, M³⁺)₄O₁₀(OH)₂]}

All clay minerals above described present a layer structure. A small number of clay minerals, however, present fibrous structure (and morphology). They are formed by ribbons

of octahedral and tetrahedral sheets, which are packed together in a way that hole channels, parallel to the elongation direction of the fiber arises. Palygorskite and sepiolite are the main representatives of this group.

Particles of the so-called mixed-layer clay minerals present two (or more) layers of different clay minerals, which can be packed together regularly or randomly. Examples of such minerals are rectorite, chlorite/vermiculite and illite/smectite.

Table 1.1 presents a classification of the clay minerals, based on their structure, as well as some examples of each category.

1.1.2.2 Special characteristics of clay minerals

Despite the fact that there are hundreds of different clay minerals, and that they can be 1:1 or 2:1, di- or tri-octahedral, that they can have neutral or charged layers and that many different elements can be present in their structure, there are some very important characteristic properties which can be ascribed to almost all of them. These properties are obviously linked to the fact that, with few exceptions, clay minerals are layered compounds.

One of the most important properties of layered compound is the capacity to intercalate species (neutral atoms, ions or molecules) into the interlayer spaces. The study of intercalation reactions in clay minerals is a very large research field *per se*, and intercalation compounds of almost all clay minerals are described in the literature. The synthesis of different intercalation compounds is of vital importance in obtaining clay mineral/organic polymers nanocomposites, which present improved characteristics compared to non-intercalated (traditional) nanocomposites (Lagaly, 1999; LeBaron *et al.* 1999; Gardolinski *et al.*, 2000; Gardolinski, 2001). The study of intercalation compounds of clay minerals is also of great importance in areas such as catalysis, fixation of pesticides, energy accumulation devices (batteries) and many others (Gardolinski, 2001). The spectroscopic study of intercalated molecules into the confined interlayer spaces of the clay minerals also gives new insights not only about the interaction between the clay mineral surfaces and the intercalated molecules but also in the behaviour of the intercalated molecules when severely sterically limited (Gardolinski, 2001).

Another very important characteristic of many clay minerals is their high cation exchange capacity (it can be as high as > 2 meq/g). This fact is mainly related to the presence of charged layers, and is mainly due to the large surface area they present (normally between 30 and 100 m²/g). In addition, the external surfaces of clay mineral particles possess a very

high adsorption capacity, derived from various factors: hydroxyl groups on 1:1 structures can easily build hydrogen bonds with other molecules; crystal borders are filled with hydroxyl groups which can be easily protonated or deprotonated, depending on the pH of the dispersion; besides the fact that silica-like surfaces have good adsorption sites (Jasmund and Lagaly, 1993).

Also noteworthy is the possibility to split the clay mineral layers into isolated units, in a process called delamination. Delaminated clay minerals present much higher surface areas and much smaller particle sizes. This process is of high importance in many industrial applications, when a smaller amount of clay mineral would fulfill the same needs as a higher amount of a non-delaminated material (in the synthesis of nanocomposites, for example). Delaminated clay minerals can also form much more stable colloidal dispersions as non-delaminated ones, due to the much higher interaction with the liquid phase (Lagaly *et al.* 1997).

1.1.2.3 Uses and applications of clay minerals

Hardly any group of substances present such a huge and diversified range of uses and applications as the clay minerals. Clay minerals are present almost everywhere, from the ceramic pieces we daily use to the most developed catalysts used in the industrial synthesis of fine chemicals; from the coating of paper to the advanced drilling sludges used in the mining of oil; from additives to paints, rubbers and plastics to the high-tech applications in nanotechnology and materials science (nanocomposites, for example). Even two such opposing application fields as pesticide formulations and human medicines make use of clay minerals. Clay minerals represent approximately 16% of the composition of the Earth's crust (Schroeder, 2004) and the worldwide total production is assumed to be around half a billion tons per year (Jasmund and Lagaly, 1993). These numbers alone show already that the market for such materials is almost universal.

1.2 Structure and Morphology of Kaolinite and its Polymorphs

1.2.1 The Kaolin Minerals

The kaolin (sub-)group of clay minerals is composed of four distinct minerals, **kaolinite**, **halloysite**, **dickite** and **nacrite**. These four species share the same chemical composition, that can be resumed as: $\text{Al}_2\text{Si}_2\text{O}_5(\text{OH})_4$, which means they are **polymorphs** (considering just the anhydrous, 7 Å form of halloysite, see below). In addition, kaolinite, dickite and nacrite are also **polytypes**, as they share the same, common structure of the individual layer, whereas only the layer-stacking scheme is different (Dera *et al.*, 2003). Theoretically, there are 52 different dioctahedral structures with periodicities between one and six layers (Zvyagin, 1962), but just the three with the lowest electrostatic bonding energies are known (Jasmund and Lagaly, 1993).

Kaolinite is by far the most abundant mineral of this group (in fact, it is the most abundant of all clay minerals). Nacrite and dickite are rather rare minerals, occurring in just a few locations.

There was for long time no definitive consent in the literature about the existence of two different mineral species of halloysite. The halloysite structure can intercalate a monolayer of water between the aluminosilicate layers. This intercalated water expands the basal spacing from 7 Å to 10 Å. The anhydrous 7-Å halloysite was also called *meta-halloysite*, while the 10-Å hydrated form was called *endellite*. The intercalated water can be easily lost by heating at ~ 60 °C or by placing the mineral in vacuum. Both species exist in nature, many times within the same deposit. These facts suggest that there is only one halloysite mineral, which can possess intercalated water or not. This that does not justify, however, the classification of the 10-Å halloysite as a different mineral species (Moore and Reynolds, 1989; Jasmund and Lagaly, 1993). In fact, the AIPEA resolution of 1980 (Bailey, 1980) recommended the use of the terms **halloysite(7Å)** and **halloysite(10Å)**. The terms meta-halloysite and endellite should not be used.

1.2.2 Kaolinite: Structure and Morphology

As already discussed, kaolinite particles are formed by regular stacking of the individual 1:1 dioctahedral layers. The layers are continuous in the X and Y crystallographic axes, and stacked along the Z axis, the XY plane being the basal plane.

The structure of the unit cell of kaolinite is triclinic, with the C1 space group. The unit cell parameters are given in Table 1.2.

Table 1.2: Crystallographic data for the kaolin group minerals (from Jasmund and Lagaly, 1993 and Giese, 1991).

	Space Group	a_0 (Å)	b_0 (Å)	c_0 (Å)	α (°)	β (°)	γ (°)
Kaolinite	C1	5.16	8.94	7.40	91.7	104.9	89.8
Halloysite	Cc	5.14	5.90 ^a 8.90 ^b	14.9 ^a 20.7 ^b		101.9 ^a 99.7 ^b	
Dickite	Cc	5.14	8.92	14.39		96.7	
Nacrite	Cc	8.91	5.15	15.70		113.7	

^a halloysite(7Å)

^b halloysite(10Å)

The vertical distance (along the Z axis) between two adjacent layers, which is denoted the basal spacing (d_L) is indicated by

$$d_{001} = c_0(1 - \cos^2 \alpha - \cos^2 \beta)^{1/2} = d_L = 7.16 \text{ \AA} \quad (\text{Eq. 1.1})$$

Figure 1.3 presents a schematic view of the kaolinite structure, with the designation of the XY plane and the Z axis. Two types of hydroxyl groups are present in the structure. One type of hydroxyl groups is located directly on the interlayer basal surfaces, pointing to the interlayer space. These hydroxyl groups are responsible for the hydrogen bonds with the oxygen atoms of the adjacent layers, responsible for the cohesion between the layers. They can also interact with any ions or molecules intercalated between the kaolinite layers (section 2.7.1). Another type of hydroxyl groups is present on the other face of the octahedral sheet of the kaolinite layers. These are located inside the layers, between the octahedral and tetrahedral sheets, and cannot form hydrogen bonds with adjacent layers. The different hydroxyl groups are called “**inner-surface**” and “**inner**” hydroxyl groups, respectively.

In fact, each hydroxyl group (from the four represented in the molecular formula) is different from the others, as the three inner-surface hydroxyl groups are oriented in different angles in relation to the (001) plane. Table 1.3 presents two sets of these angles, as well as the bond distances between O and H and the bond distances between OH and O in the interlayer hydrogen bonds. The two different sets of values arise from different experimental methods. Bish (1993) obtained the crystal structure of kaolinite from neutron powder diffraction data and Rietveld refinement at 1.5 K. Neder *et al.* (1999) used synchrotron radiation applied in a single crystal at room temperature to obtain his data. Although the values show some great differences, it is clearly seen that all hydroxyl groups are different, which should also imply different reactivities for each of the inner-surface hydroxyl groups. It is also seen that the inner-hydroxyl groups are located almost parallel to the (001) basal planes of the crystal.

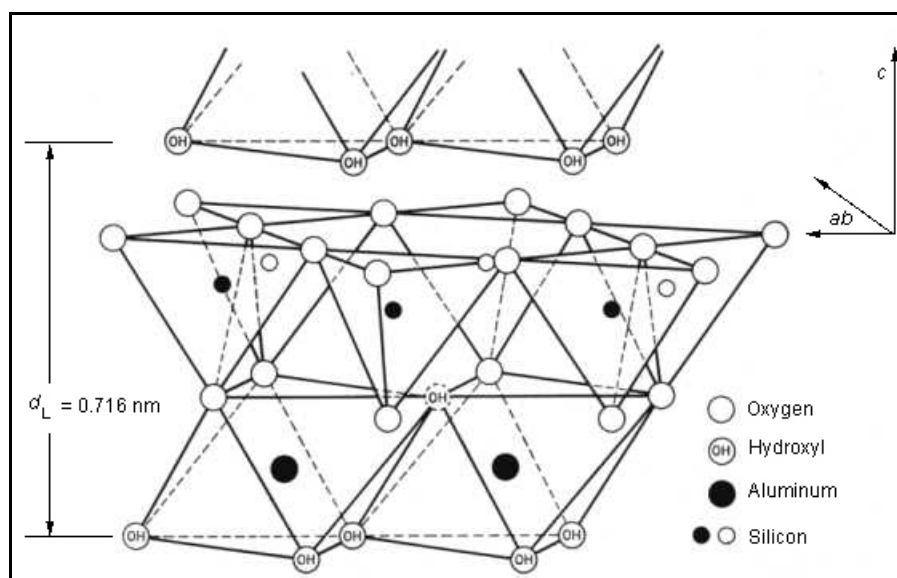


Fig. 1.3: Schematic view of the structure of kaolinite, showing the crystallographic c axis, ab basal plane and basal spacing (d_L) (adapted from Grim, 1968).

The inner-hydroxyl groups are, in reality, not totally isolated or closed inside the kaolinite layers. They are located inside the **ditrigrinal cavity** of the tetrahedral sheet. From the pseudo-hexagonal arrangement of the silica tetrahedra, holes or cavities arise in the structure of the sheet (as seen in Fig 1.1b). The arrangement of the tetrahedral and octahedral sheets is so that the inner-hydroxyl groups are located just above these holes (as seen in Fig. 1.3). Due to this structural feature, ions or molecules which could be present between the kaolinite layers (intercalation, see 2.7.1) could also interact with the inner-hydroxyl groups by

keying into the ditrigonal holes in the tetrahedral faces of the kaolinite layers. Figure 1.4 shows a schematic view of the kaolinite structure, with the positioning of the hydroxyl groups.

Table 1.3: Structural parameters for the OH groups in kaolinite

	O-H (Å)	angle of OH with (001) plane (°)	OH...O (Å)
OH(1) inner-hydroxyl	0.975 ^a 0.75 ^b	0.38 ^a 12 ^b	-
OH(2) inner-surface hydroxyl	0.982 ^a 0.76 ^b	73.16 ^a 64 ^b	3.087 ^a 3.088 ^b
OH(3) inner-surface hydroxyl	0.976 ^a 0.77 ^b	68.24 ^a 73 ^b	2.980 ^a 2.989 ^b
OH(4) inner-surface hydroxyl	0.975 ^a 0.88 ^b	60.28 ^a 47 ^b	2.945 ^a 2.953 ^b

^a Bish, 1993

^b Neder *et al.*, 1999

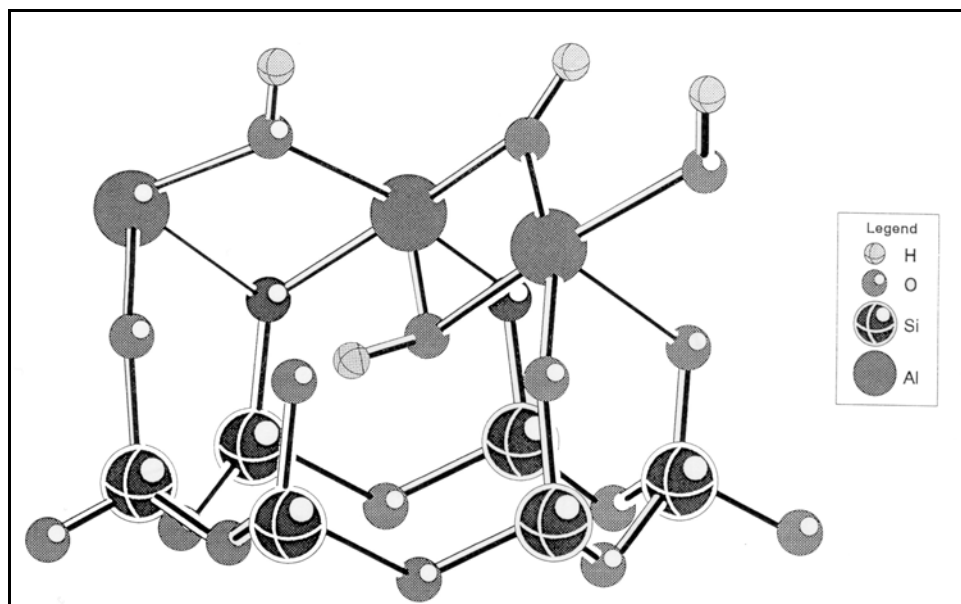


Fig. 1.4: Schematic view of the structure of kaolinite, with the positioning of the three inner-surface hydroxyl groups and the inner-hydroxyl groups. The angles with the (001) plane are not correctly scaled (Adapted from Frost, 1998)

In the so-called well-crystallized kaolinite there is a regular stacking of the layers in relation to the Y axis, the layers are exactly superimposed in relation to the Y axis, but translated by $-a_0/3$ in relation to the X axis. Figure 1.5 illustrates an ideal trioctahedral 7 Å layer in which octahedral hydroxyl groups at the top of the layer are paired with the tetrahedral oxygen atoms at the base of the overlying layer. This OH-O pairing results in the formation of long hydrogen-bonds, approximately 3.0 Å between the atom centers, that hold the neutral layers together (Bailey, 1963). The interlayer basal planes are cleavage planes, but the cleavage is not easy due to the ordered stacking of the layers, which optimizes the hydrogen-bonds between two adjacent layers.

In the kaolin group minerals the vacant octahedral site is always either B or C, these being enantiomorphic (see Figs. 1.5 and 1.6), position A always being occupied. In kaolinite, the vacant octahedral sites are always the same (either B or C), what implies in a triclinic symmetry (see Fig. 1.6).

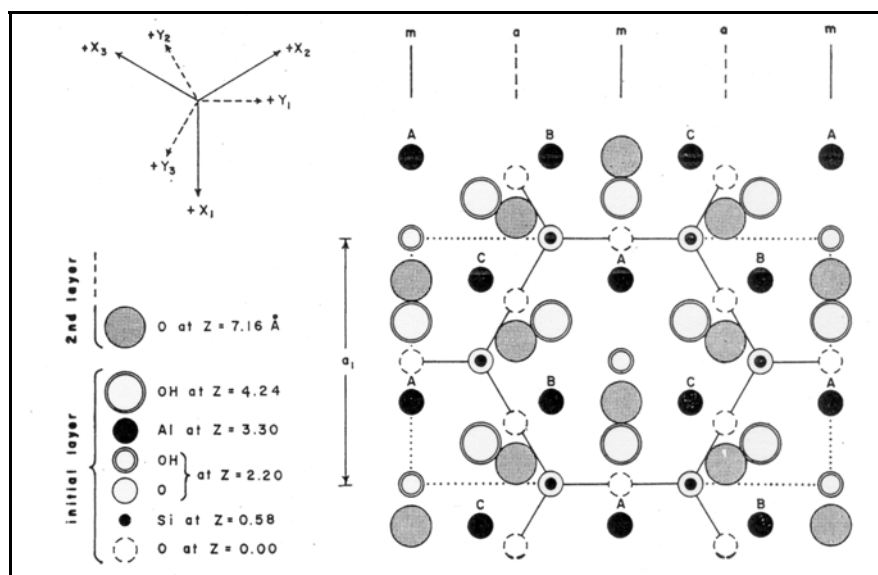


Fig. 1.5: Normal projection onto (001) of an undistorted 7 Å layer of space group Cm. The three possible octahedral sites, only two of which are occupied in the kaolin group minerals, are labeled A, B and C. The second layer has been shifted by $-a_0/3$, as in kaolinite and dickite, to provide optimized hydrogen-bonds between the paired OH and O at the layer interface (from Bailey, 1963).

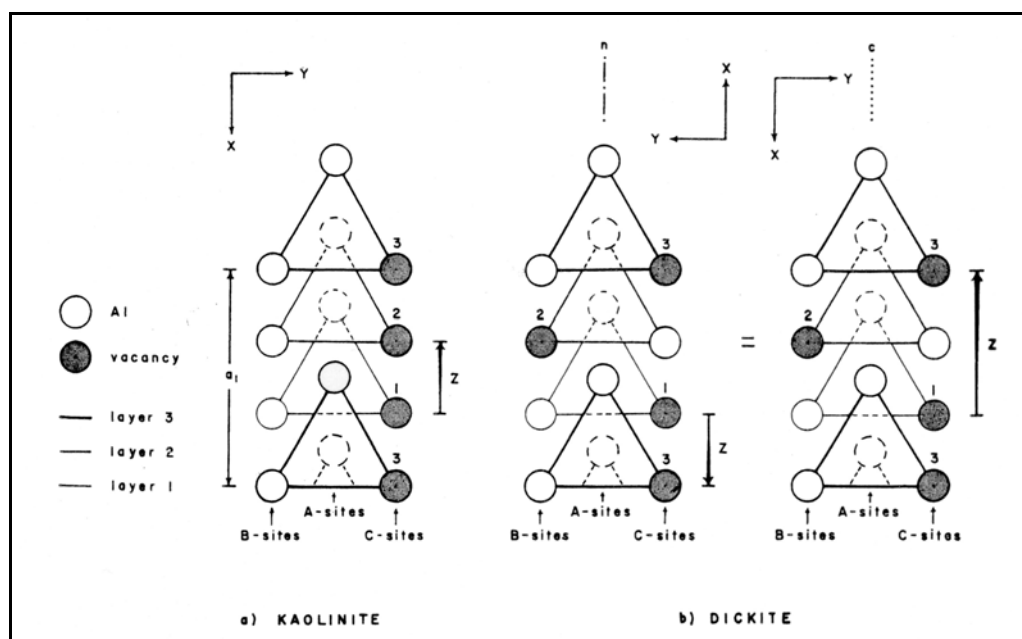


Fig. 1.6: Normal projection onto (001) of the octahedral portions of three layers (labeled 1, 2 and 3) of the kaolinite and dickite structures, showing distribution of Al atoms and vacancies over the A, B and C octahedral sites. In both structures, each layer is shifted by $-a_0/3$ ($a_1/3$) relative to the layer below. The projected Z-axis vector is shown as a solid line arrow. For dickite, the Al distribution may be interpreted as related by a n -glide plane or by a c -glide plane, depending on definition of the Z-axis vector. Two sets of octahedral positions, separated by a_1 , are shown in layer 3 to illustrate the two choices for the Z-axis vector in dickite. (adapted from Bailey, 1963).

Well-crystallized kaolinites present well constituted particles (crystallites) with a typical euhedral, hexagonal morphology, which reflects the pseudo-hexagonal structure of the layers. The hexagonal faces of these particles correspond to the crystallographic (001) basal planes. Kaolinite particles are highly anisometric, having a thickness (along the Z axis) much smaller than its other dimensions (Santos, 1989). The typical size of kaolinite particles range from 0.2 to 4 μm diameter, but macroscopic particles also described (Paetsch *et al.*, 1963). Figure 1.7 shows a TEM image of typical kaolinite particles in a platy morphology (almost isolated crystals), where the pseudo-hexagonal morphology is clearly identified. Figure 1.8 shows a SEM image of kaolinite particles, the larger units seen are sometimes also denominated as “booklets” (due to the resemblance with a book)¹. Kaolinite aggregates can also occur in a vermicular (or vermiform) morphology with very long, curved booklets, as seen in Fig. 1.9.

¹ The term “tactoid” is sometimes used as synonym; it is, however, misleading and should be avoided.

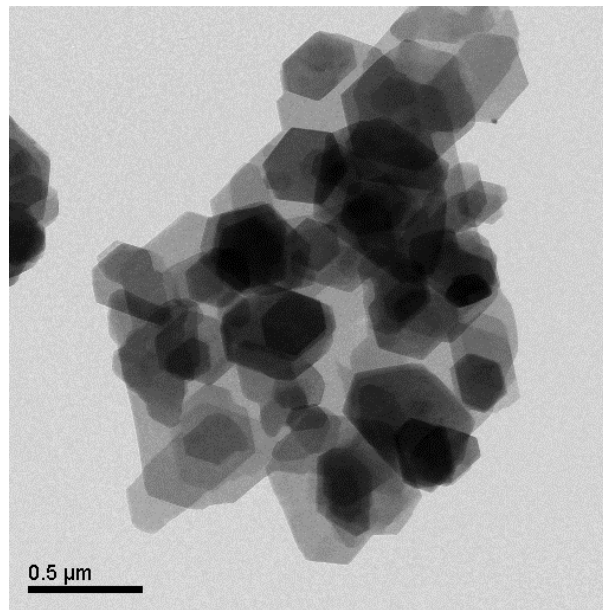


Fig. 1.7: TEM micrograph of kaolinite particles (Brazilian kaolinite, see Appendix I, Image courtesy from Prof. Dr. F. Wypych, Brazil)

Some kaolinite samples, mainly from sedimentary origin, present small, randomly distributed dislocations of the stacked layers. These dislocations occur mostly along the Y axis and are integer multiples of $b_0/3$ (Santos, 1989). These kaolinites are generally called “poorly crystallized kaolinites”, although the correct designation would be “kaolinite with disorder along the Y axis”. These kaolinites present much poorly built particles, which are thinner and smaller than particles from a well-crystallized probe.

Kaolinite normally presents very little isomorphous substitutions, especially of Si^{4+} by Al^{3+} in the tetrahedral sheets, what also accounts for the neutrality of its layers. Not uncommon is a small degree of substitution of Al^{3+} by Fe^{3+} ($< 1\%$ w/w Fe as Fe_2O_3) and in much smaller scale Si^{4+} by Ti^{4+} (Jasmund and Lagaly, 1993).

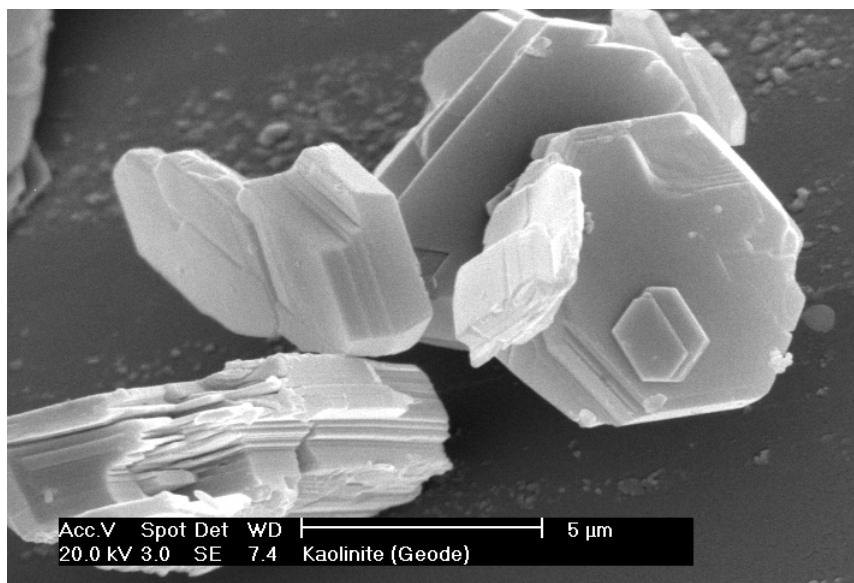


Fig. 1.8: SEM image of well crystallized kaolinite particles from the Keokuk geode, USA (Courtesy of the Clay Minerals Group of the Mineralogical Society, UK).

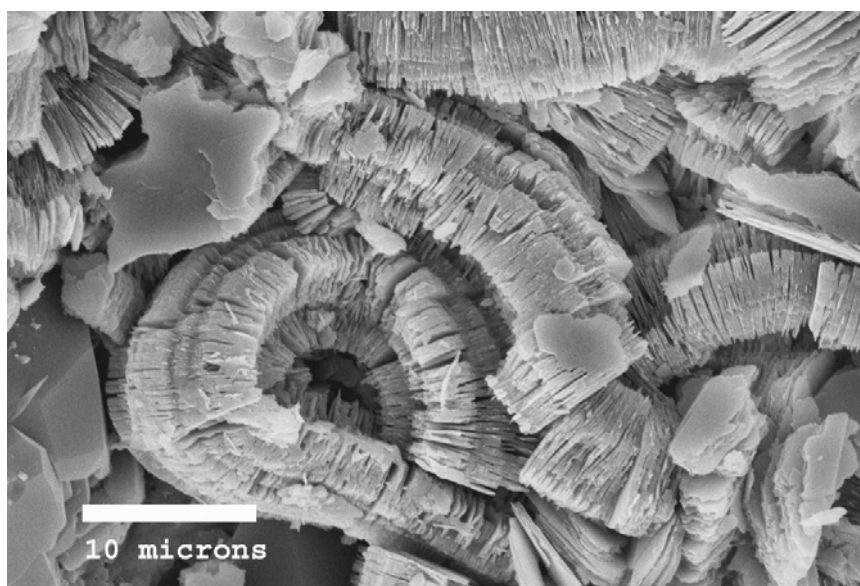


Fig. 1.9: SEM image of vermicular (vermiform) kaolinite from the Eyre Peninsula, Australia. (Courtesy of the Clay Minerals Group of the Mineralogical Society, UK)

1.2.3 Dickite and Nacrite: Structure and Morphology

Kaolinite and dickite have identical layer sequences, in which each layer is shifted by $-a_0/3$ relative to the layer below (as seen in Fig. 1.5). The two structures differ only in regard to the distribution of the vacant octahedral position in successive layers and the consequences of this distributions in terms of symmetry, layer distortion and Z-axis periodicity (Bailey, 1963).

In contrast to kaolinite, where each layer is identical and has a octahedral vacant site B (or C), dickite has the vacant sites alternating between B and C in successive layers creating a two-layer unit cell (see Fig. 1.6). This alteration of vacant sites in dickite tends to balance the stress distribution in the two layers so that the cell remains monoclinic. The pattern of vacant sites also creates c and n glide planes parallel to (010) and changes the space group to Cc. Thus, dickite can be considered as a regular alternation of right- and left-handed kaolinite layers (Bailey, 1963). The unit cell parameters of dickite are given in Table 1.2.

Dickite, as a rule, shows higher degree of crystallinity than kaolinite. This is expressed by the sharpness of the X-ray powder reflections as well as by, for a clay mineral, the unusually large size of the dickite particles (Nemecz, 1981). Fig. 1.10 presents a SEM image of typical dickite particles, with pseudo-hexagonal morphology.

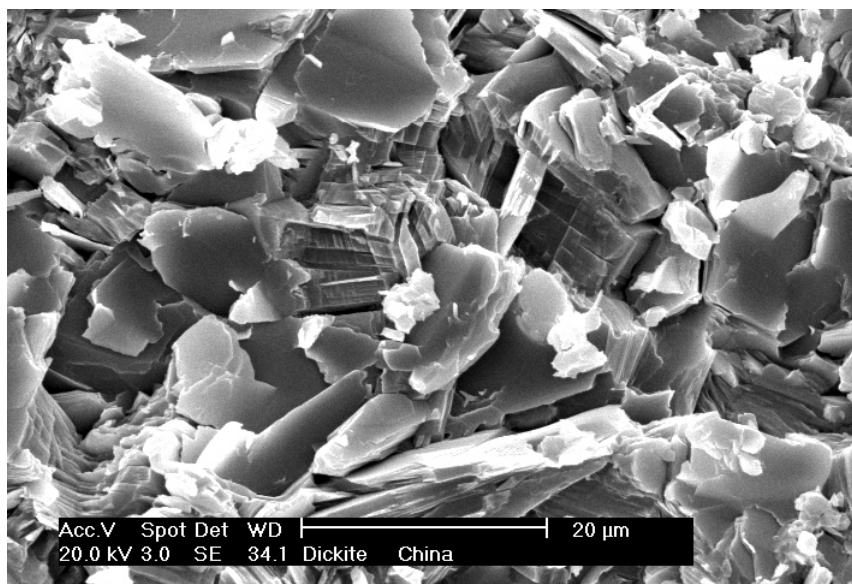


Fig. 1.10: SEM image of typical dickite particles. Note the large size of the particles, in comparison to kaolinite. (Image courtesy of the Clay Minerals Group of the Mineralogical Society, UK)

In the structure of nacrite, the vacant octahedral sites also alternate between B and C for each successive layer, as in dickite. Nacrite differs however by having each layer shifted by $-b_0/3$ in relation to the layer below, and alternate layer are rotated by 180° . The X and Y axes of dickite are, due to this fact, exchanged in relation to other clay minerals, so that the layer shifts are considered $-a_0/3$. The unit cell comprises two layers as in dickite, and the space group is Cc (Bailey, 1963). The unit cell parameters for nacrite are given in Table 1.2.

Nacrite tends to form very large particles, with pseudo-hexagonal morphology (Fig. 1.11).

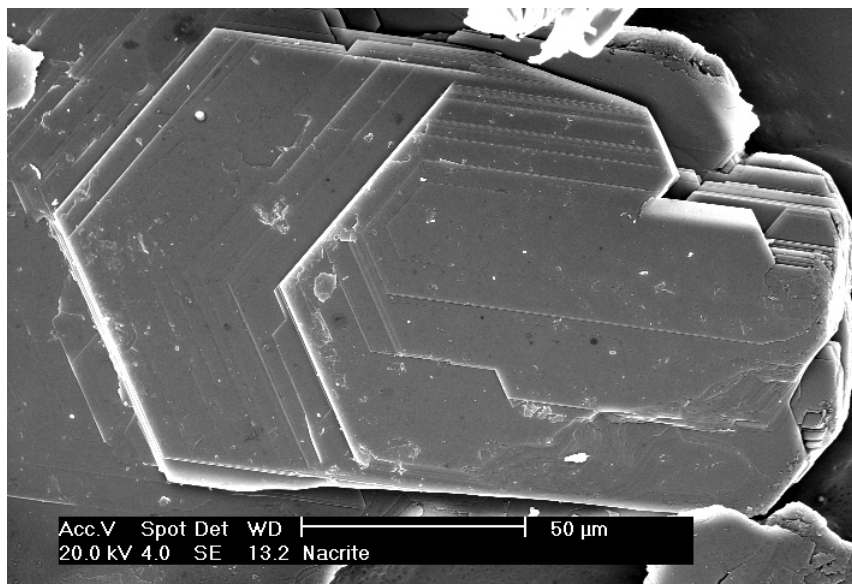


Fig. 1.11: SEM image of nacrite particles. Note the very large size of the particles. (Image courtesy of the Clay Minerals Group of the Mineralogical Society, UK)

1.2.4 Halloysite: Structure and Morphology

Halloysite is intrinsically different from kaolinite, dickite, or nacrite, as it can have a monolayer of water naturally intercalated between its layers. The structure of halloysite has posed challenges to clay scientists for many decades, but some facts are already known with certainty.

Halloysite in its hydrated form presents the approximate stoichiometry $\text{Al}_2\text{Si}_2\text{O}_5(\text{OH})_4 \cdot 2\text{H}_2\text{O}$ and basal a spacing near 10.1 Å. This halloysite(10Å) easily dehydrates in atmospheric pressures at temperatures around 60°C or *in vacuo* at room temperature. This anhydrous form has a basal spacing near 7.2 Å and is metastable, recovering its interlayer water when wet. Interstratification of hydrous and anhydrous forms during the hydration or dehydration processes cause the appearance of different peaks between 7.2 and 10.1 Å in the X-ray diffractograms (Brindley, 1984).

The accepted model of the structure of halloysite(10Å) presents a double layer unit cell with cell parameters as given in Table 1.2. The unit cell is monoclinic and the space

group is Cc. In addition, halloysite presents a highly disordered structure, with random dislocations in the X and Y directions.

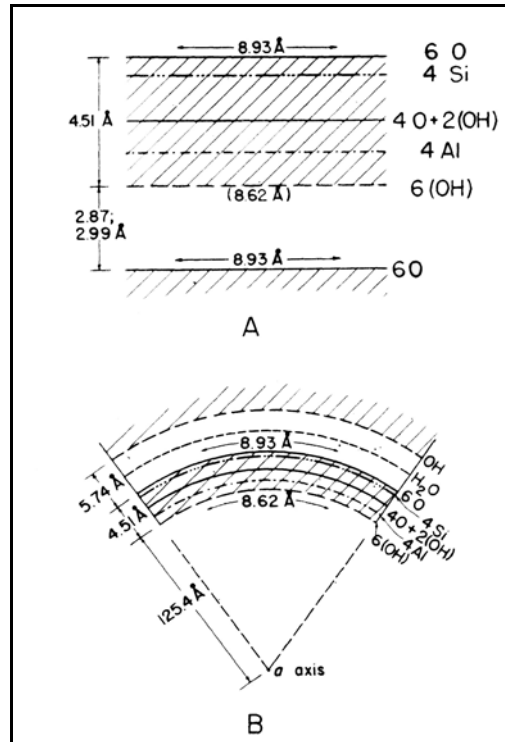


Fig. 1.11: Comparison between schematic structures of planar kaolinite (A) and tubular halloysite (B). Observe the minimum tube inner diameter of 250 Å, as calculated by Bates *et al.* 1950). (adapted from Bates *et al.* 1950)

The greatest problems involving halloysite concern its morphology. Halloysite particles normally consist of tubes, cylinders or rolls, but halloysite can also be composed of spheroidal or irregular particles. The cause of the curvature of the layers is usually attributed to the lateral misfit between the octahedral and tetrahedral sheets in the 1:1 structure. For a Si-tetrahedral sheet with a Si-O bond length of 1.62 Å, the b_0 dimension equals 9.164 Å and $a_0 = 5.02$ Å. These lateral dimensions of the tetrahedral sheet are significantly larger than those of the Al-dioctahedral sheet which has $b_0 = 8.655$ Å and $a_0 = 5.066$ Å as observed for gibbsite (Singh, 1996). In this way, the 1:1 layer tends to curve itself along the Y (or X) axes, with the silica tetrahedral sheet on the convex side of the curve in order to compensate the lateral misfit. Bates *et al.* (1950) calculated that the diameter of the so formed tubes match well with the observed minimum internal diameter of the halloysite tubes (see Fig. 1.11). Figure 1.12 presents schematically the morphology of halloysite, as proposed by Bates *et al.* (1950).

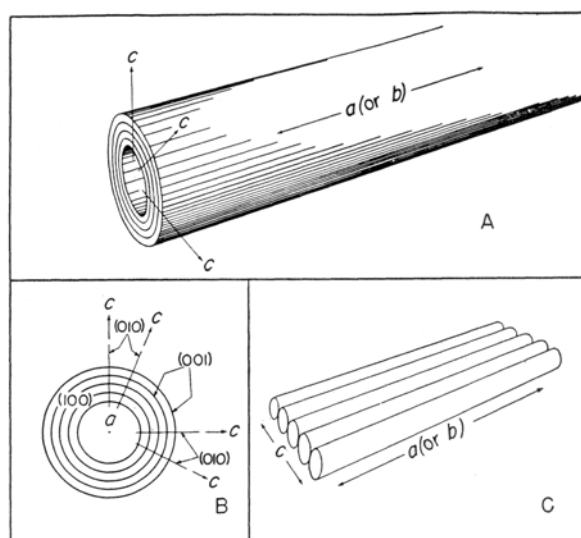


Fig. 1.12: Morphology of halloysite tubes. (A) Tube in perspective. (B) Cross section showing crystallographic axes and major planes. (C) Oriented aggregate. (adapted from Bates *et al.*, 1950)

The lateral misfit is, however, present in every 1:1 or 2:1 clay mineral structure and the vast majority of the clay minerals have a planar morphology. It was already demonstrated (Radoslovich, 1963) that rotation of adjacent tetrahedra in opposite directions corrects the lateral misfit and stabilizes the structures of the aluminosilicates. The question is why that does not happen with halloysite?

Singh (1996) showed that correction of the lateral misfit on non-hydrated 1:1 structures is accomplished by tetrahedral rotation, which is corroborated by the hydrogen bonds between the layers. However, in a hydrated structure, the hydrogen bonds are weakened and the rolling mechanism is energetically more favorable stabilizing the layers.

It is also known that repeated intercalation/deintercalation sequences of various molecules on kaolinite (ammonium acetate: Weiss and Russow, 1963; potassium acetate: Wiewiora and Brindley, 1969; Singh and Mackinnon, 1996; octylamine: Poyato-Ferrera *et al.*, 1977) induces the formation of a highly disordered, partially-delaminated kaolinite structure, which culminates in the curling of the layers to a morphology indistinguishable from the halloysite tubes. Based on these facts, it was postulated that hydration of kaolinite and formation of halloysite requires stacking disorder (Costanzo *et al.*, 1984). This paradigm can be inverted in a way that stacking disorder is seen as a consequence of the hydration of kaolinite, which causes the weakening of the interlayer hydrogen bonds and triggers the curling of the layers of halloysite.

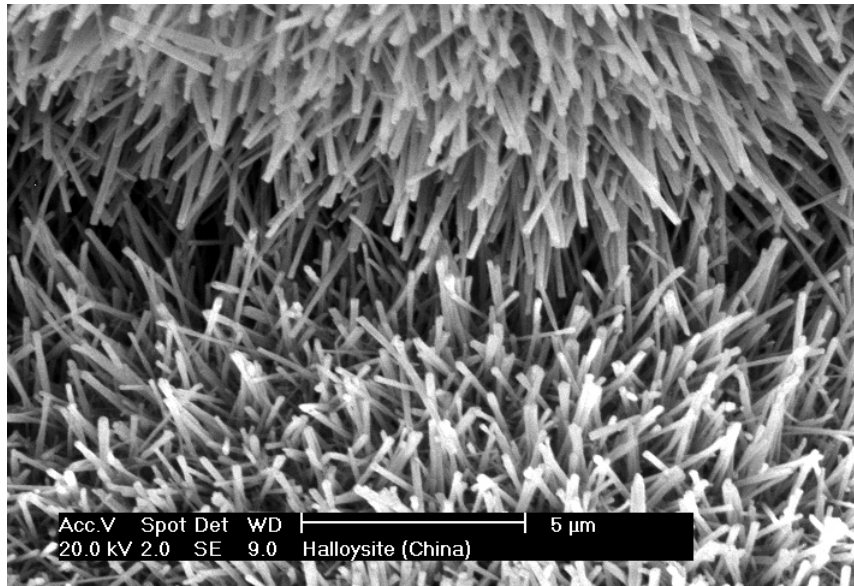


Fig. 1.13: SEM image of halloysite presenting the typical tube (rolls) morphology (Image courtesy of the Clay Minerals Group of the Mineralogical Society, UK)

Fig. 1.13 presents a SEM image of typical halloysite tubes and Fig. 1.14 a TEM image of a transversal section of halloysite tubes. It can also be observed that there are particles presenting planar domains, which are just kinked in pentagonal or hexagonal angles (100° - 130°) to form “prismatic rolls” or polygonal spirals. Robertson and Eggleton (1991) suggested that in the planar domains of the plates, kaolinite structure is still present, while in the curved domains, the structure is hydrated. This process of domain formation of halloysite in kaolinite plates is illustrated in Fig. 1.15.

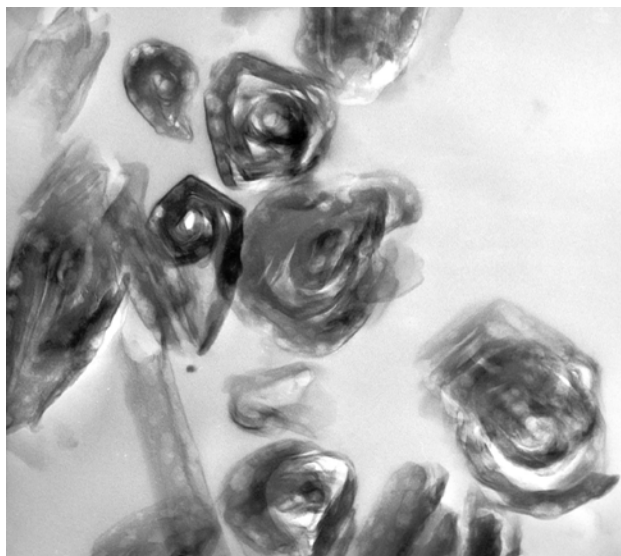


Fig. 1.14: TEM image of a transversal section of halloysite tubes. Note that the tubes consist of rolled plates which, in many domains, still conserve planar morphology and are kinked in pentagonal or hexagonal angles (100° - 130°), forming polygonal spirals. (Image courtesy of Imerys Tableware New Zealand Ltd.)

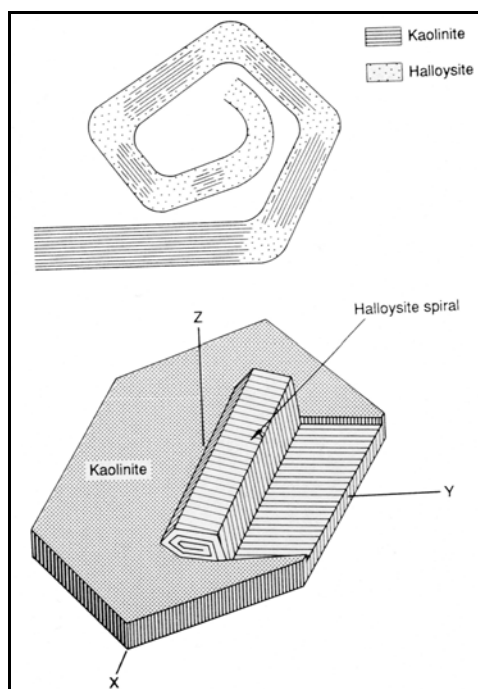


Fig. 1.15: (Upper) Model for halloysite spiral development. Hydration of kaolinite to halloysite has occurred at points along the kaolinite crystal. At these points halloysite curls. Intervening kaolinite relics provide localized rigidity, so a polygonal spiral develops. As these relics are progressively consumed, the halloysite curls smoothly. (Lower) Halloysite spiral developed on and still attached to a kaolinite plate, by rolling up part of the plate (from Robertson and Eggleton, 1991).

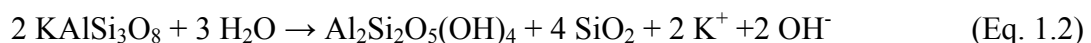
1.3 Genesis and Occurrence

1.3.1 The Genesis of Kaolin Minerals

The kaolin mineral deposits can have different origins, as they can be formed either by metamorphic or sedimentary processes. Metamorphic kaolins, also called primary kaolins, are classified into **residual** and **hydrothermal**. These deposits were formed in-situ, by alteration of crystalline rocks such as granites and rhyolites. The alteration results from surface weathering, groundwater movement below the surface (Residual formation) or hydrothermal action. **Sedimentary** kaolins are also called of secondary origin, as they were formed elsewhere, and eroded, transported and deposited as beds or lenses associated with other sedimentary rocks in the final deposits (Murray, 1991).

Kaolinite can be found in sedimentary, residual or hydrothermal deposits. Halloysite occurs as weathering or as hydrothermal product. It is uncommon in sedimentary deposits. Dickite occurs as a hydrothermal mineral and occasionally as an authigenic sedimentary mineral. Nacrite occurs only in hydrothermal environments (Murray, 1991).

The physical and chemical conditions under which the kaolin minerals form are relatively low temperatures and pressures. The most common parent minerals from which they form are feldspars and muscovite, both of which contain the necessary alumina and silica. The transformation of potassium feldspar (KAlSi_3O_8) into kaolinite occurs by intense weathering of the feldspar and leaching of K^+ and SiO_2 according to the idealized equation:



All of the potassium must be lost in solution because if some is retained, illite will form rather than kaolinite (Murray, 1991).

Granites and rhyolites weather readily to kaolinite and quartz under favorable conditions of high rainfall, rapid drainage, temperate to tropical climate, low water table and adequate ground water movement to leach the soluble components.

The exact conditions of formation of halloysite versus kaolinite are still matter of debate. Papoulis *et al.* (2004) showed that in the weathering of some plagioclase deposits there are clear stages in the formation of halloysite and its subsequent transformation into kaolinite. Concomitant with the kaolinization of halloysite is a enrichment of iron in the

mineral structure as well as a diminution of the aluminum concentration. It is suggested that the compositions of the ambient solutions are the main factor dictating the nature of the solid phase formed. Geological processes can alter halloysite to kaolinite (Papoulis *et al.*, 2004; Jeong, 1998), but the opposite direction, the formation of halloysite from kaolinite is also very common (Loughnan and Roberts, 1981; Robertson and Eggleton, 1991; Bobos *et al.*; 2001). The reason is that these two minerals are very similar and a certain equilibrium between the two forms exists. Dickite and nacrite are rarely found in residual deposits.

Primary kaolins of hydrothermal origin generally are comprised of kaolinite with lesser amounts of halloysite and occasionally dickite and nacrite. The kaolin mineral that forms under hydrothermal conditions is largely dependent upon temperature. Nacrite and dickite may form as result of high temperature hydrothermal solutions although they are relatively rare and the temperatures are probably of the order of 100°C to 400°C (Murray, 1991).

Sedimentary or secondary kaolin deposits are not as common as primary deposits, however, some large deposits are known (USA, Brazil, Australia). The largest sedimentary deposits that are preserved in the rock record are Cretaceous or younger in age and were deposited in deltaic, lagoonal, estuarine, or lacustrine environments. Kaolinite is the dominant kaolin mineral in the secondary deposits, with halloysite rare, dickite very rare and nacrite not present. Authigenic halloysite and dickite have been reported in sedimentary rocks (Murray, 1991).

1.3.1 Occurrence of Selected Kaolin Deposits

Deposits of kaolin minerals are found virtually all around the globe, in most of the countries. A few of the most important or unusual kaolin deposits are here briefly described in the following tables, they are separated into hydrothermal, residual, mixed hydrothermal-residual and sedimentary origins. All information, unless otherwise noted, is derived from Murray (1991).

Table 1.4: Some hydrothermal kaolin deposits, according to Murray (1991).

Country	Mine/Place, Location	Origin	Composition	Impurities	Major Uses	Observations
China	near Suzhou, Jingsu province	kaolinization of various rock types	kaolinite and halloysite	alunite, pyrite, sericite, quartz, quartz and chalcedony	ceramics, cement, fillers for papers, rubber and paint	very large reserve: over 20 Mt
Italy	Locchera, Sardinia	from Tertiary rhyolite ignimbrites and andesitic-basaltic lavas	well-crystallized kaolinite, small amounts of halloysite, dickite and allophane	crystalite, quartz, opal, alunite, sulfates and residual feldspar	cement, ceramics and refractories	
Japan	Itaya, Okayama prefecture	from Pleistocene volcanic and pyroclastic rocks	kaolinite, pyrophyllite and diaspore, small amounts of dickite, nacrite and alunite		paper fillers and refractories	
Mexico	near Guanajuato	from upper Cenozoic volcanic rocks	disordered kaolinite	very fine quartz	fillers for paper rubber and plastics, paint extenders, ceramic and refractories	Mexico has at least 9 mining locations. Total national production of kaolins is greater than 100 kt/year
	General Saragosa, near San Luis Potosi	argillation of rhyolite flow-breccia and welded tuff	poorly ordered kaolinite, small amount of halloysite	crystalite and alunite	refractories	
	Nayarit	Cenozoic volcanic rocks of andesitic to rhyolitic composition	kaolinite and dickite, minor amounts of nacrite. Traces of halloysite	quartz and crystalite		
USA	Little Antelope Valley, California	alteration of rhyolites	kaolinite and quartz	crystalite opal, alunite	fillers for paper, plastics and rubber, cement and stucco	
	Dragon mine, Utah	replacements of lower Paleozoic limestone near the contact with the porphyry	halloysite	very fine grained pyrite	catalysis	one of the most important sources for very pure halloysite, almost totally mined.

Table 1.5: Some residual kaolin deposits, according to Murray (1991).

Country	Mine/Place, Location	Origin	Composition	Impurities	Major Uses	Observations
Argentina	Chubut river valley, Patagonia	from rhyolitic volcanic and related pyroclastic rock of Jurassic age	kaolinite and minor amounts of halloysite	quartz	ceramics and refractories. Better quality as paper and paint fillers	
Australia	Ballarat and Pittong, NW of Melbourne	alteration of late Devonian granites	kaolinite and minor amounts of halloysite	quartz	filler for paper, plastic rubber and paint, ceramics	
China	Gaoling, Kiangsi province	weathering of granites	kaolinite and halloysite	quartz and muscovite	ceramics, including fine china	The Gaoling mine originated the mineral name
Czech Rep.	near Karlovy Vary	weathering of granites	kaolinite and minor amounts of halloysite	quartz and illite	filler for paper and rubber, ceramics and refractories	
Germany	Kemmlitz, Sachsen	from volcanic ignimbrites and porphyritic andesites	kaolinite	quartz and illite-smectite	fillers in paper, paint, plastics and rubber, ceramics	
	Seilitz, near Meissen	alteration of pitchstone, felsite and quartz porphyry	kaolinite		fine china	Oldest mine in Europe (1764). Worldwide famous chinaware
Indonesia	Belitung and Bangka islands	alteration of porphyritic biotite granite	kaolinite and minor amounts of halloysite	quartz	filler for paper, whiteware and ceramics	
Ukraine	Proslanovskoe	weathering of granites and feldspathic or micaceous acid rocks	kaolinite	mica and quartz	fillers for paper and rubber, ceramics	
South Africa	near Grahamstown, Cape province	from Permian tillites and Carboniferous shales	fine particle size kaolinite	quartz, feldspar and muscovite	ceramics, fillers for paper, rubber, paint and plastics, carrier for insecticides	

Table 1.6: Some mixed hydrothermal and residual kaolin deposits, according to Murray (1991).

Country	Mine/Place, Location	Origin	Composition	Impurities	Major Uses	Observations
England	Cornwall	alteration of St. Austell granite	well crystallized kaolinite	muscovite, quartz and feldspar (fine particle fraction is almost pure)	paper coating and filling, ceramics, filler in paints, plastics and rubber	one of the largest and highest quality primary kaolin deposits in the world
New Zealand	Maungaparerura and Mataury Bay	from rhyolitic flow rock	halloysite, kaolinite and allophane	50% quartz, amorphous silica and cristobalite	very high quality ceramics	high proportion of halloysite in clay fraction produces a material with elevated whiteness

Table 1.7: Some sedimentary kaolin deposits, according to Murray (1991).

Country	Mine/Place, Location	Origin	Composition	Impurities	Major Uses	Observations
Australia	Weipa, Cape York peninsula	late Cretaceous or early Tertiary kaolinitic sands	kaolinite	quartz, smectite	paper coating	
Brazil †	Jari and Capim river basins, amazon region	Plyocenic sands, sandy clays, kaolin and conglomerates of lateritic origin, modified by reduced lacustrine and/or swamp environment	well crystallized kaolinite	quartz, illite-muscovite, anatase and hematite	primarily for paper coating	Brazil has the world's second largest kaolinite deposit (~ 41 %), with a exceptionally high quality product.
Germany	near Hirschau, Bayern	kaolinization of akrosic sand of Triassic age	kaolinite	quartz, smectite and illite	paper filler and coating, ceramic	
Spain	from Guadalajara to Valencia region	kaolinitic akrosic sands from Cretaceous age	kaolinite	quartz, feldspar	ceramics, filler for paper, plastic, rubber and paint	
Suriname	Oncerdach Series, Moengo area	Eocenic kaolin sands	kaolinite	quartz, bauxite, gibbsite and mica	not mined (suitable for paper coating)	
USA	Georgia and South Carolina	late Cretaceous deposits in estuaries, lagoons, oxbow lakes and ponds, in an area about 30x50 km wide, derived from granites and gneisses of the Piedmont plateau	kaolinite	quartz, muscovite, biotite, smectite	paper coating, ceramics and fillers	USA has the world's largest kaolin reserves (~ 48%). Georgia resources, with over 5 billion tons are the largest reserve of high quality kaolin in the world.

† Data from Costa and Moraes (1998) and Mártires (2003, 2004)

1.4 Mining and Production

1.4.1 The Mining and Processing of Kaolin Minerals

The mining and processing of clay minerals, especially of kaolins can vary according to the type of deposit, type and quantity of impurities, destination of the mineral among many others. Many different factors may influence the whole process, but the basic principles of mining and processing are roughly the same.

Kaolin minerals are obtained from open pit surface mines. One of the only important exceptions is the mine of the Meissen China Manufacture, near Seilitz, Sachsen (Germany). The kaolin in this subterranean tunnel mine is still handpicked as it was for centuries ago. All the mine production is used in the manufacture of fine china of worldwide fame.

In almost all other deposits, after conventional extraction with bulldozers or with high-pressure water jets (hydromonitor), the raw material is transported to the processing facility. Large producers extract kaolin from different mines simultaneously, and mix the products according to their properties prior to further processing, in order to obtain a blend that will have the right characteristics for its applications.

The raw material is mixed with water and milled to a fine paste (blunging), at the same time dispersion agents are also added to the mixture (usually soda). During this process, a dispersion of the fine particle size kaolin minerals (2-100 μm) is formed, while quartz, feldspars and other sandy contaminants with large particle size are separated by sedimentation or filtration (de-gritting). The kaolin dispersion is then ready to be separated by particle size. Hydrocyclones are used to fractionate the dispersions up to portions with 5-20 μm particle size. For even finer fractionating, centrifuges are used. After the separation and classification of different particle sizes, the dispersions are kept in homogenization silos in order to obtain a product with constant quality.

The resulting dispersions have up to 95 % (w/w) of water. In further processing, they are flocculated and sedimented, sometimes with addition of organic flocculation agents. This processes can reduce the water content to ~ 40 %. The resulting heavy dispersions are further dried by filtering techniques (chamber-filter pressing, vacuum filtration, etc.) up to water contents around 20 %. Depending on the destination of the kaolin, a more complete drying (up to < 1 % water) can be obtained by conventional thermal methods, dry-freezing or spray-drying, followed by dry milling of the product.

According to the destination of the final material, the kaolin mineral can be further treated to obtain specific properties needed. Among these techniques one could cite the magnetic separation of iron contaminants, which impart a yellow tinge to the kaolin and is extremely undesirable for the paper industry as well as chemical bleaching, ozonization or “delamination”¹ (Jasmund and Lagaly, 1993).

1.4.2 Worldwide Production of Kaolin Minerals

The worldwide reserves of kaolin minerals are estimated to be around 17.3 billion tons. Even when there are deposits in many different countries (see 1.3.1), most of them are highly concentrated. Alone USA, Brazil and Ukraine detain almost 95 % of the total. The country concentrating the largest worldwide reserves is the USA (~ 47 %), most of it at the Georgia region. Brazilian reserves (~ 41 % of the worldwide deposits) are 95 % concentrated in the amazon region, mostly in the Jari and Capim river basins (Mártires, 2003, 2004). Table 1.7 presents a rough distribution of the kaolin reserves around the globe, as well as the production for each country, during 2003.

Table 1.7: Distribution of worldwide kaolin reserves and production during 2003, according to Mártires (2003, 2004).

Country	Reserves		Production	
	(10 ³ t)	(%)	(10 ³ t)	(%)
USA	8 290 500	47.8	8 010	17.8
Brazil	7 179 126	41.4	5 206	11.5
Ukraine and CIE^a	979 000	5.6	8 000	17.7
UK	257 500	1.5	2 400	5.3
China	179 000	1.0	-	-
Others	473 000	2.7	21 484	47.6
Total	17 358 126	100	45 100	100

^a CIE = Commonwealth of Independent States

¹ The term delamination is used here as it is industrially known. For a discussion on the terms exfoliation and delamination, see section 2.8.

From the data above is clearly seen that the countries with the greatest reserves are also the major kaolin producers. Two other facts are also noteworthy: Brazil detaining more than 40 % of the reserves, occupies only the third place on production, which means it's producing capacity can still be greatly expanded. In fact, the Brazilian amazonic reserves are of a kaolinite with exceptionally high quality, which attends the most rigid parameters for the noble application in paper coating. These reserves surpass in a size *versus* quality evaluation any other deposits in the world. Another interesting fact is that the UK, having no more than 1.5 % of the world reserves, responds with more than 5 % of the production. This fact is due to the great tradition of the Cornwall kaolins and the high quality of its products.

Few companies detain almost the total kaolin production around the globe, among them Imerys (France) with mines spread in many counties (and since 1999 detaining also control of the traditional English China Clays International (UK)); J. M. Huber (USA) and CADAM (Brazil). The 2005 market forecast for kaolin minerals is estimated to be around 4.05 billion US dollars (Gobi, 2002).

1.5 Traditional Uses and Importance

The worldwide annual production and market numbers for kaolin minerals (annual worldwide production ~ 45.1 million tons, annual market ~ 4.05 billion US dollars) clearly indicated that kaolin minerals have an immense industrial and technological importance and represent a huge commercial market.

Particle size, shape, and distribution of kaolin minerals are important physical properties, which are strongly related to their many applications. Other important characteristics are surface area and surface charge. They have direct influence on many other properties such (low and high) shear viscosity; absorption; plasticity; green, dry and fired strength; casting rate; permeability; and bond strength. These properties, along with color and brightness, are all of high industrial importance, and play an important role on the application fields and prices of kaolin samples from different sources. In almost every application, the kaolin minerals are functional and not just inert components of the system (Murray, 2000).

It would be impracticable to detail here all the application fields for kaolins, the most important and/or notable of them, however are briefly described or cited below (data from Santos, 1989; Jasmund and Lagaly, 1993 and Murray, 2000).

Ceramic Industry: Although the use of clays as raw material for ceramics is the oldest and one of the more traditional applications known, it responds today for only ~ 20 % of the worldwide kaolin consumption. That does not mean that ceramic industry is using less of it today, but rather that other applications have now a much higher need for kaolin minerals. Fine ceramics, china, whiteware, sanitaryware, pottery, tableware, insulators, many refractories and almost all other ceramic-related industries use kaolin minerals as the primary raw material in addition to small amounts of silica (quartz sand), feldspars or other components. Different grades of kaolin minerals are suited for different kinds of ceramics. Usually, only the purest and whitest kaolins are used in the manufacture of fine china. The halloysites of New Zealand find here a special place, since they are considered the whitest kaolins available at industrial scales.

Paper Industry: By far the largest consumer of kaolins is the paper industry, as it alone responds for ~ 50 % of all consumption. Kaolins have two main distinct applications in the manufacture of paper, as filler or as coating. The use of kaolin as paper filler has decreased due to the crescent use of basic-pulp technologies, which makes possible the use of calcium carbonate. The use as paper coating material only tends to grow, as there is an ever-growing

demand for high quality papers. Also here only a few kaolins are suitable, as it has to be free from silica and possess an elevated whiteness. Amazonian kaolins are among the most suited to paper coating, turning the huge deposits in Brazil in a high-valued strategic reserve for the country.

Paints, Inks and Enamels: In the fabrication of paints, inks and enamels, kaolins are traditionally used as both fillers and extenders. Calcined kaolin, with high content of needle-like mullite crystals, which have a high light refraction capacity, are also used in substitution of the expensive TiO₂ pigments in paints.

Rubbers and Plastics: Kaolins are also extensively used as inorganic fillers in rubbers and plastics. The fire-retardant and anti-dropping qualities that kaolins impart to these materials, especially to electrical cable insulation are of immense importance nowadays, not to mention the improvement of mechanical properties.

Fungicides, Pesticides and Insecticides: Kaolins find here a valuable use as inert carriers for the active ingredients.

Pharmaceuticals: High quality kaolins are used as filler, binding and carriage material in the fabrication of pills and other pharmaceuticals.

Fiberglass: Impure kaolins, which are not suitable to other industries, have also found use in the obtention of glass fibers.

Cement: Kaolin clays are very important ingredients in the cement industry, providing aluminum and silicon to the mixture.

Cracking Catalysts: Acid treated halloysitic clays are one of the most efficient cracking catalysts used by the oil industry.

Other important applications for kaolins are carriers for automobile catalysts; in the fabrication of molecular sieves and cation exchangers, diverse catalysts, sialons, adhesives and crayons; etc.

1.6 Conclusion

Kaolin minerals, especially kaolinite, are among the most important industrial minerals today. They are indispensable in many different sectors and branches, having a huge worldwide market. These 1:1 dioctahedral aluminosilicates are formed by alteration of granites, feldspars or other clays and are found either in primary or secondary deposits. They can be found in almost all countries of the world, the largest and highest-quality reserves, however, being concentrated in just a few locations, turning them into strategic sources for the countries which have access to them. Constantly increasing industrial and technological standards drive the processing and beneficiation of kaolins into new improvements.

CHAPTER 2
KAOLINITE CHEMISTRY

2.1 Introduction

In this chapter, some basic aspects of the chemistry of kaolinite will be exposed and discussed. Thermal behavior and dehydration, as well as the TG/DTA analysis of the mineral will constitute the first topic. A short introduction on some important aspects of the most important analytical methods applied to the study of kaolinite and its derivatives, X-ray diffractometry and FTIR analysis, will also be given.

The external surface of kaolinite particles will then be the theme of discussion, with some insights on the surface charge and cationic exchange capacity, adsorption and surface grafting reactions.

A detailed study of kaolinite intercalation reactions and derivatives will be presented, as well as a discussion and review of the interlayer-grafted derivatives obtained from kaolinite which were already described in the literature. The syntheses of new grafted derivatives of kaolinite is one of the main objectives of this work, so it would be relevant to present a detailed insight on these compounds.

Some non-topotactic reactions of kaolinite will also be briefly presented. The phenomena of delamination and exfoliation on kaolinite will be precisely defined, and a discussion on the methods already discussed on these matters will also be presented.

The chapter ends with a brief introduction on the rheological properties of kaolinite aqueous dispersions, as results of the flow properties of grafted kaolinite derivatives are going to be presented in Chapter 4.

2.2 Thermal Behavior and Dehydration

According to Brindley and Lemaitre (1987), the thermal reactions of clay minerals can be conveniently separated into four categories:

1. Low-temperature reactions below ~ 400 °C.
2. Intermediate-temperature reactions, mainly between 400 and 750 °C.
3. High-temperature reactions, above 750 °C.
4. Oxidation reactions.

The phenomena occurring up to 400 °C are mostly related to the elimination of water molecules present in the clay mineral. These molecules can be adsorbed to the surfaces or intercalated. The intercalated water molecules may be part of the hydration sphere of cations or simply hydrogen bonded to the interlayer surfaces.

Kaolinite does not present either interlayer cations or naturally intercalated water (see Chapter 1 for a discussion of the hydrated halloysite structure). This being the case, all phenomena observed in the thermal analysis of pure kaolinite in the low-temperature region are attributed to the elimination of water molecules adsorbed to the external surfaces of the particles. In the TG/DTA curves of kaolinite (Fig. 2.1), this process is observed as a loss of ~ 0.5 % of mass up to 400 °C, accompanied by a faint endothermic band (in Fig. 2.1 not clearly visible due to the inclined baseline).

In the intermediate-temperature region is located possibly the most important thermal reaction of kaolinite, the elimination of water molecules by the dehydroxylation process, according to the equation:



The dehydroxylation of kaolinite samples is observed in the TG/DTA analysis (Fig. 2.1) as a mass loss beginning after 400 °C and completed around 650 °C though some additional small mass loss is usually observed up to 800 °C. This mass loss corresponds to a theoretical value of 13.96 % according to Eq. 2.1. The process is endothermic, and an intense endothermic peak is observed in the DTA curve around 550-600 °C. Crystallinity and particle size of the sample can strongly influence these temperatures, with small, poorly crystallized particles presenting lower dehydroxylation temperatures than high ordered samples with larger particles (Brindley and Lemaitre, 1987).

The product formed after dehydroxylation is called metakaolinite and is usually almost amorphous (after XRPD data), though the dehydroxylation process is topotactic and

the particles retain the pseudo-hexagonal morphology. It was showed that structural order persists within individual layers of metakaolinite, but not between them (Brindley and Lemaitre, 1987).

The mechanism of the dehydroxylation reaction is not yet fully understood. A homogeneous mechanism suggests that in two neighboring hydroxyl groups having different acidities the proton of the more acidic one will react with the less acidic to form water. This water molecule would diffuse through the interlayer spaces until be eliminated from the particle. The heterogeneous mechanism suggests that free protons are produced in some region of the structure. These protons migrate to elimination regions where they can react with hydroxyl groups forming water. The increase of the electrical conductivity of kaolinite around the dehydroxylation temperature may be linked to proton delocalization and is an indicative of the heterogeneous mechanism (Brindley and Lemaitre, 1987).

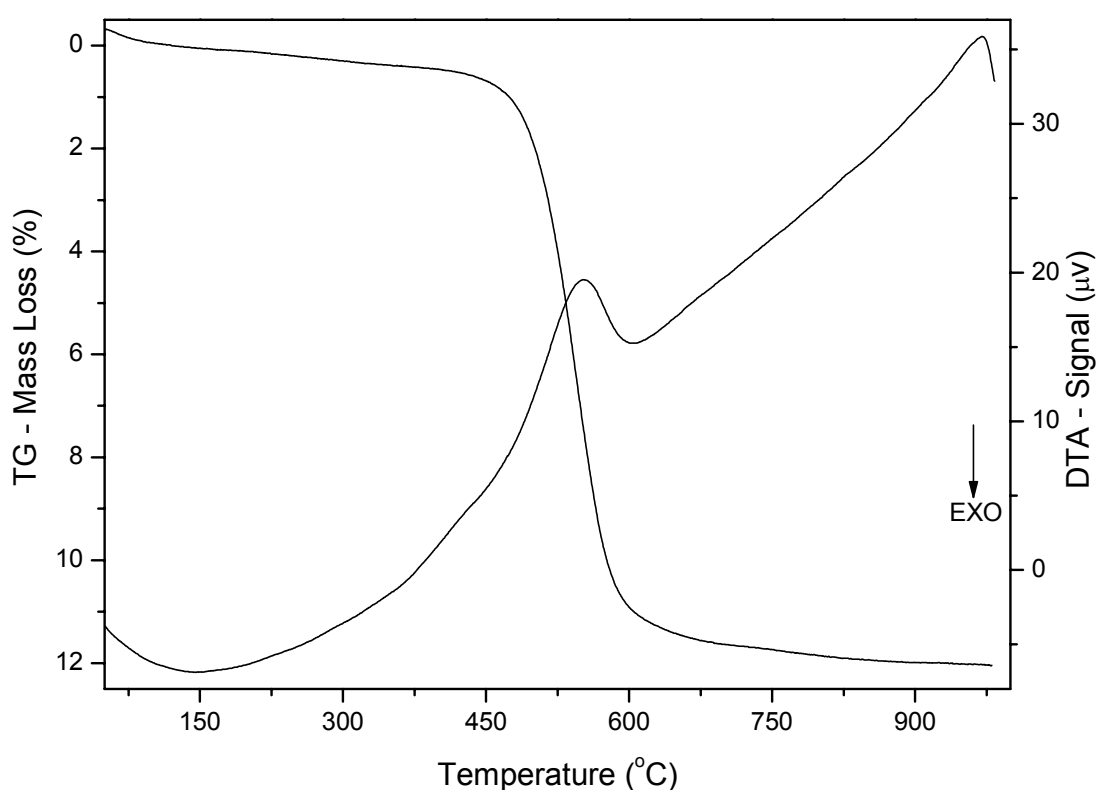


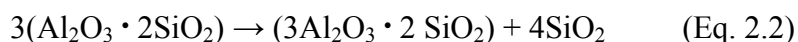
Fig. 2.1: TG/DTA curves of raw kaolinite (SPS kaolinite from Cornwall, UK).

Infrared emission spectroscopy (IES) studies of the dehydroxylation of kaolinite suggested that two different mechanisms are involved in the process (Frost and Vassallo,

1996). This may indicate that homogeneous and heterogeneous mechanisms occur simultaneously, but a final elucidation of the mechanism was not yet described. The IES results also showed that the dehydroxylation mechanisms are different for kaolinite, halloysite and dickite.

Diffusion of the formed water molecules certainly plays an important role in the dehydroxylation process. Kaolinite samples of different crystallinities and particle sizes differ in their thermal behavior, with smaller and poorly crystallized samples leading to lower dehydroxylation temperatures. However, the rate controlling step of the dehydroxylation reaction is, most likely, not the diffusion of water but the removal of the accumulated water from the surfaces of the particles (Brindley and Lemaitre, 1987).

The first thermal phenomenon of the high temperature region is observed in DTA curves (Fig. 2.1) as a slight endothermic event immediately followed by an exothermic peak, around 950-975°C. In poorly crystalline kaolinites, the exothermic peak is broadened and occurs at lower temperatures, around 940 °C (Jasmund and Lagaly, 1993). The exact identity of these transformations is still unclear. It has been attributed to many different reactions including recrystallization of γ -alumina, nucleation of mullite, recrystallization of a mixed Si-Al spinel, or recrystallization of silica into high-quartz (Delmon *et al.*, 1978). The exothermic formation of mullite and cristobalite occurs at 1000-1100 °C, but there is still unclear which phase or phases are present between 950 °C and 1100 °C. In any case, these reactions are topotactic and lead to the formation of free silica, according to the equation:



Around 1450 °C the exothermic crystallization of cristobalite is observed. Finally, around 1750 °C the system melts.

Oxidation reactions are usually not observed in raw kaolinite, which does not present variable-valence cations, except for traces of isomorphically substituted iron ions.

2.3 X-Ray Diffraction

As of all clay minerals and any other layer compounds, the X-ray diffraction is possibly the most characteristic and widely used characterization method. Many structural and morphological characteristics of kaolinite can be directly or indirectly deduced from its XRPD patterns, including, but not being restricted to crystallinity (degree of stacking disorder), presence of other polytypes and/or spurious crystalline contaminants and average particle size. In addition, the determination of the basal spacing of the sample is of highest importance when studying intercalation reactions.

Due to the broad spectrum of applications and the large volume of specialized publication on X-ray diffraction of clay minerals and kaolinite, just some of the most basic characteristics of this clay mineral are introduced and briefly discussed here.

The diffraction pattern of kaolinite is characterized by the strong basal reflections, which present much higher intensities than the non-basal reflections in any sample that is not prepared with extreme care to avoid preferential orientation of the particles. As the majority of the reactions commonly studied involving kaolinite do not alter its structure, but can change the basal spacing by intercalation, the basal reflections are the only ones that have real importance in such systems.

Fig. 2.2 shows the X-ray diffraction pattern of a well-crystallized kaolinite from Cornwall (UK). This sample was prepared by slow evaporation of an aqueous dispersion of kaolinite, in such a way that the particles could orient themselves with the basal planes parallel to the surface of the sample-holder. This texture effect is clearly observed by the extremely higher intensity of the basal reflections in relation to the non-basal ones, as above discussed.

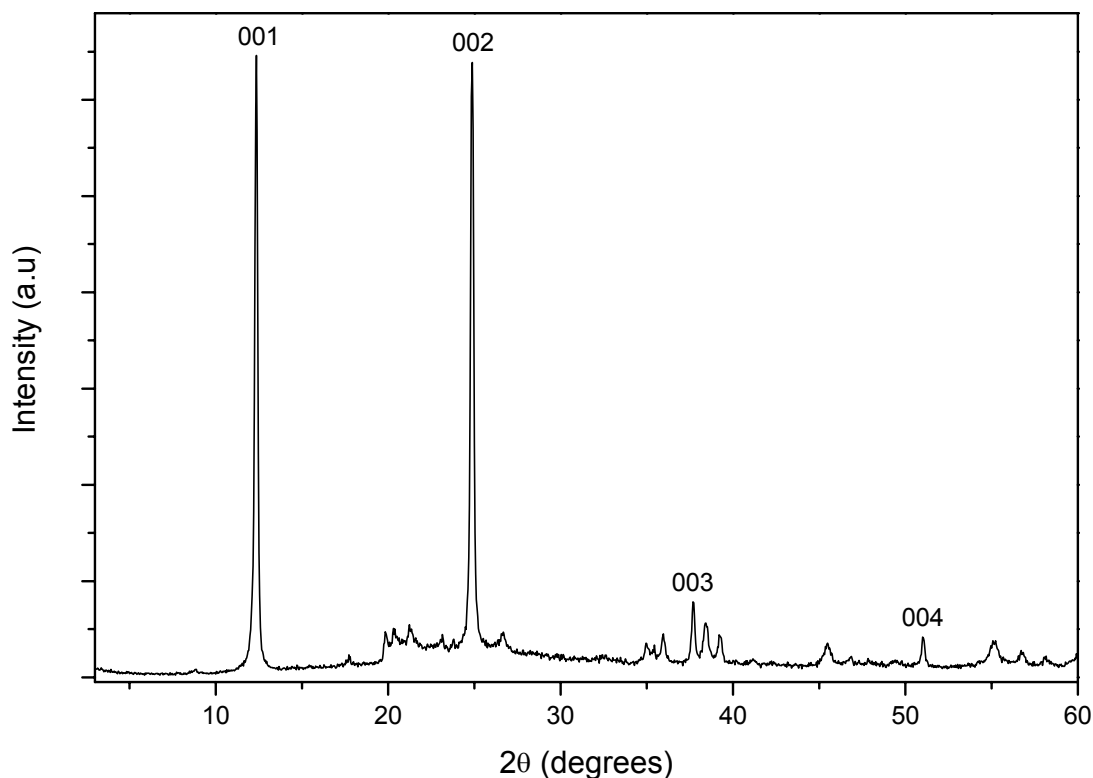


Fig. 2.2: XRPD pattern of the SPS kaolinite from Cornwall, UK.

Table 2.1 presents the main $d_{(hkl)}$ values of a randomly oriented well-crystallized kaolinite sample as well as the relative intensity of the reflections and their indexing. The comparison of these values with an unknown sample is a useful method to differentiate samples possibly constituted of the polytypes kaolinite, dickite and nacrite (Grim, 1968).

The (006) reflection is usually used to distinguish between di-octahedral kaolins and tri-octahedral serpentines, since this reflection appears at 1.49 Å in kaolins and at 1.54 Å in serpentines (Jasmund and Lagaly, 1993).

Table 2.1: Observed XRPD data for randomly oriented kaolinite: interplanar spacing (d), relative intensity (I) and indices (hkl), until the 004 reflection ($2\theta \sim 51.2^\circ$, $\text{CuK}\alpha$). Adapted from Bailey, 1984.

d (Å)	I	hkl	d (Å)	I	hkl
7.16	10+	001	2.379	6	003
4.46	4	020	2.338	9	$20\bar{2} + 1\bar{3}1$
4.36	5	$1\bar{1}0$	2.228	8	131
4.18	5	$11\bar{1}$	2.247	2	$13\bar{2}$
4.13	3	$1\bar{1}\bar{1}$	2.186	3	201
3.845	4	$02\bar{1}$	2.131	3	$02\bar{3}$
3.741	2	021	2.061	2	$2\bar{2}\bar{2}$
3.573	10+	002	1.989	6	$20\bar{3} + 1\bar{3}2$
3.372	4	111	1.939	4	132
3.144	3	$11\bar{2}$	1.896	3	$13\bar{3}$
3.097	3	$1\bar{1}\bar{2}$	1.869	2	042
2.753	3	022	1.839	4	$1\bar{3}\bar{3} + 202$
2.558	6	$1\bar{3}0 + 20\bar{1}$	1.809	2	$11\bar{4} + 2\bar{2}\bar{3}$
2.526	4	$13\bar{1}$	1.781	4	004
2.491	8	$1\bar{3}\bar{1} + 200$			

Fig. 2.3 presents the XRPD patterns for three kaolinite samples with different degrees of crystallinity. The transition from well-crystallized to poorly crystallized structures is observed as a broadening and weakening of the reflections with the complete elimination of the weaker ones. There is a tendency for adjacent reflections to collapse into non-resolved broadened reflections. The basal reflection also increases from 7.16 Å to 7.20 Å in very poorly crystallized samples. The group of reflections from (020) to (002) particularly reflects the change to lower crystallinity. In this region the clearly resolved doublet ($11\bar{1}$) and ($1\bar{1}\bar{1}$) of well-crystallized material yields a single broadened reflection, a good evidence for the decrease in crystallinity (Grim, 1968).

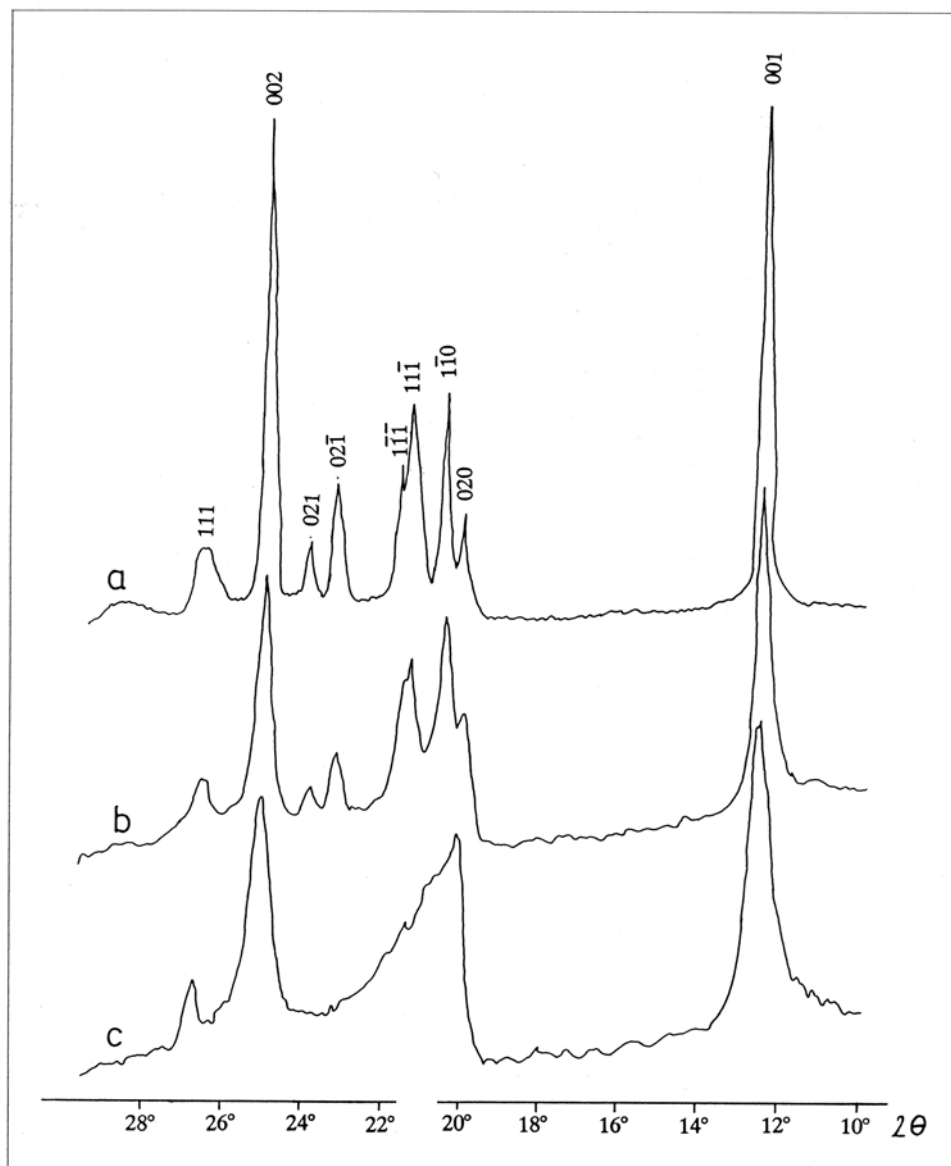


Fig. 2.3: XRPD patterns of kaolinites with different degrees of crystalline order: (a) kaolinite from Keokuk geodes, Iowa, USA; (b) kaolinite from the main bed at the Rohrhof mine near Maxhütte, Germany; (c) poorly crystallized kaolinite from the bed 13 at the Rohrhof mine. Adapted from Jasmund and Lagaly, 1993

Because of the importance of estimating, even in a relative sense, the degree of disorder of a given kaolinite, empirical relations have been used. The most widely used relation for the kaolin minerals is that proposed by Hinckley (1963), and termed the “crystallinity index” (nowadays commonly referred as “Hinckley index”). This index is the ratio of (i) the sum of the heights of the reflections $(1\bar{1}0)$ and $(11\bar{1})$ measured from the inter-peak background, and (ii) the height of the $(1\bar{1}0)$ reflection measured from the general

background (Fig. 2.4). The justification for this rather arbitrary procedure was that as the crystallinity decreased, the proportion of random shifts between adjacent layers by $\pm nb_0/3$ increased, resulting in a decrease in resolution of neighboring reflections and an increase in the inter-peak diffraction intensity. At the same time, an increase in the frequency of defects would decrease the absolute intensity of the $(1\bar{1}0)$ reflection. The algebraic combination of these two estimates yields a dimensionless number which normally varies between 0.2 and 1.5; the larger the value of the index (H_i), the greater the crystallinity (Plaçon *et al.*, 1988).

H_i has two main virtues: the procedure requires only a normal XRPD scan from a reasonably unoriented sample, and the calculation is very simple. In addition, the ability to rank kaolinites according to changes in their XRPD patterns is useful. However, due to the complexity of the defects and stacking faults occurring in kaolinites, it cannot be explained what H_i in fact measures (Plaçon *et al.*, 1988).

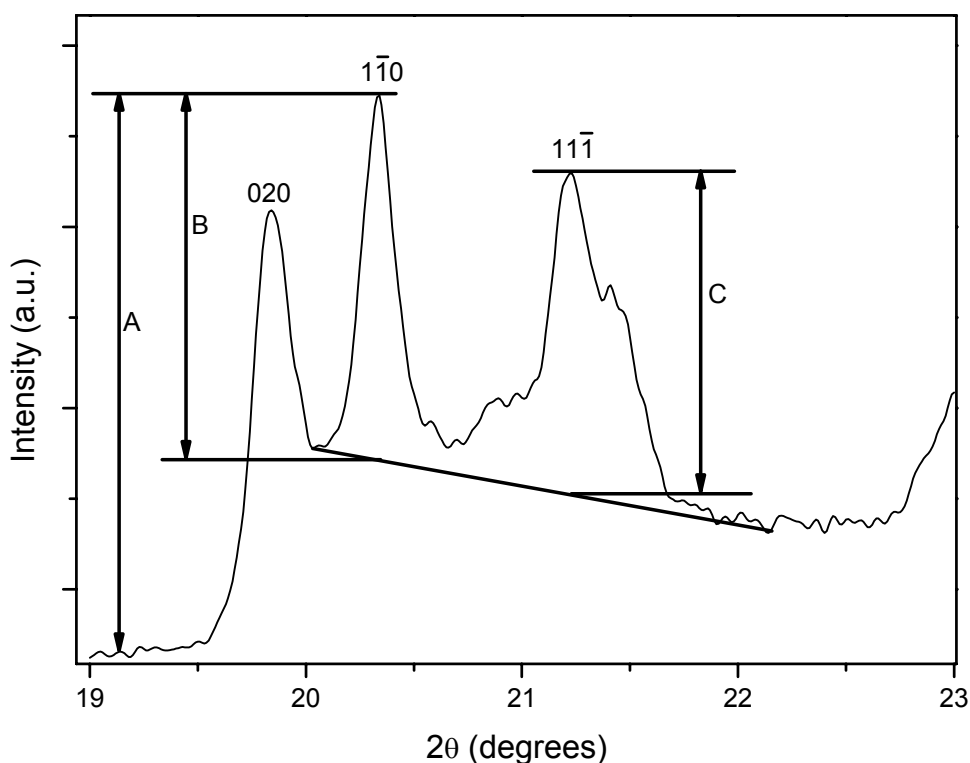


Fig. 2.4: Calculation of the Hinckley crystallinity index for kaolinite: $H_i = \frac{B+C}{A}$.

Many other methods for the quantitative evaluation of disorder in the crystalline structure of kaolinite had been proposed (Brindley, 1984), but for reasons above cited H_i is still vastly used to roughly categorize a kaolinite sample. Among these other methods, one could cite the Stoch index, which relates the intensities of the (020) and (1 $\bar{1}$ 0) reflections or the Aparicio-Galán-Ferrell index, which relates the intensities of the (020), (1 $\bar{1}$ 0) and (11 $\bar{1}$) reflections as obtained by a mathematic fitting of the XRPD pattern (Aparicio *et al.* 2004). All these three indices are based almost on the same reflections but the H_i is influenced by the presence of quartz, feldspar, iron hydroxide gels, illite, smectite and halloysite. On the other hand, the Stoch index can be used in the presence of quartz, feldspar and amorphous silica and iron hydroxides, but not in the presence of other phyllosilicates. Finally, the Aparicio-Galán-Ferrel index is less influenced by associated minerals and amorphous phases than the Hinckley and Stoch indices (Aparicio *et al.*, 2004).

2.4 FTIR Spectroscopy

The FTIR analysis of kaolinite (and other clay minerals) can provide important insights not only on the structure and interactions between the composing atoms of the mineral, but also on the interaction with guest species, presence of adsorbed water and/or other mineral species, particle size and orientation as well as the degree of crystalline order (Jasmund and Lagaly, 1993; Russell and Fraser, 1994).

The MIR (from 4000 cm^{-1} to 400 cm^{-1}) absorption spectrum of kaolinite presents many characteristic bands, which can be divided in two main groups: hydroxyl stretching bands in the high frequency region and skeletal (lattice) bands in the low frequency region, also including the hydroxyl deformation bands. Fig. 2.5 shows the FTIR spectrum of kaolinite between 4000 cm^{-1} and 400 cm^{-1} , presenting the identification of the bands.

The assignment of the MIR absorption bands of kaolinite is still not completely settled. Some of the bands can be unambiguously attributed to specific vibrational modes, other bands however, are assigned to different modes according to different authors. A detailed description of these bands is later provided, taking into account the most common assignments. Table 2.2 presents a concise description of the assignments of the bands on the FTIR spectrum according to various sources.

The hydroxyl stretching region is characterized by the presence of two major bands at 3695 cm^{-1} and $3620\text{ cm}^{-1\dagger}$. Two other bands with weak intensity are also observed at 3669 cm^{-1} and 3652 cm^{-1} . There are no divergences in the literature about the identity of these bands. The three most energetic ones (3695 , 3669 and 3652 cm^{-1}) are attributed to stretching of the inner-surface hydroxyl groups, while the band on 3620 cm^{-1} is attributed to the stretching of the inner hydroxyl (Frost *et al.*, 1993; Frost and Vassallo, 1996; Johansson *et al.*, 1998; Michaelian *et al.*, 1998; Bougeard *et al.*, 2000 and Balan *et al.*, 2001). Using *ab initio* quantum mechanical computations of the theoretical spectrum of kaolinite, Balan *et al.* (2001) were able to assign the 3695 cm^{-1} band to the in-phase stretching of the three inner-surface hydroxyl groups and the 3669 cm^{-1} and 3652 cm^{-1} bands to the anti-phase stretching modes of these hydroxyl groups, in agreement with the assignment done by Farmer (1974).

[†] The values for the band absorption centers here presented are relative to the SPS kaolinite from Cornwall, measured as described in Appendix I. However, these values show very little variation from the standard values usually presented in the literature so that all bands can be correlated to the literature values without any problem.

Shoval *et al.* (1999) showed by curve fitting that a fifth hydroxyl stretching band is present in the MIR spectrum of kaolinite. This band, located at $3688\text{--}3689\text{ cm}^{-1}$, is easily identifiable in the Raman spectrum of kaolinite, but is hidden in the FTIR spectrum by the 3695 cm^{-1} band, being identified only by curve fitting methods. Neither of the computer simulation studies of the theoretical spectrum of kaolinite by Bougeard *et al.* (2000) and Balan *et al.* (2001) predicted this band, but both could reproduce the positions and intensities of the experimental bands with great accuracy.

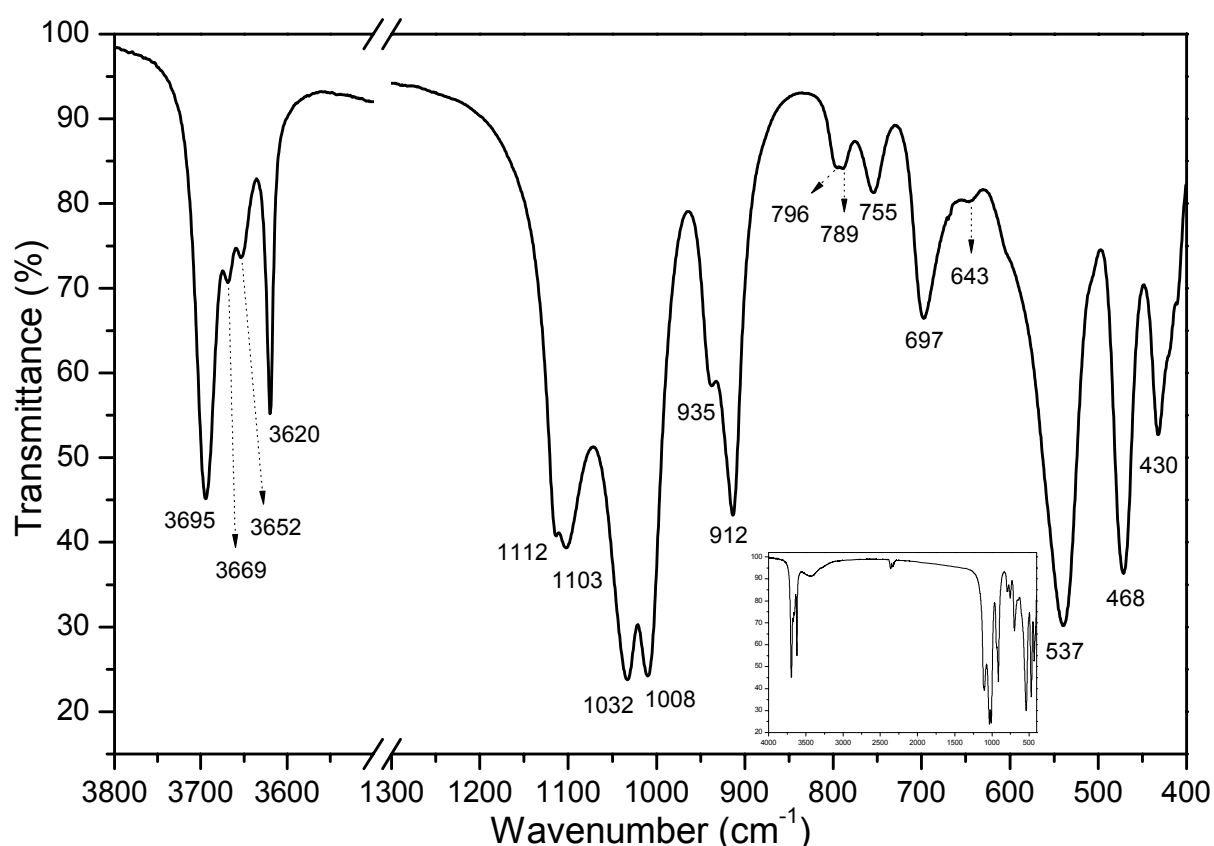


Fig. 2.5: FTIR spectrum of kaolinite (SPS kaolinite from Cornwall, UK) showing the hydroxyl stretching region ($3800\text{--}3500\text{ cm}^{-1}$) and the skeletal (lattice) bands region ($1300\text{--}400\text{ cm}^{-1}$). Inset shows the whole spectrum from 4000 cm^{-1} to 400 cm^{-1} .

The next four bands in the spectrum of kaolinite (1112 cm^{-1} , 1103 cm^{-1} , 1032 cm^{-1} and 1008 cm^{-1}) also have a consensual assignment by the different literature sources. These are the most intense Si-O stretching modes, and can be observed in most of the silicate minerals (Farmer, 1974). Balan *et al.* (2001) assigned the 1112 cm^{-1} band to the symmetric stretching of

the equatorial Si-O bonds, while the anti-symmetric stretching of these groups are assigned to the bands at 1032 cm^{-1} and 1008 cm^{-1} . The band at 1103 cm^{-1} is attributed to the in-phase stretching of apical Si-O bonds. These theoretical results are also in agreement with the assignment proposed by Farmer (1974). Johansson *et al.* (1998) attributed the 1034 cm^{-1} (1032 cm^{-1}) band to a Si-O-Si stretching mode (ν_3 (f_2) mode of the SiO_4 tetrahedron).

The bands at 935 cm^{-1} and 912 cm^{-1} are not due to any lattice vibrations, but are consensually attributed to hydroxyl vibration modes. Most sources assign these bands to the deformation of the Al-OH bonds, in a movement sometimes called “hydroxyl libration”¹. The band at 935 cm^{-1} is derived from the inner-surface hydroxyl groups, while the band at 912 cm^{-1} is caused by the inner hydroxyls. Bougeard *et al.* (2000) attributed these bands to the in-plane bending modes of the hydroxyl groups. It is not completely clear if the authors meant the same movement described elsewhere as deformation or libration.

As the frequency decreases, the assignment of the remaining bands on the kaolinite FTIR spectrum becomes more difficult and different sources attribute different origins for most of the bands. This is mostly due to the fact that these bands can be composed of the vibrational modes of different groups, with coupling of vibrations from tetrahedral and octahedral sheets being common (Farmer, 1974; Bougeard *et al.*, 2000).

The bands at 796 cm^{-1} and 789 cm^{-1} are not always detected separately, and as consequence, sometimes only one band is described in this region. Frost *et al.* (1993) identifies only a band at 795 cm^{-1} and assigns it to a hydroxyl translation mode. The theoretical computation of the FTIR spectrum performed by Bougeard *et al.* (2000) predicted a band at 788 cm^{-1} and assigned it to a Si translation mode.

The bands at 755 cm^{-1} and 697 cm^{-1} were assigned to Si-O stretching modes by Bougeard *et al.* (2000) and to AlO-H deformations by Michaelian *et al.* (1998). Frost and coworkers first attributed these bands to OH bending vibrations (Frost *et al.*, 1993) but latter on only the band at 754 cm^{-1} (755 cm^{-1}) was described, and assigned to a Si-O-Al translation mode (Johansson *et al.*, 1998).

The very weak band at 643 cm^{-1} is not always cited, Johansson *et al.* (1998) assigned this band to another Si-O-Al translation mode, while Bougeard *et al.* (2000) attributed the same band to a Al-O stretching mode.

¹ Loh (1973) defined the hydroxyl libration as “the motion of the OH ion such that the proton remains parallel to the cleavage or moves away from it”.

Table 2.2: Proposed assignments of the kaolinite IR absorption bands between 4000 cm^{-1} and 400 cm^{-1} , according to Frost *et al.* (1993); Frost and Vassallo (1996); Johansson *et al.* (1998); Michaelian *et al.* (1998); Bougeard *et al.* (2000) and Balan *et al.* (2001). The bands with different assignments depending on the author are indicated with the respective source.

Band center (cm^{-1})	Probable assignment
3695	inner-surface OH in-phase stretching
3669	inner-surface OH anti-phase stretching
3652	
3620	inner OH stretching
1112	equatorial Si-O bond symmetric stretching
1103	apical Si-O bond in-phase stretching
1032	equatorial Si-O bond anti-symmetric stretching
1008	
935	inner-surface OH in-plane bending ^a inner-surface Al-OH libration/deformation ^{b,c}
912	inner OH in-plane bending ^a inner Al-OH libration/deformation ^{b,c,d}
796	Si translation ^a
789	OH translation ^{b,d}
755	Si-O stretching ^a OH translation ^{b,d} Al-OH deformation ^c Si-O-Al translation ^d
697	Si-O stretching ^a OH translation ^b Al-OH deformation ^c
643	Al-O stretching ^a Si-O-Al translation ^d
537	O-Si-O/O-Al-O bending + Al-O/Si-O stretching ^a Si-O-Al deformation ^b Al-O deformation ^c Si-O-Si stretching ^d
468	O-Si-O/O-Al-O bending + Al-O/Si-O stretching ^a Si-O bending ^b / deformation ^c Si-O-Si stretching ^d
430	O-Al-O bending (small contribution of O-Si-O bending) ^a Si-O deformation ^c Si-O-Si stretching ^d

^a Bougeard *et al.*, 2000.

^b Frost *et al.*, 1993; Frost and Vassallo, 1996.

^c Michaelian *et al.*, 1998.

^d Johansson *et al.*, 1998.

The 537 cm^{-1} band has been attributed to most different vibrations, Frost and coworkers initially attributed a band at 540 cm^{-1} to Si-O-Al deformation (Frost *et al.*, 1993) but latter on described a band at 553 cm^{-1} (detected by DRIFT) assigned to Si-O-Si stretching

(ν_4 (f_2) mode of the SiO_4 tetrahedron) latter on (Johansson *et al.*, 1998). Michaelian *et al.* (1998) assigned a band at 552 cm^{-1} to a Al-O deformation, while Bougeard *et al.* (2000) predicted a band at 538 assigned to O-Si-O/O-Al-O bending plus a contribution of Si-O/Al-O stretching.

Frost *et al.* (1993) assigns the 468 cm^{-1} and 430 cm^{-1} bands to ν_6 (e) and ν_3 (a_1) modes of the SiO_4 tetrahedra. Latter on these bands were assigned to ν_4 (f_2) and ν_4 (e) modes of Si-O-Si bonds on the SiO_4 tetrahedra (Johansson *et al.*, 1998). Michaelian *et al.* (1998) attributed these bands to a Si-O deformation. Bougerad *et al.* (2000) predicted bands at 488 cm^{-1} and 430 cm^{-1} . The band at 488 cm^{-1} was attributed to O-Al-O and/or O-Si-O bending plus a contribution of Al-O and/or Si-O stretching. The band at 430 cm^{-1} was attributed to a O-Al-O bending with minor contribution of O-Si-O bending.

Adsorbed water is almost always present in kaolinite and is observed in the FTIR spectrum as a strong broadened OH stretching band around 3435 cm^{-1} and as a OH bending band of medium intensity around 1630 cm^{-1} (van der Marel and Beutelspacher, 1976).

Crystalline disorder in kaolinite is detectable mainly in the hydroxyl-stretching region, although some general broadening of all bands in the spectrum may also occur. Whereas the 3695 cm^{-1} and 3620 cm^{-1} bands remain essentially unchanged, the 3669 cm^{-1} and 3652 cm^{-1} doublet is replaced by a single broad band at 3653 cm^{-1} in disordered kaolinites (Russel and Fraser, 1994). The intensity ratio of the hydroxyl stretching bands is affected not only by the crystallinity, but also by the particle size, orientation of the particles and incidence angle of the IR beam (Jasmund and Lagaly, 1993).

Isomorphic substitution of Al by Fe in the kaolinite structure can cause the appearance of a small inflexion at 3600 cm^{-1} and a weak band near 880 cm^{-1} , corresponding to the stretching and bending modes of the Fe-OH bonds (Russel and Fraser, 1994).

To avoid perturbations due to Christiansen-Effect in oriented kaolinite samples, the equivalent spherical diameter of the particles should be below $1\text{ }\mu\text{m}$. In samples with very small particle sizes, the particles below $0.2\text{ }\mu\text{m}$ size should be discarded, in order to diminish the intensity of the adsorbed water bands. Consequently, size fractions from $0.2\text{-}0.5\text{ }\mu\text{m}$ and $0.5\text{-}1.0\text{ }\mu\text{m}$ provide the optimal FTIR spectra (Jasmund and Lagaly, 1993).

2.5 Surface Reactions and Phenomena

One of the most important surface properties of kaolinite is its surface charge. It has a major influence on the type and magnitude of the interparticle interactions, the cation exchange capacity of the material, the adsorption behavior and on eventual catalytic properties of the particles. A brief introduction to these subjects is presented.

The surface of kaolinite particles is also a reactive site for topotactic reactions with organic or inorganic molecules, forming derivatives that can present some interesting characteristics. These surface modifications are also briefly discussed.

2.5.1 Surface Charge and Cation Exchange

It has been long accepted that the surface charges in kaolinite particles may have two different origins: (i) negative charges from isomorphous substitution of Si^{4+} by Al^{3+} in the tetrahedral sheets and, (ii) pH dependent charges arising from protonation/deprotonation of aluminol and silanol groups located on the lateral edges of the particles (Bolland *et al.*, 1976; Jasmund and Lagaly, 1993).

However, based on the consideration of surface charge density, Zhou and Gunther (1992) noted that the ionization of edges alone could not explain the magnitude of the changes in the cation exchange capacity (CEC) of kaolinite with the pH. Thus, they concluded that the basal surfaces should also contribute to these charges. The charges on the basal surfaces would be always negative but the magnitude would be pH dependent. This result would imply that the basal surfaces of kaolinite are ionizable in aqueous solutions. These results were later confirmed by CEC studies by Ma and Eggleton (1999).

Brady *et al.* (1996) showed, based on computational modeling of the kaolinite surface charges and on morphological data from SFM, that the edge site contribution to the total kaolinite surface area is higher than so far accepted (from 10 to 50 % of edge area) and that no basal plane participation is required to explain the total surface charge of kaolinite. These results are in opposition to what was discussed above, but attested by other results (on the hydrophobicity of kaolinite surfaces, or the lower reactivity of basal aluminol groups in comparison to edge aluminols, for example).

There is still no universally accepted explanation for which group(s) controls pH-dependent charged sites on kaolinite. It may even be the case that for different kaolinites, the

predominant charged site(s) varies with bulk composition or defect structure (Brady *et al.*, 1996).

The cation exchange capacity (CEC) of kaolinite is essentially a function of its surface charge, among other minor factors. Typical experimental CEC values for kaolinites are found between 0.01 and 0.1 meq/g (Jasmund and Lagaly, 1993). This variation is a function of many factors, including the origin of the sample, particle size, amount of crystalline defects and pre-treatment of the sample (the factors that usually influence the surface charge of the mineral) but also of the method used to determine the CEC value. For comparison, montmorillonites have experimental CEC values between 0.7 and 1.2 meq/g and vermiculites between 1.30 and 2.10 meq/g (Jasmund and Lagaly, 1993).

2.5.2 Adsorption

Kaolinite is able to adsorb a great variety of organic and inorganic species (physisorption, chemisorption and ionic exchange with cationic species), however, not so efficiently as other clay minerals with higher surface area, charge and CEC values like the smectites. Due to its high availability and lower cost in comparison to other clay minerals (see Chapter 1), it can be largely used for industrial purposes, like for water treatment facilities, for example (Santos, 1989). A few other notable examples of the importance of the study of the adsorption of substances on kaolinite are shown by the next examples. Adsorption of inorganic cations to kaolinite has been studied also with the aim to control and immobilize toxic or radioactive wastes (Tarasevich and Klimova, 2001; Osmanlioglu, 2002). The adsorption and immobilization of enzymes on kaolinite, for biocatalytic purposes has been also described (Basyaruddin *et al.*, 2005). Adsorption on kaolinite and other clay minerals also play an important role in the soil science either in the obtention of new pesticide formulations or in the understanding of the interactions of fertilizers and pesticides with the clay fraction of the soil (Lagaly, 2001).

One of the most studied and promising applications of adsorption on kaolinite is, however, the synthesis of nanocomposites between organic polymers and kaolinite (Lagaly, 1999; LeBaron *et al.*, 1999; Gardolinski *et al.*, 2000; Gardolinski, 2001). The improvement of the mechanical, thermal and chemical properties of polymers by addition of small quantities of mineral charges is known since many years. However, the possibility to obtain

nanocomposites with optimized properties can be achieved only with a deep understanding of the interactions between the organic phase and the clay mineral surfaces. Chemical modification of the clay external surfaces, intercalation of the polymer matrix and partial delamination can lead to an even greater interaction between the phases (LeBaron *et al.*, 1999; Gardolinski, 2001).

The understanding of the adsorption and interactions of kaolinite with surface active agents and polymers is also of great importance in the processing of the raw mineral in the mining plants and during other industrial processes (Besra *et al.*, 2002).

Adsorption/desorption of water to/from kaolinite surfaces is briefly discussed in section 2.2.

2.5.3 Topotactic Reactions at the External Surfaces (*Surface Grafting*)

As discussed above, one of the possible ways to modify chemically the external kaolinite surfaces is ionic exchange with polyatomic cations, building ionic bonds between the cation and the clay surface. In addition, it is also possible to modify the external surfaces of kaolinite by the reacting appropriate molecules with the silanol or aluminol groups present at the edges and basal surfaces of the particles, with the formation of covalent bonds between the clay mineral surface and the reacting molecules. This process is also called “surface grafting”. Grafting at the interlayer surfaces of kaolinite is discussed at section 2.7.2.

Various different surface grafting reactions of kaolinite were already discussed. Most of them occur with the silanol and aluminol groups at the edges of the particles, as these are more reactive than the exposed aluminol groups of the octahedral basal surface (Brady *et al.*, 1996). Some of the molecules found to react with kaolinite with the formation of grafted derivatives are:

- Diazomethane: formation of methyl kaolinite (Santos, 1989).
- Carboxylic acid chlorides: formation of acetyl and benzoyl kaolinite (Santos, 1989).
- Thionyl Chloride: formation of kaolinite chloride (Fedoseev and Kucharskaja, 1963; Santos, 1989). This compound can react further with other substances producing new derivatives:

- ◇ benzene- AlCl_3 : formation of phenyl kaolinite in a Friedel-Craft reaction (Santos, 1989).
- ◇ phenyl-magnesium bromide: formation phenyl kaolinite with the Grignard reagent (Fedoseev and Kucharskaja, 1963; Santos, 1989).
- Phenylbenzene and benzylbenzene: reaction with ultra-sound energy input, formation of phenylphenoxy- and benzylphenoxy-kaolinite (Fedoseev and Kucharskaja, 1963).
- Ethylpolysiloxane: reaction with ultra-sound energy input, formation of ethylpolysiloxyl kaolinite, a strongly hydrophobic derivative (Fedoseev and Kucharskaja, 1963).
- Chlorosilanes: the most common surface grafting reactions of kaolinite. Formation of $(\text{Si-O})\text{-Si-R}_3$ or $(\text{Al-O})\text{-Si-R}_3$ bonds (Santos, 1989; Braggs *et al.*, 1994)

Chlorosilane derivatives of kaolinite were shown to form nanocomposite with various organic polymers presenting improved mechanical properties in contrast to nanocomposites obtained from unmodified kaolinite (Domka *et al.*, 2002; 2003; Buggy *et al.*, 2005). Electrochemical and rheological properties of a chlorodimethyl octadecylsilane derivative of kaolinite were also discussed (Braggs *et al.*, 1994). These authors proposed that such derivatives might have an industrial importance, as there was an insignificant change in the flocculation behavior of silanized kaolinite dispersions with the variation of the pH value. Silanized kaolinites were also studied as support for anionic Fe(III)-porphyrins used as catalyst for oxidation reactions (Nakagaki *et al.*, 2004). The effects of calcination of kaolinite prior to silanization (silanization of metakaolinite) have also been discussed (Price and Ansari, 2003).

2.6 Topotactic Interlayer Reactions

The topotactic interlayer reactions comprise two processes, with the same basic principle: intercalation and grafting. Intercalation reactions in kaolinite are known since the beginning of the 1960's and are still much studied. A short historical review on these reactions is presented, and some chemical aspects of the intercalation phenomenon in kaolinite are briefly discussed.

The first examples of interlayer functionalization (grafting) on kaolinite were described in 1993. Until now not much attention has been directed to this theme, indicated by the few publications of two or three different research groups around the world. As the main objective of this work consisted on the synthesis of new grafted kaolinite derivatives, a more in-depth discussion of the results published so far is presented.

2.6.1 Intercalation

2.6.1.1 Historic development

The first example of an intercalation reaction on a layered matrix was given by Ulrich Hofmann and Alfred Frenzel in 1930 and dealt with the reaction of graphite with concentrated sulfuric and nitric acids (proton intercalation) (Hofmann and Frenzel, 1930). Although these reactions were not new, it was the first time that the basal expansion of the matrix was described. It did not take long to unveil that clay minerals were also prone to "Innerkristalline Quellung" (inner-crystalline swelling). Hofmann *et al.* (1933) showed that montmorillonite could be intercalated with water, affecting its basal spacing, as detected by X-ray diffractometry.

Kaolinite was, after these discoveries, for long time considered as non-expandable clay, as no intercalation reaction could be achieved. The only kaolin mineral already known to intercalate other molecules was halloysite. Gastuche *et al.* (1954) tried to break the interlayer hydrogen bonds of kaolinite by reaction with proton acceptors (nitrobenzene and nitromethane). Although the treated samples showed a small degree of rolling of the borders of the thinner particles, no modification of the basal spacing of kaolinite was obtained with nitromethane. Curiously, the reaction with nitrobenzene yielded a product with basal spacing of 7.7 Å (and some curling of the particle borders). However, this expansion of 0.55 Å could

not be explained by the intercalation of the organic molecule. The authors also described that ethylene glycol was unable to intercalate into these modified kaolinites. In this way, kaolinite continued to be generally regarded as a non-expandable clay mineral, what was also contributed by the fact that this pioneer work was unfortunately completely forgotten by the scientific community.

This situation changed completely in 1961, when Koji Wada, from the Kyushu University in Fukuoka (Japan) published a paper on the intercalation of potassium acetate on kaolinite. Dry or wet grinding of kaolinite (and halloysite) with potassium acetate caused the expansion of the basal spacing of the clay mineral from 7.1 Å to 14.2 Å (Wada, 1961). By heating the intercalation compound to 100 °C the basal spacing contracted to 11.4 Å, showing that a monolayer of water was co-intercalated in the 14.2 Å phase. The author also comments that grinding of kaolinite with ammonium chloride produced a poorly crystalline phase with a basal spacing around 10 Å. Washing the potassium acetate intercalate with an aqueous solution of ammonium chloride formed the ammonium chloride intercalation compound, with a much higher crystallinity than the phase obtained by grinding. Curiously, Andrew *et al.* (1960) reported the intercalation of potassium acetate in kaolinite (and dickite) prior to the publication of Wada. However, they cited Wada's article of 1961 as "in press", in such a way that the credit of the first report must go to the second published paper on the issue. These authors also reported that by washing the potassium acetate intercalate with concentrated aqueous solutions of some salts, other intercalation compounds were obtained. These were: ammonium acetate ($d_L = 14.2$ Å), potassium carbonate ($d_L = 13.6$ Å), ammonium nitrate ($d_L = 11.5-11.6$ Å) ammonium chloride ($d_L = 10.2$ Å) and potassium chloride ($d_L = 9.9$ Å). The intercalation method was improved by the overnight resting of the pre-ground mixture, thus obtaining products with much less crystalline disorder than using the method described by Wada (1961).

Working independently of Wada, and without knowledge of his research, Armin Weiss (former PhD student of U. Hofmann in Darmstadt) at the University of Heidelberg, latter on in Munich (Germany), published his results on the intercalation of urea on kaolinite in the same year as Wada (1961). The basal spacing of the mineral was shown to expand from 7.16 Å to 10.68 Å after reacting with a saturated aqueous solution of urea or with the melted substance (Weiss, 1961). After washing the urea-kaolinite compound, Weiss reported that the basal spacing would not return to the original 7.16 Å, instead a phase with basal spacing

around 8.3 Å would be formed¹. In the same publication, Weiss commented that besides urea, other amides such as formamide, acetamide, chloroacetamide and thiourea were intercalated. He did not provide, however, any data on those compounds at that point. In another study, Weiss (1963) commented that urea-kaolinite was found in a clay mineral accumulation between the cracks of a granite formation under an old animal barn in Bayern (Germany). The kaolinite formed by the weathering of the granite matrix had been naturally intercalated with the urea that percolated the soil coming from the decade-long accumulating animal feces on the surface.

Latter on, Weiss and coworkers described the intercalation of hydrazine hydrate on kaolinite, forming of a phase with $d_L = 10.41$ Å (Weiss *et al.*, 1963a). Kinetic and thermodynamic studies of the intercalation with hydrazine were described. It was also observed that smaller kaolinite particles intercalate much more slowly than larger particles, and sometimes were not able to react completely (until a intercalation ratio of 100 %).

Also in 1963, Weiss and coworkers discussed the intercalation of kaolinite with many other molecules. The molecules that could intercalate directly into the raw mineral were divided into two groups: those that build strong hydrogen bonds like hydrazine and formamide, and the alkali and ammonium salts of small carboxylic acids like potassium, rubidium and cesium acetates and potassium propionate (Weiss *et al.*, 1963b). They also described the intercalation of molecules that would not intercalate directly in raw kaolinite. These molecules could be intercalated either by simultaneous reaction with a carrier (Schlepper) like hydrazine or by the reaction of an intercalation compound with the other substance, in a displacement reaction (Verdrängung). The new molecules which could be intercalated directly (by reaction with the saturated aqueous solutions) described in this publication were: acetamide ($d_L = 10.92$ Å), cesium acetate ($d_L = 14.68$ Å), rubidium acetate ($d_L = 14.42$ Å), ammonium acetate (14.05 Å and 17.15 Å), potassium propionate ($d_L = 14.01$ Å) and potassium cyanoacetate ($d_L = 12.98$ Å). With hydrazine as carrier, the following molecules could be intercalated: potassium glycinate ($d_L = 12.44$ Å or 15.6 Å, text unclear!), potassium oxalate ($d_L = 10.28$ Å), potassium alaninate ($d_L = 12.45$ Å), potassium lysinate ($d_L = 14.88$ Å), potassium lactate ($d_L = 11.18$ Å), sodium acetate ($d_L = 10.06$ Å), lithium acetate ($d_L = 9.95$ Å), glicerol ($d_L = 10.5$ Å), n-octylamine ($d_L = 31.71$ Å) and benzidine (10.28 Å and 20.78 Å by reaction of the intercalate with melted benzidine). Using the 17.15 Å phase of the

¹ This 8 Å phase is identified today as a kaolinite monohydrate (Costanzo *et al.*, 1984b), see section 2.6.1.7.

potassium acetate intercalate as precursor, the following molecules were intercalated by displacement reactions: n-decylammonium chloride ($d_L = 34.99 \text{ \AA}$), trimethyl cetyl ammonium chloride ($d_L = 41.14 \text{ \AA}$) and n-octylamine ($d_L = 31.71 \text{ \AA}$). Also described was the formation of the intercalation compounds with calcium acetate ($d_L = 10.42 \text{ \AA}$) and with hydrazinium acetate ($d_L = 10.76 \text{ \AA}$) (the text is not clear by which process these compounds were obtained). Finally, the authors comment that using displacement reactions a great number of other molecules could be intercalated. In fact, in after a following publication (Weiss *et al.*, 1966a) and the PhD Dissertations of three students of A. Weiss (Thielepape, 1966; Mai, 1969; Orth, 1970) around 300 new intercalation compounds have been described. The authors also showed that the other kaolin minerals (dickite, nacrite, and halloysite) reacted with most of these substances in a similar way, producing analogous intercalation compounds. It is, however, much beyond the intentions of this work to detail all these compounds.

The dimethyl sulfoxide derivative (K-DMSO) is one of the most important and well-described intercalation compounds of kaolinite. It is used almost as the “standard” intercalation compound to obtain other derivatives by displacement reactions. This is mainly due to its ease of preparation, higher thermal stability (in comparison with K-hydrazine, for example), lower toxicity (in comparison with hydrazine or NMF, for example), and lower cost of the reactant (see section 3.2). Gonzalez-Garcia and Sanchez-Camazano (1965) were the first authors to publish on the intercalation of DMSO into kaolinite, as well as in various other clay minerals. On the following year these authors published a more in-depth study of the kaolinite and halloysite derivatives with DMSO and other polar liquids (Sanchez-Camazano and Gonzalez-Garcia, 1966). However, Weiss *et al.* (1966a), when describing the K-DMSO compound they obtained (without the knowledge of above mentioned results), commented that the reaction of kaolinite with DMSO was already discussed by H. van Olphen during the International Clay Conference in Stockholm, in 1963.

It is fair to say that the work developed by Armin Weiss and his coworkers in the 1960 decade was the main cornerstone of the research on kaolinite intercalation derivatives, even if most of their results remained hidden from the general academic world, by not being published in international journals in English. This fact is sadly confirmed by the various cases of later publications of studies on intercalation compounds previously described by them, without any mention (or knowledge) of the work already done in Germany.

2.6.1.2 Direct intercalation reactions

The molecules that intercalate in direct reaction with kaolinite can be roughly separated in four groups (Weiss *et al.*, 1966a; Raussel-Colom and Serratos, 1987; Jasmund and Lagaly, 1993, Thompson *et al.*, 1993):

- Molecules capable of forming strong hydrogen bonds, and having donor and acceptor groups for hydrogen bonds in different atoms: urea, formamide, hydrazine, etc. Molecules where the donor and acceptor group is provided by the same atom, will not intercalate (water, alcohols).
- Molecules with a betaine-like (mesomeric) structure, having a large dipole moment: dimethyl sulfoxide, pyridine N-oxide, etc.
- Alkali and ammonium salts of low molecular weight carboxylic acids: ammonium acetate, potassium propionate, etc.
- Alkali halides: sodium chloride, potassium iodide, etc.

These compounds intercalate either from the liquid form (hydrazine), the melt (acetamide), concentrated aqueous solutions (10 mol/l solution of urea) or directly from the solid, in a solid-state reaction (potassium acetate, alkali halides).

Generally, small polar molecules capable of forming hydrogen bonds are easily intercalated on kaolinite. However, additional factors determine whether or not a molecule will intercalate, since a large number of molecules that fulfill the requirements above will not intercalate directly, but form very stable intercalates by displacement reactions, as dimethyl acetamide, for example (Olejnik *et al.*, 1970).

2.6.1.3 Interlayer forces in kaolinite

According to Cruz *et al.* (1973) interlayer bonding in the kaolinite particles arises from van-der-Waals attraction between layers, from hydrogen bonding between octahedral hydroxyl groups on one layer and tetrahedral oxygen atoms of the adjacent layer, and from electrostatic interactions arising from the fact that each layer, although electrically neutral, bears a net fractional charge of opposite sign on each basal surface. Calculations based on simplified assumptions have led the above authors to estimate the total cohesion energy as 210 kJ per formula unit, the main part of which arises from the electrostatic energy term.

For penetration of organic molecules, sufficient energy must be provided to overcome the cohesion between layers. The intercalation process are envisaged as resulting from the

tendency of the dipolar kaolinite layers to become solvated with molecules (Raussel-Colom and Serratos, 1987).

Infrared spectra of intercalated kaolinites give some evidence on the type of interaction between the organic molecules and the mineral matrix. When an organic substance is intercalated, the bands corresponding to inner-surface hydroxyl groups are displaced to lower frequencies, clearly demonstrating the existence of hydrogen bonds between these hydroxyl groups and the intercalated molecules. The strength of the hydrogen bonds may be estimated from the frequency shifts observed (Raussel-Colom and Serratos, 1987). By this procedure, Cruz *et al.* (1973) have calculated the contribution of hydrogen bonding to the net enthalpy change for the intercalation of dimethyl sulfoxide into kaolinite as 46 kJ per formula unit, which is less than the 210 kJ necessary to overcome the cohesion of the layers. They conclude that other factors must contribute to the energy balance, and postulate an additional contribution, either due to a decrease of the electrostatic attraction caused by a higher dielectric constant in the interlayer volume after intercalation, or due to a compensation of the internal dipole moment of the kaolinite layers by the dipole moment of the intercalated phase.

2.6.1.4 Reaction mechanisms

The intercalation reaction starts at the edges of the kaolinite particles and molecules penetrate towards the interior with the same rate between each pair of layers. That part of the particle where molecules have penetrated has a basal spacing about 50% greater than the original 7.1 Å phase. Molecules act as wedges on the kaolinite particles and cause the layers to be elastically deformed at the interphase (Fig. 2.6a). Because of their unsymmetrical structure, all layers in the particle are bent in only one direction (Raussel-Colom and Serratos, 1987).

The reaction is initiated with a reorientation of the interlayer hydroxyl groups and/or proton migration under the influence of the guest molecules adsorbed at the external surfaces of the particles. The elastic deformation thus caused opens the interlayer spaces to the guest molecules. The deformation of the layers and the accompanying stacking disorder are not totally excluded from the structure after deintercalation (Jasmund and Lagaly, 1993).

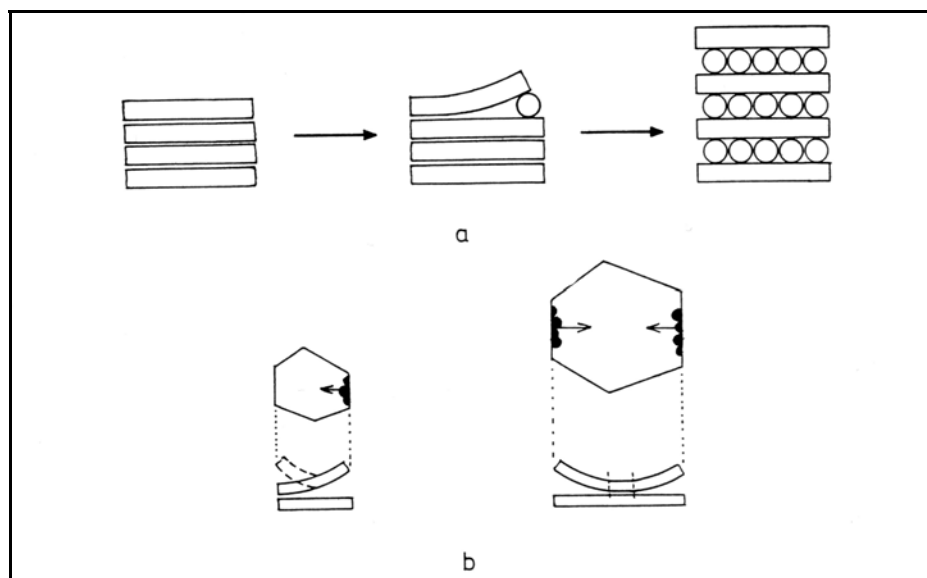


Fig. 2.6: Intercalation mechanism on kaolinite: (a) Beginning of the reaction with elastic deformation of the layers and final state with uniform expansion of the interlayer spaces. (b) Progression of a single reaction front in a small particle ($< 0.5 \mu\text{m}$) and formation of multiple reaction fronts in larger particles. From Jasmund and Lagaly (1993).

According to Weiss *et al.* (1969) the kinetics of the intercalation reaction cannot be described by a simple diffusion process, the relationship between the fraction of reacted kaolinite and the time being best expressed by the logarithmic equation

$$\sqrt{-\ln(1-\alpha)} = \kappa t \quad (\text{Eq. 2.1})$$

that is, by an expression describing reactions which are typically cooperative. The length of the elastically deformed zone in the interior of the crystal is taken as the "cooperative action length" (a_0) and depends on the net increase in basal spacing as well as on the elastic properties of the layers, which are themselves related to the crystallinity of the kaolinite used: the better the crystallinity, the longer a_0 and the faster the reaction, since the weaker cohesion on that zone of the crystal favors further penetration (Raussel-Colom and Serratos, 1987).

The ratio between a_0 and particle diameter becomes crucial in determining the mechanism of reaction. Thus, for large particles, intercalation starts from all edges but, for particles which are too small, the elastic deformations induced by molecules penetrating from one side are transmitted across the entire particle causing a contraction of the layers on the opposite side. Intercalation from that side is hindered, so that for small particles the reaction proceeds at a slow rate via a "one-side mechanism". For large particles, where nucleation can

start from all edges, the reaction proceeds faster via a "ring mechanism" (Fig. 2.6b) (Raussel-Colom and Serratosa, 1987).

Jackson and Abdel-Kader (1978) explained the intercalation phenomenon in kaolinite as a diffusion process, the driving force of which would be strong hydrogen bond formation between the intercalation agent and the hydroxyl groups of the octahedral sheet. The release of the original particle interlayer bonds could be a primary or secondary effect of the intercalation agent. The kaolinite intercalation process would result from a compensation of interlayer dipole moment by the dipole moment of the intercalation phase. A large dipole moment of a polar organic compound combined with a significant number of intercalated molecules per unit cell would favor the formation of a stable intercalation compound. Therefore, the conventional intercalation agents (potassium acetate, DMSO or hydrazine) with relatively low dipole moments and polarizability fail to intercalate kaolinite samples with small particle size having a higher degree of interlayer bond strength with a higher value of dipole moment. Dry grinding of these samples would increase the crystalline disorder and partially exfoliate the kaolinite particles, what would make possible the intercalation with the above mentioned molecules (Jackson and Abdel-Kader, 1978). This explanation is very simplified and fails to explain the influence of all the factors affecting the intercalation process and reaction rates (see next section).

2.6.1.5 Factors affecting the reaction rate

The effect of particle size distribution and of degree of crystallinity on the intercalation properties of different kaolinites has been investigated by several authors, but their conclusions do not always agree (Bodenheimer *et al.*, 1967; Range *et al.*, 1969; Wiewiora and Brindley, 1969). According to the model of Weiss *et al.* (1969) both the size and crystallinity should have analogous effects on the reaction rate but, since they are not always directly correlated, the combined effect of both may be difficult to assess by measuring only the fraction of material that has reacted after a selected reaction time. More definite patterns are observed when the complete kinetics of the reaction is studied and the intercalation properties are expressed as a function of the reaction rate. For a given kaolinite, intercalation rates first increase with particle size and then decrease, a trend also observed for the variation of the index of crystallinity of the different size fractions (Raussel-Colom and Serratosa, 1987).

Supported by FTIR analyses of intercalated kaolinites, Deng *et al.* (2002) proposed that structural stress would be a major controlling factor governing the intercalation process. As discussed in the previous chapter, the misfit between octahedral and tetrahedral sheets on the kaolinite layer imposes structural stress on the structure. According to these authors part of this stress can be relieved when kaolinite is intercalated. The faster intercalation rates of the coarse fractions would be dictated by the larger structural stress accumulated from the misfit inside the layers. The authors claimed that the changes in the structure of kaolinite detected by FTIR were caused by releasing of the structural stress. The experimental data supported the hypothesis that the finer particles have slower intercalation rates due to the less structural stress on their layers. The authors also comment that the unusual size effect on intercalation rate of kaolinite could not be explained by crystallinity differences as previously reported (Wiewiora and Brindley, 1969), because the particles in the clay fractions had lower crystallinity than the silt particles and there was no consistent crystallinity trend associated with the particle size among the studied clay fractions (Deng *et al.*, 2002).

Reaction rates are also affected by factors that bear no relation to the properties of the mineral. These properties include the molecular size and geometry of the intercalating material, the degree of association of the liquid or solution, the concentration of the solutions, the solution pH, and also the reaction temperature (Olejnik *et al.*, 1970; Raussel-Colom and Serratosa, 1987).

The effects of addition of water to the intercalating agent have been studied for the reaction of kaolinite with hydrazine (Weiss *et al.*, 1963b), with formamide and with *N*-methylformamide (Olejnik *et al.*, 1970). In all cases, the reaction rate was significantly increased when water was added, becoming maximum at a certain water content that varies widely with the system involved. Thus, the maximum rate was attained at 10% water content for formamide-water and for *N*-methylformamide-water, while for hydrazine-water the maximum rate was attained at a concentration of 10 mol/l (approximately 68% water in the mixture).

In the pure liquids, the molecules are either hydrogen-bonded or in dipole-associated polymeric networks, with very few free or unbonded molecules coexisting at normal temperature. It has been suggested (Olejnik *et al.*, 1970) that the addition of water or other polar molecules favors intercalation because the associated structure of the pure liquid is broken up, thus increasing the proportion of unbonded molecules. However, if excess water is added, then the solute becomes solvated by the solvent, and molecules free to

intercalate are fewer. The rate thus passes through a maximum because of the competition for unsolvated molecules between the kaolinite crystal and the liquid phase (Raussel-Colom and Serratosa, 1987).

Higher temperature should also favor intercalation because of its disruptive effect on the liquid structure (Raussel-Colom and Serratosa, 1987). This is in accordance with the increased rates reported for the intercalation of urea (Weiss *et al.*, 1963b) and dimethyl sulfoxide (Weiss *et al.*, 1966a) into kaolinite.

No definite relationship exists between molecular size and intercalation ability. Considering that the work needed for lattice expansion should be the greater the larger the resulting d_{001} spacing, it might be expected that rates would increase with decreasing molecular weight of the intercalating agent (Raussel-Colom and Serratosa, 1987). However, rate determinations for compounds from homologous series such as formamide and acetamide and their monomethyl and dimethyl derivatives do not indicate such a tendency (Olejnik *et al.*, 1970). Undoubtedly, any possible influence of molecular size is overshadowed by differences in the extent of molecular association in the liquids or melts (Raussel-Colom and Serratosa, 1987).

The intercalation of organic salts (the NH_4^+ , K^+ , Rb^+ and Cs^+ acetates) is strongly influenced by the pH value of the saturated solution used. The reaction takes place in an alkaline medium only, the maximum rate being attained in the pH range of 8 to 11. At pH values higher than 13 the reaction is also inhibited (Weiss *et al.*, 1963b; 1966a). No explanation has been so far offered for this behavior.

2.6.1.6 Displacement reactions

Once the kaolinite layers are separated in an intercalation compound, the intercalated molecules may be displaced by contact with other organic or inorganic compounds that do not react directly with the mineral. Indirect intercalation compounds have been prepared by displacement reactions with a very large variety of substances. These include, among many others:

- Polar organic compounds: acetone, glycols, acetonitrile and nitrobenzene (Sanchez-Camazano and Gonzalez-Garcia, 1966).
- Organic bases: alkyl- and aromatic amines, alkylene diamines, pyridine, purines and pyrimidines, morpholine (Weiss *et al.*, 1966a).

- Amino acids, peptides and their salts: potassium glycinate, alaninate and lysinate (Weiss *et al.*, 1963b).
- Other organic salts: sodium acetate and potassium oxalate and lactate (Weiss *et al.*, 1963b).
- Inorganic Salts: alkali halides, transition metal chlorides, potassium phosphate, potassium carbonate (Andrew *et al.*, 1960; Weiss *et al.*, 1966a; Thielepape, 1966).
- Organic polymers: either by in-situ polymerization of the intercalated monomer: poly(acrylamide), poly(acrylonitrile) and poly(vinylpyrrolidone) (Sugahara *et al.*, 1988; 1990; 1992), or by displacement with the polymer: poly(ethyleneglycol) and poly(hydroxibutirate) (Tunney and Detellier, 1996b; Gardolinski *et al.*, 2000).
- Metal and metal oxide nanoparticles, by the reduction of intercalated salts: Ag, Rh and ZnO (Patakfalvi *et al.*, 2003; Papp *et al.*, 2004; Németh *et al.*, 2004)
- Water: see section 2.6.1.7.

The most common intercalation compounds used as precursors for the displacement reactions are K-DMSO, K-hydrazine, K-potassium acetate and K-NMF. The intercalation compound with methanol, obtained by the exhaustive methanol washing of the K-DMSO or K-NMF compounds, can be used as a very versatile precursor in the intercalation of molecules which will not intercalate by displacement reactions starting with the usual precursors (Komori *et al.*, 1998).

The stability of the intercalation compounds obtained via displacement reactions is very variable. Some of the compounds are stable only in the presence of an excess of the guest molecule, and deintercalate readily when the sample is dried, recovering raw kaolinite (K-acetone, K-methanol). Other compounds are indefinitely stable in ambient conditions (derivatives with alkali halides or organic polymers), some of the organic derivatives even present remarkably high thermal stabilities (K-NMP is stable until ~ 430 °C: Gardolinski *et al.*, 1999). However, as a general characteristic of all intercalation compounds, the guest molecules can be more or less easily removed from the interlayer spaces by leaching (washing) with the appropriate solvent (water, acetone, ether, dioxane, etc.), which will depend on the solubility and polarity of the guest molecule.

2.6.1.7 Hydrated kaolinite

Water cannot be intercalated directly in kaolinite even under extreme conditions. The difficulty to obtain a kaolinite hydrate was subject of much discussion prior to the discovery of the intercalation reactions of kaolinite since halloysite naturally occurs with intercalated water (see Chapter 1).

This scenario began to change when Weiss (1961; 1963b) noticed that washing the urea-kaolinite compound produced a phase with $d_L = 8.33 \text{ \AA}$. Later, van Olphen and Deeds (1963) prepared a $d_L = 8.45 \text{ \AA}$ hydrate of dickite by exhaustive water washing of urea and potassium acetate intercalates. Wada (1965) studied the intercalation of water in kaolin minerals by washing the potassium acetate intercalation compounds of kaolinite, dickite, nacrite and halloysite and found that nacrite formed a hydrate with $d_L = 8.35 \text{ \AA}$. He was not able to form the hydrated dickite phase described above. Range *et al.* (1968) commented that, after washing the hydrazine-kaolinite compound with water, the basal spacing of the product changed from the original 10.72 \AA to $10.1\text{-}10.2 \text{ \AA}$. This phase collapsed after air drying to a phase with $d_L = 8.2\text{-}8.4 \text{ \AA}$. They interpreted these phases as two different forms of a hydrated kaolinite. More than ten years latter, Costanzo *et al.* (1980) described a new method to obtain hydrated kaolinite. It consisted in the reaction of NH_4F with a K-DMSO phase in excess liquid DMSO followed by washing with water. This method yielded a 10.01 \AA phase attributed to a kaolinite dihydrate ($\text{Al}_2\text{Si}_2\text{O}_5(\text{OH})_4 \cdot 2\text{H}_2\text{O}$). In a following investigation (Costanzo *et al.*, 1982), K-DMSO was washed with methanol prior to the treatment with ammonium fluoride, and a quasi-stable kaolinite dihydrate was obtained. It was even stable for an indefinite period when kept below $10 \text{ }^\circ\text{C}$ but dehydrated to the 8.6 \AA phase at room temperature during drying. Instead of using K-DMSO, the use of kaolinite intercalated with hydrazine, formamide or NMF also yields similar results. However, among all alkali fluorides and ammonium halides, only NH_4F produces satisfactory results, with the obtention of small amounts of the 10 \AA phase with KF, RbF and CsF and no formation of the 10 \AA hydrate with the other salts (Costanzo *et al.*, 1984a). Costanzo *et al.* (1984b) showed that by different synthetical routes involving the ammonium fluoride method, four different hydrates could be obtained: 8.4 \AA , 8.6 \AA , unstable 10 \AA and quasi-stable 10 \AA .

The formation of the hydrate by the fluoride method was explained by the substitution of interlayer hydroxyl groups by fluoride ions. This alters the nature of, and weakens the interlayer bonds, favoring the intercalation of water molecules (Costanzo *et al.*, 1984a) beside

the fact that fluorination at the particle edges would reduce the possibility of collapse being initiated at the edges (Raythatha and Lipsicas, 1985).

Raythatha and Lipsicas (1985) demonstrated that the kaolinite dihydrate could also be obtained by washing K-DMSO with methanol and then with water, without the need of the ammonium fluoride treatment, in a similar way to the formation of the hydrate by washing of K-hydrazine or K-urea compounds. Tunney and Detellier (1994b) described the formation of an analogous monohydrate ($d_L = 8.4 \text{ \AA}$) by washing the kaolinite-ethylene glycol intercalation compound (obtained by displacement from K-DMSO).

In the monohydrate (8.4 \AA) the water molecules are assumed to interact strongly with the matrix, being keyed into the ditrigonal holes of the silica sheet. The dihydrate has a second layer of intercalated water, which interacts more weakly with the kaolinite interlayer surfaces and has greater mobility (Costanzo *et al.*, 1984b). During the dehydration of both phases, strong interstratification occurs, and different broadened reflections between 10 \AA and 8.4 \AA and between 8.4 \AA and 7.1 \AA can be observed (Costanzo and Giese, 1985; Naamen *et al.*, 2003).

While the 10 \AA dihydrate is very unstable and collapses to the 8.4 \AA monohydrate readily when dried, the monohydrate is more stable, and the basal spacing of kaolinite (7.1 \AA) is completely recovered only by heating to $250 \text{ }^\circ\text{C}$ (Gardolinski *et al.*, 2003). This is due to the fact that the presence of even very few interstratified layers of the mono- and dihydrates in a kaolinite particle contribute significantly to the dislocation of the 7.1 \AA reflection in the X-ray diffractograms (Naamen *et al.*, 2003).

2.6.2 Interlayer Grafting

2.6.2.1 Definition and peculiarities

The term “grafting” designates topotactic reactions of organic or inorganic molecules with any reactive group at the external or interlayer surfaces of clay mineral particles, forming covalent bonds between the grafting molecule and the clay matrix.

Most of the grafting reactions described in the literature involve 2:1 clay minerals and proceed at the external basal surfaces and lateral edges of the particles, as these are the sites where the hydroxyl groups are present (like silanol and aluminol groups). Interlayer grafting reactions are not possible in the raw 2:1 clay minerals, as the interlayer silica

surfaces do not present reactive sites. Chemical treatments of the mineral can, however, produce enough interlayer hydroxyl groups by partial or total removal of octahedral atoms (Raussel-Colom and Serratosa, 1987). The majority of the grafting reactions described with 2:1 clay minerals involve the silanization of smectites.

1:1 clay minerals present a great advantage to 2:1 minerals as they have “exposed” hydroxide sheets as basal surfaces in addition to the silica surfaces. In kaolinite, many different molecules can have access to these acidic aluminol groups, since intercalation is not a difficult task as shown by the large number of intercalation compounds with many kinds of molecules (see previous section). However, the reaction of the aluminol groups with intercalated molecules, with the formation of covalent Al-R bonds (generally Al-O-C) was described only in 1993, and, until the beginning of this study, the reaction of only a few similar molecules was reported.

To obtain a grafted derivative, a series of phenomena must be in fine balance: The grafting agents must have access to the interlayer surfaces by intercalating in kaolinite either directly or indirectly. The diffusion rates of intercalated molecules coming out of the matrix and of grafting agents being intercalated (considering a displacement reaction) must match, so that no layer collapse will occur. The grafting agents must not react with the intercalated molecules, at least not in a way that will compete with the grafting process. The grafting agents must react with the interlayer hydroxyl groups at reasonable temperature, to avoid their decomposition. Any reaction intermediates formed must not disrupt the process (e.g. by reacting with the grafting agent or being deintercalated). Byproducts of the grafting reaction (often water) must diffuse out of the interlayer space fast enough to allow the reaction to proceed, not shifting the equilibrium into the opposite direction. The grafted product must be stable at the reaction temperature as well as during any post-reactional treatments. It is clearly seen that it will not be trivial to find reactions in which these and other factors will be so finely tuned that a grafted derivative will be formed.

All grafted derivatives from kaolinite described in the literature were obtained from a pre-expanded product (mainly with DMSO), as the grafting agents were unable to intercalate directly. All products were obtained in similar reactions as the grafting agents had functional alcohol groups. Derivatives were obtained with methanol, diols, diol mono-ethers, polyols and aminoalcohols in esterification-like reactions with the acidic aluminol hydroxyl groups (detailed mechanistic studies were not performed so far).

Analogous alcohol derivatives obtained from various aluminium sources have been already known for some time. Reaction of gibbsite, aluminium alkoxides or even aluminium metal with glycols, alcohols, aminoalcohols or other similar molecules produce, under certain conditions, grafted organic derivatives of layered aluminium (hydr)oxide of the boehmite structure (Inoue *et al.*, 1986; 1988; 1991a; 1991b; 2000). These compounds, also called *alkoxyalumoxanes* can be regarded as grafted derivatives analogous to kaolinite, obtained from the gibbsite sheet alone. It was reasonable to expect that at least some of the molecules that react with gibbsite would react with kaolinite, once they have access to the interlayer space.

2.6.2.2 Kaolinite interlayer-grafted derivatives

Based on the results obtained by Inoue and coworkers described above, Christian Detellier and his coworkers at the University of Ottawa (Canada) began the research on the grafting of kaolinite using similar grafting agents. The first interlayer-grafted derivatives of kaolinite were described in 1993 (Tunney and Detellier, 1993). These researchers refluxed dispersions of the DMSO intercalate of kaolinite with ethylene glycol, ethylene glycol methyl ether, di(ethylene glycol) buthyl ether, 1,2-propanediol and 1,3-propanediol for periods from 12 to 18 hours, washed the products with methanol, ethanol or water and dried them under vacuum at 120 °C (Table 2.3). The authors showed that the alcohol-like molecules had reacted with the kaolinite interlayer aluminol groups in an esterification-like reaction, with the formation of Al-O-C covalent bonds. Though detailed analyses only of the ethylene glycol derivative (EG) were provided, there was no reason to imagine that the other derivatives would not be analogous to K-EG. These analyses included MAS-NMR spectra of the K-EG derivative, which pointed to the successful grafting, with the formation of the Al-O-C bond. It was proposed that the non-grafted hydroxyl group of the ethylene glycol molecules keys into the ditrigonal cavity of the silica sheets, increasing the basal spacing by 2.3 Å in relation to raw kaolinite.

In the following year, the same researchers published a more in-depth study of this K-EG compound, with a discussion of the role of water during the reaction, stability towards washing/hydrolysis and the distinction between the 9.4 Å grafted phase and a 10.8 Å intercalated phase (Tunney and Detellier, 1994a).

Table 2.3: Interlayer-grafted derivatives of kaolinite described until August 2005.

Grafted molecule	Basal spacing (Å)	Stoichiometry	Reference
Methanol	8.2	$\text{Al}_2\text{Si}_2\text{O}_5(\text{OH})_{3.13}(\text{OCH}_3)_{0.87}$	Tunney and Detellier, 1996a
	8.6/8.2 ^a	$\text{Al}_2\text{Si}_2\text{O}_5(\text{OH})_{3.64}(\text{OCH}_3)_{0.36}$	Komori <i>et al.</i> , 2000
	8.6/8.2 ^a	$\text{Al}_2\text{Si}_2\text{O}_5(\text{OH})_{3.60}(\text{OCH}_3)_{0.40}$	Itagaki and Kuroda, 2003
Ethylene glycol	9.5	-	Tunney and Detellier, 1993
	9.4	$\text{Al}_2\text{Si}_2\text{O}_5(\text{OH})_{3.2}(\text{OCH}_2\text{CH}_2\text{OH})_{0.8}$	Tunney and Detellier, 1994a
1,2-Propanediol	10.9	-	Tunney and Detellier, 1993
	10.8	$\text{Al}_2\text{Si}_2\text{O}_5(\text{OH})_{3.37}(\text{C}_3\text{H}_3\text{OH})_{0.63}$	Itagaki and Kuroda, 2003
1,3-Propanediol	9.8	-	Tunney and Detellier, 1993
	11.1	$\text{Al}_2\text{Si}_2\text{O}_5(\text{OH})_{3.32}(\text{C}_3\text{H}_3\text{OH})_{0.68}$	Itagaki and Kuroda, 2003
	11.0 ^b	$\text{Al}_2\text{Si}_2\text{O}_5(\text{OH})_{3.39}(\text{C}_3\text{H}_3\text{OH})_{0.61}$	Itagaki and Kuroda, 2003
1,2-Butanediol	11.8	-	Murakami <i>et al.</i> , 2004
1,3-Butanediol	11.6	-	Murakami <i>et al.</i> , 2004
Adonitol	8.4	-	Brandt <i>et al.</i> , 2003
Dulcitol	11.4	-	El Bokl and Detellier, 2005
D-Sorbitol	11.0 ^c	-	Brandt <i>et al.</i> , 2003
D-Mannitol	11.4	-	El Bokl and Detellier, 2005
Ethylene glycol methyl ether	10.6	-	Tunney and Detellier, 1993
Di(ethylene glycol) butyl ether	11.2	-	Tunney and Detellier, 1993
Ethanolamine	10.7	$\text{Al}_2\text{Si}_2\text{O}_5(\text{OH})_{3.0}(\text{OCH}_2\text{CH}_2\text{NH}_2)_{1.0}$	Tunney and Detellier, 1997
3-Amino-1-propanol	11.1 ^d	-	Tunney and Detellier, 1997

^a hydrated/anhydrous products

^b “bridge grafted” (see text).

^c Value not presented in the publication text, but indicated in a personal communication with the authors.

^d It is not clear in the reference text if the product is really grafted or if the organic molecules are only intercalated (see text).

Tunney and Detellier also described the grafting of methoxy groups by reacting methanol with K-DMSO and K-NMF (Tunney and Detellier, 1996a). The reactions were performed in autoclaves, in order to achieve high temperatures (190-270 °C). The authors

proposed that every third interlayer hydroxyl group was grafted, in such a way that every ditrigonal cavity would host a keyed methoxy group, resulting in a “*non-centrosymmetric two-dimensionally ordered organomineral assembly*”.

Later on, the same group described the reactions of aminoalcohols with kaolinite, forming grafted derivatives from the K-DMSO and K-NMF intercalation compounds (Tunney and Detellier, 1997). The derivative obtained from ethanolamine in a reflux reaction (as with the diols) was carefully studied, and results similar to the other grafted derivatives were obtained, including high thermal stability, stability towards washing and characteristic changes on the FTIR spectrum. A compound obtained from the reaction with 3-amino-1-propanol was also described. The yield for this reaction was much lower than for the other grafting reactions already described (58 % against more than 90 %) and the FTIR spectrum for this compound was not so widely changed as the spectrum of the ethanolamine derivative. The authors do not clearly state if this product consists of a grafted phase or if the organic molecules are just intercalated. Reactions of K-DMSO with ethylene diamine, DL-1-amino-2-propanol and nitroaniline were also performed, but no new phases were obtained.

The next grafted derivative of kaolinite reported on the literature was presented by the group of Kazuyuki Kuroda from the Waseda University in Tokyo, Japan (Komori *et al.*, 2000). These researchers reported that methoxy groups from methanol could be grafted on kaolinite using the K-NMF compound at room temperature, without the need of the thermal treatment described by Tunney and Detellier (1996a). The ratio of methoxy groups grafted per unit formula of kaolinite was lower than the values obtained by Tunney and Detellier (Table 2.3), but the experimental conditions of the synthesis were simpler. The 8.6 Å phase obtained collapsed to the 8.2 Å phase described by Tunney and Detellier after heating under vacuum, showing that the product contained intercalated water. MAS-NMR measurements strongly indicated the formation of Al-O-C bonds by the grafting at room temperature.

Some years later, Itagaki and Kuroda (2003) obtained in a so-called “transesterification” reaction other grafted derivatives from the above describes methanol-kaolinite. During this process, the methoxy groups grafted to the clay mineral surfaces are exchanged by the grafting groups of other alcohol-like molecules. In this case, 1,2- and 1,3-propanediols (12PD and 13PD) were refluxed with methoxy-kaolinite to obtain the diol derivatives, and methanol as byproduct. It was shown that the methoxy groups are really exchanged by the diols and that additional interlayer hydroxyl groups are esterified with the diols, as the amounts of alkoxy groups in the products was higher than in the original

methoxy-kaolinite (see Table 2.3). By extending the reaction time from 1 to 5 days for 13PD, a product was obtained which presented a 0.1 Å smaller basal spacing than the product from the faster reaction. This was explained by the formation of a “bridge” grafted derivative, in which both hydroxyl groups of the diol reacted with kaolinite.

In 2003 the research group of C. Detellier opened a new possibility of grafting kaolinite by the reaction of K-DMSO with some polyhydroxy alcohols (alditols) (Brandt *et al.*, 2003). Intercalation compounds from D-sorbitol and adonitol were obtained from the reaction of the melted polyol with K-DMSO ($d_L = 11.9$ Å and 10.4 Å respectively). After thermal treatment of the intercalates (200 °C, 1h) the basal spacing was reduced due to the grafting of the intercalated polyols (K-adonitol: $d_L = 8.4$ Å) analogously to the intercalation and grafting of ethylene glycol (Tunney and Detellier, 1994a) and methanol (Tunney and Detellier, 1996a). The basal spacing of the product grafted with D-sorbitol was, however, not reported. It was proposed that the intercalated alditol chains are arranged in a flattened horizontal monolayer between the kaolinite layers but no structural model of the grafted derivatives was designed which could account for the reduction in the basal spacing by 2 Å.

In 2004 the group of K. Kuroda reported two new grafted derivatives obtained by the transesterification method already discussed (Murakami *et al.*, 2004). Starting with methoxy-kaolinite, 1,2- and 1,3-butanediols were grafted on kaolinite, in reactions analogous to the ones described in the year before.

Finally, in 2005, the group of C. Detellier presented more results on the grafting with alditols (El Bokl and Detellier, 2005). Dulcitol and D-mannitol were grafted by the procedure described previously. After thermal treatment, the grafted phases presented basal spacings of 11.4 Å.

During our research we were able to greatly expand the number of grafted kaolinite derivatives by reacting the K-DMSO intercalate with many n-alkanols, diols and glycol mono-ethers (see Chapter 3).

All grafted molecules so far discussed are very similar, sharing an alcohol structure (alcohols, diols or polyols) and the reactions proceed only by using the pre-expanded kaolinite. However, in 1998, the grafting of phenylphosphonic acid into raw kaolinite was described (Guimarães *et al.*, 1998). This report was followed by a description of the intercalation of hexylamine into this so called kaolinite-phenylphosphonate (Guimarães *et al.*, 1999) and a thermal stability study of the product using TG-EGA and VT-DRIFTS (Breen *et al.*, 2002). This reaction was completely different from all previously (and afterwards)

described reactions, as the grafting agent was a strong acid (in comparison to alcohols) and the reaction would take place without pre-expansion of the kaolinite interlayer spaces. Chapter 6 presents an in-depth study of this reaction, as well as reactions of kaolinite and gibbsite with similar acids. We establish that kaolinite reacts with phenylphosphonic acid (and similar acids) in a non-topotactic reaction, with the dissolution of the clay mineral structure and new-formation of a layered aluminum phenylphosphonate. A grafted kaolinite derivative was not produced (Gardolinski *et al.*, 2004).

2.7 Non-Topotactic Reactions

In opposition to topotactic reactions, which can be neatly grouped in surface and interlayer modification, non-topotactic reactions are much varied and, therefore, difficult to present in a simple classification. In a general manner, however, the non-topotactic reactions of kaolinite can also be divided in two major groups: reactions in solution and solid-state reactions.

Reactions in solution involve the dissolution of the structural gibbsite and/or silica sheets, with or without the formation of new solids. The kaolinite structure can be decomposed by inorganic acids, like HCl or HNO₃, in a proton promoted dissolution mechanism; by organic acids, like oxalic acid, in a ligand promoted dissolution mechanism (Sutheimer *et al.*, 1999); by alkalis with the formation of silicates and aluminates; by fluoride ions with the formation of soluble fluorosilicic species; or by phosphate or many other phosphor-containing ions with the formation of complex aluminophosphates (Weiss *et al.*, 1995; Gardolinki *et al.*, 2004), among others. Generally, acids tend to attack the octahedral sheet, leaching aluminum ions and leaving amorphous silica, while alkalis will rather dissolve the silica, leaving insoluble aluminum oxide or even solubilizing the hole matrix (Grim, 1968). Dissolution rates of kaolinite are usually dependent of the particle size but structural disorder plays also an important role (Sutheimer *et al.*, 1999).

The interaction of kaolin minerals and other soil components with phosphates, polyphosphates, cyclophosphates and many phosphor-containing organic substances is of great importance in soil and environmental science, as a large number of fertilizers, pesticides and insecticides contain such components (Weiss *et al.*, 1995).

The reactivity and ease of dissolution of kaolinite is greatly improved by calcination of the mineral prior to chemical attack. Metakaolinite is more easily attacked by acids and alkalis than the original mineral. Selective leaching of the octahedral sheets of metakaolinite, to obtain planar or even rolled silica sheets (nanotubes) was already discussed (Dong *et al.*, 2003).

The dissolution of kaolinite in alkalis, especially in NaOH, gained much attention as it is a pathway for the synthesis of zeolites (Rocha *et al.*, 1991; Murat *et al.*, 1992; Gualtieri *et al.*, 1997). These processes usually involve the hydrothermal treatment of metakaolinite with aqueous solutions of NaOH, with formation of zeolite Na-A, zeolite 4A or cubic zeolite P.

The solid-state reactions of kaolinite leading to ceramic materials and Portland cement were (and still are) subject of innumerable studies due to their great industrial importance

(Grim, 1962; Jasmund and Lagaly, 1993). Other thermal solid-state reactions, however, gained by far not so much attention, only a few of them are cited below, to give a broad impression of the types of reactions and kinds of products which can be obtained.

A few studies were made on the high-temperature reaction of kaolinite with various salts (Heller-Kallai and Frenkel, 1978). Metal aluminosilicates were obtained by the reaction of kaolinite with K_2CO_3 (forming $KSiAlO_4$) (Heller-Kalai and Lapidés, 2003) and $CaCO_3$ (forming $CaAl_2Si_2O_8$) (Okada *et al.*, 2003). Hercynite ($FeAl_2O_4$) was obtained by the reaction of kaolinite with Fe_2O_3 (Takeuchi *et al.*, 2000). Fukase *et al.* (1996) described the synthesis of “fluorine muscovite” by the reaction between kaolinite and K_2SiF_6 .

2.8 Exfoliation and Delamination

Delamination and exfoliation are terms used in current literature, unfortunately neglecting distinction or precision. To discuss these topics further, a precise definition is necessary. When dealing with clay minerals (and many other layered materials) a clear distinction between both terms is easily established: *Exfoliation is defined as the decomposition of large aggregates (booklets) into smaller particles. Delamination denotes the process of separation of the individual layers of the particles.*

Exfoliation mostly involves the mechanical disruption of the solid, which can be achieved by grinding, extruding, or similar processes. On the other hand, mechanical processes may not be efficient enough to separate the individual layers of the clay mineral in structures with strong interlayer interactions like kaolinite. In these cases, delamination must involve chemical processes, which influence the interlayer cohesive forces.

Exfoliation of kaolinite is an important industrial procedure. For instance, it influences the rheological properties of dispersions used in the ceramic industry and the coating properties of the kaolins used in the paper industry. Exfoliated kaolins usually have a higher aggregate value than the raw material, and the exfoliation process can expand the usability of reserves otherwise unsuited for many applications (Jasmund and Lagaly, 1993).

Industrial (and experimental) exfoliation of kaolins is obtained by mechanical processes (Tari *et al.*, 1988; Jasmund and Lagaly, 1993; Maxwell and Malla, 1999) but chemical approaches were also discussed, as these can be much more efficient than simple mechanical processes (Weiss, 1963; Lahav, 1990; Tsunematsu *et al.*, 1992; Maxwell and Malla, 1999; Tsunematsu and Tateyama, 1999; Gardolinski *et al.*, 2001; Tripelhorn *et al.*, 2002). These processes are based on the intercalation of molecules such as urea or potassium acetate, concomitant (or not) with mechanical treatments. The following washing/deintercalation steps, accompanied by mechanical disruption (grinding, ultrasound), can exfoliate kaolinite much efficiently, separating the agglomerates into very small particles.

Weiss (1963) showed that the exfoliation of kaolinite by grinding a kaolinite-urea intercalation compound is many times more efficient than the simple grinding of the raw mineral. He proposed that this process was already in use in ancient China (using urine as a source of urea), and was one of the major “secrets” involved in the obtention of very high-quality Chinese porcelain, unparalleled in the rest of the world for centuries.

True delamination of kaolinite into stable aluminosilicate monolayers was not yet achieved. The delamination process previously described by Lahav (1990) with the alleged formation of single layers by combined dimethyl sulfoxide and ammonium fluoride treatment was shown to be based on misinterpreted data. In fact, the amount of finer fractions was increased insignificantly and only platy particles were formed (Chekin, 1992). These remarks were corroborated by later results on particle size (see Appendix II) and microscopical analysis (unpublished results) of the kaolinite treated by Lahav's method.

The chemical exfoliation using ammonium acetate (Weiss and Russow, 1963) or potassium acetate (Singh and Mackinnon, 1996), however, was studied in detail. Many (more than 30) cycles of intercalation/deintercalation (washing with water) exfoliated the particles forming thinner lamellae, which eventually curled to halloysite-like tubes and/or polygonal spirals. Briefly described were similar results where a kaolinite previously intercalated with *n*-octylamine (or decylamine) was washed with ethyl ether (Poyato-Ferrera *et al.*, 1977; Weiss *et al.*, 1981).

The microscale morphology of the tubes and polygonal spirals obtained by the intercalation/deintercalation cycles of kaolinite with potassium acetate was shown to be indistinguishable from that of natural halloysite, presenting a highly disordered structure with intercalated water (Singh and Mackinnon, 1996). It was shown that kaolinite layers curl to compensate the lateral misfit between the octahedral and tetrahedral sheets, when the interlayer hydrogen bonds are sufficiently weakened (see sections 1.2.4 and 5.3.3). In planar particles, the misfit is compensated by rotation of the [SiO₄] tetrahedra. The curling mechanism is energetically more favorable than tetrahedral rotation, but can only proceed in sufficiently thin particles with a highly disordered structure and, consequently, strongly weakened interlayer hydrogen bonds, as in the case of the samples after potassium or ammonium acetate treatments (Singh, 1996). The rolling of the octylamine-intercalated kaolinite after washing with ether can be interpreted in the same way. The high basal spacing of the intercalate hinders the formation of hydrogen bonds between the kaolinite layers, which are readily separated by solvent leaching.

The rolling of very thin kaolinite particles poses an obstacle on the further separation of the layers in order to obtain fully delaminated samples, as the layers will tend to adhere together, stabilized as tubes and spirals. A more efficient method is needed to increase the degree of delamination of kaolinite. Chapter 5 reports the results on the development of an

optimized delamination method for kaolinite. Using this new method, the highest possible degree of delamination was achieved, with the formation of rolled single layers of kaolinite.

2.9 Rheological Properties of Kaolinite Aqueous Dispersions

The understanding of the properties of the system kaolinite/water is of great industrial importance. Ceramic, paper and pharmaceutical industries constitute the largest consumers of kaolin worldwide (see section 1.5), and aqueous dispersions of kaolinite are often formed at some point during its processing or use. It is, therefore, important to know how these dispersions behave and how the addition of other substances influences the properties of the system. Some of the most basic rheological properties of the kaolinite/water system are briefly described.

In general, the flow behavior, viscosity, yield point, thixotropy and antithixotropy, and other rheological properties of clay mineral dispersions are defined and influenced by:

- intrinsic properties of the clay mineral (particle size, charge, counterions, surface defects, etc.),
- presence of accessory minerals,
- solid content of the dispersion,
- type and concentration of ions, mostly by the proportion of Na^+ and Ca^{2+} cations,
- pH value,
- salt concentration,
- admixtures.

By the addition of substances like phosphates, soda or polyanions the flow behavior can be drastically changed (Jasmund and Lagaly, 1993).

In acid medium the yield point of kaolinite dispersions is dictated by the formation of cardhouse structures (edge-face interactions, forming a tri-dimensional framework). Increasing pH values will decrease the yield point, until a minimum value is attained (Fig. 2.7A), due to the break-down of the edge(+)/face(-) contacts, as the edges will be progressively negatively charged.

If sodium ions are present as counterions, kaolinite dispersions can stay fluid at relatively high solid contents. With increasing solid content, the degree of thixotropy increases (Fig. 2.8a). By the addition of calcium chloride, stable framework structures are built due to edge/edge-contacts, and the yield point increases significantly. One should note that after a critical CaCl_2 concentration, the flow behavior inverts from thixotropic to antithixotropic (Fig. 2.8b) (Jasmund and Lagaly, 1993).

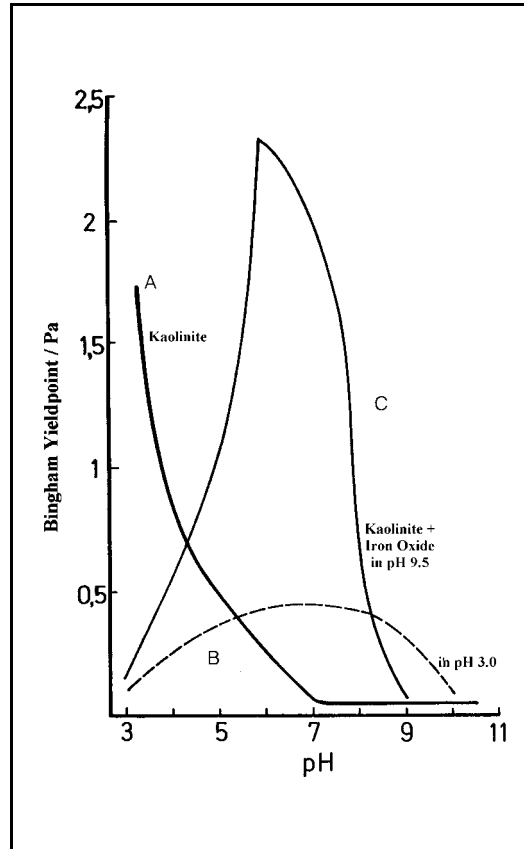


Fig. 2.7: Bingham yield points of sodium kaolinite dispersions (9 % solid content) as a function of the pH value (curve A) and in presence of iron oxide (curves B and C) (adapted from Jasmund and Lagaly, 1993).

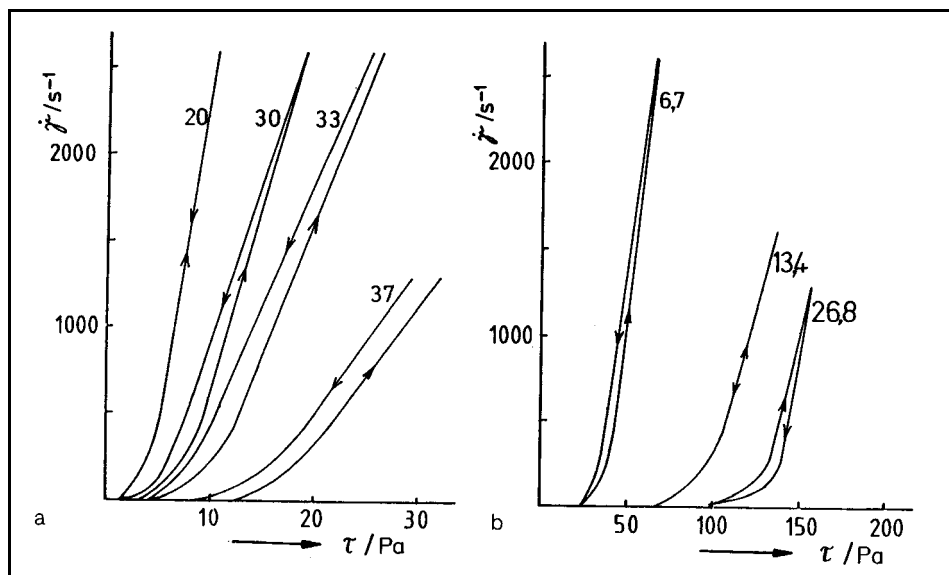


Fig. 2.8: Flow behavior of kaolinite (kaolin from Zettlitz, Czech Republic): (a) Sodium exchanged kaolinite, solid content = 20-37 %. (b) Effects of the addition of 6.7 to 26.8 mmol/l CaCl₂ to a 40 % sodium kaolinite dispersion (from Jasmund and Lagaly, 1993).

Fig. 2.9 demonstrates the liquefaction by the addition of sodium diphosphate to a kaolinite dispersion. Even small amounts of diphosphate anions destroy the edge(+)/face(-) contacts and transforms the pseudoplastic mass in a Newtonian dispersion. According to the DLVO theory, the addition of salt makes the interactions between the kaolinite particles attractive. The formation of a new framework structure consisting of face/face contacts increases the yield point again (Jasmund and Lagaly, 1993).

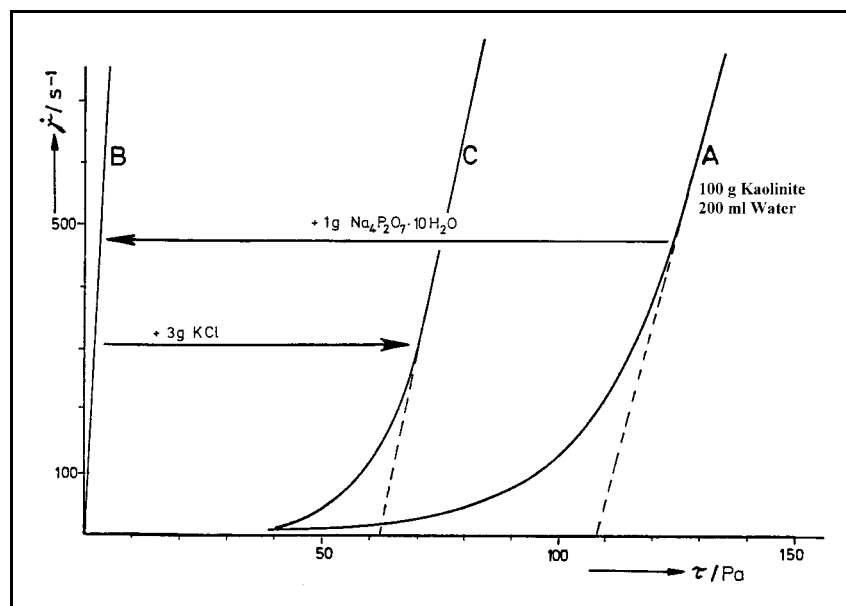


Fig. 2.9: Liquefaction of kaolin (English china clay) by addition of diphosphate and re-solidification by addition of KCl (adapted from Jasmund and Lagaly, 1993).

Few is known about the influence of admixtures in kaolinite dispersions. An instructive example is the flow behavior of kaolinite dispersions in the presence of iron oxide (ferrihydrite) (Fig. 2.7). Iron oxides, depending on the modification, crystallinity and history, are positively charged between pH 6 and 9. The yield point decisively depends on the conditions under which the iron oxide comes into contact with kaolinite. In curve B, iron oxide was added to the 9 % dispersion of sodium-kaolinite at pH = 3. The positive iron oxide particles, which adsorb preferentially on the surfaces of the clay mineral, neutralizes the kaolinite particles, so that no framework can be formed: the yield point disappears. When the pH is raised by the addition of NaOH, increasing negative charges are built at the edges and edge(-)/face(+) contacts are formed: the yield point increases. As the iron oxide is also increasingly re-charged with increasing pH, the edge(-)/face(+) contacts disappear again and the yield point decreases. The yield point is zero when the iron oxide is added to a kaolinite

dispersion at pH = 9.5 (curve C). By the addition of acid, the iron oxide becomes increasingly positively charged and bridges the negative kaolinite particles in a rigid framework. The yield point increases to a sharp maximum. Too high positive charging of the iron oxide particles promotes their adsorption on the kaolinite basal surfaces. The kaolinite(-)/iron oxide(+)/kaolinite(-) framework breaks up and the yield point decreases strongly, finally reaching a similar condition as in curve B (Jasmund and Lagaly, 1993).

Chemical modification of the kaolinite surfaces can be an effective way to control the flow properties of kaolinite dispersions. Until now, there are no studies on this subject. We report, in Chapter 5, the effects of the interlayer and surface grafting of alcohol-like molecules on the flow properties of kaolinite dispersions. The changes and, to some point, the control of the flow properties of the dispersions was successfully achieved by chemical modification of the kaolinite, and are for the first time, described.

2.10 Conclusion

X-Ray diffractometry, FTIR spectroscopy and thermal analysis constitute the most important analytical methods when investigating kaolinite and its derivatives. Kaolinite shows a smaller cationic exchange and adsorption capacity than many other clay minerals. Nevertheless, its high availability and low cost turn this clay mineral into an interesting industrial material. Chemical modification of kaolinite can take place either on the external surfaces or also in the interlayer surfaces. Total delamination of kaolinite will curl the layers to an halloysite-like morphology. Modified kaolinites might present a great industrial importance, as many different properties of the material can be tuned in a more or less controllable way, rendering its industrial use rentable where unmodified kaolinite would not even be a choice. In addition, the preparation of nanocomposites [modified clay mineral/organic polymer] with improved properties due to an optimized interaction between the phases is one of the major challenges in kaolinite chemistry.

CHAPTER 3
PREPARATION AND CHARACTERIZATION OF
GRAFTED KAOLINITE DERIVATIVES

3.1 Introduction

As previously discussed, a more in-depth study of the grafting reactions of kaolinite was one of the major aims of this work. Our studies started with the synthesis of the phenylphosphonic acid (PPA) derivative and by the reaction of kaolinite with similar substances. The research on such reactions brought unexpected results, with the conclusion that PPA does not react topotactic with kaolinite. Instead, the clay mineral structure is destroyed and aluminum compounds were obtained. Chapter 6 contains a detailed discussion of these results.

After having narrowed the spectrum of substances that form grafted derivatives by a topotactic reaction with kaolinite to alcohol-like molecules, we started a systematic study of such reactions, using many different grafting agents. Pre-expanded kaolinite was reacted with a series of diols, glycol mono-ethers and alcohols. Most reactions were successful, and many new grafted derivatives were obtained. The following sections describe these syntheses as well as the characterization of the compounds.

3.2 Preparation of Precursors

None of the grafting agents used were capable of intercalating in the raw kaolinite (control reactions with raw kaolinite were made, and are discussed in the sequence). To give the grafting agents access to the interlayer hydroxyl groups of kaolinite, the clay mineral was previously expanded with one of the usual intercalation agents, such as DMSO, NMF, urea, hydrazine or potassium acetate.

The DMSO intercalated compound was preferred because of its higher thermal stability (in contrast to the hydrazine intercalation compound, which deintercalates readily at room temperature), low toxicity (in contrast to NMF or hydrazine), possibility to eliminate excess non-intercalated material by drying (in contrast to urea or potassium acetate) and the ease of preparation.

3.2.1 Preparation of the Kaolinite-DMSO Intercalation Compound

This well-known intercalation compound was obtained by the reaction of raw kaolinite with liquid DMSO. According to Olejnik *et al.* (1968) the DMSO was adjusted to a water content of 9 % (v/v) to obtain the maximal intercalation speed. Typically, 50 g kaolinite was reacted with 100 ml DMSO/water solution. The dispersion was sonicated for 30 minutes in a ultrasonic water-bath (ultrasonic lab cleaner) at 60 °C and then kept under agitation at room temperature for 2 weeks. The mild ultrasonic treatment was found to decrease the time needed for almost total intercalation in more than one week, without noticeable decrease in the crystallinity of the product as interpreted from XRPD data (results not shown). After this period, the resultant thick dispersion was centrifuged and the sediment dried at 50 °C for 3 days to eliminate the excess DMSO. No washing with dioxane was performed (Tunney and Detellier, 1993) as this was found to deintercalate a part of the DMSO, regenerating raw kaolinite with a $d_L = 7.15 \text{ \AA}$ (results not shown). The product obtained from the English SPS kaolinite will be denoted simply as K-DMSO and the one from the Brazilian amazonic kaolinite as K_{RC} -DMSO.

The XRPD patterns of the DMSO intercalates obtained from SPS and Brazilian kaolinite are shown on Fig. 3.1. The products show the intense reflection corresponding to a $d_L = 11.2 \text{ \AA}$. An intercalation ratio > 99 % was reached for the SPS kaolinite and ~ 97 % for

the Brazilian kaolinite. A resulting basal expansion of 4.0 Å is in accordance with the reference values (Gonzalez Garcia and Sanchez Camazano, 1965; Weiss *et al.*, 1966a).

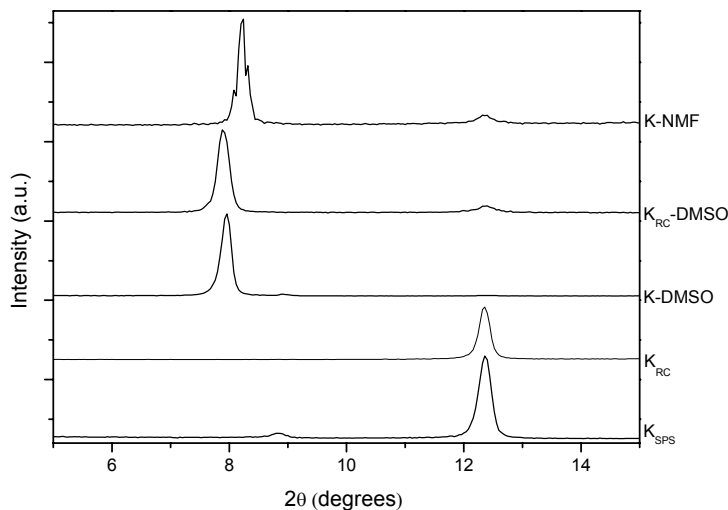


Fig. 3.1: XRPD patterns of SPS kaolinite (K_{SPS}), Brazilian kaolinite (K_{RC}), K-DMSO, K_{RC} -DMSO and K-NMF.

3.2.2 Preparation of the Kaolinite-NMF Intercalation Compound

Intercalation of NMF in the SPS kaolinite was obtained by a similar process. Typically, 50 g of kaolinite was dispersed in 100 ml of pure NMF. The system was sonicated for 30 minutes in a ultrasonic water-bath (ultrasonic lab cleaner) at 60 °C and then kept under agitation at room temperature for 2 weeks. After this period the resultant thick dispersion was centrifuged and the sediment dried at 50 °C for 2 days, in order to eliminate the excess NMF. This compound will be denoted as K-NMF.

Fig. 3.1 shows the XRPD pattern of the K-NMF compound. The product is identified by a strong reflection corresponding to a $d_L = 10.7$ Å. An intercalation ratio of ~ 96 % was reached. A resulting basal expansion of 3.6 Å is in accordance with the reference value (Weiss *et al.*, 1966a).

3.3 Grafting of Organic Molecules

For the grafting of kaolinite we tried to react molecules similar to the ones already known to form grafted derivatives. At the beginning of this study, following grafted derivatives have already been described (Table 3.1):

Table 3.1: Grafted derivatives of kaolinite described until the beginning of 2002.

Derivative	Reference
K-Ethylene glycol	Tunney and Detellier, 1993 Tunney and Detellier, 1994a
K-Ethylene glycol methyl ether	Tunney and Detellier, 1993
K-Di(ethylene glycol) butyl ether	Tunney and Detellier, 1993
K-1,2-Propanediol	Tunney and Detellier, 1993
K-1,3-Propanediol	Tunney and Detellier, 1993
K-Methanol	Tunney and Detellier, 1996a Komori <i>et al.</i> , 2000
K-Ethanolamine	Tunney and Detellier, 1997
K-3-Amino-1-propanol ^a	Tunney and Detellier, 1997

^a reference text not clear on this compound, see section 2.6.1.2

The table above does not contain the PPA derivatives, for the motives already discussed (Section 3.1).

All the grafting agents listed in Table 3.1 present an alcohol-like structure. Ethylene glycol and the propanediols are diols. Ethylene glycol methyl ether and di(ethylene glycol) butyl ether are ethers, but also have a alcohol-like hydroxyl group. Ethanolamine and 3-amino-1-propanol are amino-alcohols.

Having these facts in mind, we decided to concentrate our grafting studies on three groups of compounds: diols, glycol mono-ethers and simple alcohols.

3.3.1 Reaction with Diols

3.3.1.1 Grafting reactions

We tried to react kaolinite with a series of diols (Fig. 3.2), beginning by the repetition of the already known reactions with ethylene glycol and 1,2- and 1,3-propanediols and trying new reactions with all four positional isomers of butanediol as well as with 1,6-hexanediol and 1,8-octanediol. We also tried the grafting reaction with the branched-chain 2,2-dimethyl-1,3-propanediol.

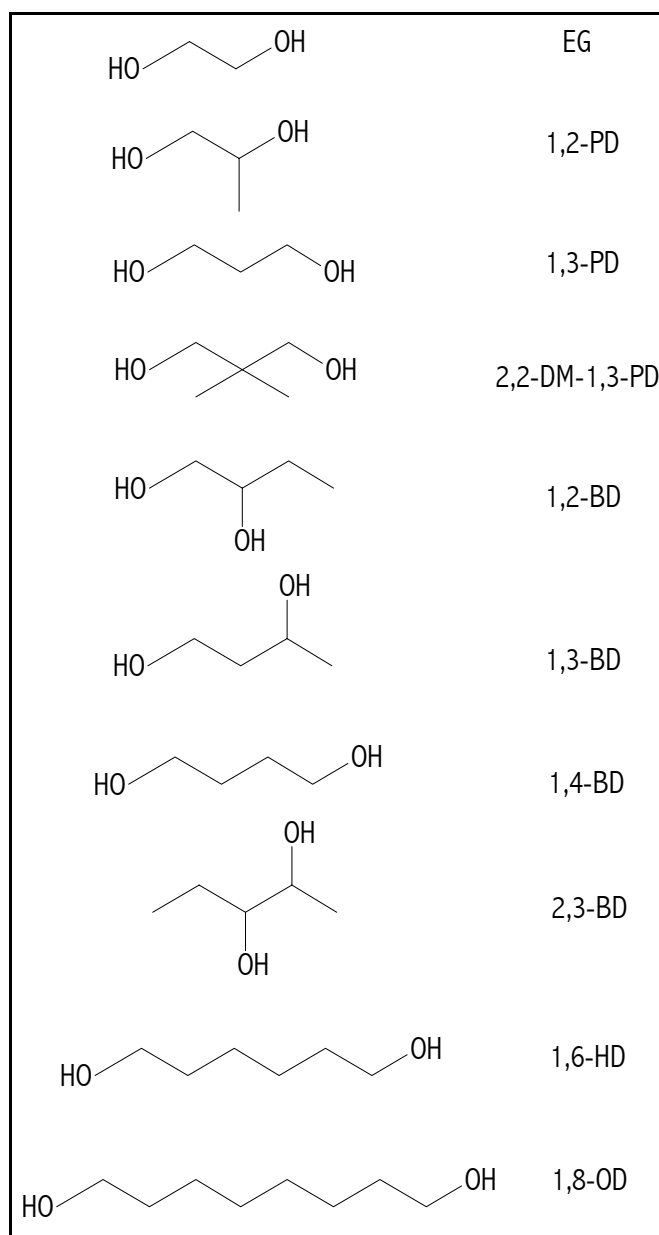


Fig. 3.2: Diols used in grafting reactions with K-DMSO.

The reactions were made by dispersing 10 g K-DMSO in ~ 80 ml of the liquid diol and refluxing this mixture with constant stirring to the boiling of the diol (or to the limit temperature of 230 °C) under N₂ atmosphere for 24 hours. When the diol was solid at room temperature (2,2-dimethyl-1,3-propanediol, 1,6-hexanediol and 1,8-octanediol) the K-DMSO was ground by hand with ~ 50 g diol and this mixture was then slowly melted and refluxed as the other samples. Table 3.2 lists all the reactions and the name given to each product.

After refluxing, the samples were cooled to room temperature and centrifuged to remove excess diol, and the resultant product was washed. In the case of solid diols, a small amount of ethanol was added to the product (while still liquid) to avoid total solidification and allow centrifugation.

The washing phase was essential, not only to eliminate the excess diol but mostly to assure that only grafted molecules would be present in the interlayer spaces of kaolinite: Characteristic of intercalation compounds is that the intercalated moieties can be deintercalated by washing with the appropriate solvent.

Bearing that in mind, the reaction products were quickly washed in an initial step with water, in order to remove the excess diol, and centrifuged. Subsequently, the products were washed at least twice with water, ethanol, acetone, ethyl ether and finally with cyclohexane (in this sequence). Each individual washing step lasted from 3 to 15 h (stirring time). The whole washing process needed typically 4 to 5 days.

The washed products were dried at 60 °C for 20 h and stored for further use.

3.3.1.2 Characterization

Fig. 3.3 shows the XRPD patterns of the products obtained in reaction of K-DMSO with diols, the basal spacings of the products are listed in Table 3.2. K-EG presented a basal spacing of 9.3 Å, in accordance with the expected value of 9.4 Å (Tunney and Detellier, 1993) and 9.5 Å (Tunney and Detellier, 1993). The reaction with 1,2-propanediol (K-12PD) yielded a phase with a basal spacing of 10.8 Å, in accordance with the previously described values of 10.9 Å (Tunney and Detellier, 1993) and 10.8 Å (Itagaki and Kuroda, 2003). The reaction with 1,3-propanediol (K-13PD) yielded a product with a basal spacing of 9.6 Å attesting the value of 9.8 Å obtained by Tunney and Detellier (1993), but differing from the value of 11.0 and 11.1 Å described by Itagaki and Kuroda (2003). It must be remembered, however, that the products described by Itagaki and Kuroda (2003) were obtained not by direct grafting as here described, but by the transesterification from the methanol-kaolinite

derivative. These authors assumed that the 11.1 Å phase of the derivative with 13PD would correspond to a case where the organic molecules are grafted by one alcohol ending only. The 11.0 Å phase (obtained by extending the reaction time from 1 to 5 days) was attributed to a bridge-like grafting, by the diol reacting at both alcohol groups. As our product presented a basal spacing of 9.6 Å, this assumption could not be further analyzed. In a control reaction, the reaction time of our synthesis was extended to 5 days. In this case, the same phase with a basal spacing of 9.6 Å was also obtained (results not shown).

The content of recovered raw kaolinite in the compounds above described was very low (< 2%), indicating a very high grafting efficiency with the diols.

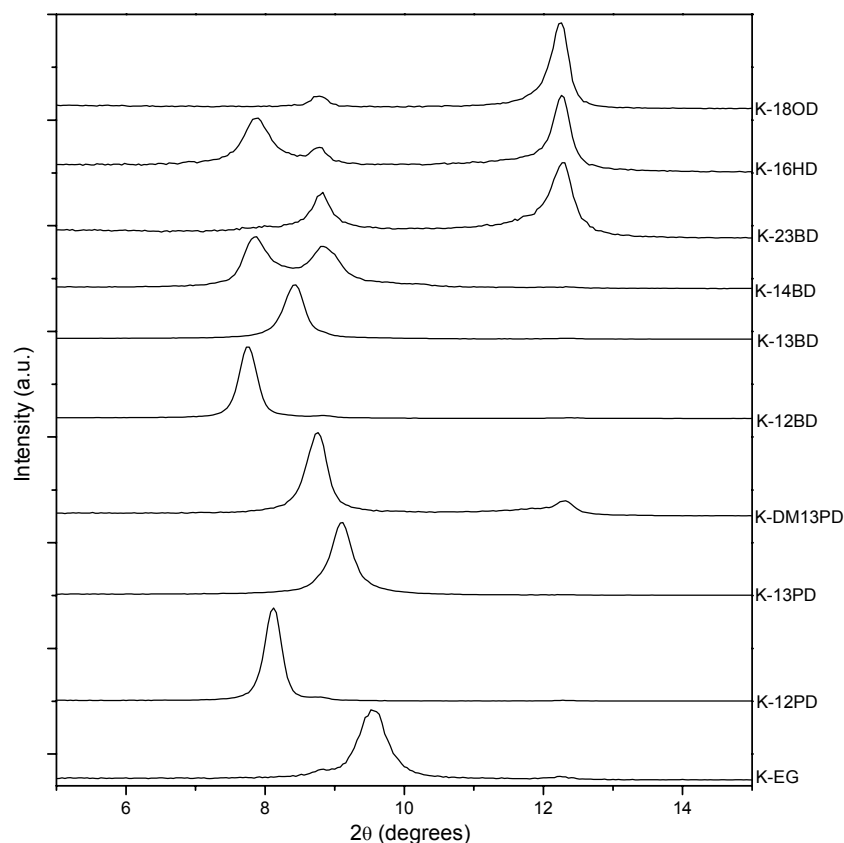


Fig. 3.3: XRPD patterns of the reaction products of K-DMSO with diols

Reacting K-DMSO with 2,2-dimethyl-1,3-propanediol for 24 h (K-DM13PD) resulted in the formation of a phase with a basal spacing of 10.1 Å (0.5 Å higher than the 13PD compound). Approximately 15% of raw kaolinite were also detected, indicating a partial

collapse of the intercalated precursor during the grafting reaction, which was not observed during the reaction with the unbranched diol.

Table 3.2: Diol-grafted kaolinites, basal spacings (d_L) and comparison with literature values ($d_L(\text{lit})$).

Diol	Product	d_L (Å)	$d_L(\text{lit})$ (Å)
Ethylene glycol	K-EG	9.3	9.5 ^a
			9.4 ^b
1,2-Propanediol	K-12PD	10.9	10.9 ^a
			10.8 ^c
1,3-Propanediol	K-13PD	9.6	9.8 ^a
			11.0-11.1 ^c
2,2-Dimethyl-1,3-propanediol	K-DM13PD	10.1 ^d	-
1,2-Butanediol	K-12BD	11.4	11.8 ^e
1,3-Butanediol	K-13BD	11.3	11.6 ^e
1,4-Butanediol	K-14BD	11.3 (55%)	-
		10.0 (45%)	
2,3-Butanediol	K-23BD	10.1 ^f	-
1,6-Hexanediol	K-16HD	11.1 ^g	-
1,8-Octanediol	- ^h	-	-

^a Tunney and Detellier (1993)

^b Tunney and Detellier (1994a)

^c Itagaki and Kuroda (2003)

^d ~ 15% unreacted kaolinite

^e Murakami *et al.* (2004)

^f ~ 65 % unreacted kaolinite

^g ~ 70 % unreacted kaolinite

^h no product formed, raw kaolinite with $d_L = 7.15$ Å recovered

The reaction of K-DMSO with 1,2-butanediol yielded a product (K-12BD) with a basal spacing of 11.3 Å. 1,3-Butanediol reacted to form a product (K-13BD) with a basal spacing of 10.4 Å. Both products presented basal spacings slightly smaller than the samples described by Murakami *et al.* (2004) ($d_L = 11.8$ and 11.6 Å), obtained from transesterification of the methanol-kaolinite compound. It was proposed that methanol molecules (or methoxy groups) would be co-intercalated in the interlayer spaces (Itagaki and Kuroda, 2003; Murakami *et al.*, 2004), what could account for the higher basal spacings of these compounds. The reaction with 1,4-butanediol yielded two phases, with basal spacings of 11.3 Å and 10.0 Å, with an approximate ratio of 55 % to 45 %. These two phases possibly reflect two different

arrangements of the diol molecules in the interlayer spaces. Reacting K-DMSO with 2,3-butanediol (K-23BD) produced a small amount (~ 35%) of a phase with basal spacing of 10.1 Å but recovered ~ 65% of unreacted kaolinite, showing a collapse of the intercalated precursor during the grafting reaction. Possibly, some kind of steric hindrance to the grafting is responsible for this fact (see section 2.6.2.1).

The reaction with 1,6-hexanediol yielded ~ 30 % of a phase with a basal spacing of 11.1 Å, and recovered ~ 70 % of unreacted kaolinite. In the diffraction pattern (Fig. 3.3) a reflection corresponding to a basal spacing of 10.0 Å is also observed. This reflection is attributed to the 5 % mica present in the original kaolinite sample. As the crystallinity of the final product is reduced, (diffraction pattern is vertically expanded for clarity reasons), the mica, which is not affected by this treatment, is now clearly identifiable. The mica reflection at 10.0 Å is not to be confused with the reflection at 10.0 or 10.1 Å present in some other compounds (K-DM13PD, K-14BD or K-23BD). The intensity of these other phases is always too high to be attributed to the 5% mica present on the kaolinite sample. Only in K-16HD and K-18OD is this reflection attributed to mica.

Reacting K-DMSO with 1,8-octanediol did not produce any grafted phase, instead, raw kaolinite was recovered. The crystallinity of the kaolinite was much reduced, as attested by the comparison with the intensity of the mica reflection at 10.0 Å.

These results show that the reactivity of kaolinite towards esterification with diols decreased quickly with the increase of the alkyl chain length, as butanediols reacted quantitatively, hexanediol yielded just 30 % product and octanediol did not react at all.

Fig. 3.4 and 3.5 show the FTIR spectra of the diol-grafted kaolinites. The most significant changes after grafting are noticed at the bands attributed to the hydroxyl groups. The inner-surface hydroxyl bands (3694, 3668, 3652 and 938 cm^{-1}) of the grafted kaolinites were weakened or even absent in some cases (in relation to the inner-hydroxyl bands at 3620 and 912 cm^{-1} , whose intensities should not be affected by grafting). New bands observed in the 3650-3300 cm^{-1} and 3000-2800 cm^{-1} regions are related to the interaction of the grafted molecules with the neighboring unreacted inner-surface hydroxyl groups and to the stretching modes of C-H bonds on the organic molecules, respectively. The broad band at ~ 3450 cm^{-1} is attributed to remnants of adsorbed or even co-intercalated water. The K-16HD compound showed smaller changes, as the sample contains ~ 70% unreacted kaolinite. These results are in accordance with the previously described spectra of kaolinite grafted with ethylene glycol

(Tunney and Detellier, 1994a), 1,2- and 1,3-propanediols (Iatagaki and Kuroda, 2003) and 1,2- and 1,3-butanediols (Murakami *et al.*, 2004).

All compounds presented a weak broad band around 1630 cm^{-1} also indicating remnants of adsorbed water on the kaolinite particles (Tunney and Detellier, 1994a). K-13PD and K-13BD also had a weak band at 1693 cm^{-1} . This band can either be attributed to a carbonyl group resulting from oxidation of the diols but also to the deformation mode of intercalated water (Brandt *et al.* 2003). It is also possible that the two phenomena occur in the same product.

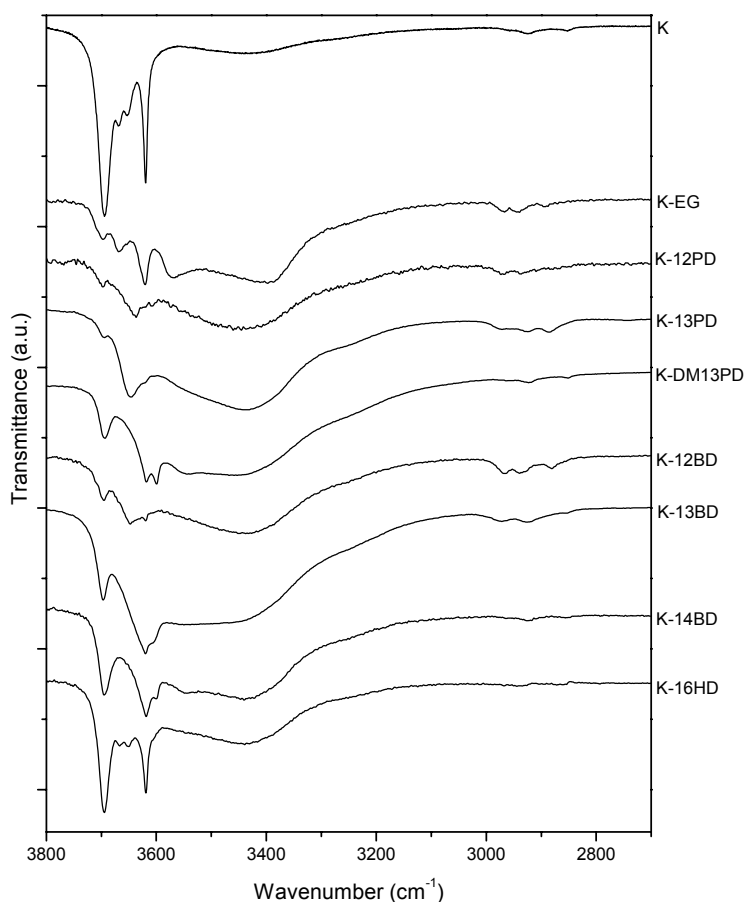


Fig. 3.4: FTIR spectra of the diol-grafted kaolinites between 3800 and 2700 cm^{-1} .

Hypsochromic shift of the Si-O skeletal bands between 1000 cm^{-1} and 1150 cm^{-1} is indicative of the perturbation of the tetrahedral silica surface of the layers by the organic molecules present in the interlayer spaces (Tunney and Detellier, 1994a; 1996b).

A slight bathochromic shift of the inner-hydroxyl bending mode at 912 cm^{-1} may indicate a small extent of keying of part of the organic molecules into the ditrigonal cavity of

the tetrahedral silica side of the kaolinite layers, affecting thus this otherwise “hidden” hydroxyl group (Tunney and Detellier, 1996b). However, a hypsochromic shift of the 3620 cm^{-1} band formerly also attributed to keying on the ditrigonal hole (Tunney and Detellier, 1997) was not detected.

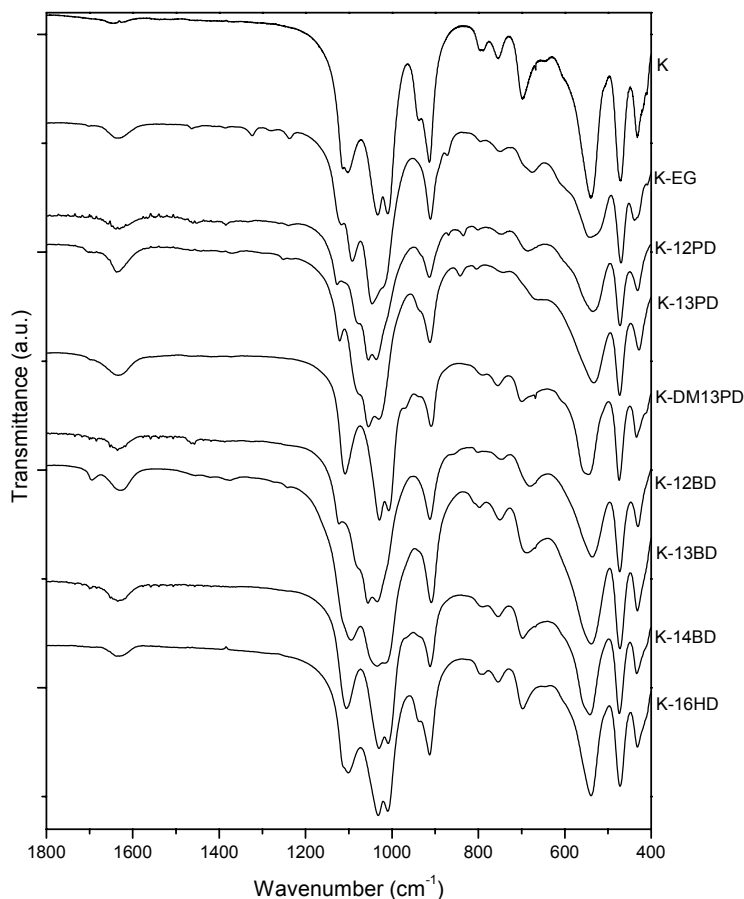


Fig. 3.5: FTIR spectra of the diol-grafted kaolinites between 1800 and 400 cm^{-1} .

The thermal behavior of the diol-grafted kaolinites varied only slightly between the different samples. The TG/DTA measurements showed exothermal processes related to the combustion and elimination of the grafted molecules associated with mass loss at 250-350 $^{\circ}\text{C}$ for all compounds, as previously described (Tunney and Detellier, 1993, 1994a, 1996a, 1997; Komori *et al.*, 2000; Brandt *et al.*, 2003; Itagaki & Kuroda, 2003; Murakami *et al.*, 2004). Fig. 3.6 exemplifies this typical behavior showing the TG/DTA curves for K-12BD and K-13BD. The thermal behavior of these two compounds is also the same as previously described by Murakami *et al.* (2004) for the products obtained by transesterification of the methanol-kaolinite.

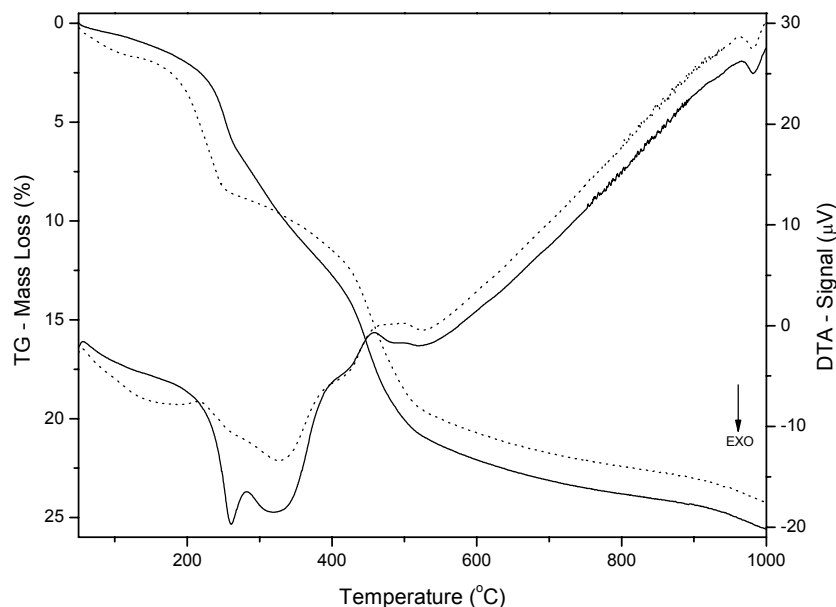


Fig. 3.6: TG/DTA curves from K-12BD (continuous lines) and K-13BD (dotted lines).

The high-temperature loss of organic matter is, alone, not a sufficient proof of chemical bonding between the grafting agent and kaolinite. Some intercalated molecules also exhibit unexpectedly high elimination temperatures. For example, the kaolinite intercalation compound with 1-methyl-2-pyrrolidone remains stable up to 431 °C (Gardolinski *et al.*, 1999).

Dehydroxylation of the unreacted OH groups of the kaolinite structure was observed at temperatures up to 100 °C below the dehydration temperature of the raw kaolinite (extrapolated onset temperatures: raw kaolinite = 500 °C; K-12BD = 423 °C; K-13BD = 417 °C). It was already demonstrated that the thermal stability of kaolinite is directly related to its crystallinity (Brindley & Lemaitre, 1987). As the dehydroxylation process is diffusion-controlled, particle size is also a very important factor (Brindley & Lemaitre, 1987). This explains the lower dehydroxylation temperatures of the grafted derivatives, which are of lower crystallinity than the raw kaolinite and possibly of smaller particle sizes after thermal decomposition of the grafted molecules.

Elemental analysis (CHNS, see Table 3.3) showed that, during grafting, elimination of DMSO from the interlayer spaces of kaolinite was almost quantitative. Only the compound K-14BD still presented some noticeable content of sulfur. This fact may be related to the two different phases observed for this sample in the XRPD patterns.

Table 3.3: Elemental analysis for the diol-grafted kaolinites.

Compound	C (w%)	H (w%)	S (w%)
K-EG	4.24	2.02	0
K-12PD	7.02	2.56	0.21
K-13PD	5.87	2.24	0
K-DM13PD	0.93	1.79	0.10
K-12BD	8.73	2.66	0.21
K-13BD	3.50	2.28	0
K-14BD	3.08	2.02	1.51
K-23BD	0.90	1.5	0.06
K-16HD	2.82	1.73	0

The low carbon content on the compounds K-DM13PD and K-23BD reveal the lower reactivity of kaolinite towards grafting with these two diols. The interlayer expansion observed is maintained by a relatively small number of organic moieties, as fewer molecules were able to graft to the inner-surface hydroxyl groups than in the other derivatives.

The carbon content of the compounds K-EG, K-12PD and K-13PD was slightly lower than the values previously reported. Tunney and Detellier (1994a) reported a carbon content of 6.51 % for kaolinite grafted with ethylene glycol. Itagaki and Kuroda (2003) obtained carbon contents of 7.60 % and 8.33/7.78 % for kaolinite grafted with 1,2-propanediol and 1,3-propanediol, respectively (the two values for the latter compound represent the simple grafted derivative and the derivative with the diol molecules grafted at both groups (bridge)). These differences may reveal a smaller reactivity of the kaolinite sample used in our experiments. Possibly, the higher amount of carbon present in the derivatives described by Itagaki and Kuroda may be related to the presence of co-grafted methoxy groups in the compounds obtained by transesterification. Another possibility that cannot be discarded is the presence of organic molecules adsorbed on the compounds described by the other authors. It may be that some residue of the grafting agents is still present on those compounds. Our washing process of the grafted kaolinites was much longer and more exhaustive than the simple washing described by the other authors.

Transmission electron micrographs of the diol-grafted kaolinites (not shown) showed that the average size and the usual pseudo-hexagonal morphology of the kaolinite particles

were unchanged. Grafting proceeds as a topotactic reaction, affecting only the interlayer space, without noticeable morphological changes of the particles.

3.3.2 Reaction with Glycol Mono-Ethers

3.3.2.1 Grafting reactions

The only examples of grafting of kaolinite with glycol mono-ethers were described by Tunney and Detellier (1993) (reaction of K-DMSO with ethylene glycol methyl ether and di(ethylene glycol) butyl ether). We tried the reaction of K-DMSO with a series of similar molecules (Fig. 3.7): ethylene glycol ethyl and hexadecyl ethers; di(ethylene glycol) methyl, butyl, hexyl, 2-ethylhexyl and decyl ethers; tri(propylene glycol) butyl ether; tetra(ethylene glycol) hexadecyl ether. We also tried to graft kaolinite with the aromatic molecules 2-phenoxy-ethanol (ethylene glycol phenyl ether) and 1-phenoxy-2-propanol (propylene glycol phenyl ether).

Typically, 10 g K-DMSO were mixed with ~ 80 ml of the liquid glycol ether and the dispersions were refluxed with constant stirring at the boiling temperature of the organic phase (or to the maximum temperature of 230 °C) under N₂ atmosphere for 24 hours. The reaction with the decyl and hexadecyl ethers were downscaled using 1 g glycol ether and ~ 0.5 g K-DMSO. In these reactions (with solid organic phase), the K-DMSO was ground by hand with the glycol ether and this mixture was then slowly melted and refluxed as the other samples. Table 3.4 lists these reactions and the name given to each product.

After refluxing, the samples were cooled to room temperature and centrifuged to remove the excess of the organic phase and the resultant product was washed. In the case of solid glycol ethers, a small amount of ethanol was added to the product (while still liquid) to avoid total solidification and allow centrifugation.

The washing steps were made in a similar way as with the diol reactions. The major difference occurred during the washing of the products with water insoluble grafting agents. In such cases, the products were washed with ethanol and acetone (1x each) prior to the normal washing cycle beginning with water described in section 3.3.1.1.

Once washed, the products were dried at 60 °C for 20 h and stored for further use.

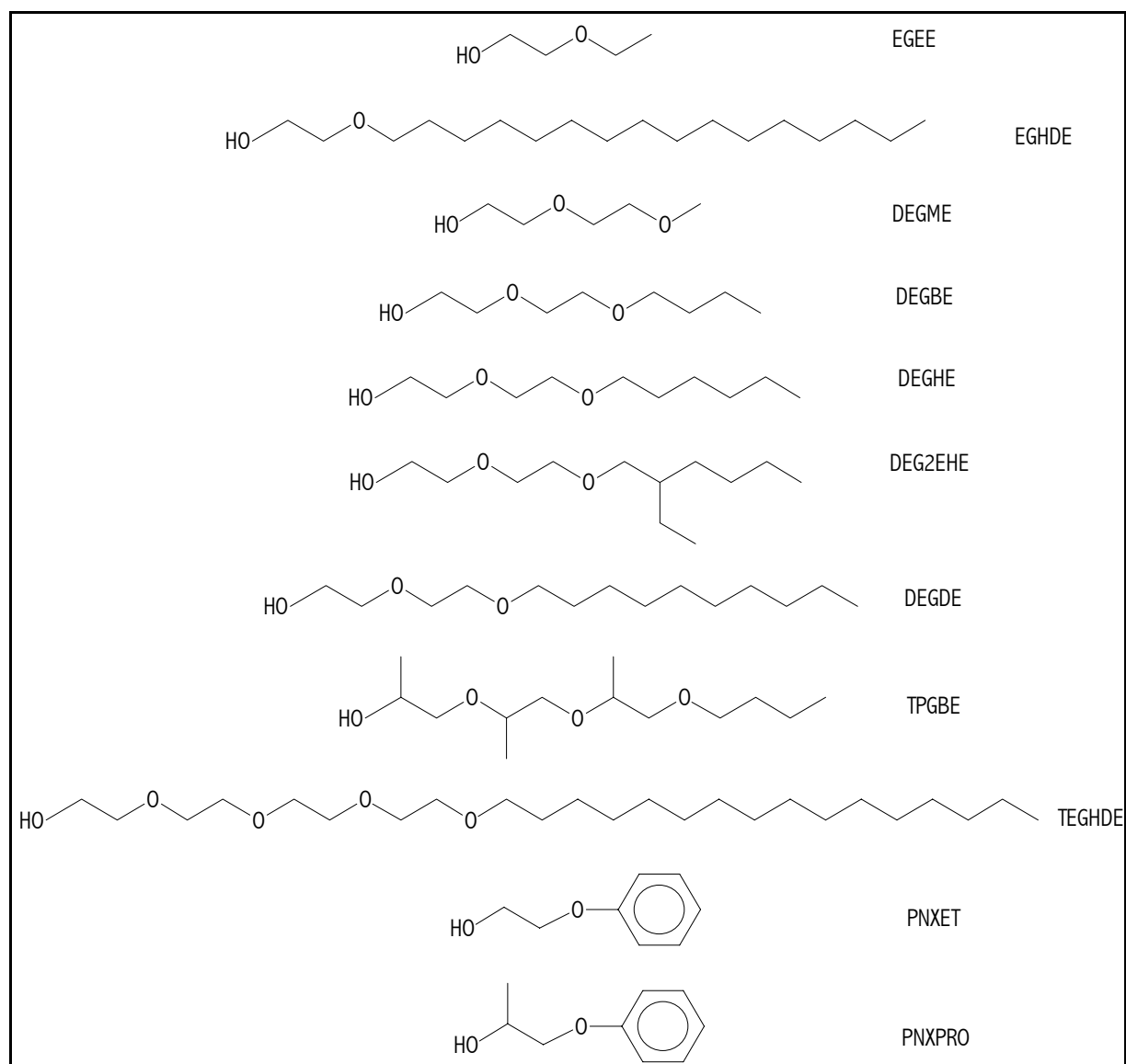


Fig. 3.7: Glycol mono-ethers used in grafting reactions with K-DMSO.

3.3.2.2 Characterization

Fig. 3.8 shows the XRPD patterns of the kaolinite derivatives obtained with glycol mono-ethers, the basal spacings of the products are listed in Table 3.4, as well as comparison values from the literature. Almost all products presented basal spacings between 10.6 and 11.3 Å, which corresponds to a monolayer of oxyethylene units sandwiched between two kaolinite layers (Tunney and Detellier, 1996b; Gardolinski *et al.*, 2000). The grafted molecules very likely are arranged in a monolayer, with the alkyl chains lying almost parallel to the kaolinite layers. An exception is the higher basal spacing of the 2-phenoxy-ethanol derivative (K-PnxEt, $d_L=13.3$ Å) indicating the grafted molecules to be inclined to the basal plane surface of the clay mineral. In a control reaction, 2-phenoxy-ethanol was reacted in the

same way as described above with K_{RC} -DMSO. The product also presented a basal spacing of 13.3 Å, but the reaction yield was much lower, with more than 60 % raw kaolinite being present in the sample. The reason for this reduced reactivity is not clear.

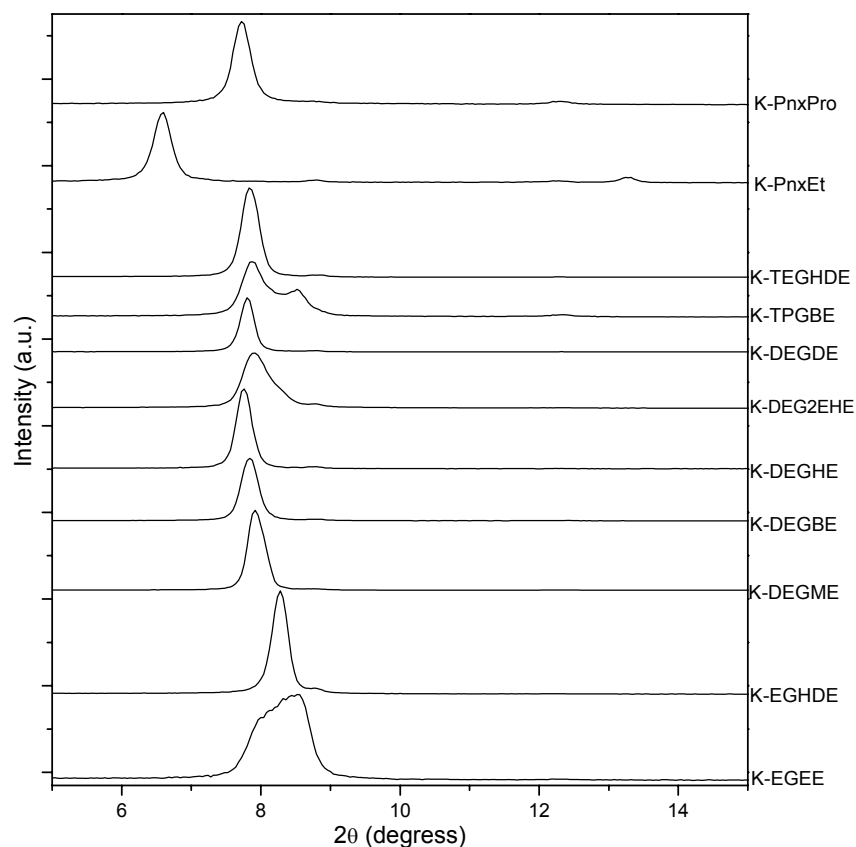


Fig. 3.8: XRPD patterns of the reaction products of K-DMSO with glycol mono-ethers

The K-EGEE compound presented an additional phase with 10.3 Å basal spacing besides the phase at 11.0 Å. The first order reflection of these two phases consisted of a partially collapsed broadened reflection. A basal spacing of 10.6 Å was reported for the ethylene glycol *methyl* ether derivative (Tunney and Detellier, 1993), showing that the phase at 10.3 Å must present a different arrangement of the organic molecules in the interlayer spaces. Also the K-TPGBE compound contained ~ 30 % of a phase at 10.3 Å.

K-DEGBE was the only compound here prepared that was already described (Tunney and Detellier, 1993). The basal spacing of 11.2 Å here obtained is exactly the same as reported previously.

Table 3.4: Glycol mono-ether-grafted kaolinites, basal spacings (d_L) and comparison with literature values ($d_L(\text{lit})$).

Glycol Ether	Product	d_L (Å)	$d_L(\text{lit})$ (Å)
Ethylene glycol ethyl ether	K-EGEE	11.0 (40%) 10.3 (60%)	(10.6) ^{a, b}
Ethylene glycol hexadecyl ether	K-EGHDE	10.6	-
Di(ethylene glycol) methyl ether	K-DEGME	11.0	-
Di(ethylene glycol) butyl ether	K-DEGBE	11.2	11.2 ^b
Di(ethylene glycol) hexyl ether	K-DEGHE	11.3	-
Di(ethylene glycol) 2-ethylhexyl ether	K-DEG2EHE	11.3	-
Di(ethylene glycol) decyl ether	K-DEGDE	11.2	-
Tri(propylene glycol) butyl ether	K-TPGBE	11.3 (70%) 10.3 (30%)	-
Tetra(ethylene glycol) hexadecyl ether	K-TEGHDE	11.3	-
2-Phenoxy-ethanol	K-PnxEt	13.3	-
1-Phenoxy-2-propanol	K-PnxPro	11.3	-

^a d_L value for the ethylene glycol methyl ether derivative

^b Tunney and Detellier, 1993

Fig. 3.9 and 3.10 show the FTIR spectra of the kaolinite glycol mono-ether derivatives. As already seen in the spectra of the diol derivatives, the major changes in relation to the spectrum of raw kaolinite was observed in the bands attributed to the hydroxyl groups. The inner-surface hydroxyl bands (3694 , 3668 , 3652 and 938 cm^{-1}) of the grafted kaolinites were weakened or even absent in some cases (in relation to the inner-hydroxyl bands at 3620 and 912 cm^{-1} , whose intensities should not be affected by grafting). New bands at 3630 - 3650 cm^{-1} and 3600 cm^{-1} are attributed to the formation of hydrogen bonds between the unreacted inner-surface hydroxyl groups of kaolinite with the oxygen atoms of the glycol ethers. It is also possible to imagine that a small amount of co-intercalated, not grafted, glycol-ether molecules (which may not have been totally removed even by the exhaustive washing process) can still exist the interlayer spaces. The diffusion-dependent elimination of such molecules would be hindered by the interaction with the grafted molecules. The interaction of these intercalated molecules with the kaolinite hydroxyl groups would contribute for the formation of the new bands. There is, however, no decisive proof of the

existence of such co-intercalated species in the grafted compounds. New bands in the 3000-2800 cm^{-1} region are attributed to the C-H stretching of the organic molecules. A broad band in the region around 3450 cm^{-1} is related to water still present in the samples.

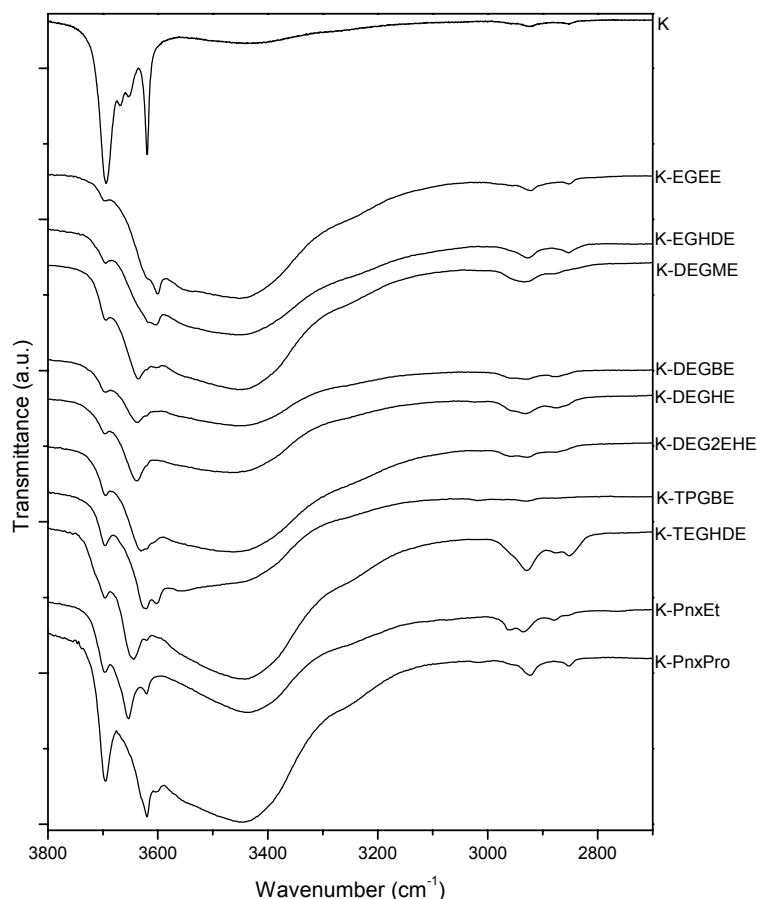


Fig. 3.9: FTIR spectra of the glycol mono-ether-grafted kaolinites between 3800 and 2700 cm^{-1} .

All compounds presented a weak broad band around 1630 cm^{-1} also indicating remnants of adsorbed water on the kaolinite particles (Tunney and Detellier, 1994a). Most of the also presented a weak band at 1693 cm^{-1} . As already discussed for the diol derivatives, this band can either be attributed to a carbonyl group resulting from oxidation of the diols but also to the deformation mode of intercalated water (Brandt *et al.* 2003).

For the lower frequencies region, almost the same remarks as presented in the interpretation of the spectra of the diol derivatives are valid. Hypsochromic shifts of the Si-O skeletal bands between 1000 cm^{-1} and 1150 cm^{-1} are indicative of the perturbation of the

tetrahedral silica surface of the layers by the organic molecules present in the interlayer spaces (Tunney and Detellier, 1994a; 1996b).

A slight bathochromic shift of the inner-hydroxyl bending mode (originally at 912 cm^{-1}) may indicate a small extent of keying of parts of the organic molecules into the ditrigonal cavities, affecting this otherwise “hidden” hydroxyl group (Tunney and Detellier, 1996b).

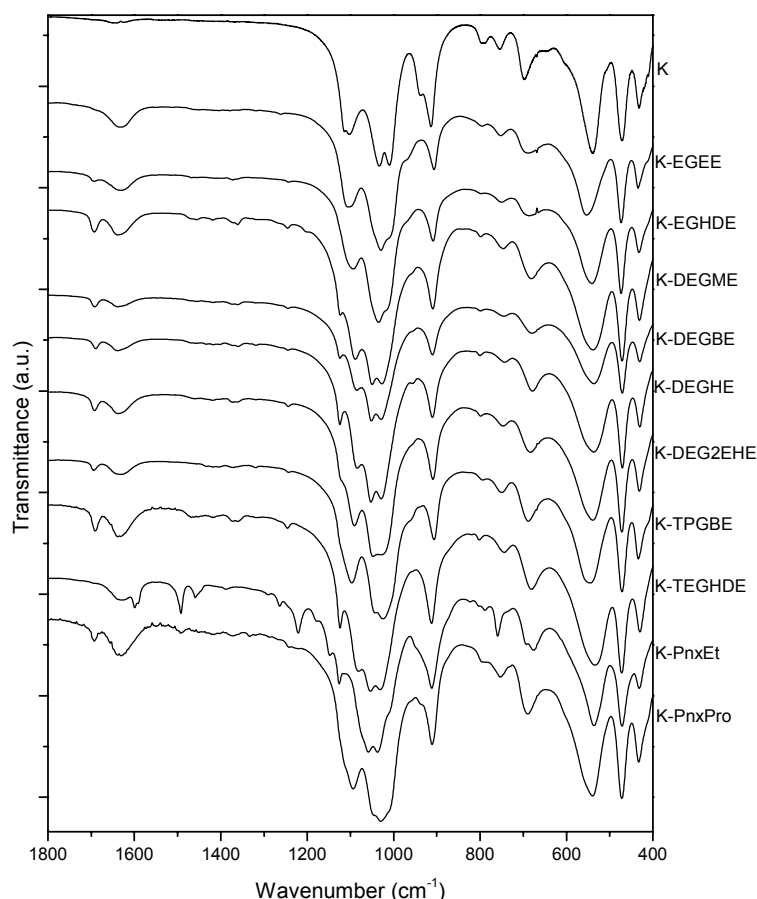


Fig. 3.10: FTIR spectra of the glycol mono-ether-grafted kaolinites between 1800 and 400 cm^{-1} .

K-PnxEt and K-PnxPro also show the characteristic bands of the aromatic phenyl group around 1400 cm^{-1} . The intensity of the bands was higher for K-PnxEt, suggesting a higher degree of grafting (as attested by the thermal and elemental analyses).

The thermal behavior of the glycol ether derivatives of kaolinite was very similar to the behavior of the diol derivatives previously discussed. After an initial small step of endothermic loss of adsorbed water at low temperatures, the organic matter was exothermically decomposed between $200\text{-}300\text{ }^{\circ}\text{C}$. This process lowered the crystallinity of the

kaolinite particles, as the dehydroxylation of the interlayer hydroxyl groups was observed at lower temperatures than in the raw kaolinite.

Fig. 3.11 shows two typical TG/DTA curves of the glycol ether derivatives. The compound K-PnxEt presented a higher thermal stability. In fact this, compound showed the highest decomposition temperature of the organic matter of all grafted derivative prepared during these studies (extrapolated onset temperature = 285 °C, exothermal events at 205 °C and 295 °C). This fact is very likely a consequence of the stronger interaction between the grafted organic molecules. As the grafted molecules are almost perpendicular to the basal plane surface, the molecules, especially the phenyl rings, can interact more strongly with each other than in the compounds with the grafted molecules lying parallel to the basal plane surface (as in K-PnxPro: extrapolated onset temperature = 200 °C, exothermal event centered at 280 °C).

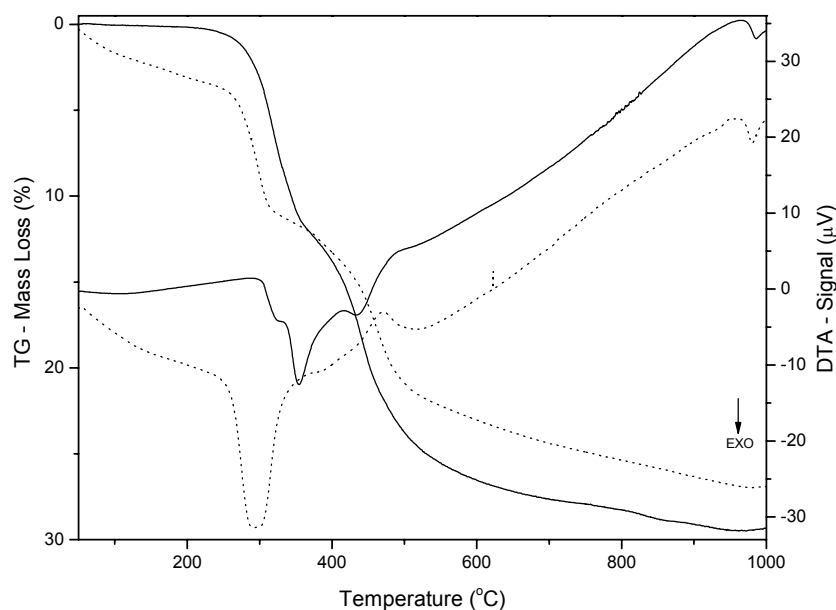


Fig. 3.11: TG/DTA curves for K-PnxEt (continuous lines) and K-DEGHE (dotted lines).

Table 3.5 shows the results of the elemental analysis of the glycol ether derivatives of kaolinite. In comparison with the diol derivatives, the elimination of DMSO was not so effective in some cases, K-DEGHE still presented 2.39 % sulfur. In other compounds, the elimination was complete. K-PnxEt had the highest carbon content of all grafted derivatives obtained (C = 14.6 %). The CHNS results and TG data indicate the stoichiometry of the formula unit for this compound as $\text{Al}_2\text{Si}_2\text{O}_5(\text{OH})_3\text{OH}_{0.52}(\text{C}_2\text{H}_4\text{OC}_6\text{H}_5)_{0.48}$

(theoretical/experimental contents: C = 14.6 % / 14.6 %, H = 2.5 % / 2.4 %, O = 12.0 % / 12.6 %). This is almost equivalent to a ratio grafting agent/kaolinite of 0.5, *i.e.* one of every six inner-surface hydroxyl groups is esterified. The organic content of 0.48 mol/formula unit is lower than for the derivatives with ethylene glycol (0.8 mol/f.u., C = 6.5 %, Tunney and Detellier, 1994a) and 1,2- and 1,3-propanediol (0.63 mol/f.u., C = 7.6 % and 0.68 mol/f.u., C = 8.3 %, Itagaki and Kuroda, 2003). This is the direct consequence of the larger size of the 2-phenoxy-ethanol molecules. The fact that the 2-phenoxy-ethanol molecules are inclined to the basal plane surface reduces the steric hindrance of the hydroxyl groups and leads to a higher degree of esterification. The 1-phenoxy-2-propanol derivative showed a much lower carbon content (C = 6.2 %) as the organic molecules are parallel to the basal plane surface, indicated by the basal spacing of 11.3 Å.

Table 3.5: Elemental analysis for the glycol mono-ether-grafted kaolinites.

Compound	C (w%)	H (w%)	S (w%)
K-EGEE	3.55	2.15	0.93
K-EGHDE	7.69	2.57	0
K-DEGME	6.22	2.37	0.88
K-DEGBE	7.3	2.53	1.06
K-DEGHE	6.8	2.49	2.39
K-DEG2EHE	5.57	2.41	0.88
K-DEGDE	6.99	2.52	0.13
K-TPGBE	6.23	2.39	2.31
K-TEGHDE	8.76	2.67	0.51
K-PnxEt	14.65	2.39	0.37
K-PnxPro	6.24	2.19	1.52

3.3.3 Reaction with Alcohols

3.3.3.1 Grafting reactions

We tried the reaction of K-DMSO with a series of different alcohols: n-alkanols from 3 to 10 and 14 carbon atoms, 2-butanol and tert-butanol, benzyl alcohol, 1- and 2-phenyl-ethanol (Fig. 3.12). The syntheses were carried out in the same way as with the diols and glycol mono-ethers. 10 g K-DMSO were dispersed in ~ 80 ml of the alcohol and refluxed with constant stirring at the boiling temperature of the organic phase (or to the maximum

temperature of 230 °C) under N₂ atmosphere for 24 hours. For the reaction with the solid 1-tetradecanol, the K-DMSO was ground by hand with the alcohol and this mixture was then slowly melted and refluxed as the other samples. Table 3.6 lists these reactions and the name given to each product.

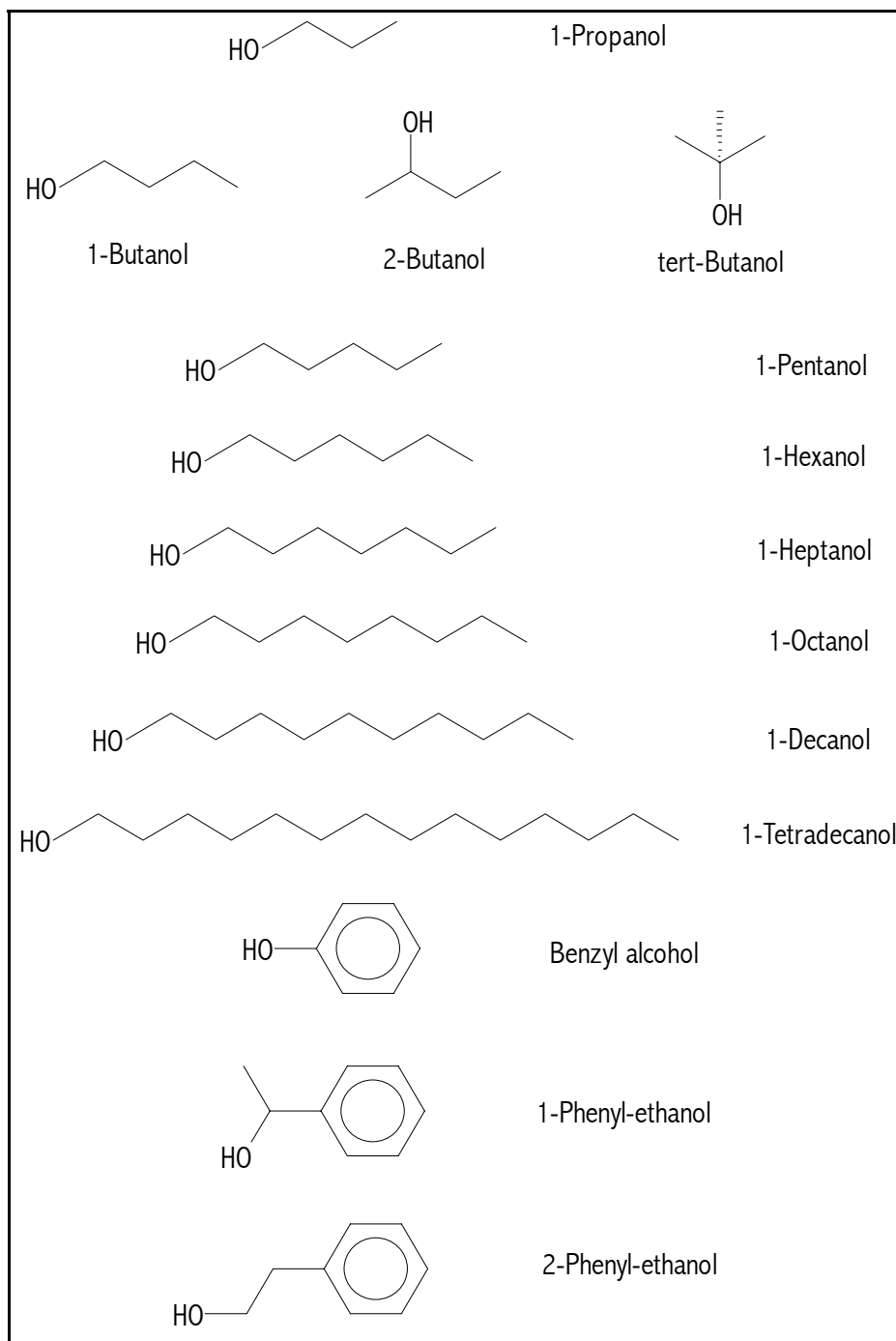


Fig. 3.12: Alcohols used in grafting reactions with K-DMSO.

After refluxing, the samples were cooled to room temperature and centrifuged to remove the excess of organic phase, and the resultant product was washed. In the reaction with 1-tetradecanol, a small amount of ethanol was added to the product (while still liquid), to avoid total solidification and allow centrifugation.

The washing steps were made in the same way as the previously described reactions (see section 3.3.1.1 and 3.3.2.1). The products from reactions with water-insoluble alcohols were washed with ethanol and acetone (1x each) prior to the normal washing cycle beginning with water described in section 3.3.1.1.

Once washed, the products were dried at 60 °C for 20 h and stored for further use.

3.3.3.2 Characterization

The XRPD patterns of the products obtained from reaction of alcohols with K-DMSO revealed that only the n-alkanols from 5 to 10 carbon atoms were grafted. The products obtained from all other reactions presented only broadened kaolinite reflections with a basal spacing around 7.1 Å, revealing the elimination of K-DMSO without the intercalation or grafting of the organic molecules. Fig. 3.13 shows the XRPD patterns of the derivatives obtained with n-alkanols. Table 3.6 lists the basal spacings of the products.

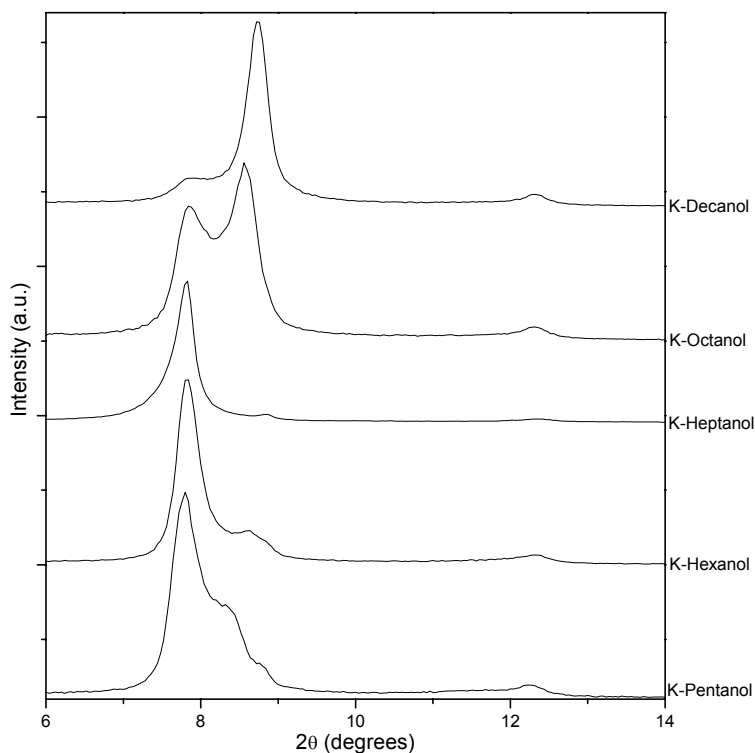


Fig. 3.13: XRPD patterns of the reaction products of K-DMSO with n-alkanols.

The diffraction patterns reveal that two different phases were obtained. K-Heptanol presented only a phase with a basal spacing of 11.3 Å, while the other alcohols produced the 11.2-11.3 Å phase and another phase with a basal spacing of 10.1-10.3 Å (similar results were also obtained in the K-14BD, KEGEE and K-TPGEBE products, as already discussed). In all cases, the content of unreacted raw kaolinite was very low, below 5 %. Fig. 3.14 shows how the content of the 11.3 Å phase varied with increasing alkyl chain length.

Table 3.6: Alcohol-grafted kaolinites and basal spacings (d_L) of the products.

Glycol Ether	Product	d_L (Å)
1-Propanol	- ^a	-
1-Butanol	- ^a	-
2-Butanol	- ^a	-
tert-Butanol	- ^a	-
1-Pentanol	K-Pentanol	11.3 (75%) 10.3 (25%)
1-Hexanol	K-Hexanol	11.3 (85%) 10.2 (15%)
1-Heptanol	K-Heptanol	11.3
1-Octanol	K-Octanol	11.3 (40%) 10.3 (60%)
1-Decanol	K-Decanol	11.2 (10%) 10.1 (90%)
1-Tetradecanol	- ^a	-
Benzyl alcohol	- ^a	-
1-Phenyl-ethanol	- ^a	-
2-Phenyl-ethanol	- ^a	-

^a no product formed, raw kaolinite with $d_L = 7.1$ Å recovered

The 11.3 Å phase is analogous to the phase obtained in most glycol mono-ether derivatives, and is consistent with the parallel arrangement of a alcohol monolayer between the kaolinite layers, as discussed previously. The exact identity and arrangement of the alcohol molecules in the 10.3 Å phases cannot be proposed based only in the XRPD data.

The fact that n-alkanols with less than 5 carbon atoms did not react with kaolinite is most possibly due to the high leaching power of these alcohols on K-DMSO. These short

chain alcohols deintercalate DMSO from the interlayer spaces recovering the raw kaolinite before the grafting reaction starts. Benzyl alcohol and 1- and 2-phenyl-ethanol also did not react with K-DMSO, in contrast to 2-phenoxy ethanol and 1-phenoxy-2-propanol. Evidently, the inductive effect of the oxygen atom of the glycol unit is needed to promote the esterification reaction. This effect also enables the reaction of large molecules such as tetra(ethylene glycol) hexadecyl ether with kaolinite, even if n-alkanols with shorter chains (1-tetradecanol) do not react.

In control reactions also K_{RC}-DMSO and K-NMF were reacted with 2-phenyl-ethanol at the same conditions as in the other cases. Both precursors, like K-DMSO, did not react and only unreacted kaolinite was detected (results not shown).

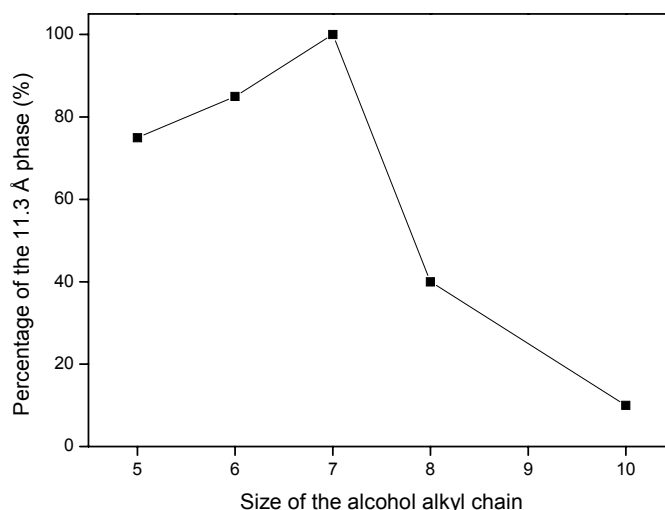


Fig. 3.14: Percentage of the 11.3 Å phase on the n-alkanol derivatives of kaolinite as a function of the number of carbon atoms in the alcohol alkyl chain.

Fig. 3.15 and 3.16 show the FTIR spectra of the n-alkanol derivatives. As expected, the major changes in relation to raw kaolinite were observed in the hydroxyl stretching region. The intensity of the band at 3695 cm⁻¹ was lowered in relation to the inner-hydroxyl band at 3620 cm⁻¹ and the small bands at 3669 cm⁻¹ and 3652 cm⁻¹ were absent in the modified kaolinites. All compounds presented a new band at 3600 cm⁻¹, but the intensity of this band on K-Heptanol was much lower than in the other alkanol-derivatives. Most of the derivatives obtained from diols and glycol ethers also presented a band at 3600 cm⁻¹, as already discussed. This band has been attributed to the hydrogen bonding between the

unreacted kaolinite hydroxyl groups and the hydroxyl or oxygen of the grafted organic molecules present in the interlayer spaces. If all interlayer alcohol molecules would be grafted to the kaolinite hydroxyl groups, this band should be absent, as the oxygen atoms of all alcohol molecules would be grafted to kaolinite and should therefore be unavailable for further hydrogen bonding.

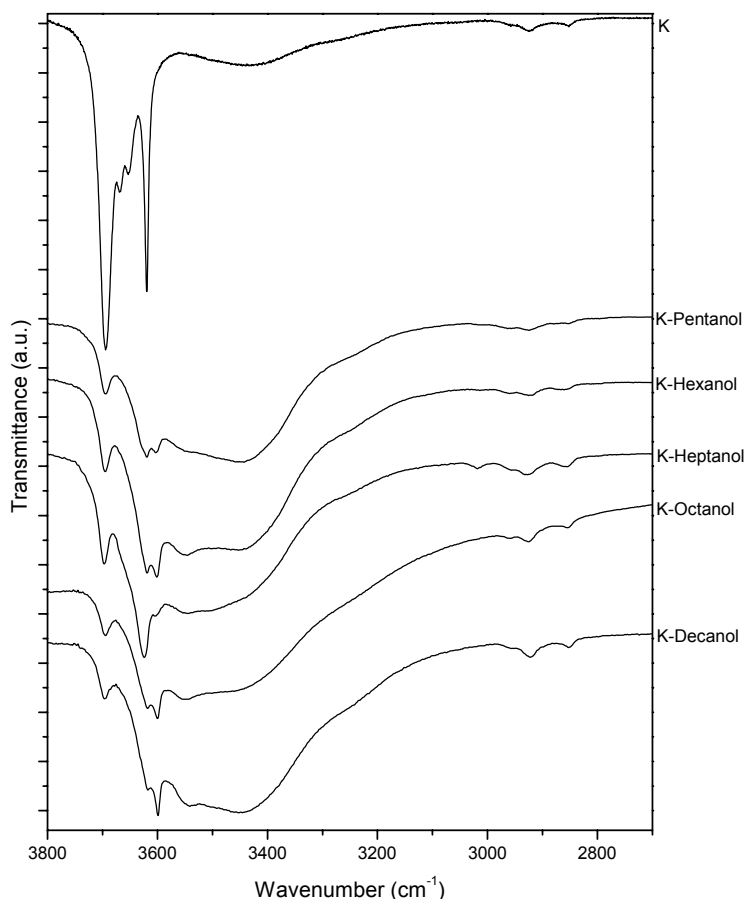


Fig. 3.15: FTIR spectra of the n-alkanol-grafted kaolinites between 3800 and 2700 cm⁻¹.

This fact suggests that some alcohol molecules in the n-alkanol derivatives are only intercalated and not grafted. As the intensity of the 3600 cm⁻¹ band was the lowest for K-Heptanol, which did not present the 10.3 Å phase, the question arises if this phase consists of kaolinite with intercalated, non-grafted alkanol molecules, and if the same conclusions are also valid for K-14BD, K-EGEE and K-TPGBE.

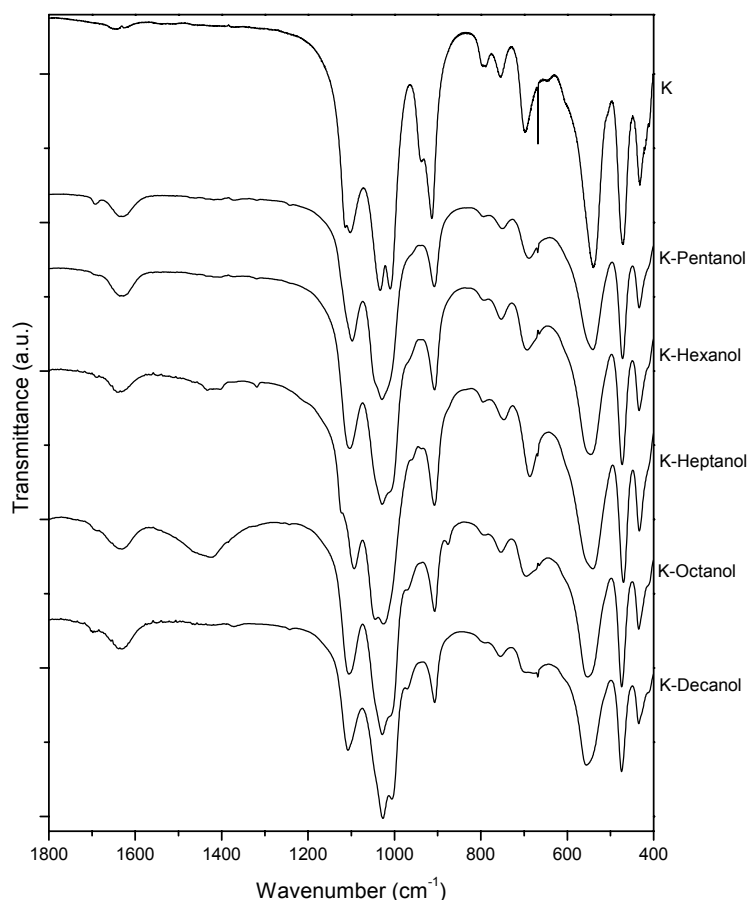


Fig. 3.16: FTIR spectra of the n-alkanol-grafted kaolinites between 1800 and 400 cm⁻¹.

It may be proposed that the grafting occurs in two successive steps. First, the matrix is fully intercalated by displacing of DMSO before the grafting reaction proceeds. In such scenario, the grafted phase, which has a higher basal spacing, is formed from the edges of the kaolinite particles to the inside, as the deformation of the layers during expansion of the interlayer space would be much higher when starting from the center of the particle. As the reaction front reaches a certain depth inside the particles, the diffusion of the water molecules formed during grafting will not be fast enough, and water will accumulate in the interlayer spaces. Accumulation of water would turn the formation of the ester unfavorable and the reaction would stop, providing the outer regions of the particles a basal spacing of 11.3 Å and the 10.3 Å for the center.

The total stability of these products against exhaustive washing is established, and constitutes an evidence against the presence of “normal” 10.3 Å intercalated phase. However, if the theory above described is taken into consideration, the intercalated phase is protected

against washing by the grafted edges of the particles, and should remain stable even after the most aggressive washing procedure, as long as the grafted molecules do not allow the diffusion of the intercalated alcohols out of the particles.

This intercalation/grafting theory, though plausible, cannot explain the variation of the ratio between the two phases with the increase of the alcohol size. Mostly, it completely fails to explain why K-Heptanol did not present the 10.3 Å phase at all. The explanation why the grafted phase would have a higher basal spacing than the intercalated phase is also not clear. During the intercalation and grafting of ethylene glycol (Tunney and Detellier, 1994a) and 1,2- and 1,3-propanediols (Itagaki and Kuroda, 2003) in kaolinite, it was showed that the grafted phases have slightly smaller basal spacings than the intercalated ones, which seems reasonable, since one oxygen and two hydrogen atoms are eliminated. In addition, extended reaction times should give enough time for all the interlayer water to diffuse out of the particles, allowing the grafting reaction to proceed. Some preliminar experiments done with extended reaction time (up to 5 days) did not showed the reduction of the quantity of 10.3 Å formed (results not shown). These results were, however, not fully conclusive, as much unreacted kaolinite was recovered, possibly due to the decomposition of the already grafted products. Based on these facts, it still not clear if the 10.3 Å phase is indeed constituted of intercalated, non-grafted molecules.

The analysis of the remaining features of the spectra of the n-alkanol kaolinites is very similar to the diol and glycol-ether derivatives. C-H stretching bands in the 2800-3000 cm^{-1} region are clearly related to the alkyl chains of the alcohol molecules. A water band at 1630 cm^{-1} was observed in all compounds as well as small bands at 1693 cm^{-1} , which was previously interpreted either by the presence of intercalated water or due to partial carbonylation of the alcohol molecules. The intensity of this band was the lowest on K-Heptanol and highest on K-Decanol. If it is caused by carbonylated alcohol molecules, free (non-grafted) alcohol molecules must be present in all derivatives, apart from K-Heptanol. This may be another evidence that the 10.3 Å phase is caused by intercalated, non-grafted molecules. On the other hand, if one assumes that water is accumulated as described above, the fact that K-Heptanol does not present the 10.3 Å phase would also explain the virtual absence of intercalated water, canceling the evidence for non-grafted alcohol molecules. The correct attribution of the 1693 cm^{-1} band could be decisive in the elucidation of this question.

The hypsochromic shift of the skeletal Si-O stretching bands was smaller than for the diol and glycol ether derivatives, indicating that the alkyl chains interact less intensively with

the tetrahedral silica surface than glycolic units. In K-Decanol, these shifts were very small, indicating that these interactions in the 10.1 Å phase are weaker than in the 11.3 Å phase.

The bending mode of the inner-surface hydroxyl groups at 935 cm^{-1} was absent in all compounds and a small bathochromic shift of the inner hydroxyl band at 912 cm^{-1} indicates the possible keying of the grafted molecules into the ditrigonal holes of the tetrahedral silica surface, as already discussed for the diol and glycol ether derivatives.

The thermal behavior of the different n-alkanol derivatives showed some important differences between them (Fig. 3.17). K-Heptanol presented a small mass loss at low temperatures and a major step of exothermic mass loss with extrapolated onset temperature of $265\text{ }^{\circ}\text{C}$. The endothermic dehydroxylation of the matrix was observed at an extrapolated onset temperature of $455\text{ }^{\circ}\text{C}$. This is the typical behavior also observed for most diol and glycol ether derivatives. K-Decanol presented a major step of mass loss ($\sim 7.8\%$) with extrapolated onset temperature of $140\text{ }^{\circ}\text{C}$, in a slight endothermic process. This was followed by a small exothermic mass loss ($\sim 1.7\%$) with extrapolated onset temperature of $260\text{ }^{\circ}\text{C}$. The endothermic dehydroxylation of the matrix was also observed at $455\text{ }^{\circ}\text{C}$. The other derivatives presented an intermediate behavior between K-Heptanol and K-Decanol.

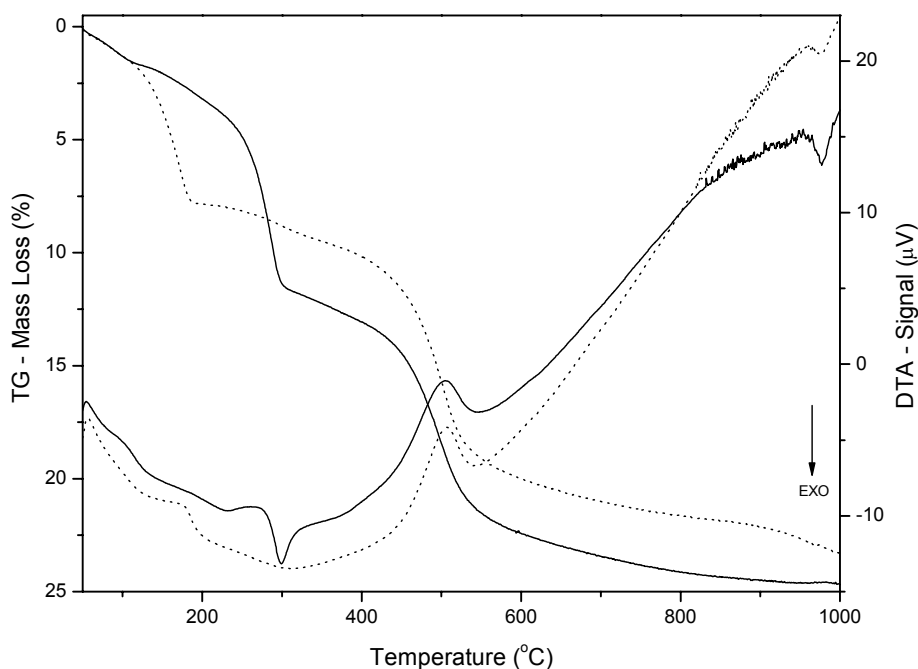


Fig. 3.17 TG/DTA curves from K-Heptanol (continuous lines) and K-Decanol (dotted lines).

This thermal behavior is a strong evidence that the 11.3 Å phase (the only one present in K-Heptanol) consists indeed of the grafted phase analogous to the diol or glycol ether derivatives. We assume that the 10.1 Å phase composing ~ 90 % of K-Decanol is responsible for the endothermic mass loss at 140 ° C. That would be a strong evidence for the assumption that in this phase the alcohol molecules are just intercalated and not grafted to the aluminol interlayer surfaces of kaolinite. The fact that the small second step of mass loss in K-Decanol presents almost the same onset temperature as in K-Heptanol is a further evidence that this step must correspond to the decomposition of the ~ 10 % of the 11.2 Å grafted-phase. If both phases are present in the same particle, as suggested above, the thermal elimination of the intercalated alcohol molecules must proceed as a diffusion process through the grafted phase present on the edges of the particles. In such case, a mechanism must be found by which water molecules would not be able to diffuse through this barrier but which would allow the alcohol molecules (or their thermal decomposition products) to be eliminated without hindrance. It becomes evident that this is a major evidence against the bi-phase particle theory above mentioned, suggesting that the two phases may be present in independent particles.

The possibility cannot be fully excluded, however, that both phases only contain grafted alcohol molecules and that structural differences between them are responsible for their different thermal behavior.

In any case, the results obtained from rheological measurements of aqueous dispersions of the modified kaolinites (Chapter 4) clearly indicate that simple adsorption of the n-alkanols on the kaolinite particles cannot explain the flow properties of the dispersions. Even if the 10.3 Å phase is indeed composed of intercalated alcohol molecules, the octahedral side of the outer basal plane surface (and the edge hydroxyl groups) of the particles is clearly grafted with the alcohols.

The elemental analysis of these compounds (Table 3.7) reveals that the elimination of DMSO was not totally complete, except for K-Hexanol. The sulfur present in these (and all other derivatives) is not direct indicative of the presence of intercalated DMSO molecules, as it is likely that this molecule would decompose at such high temperatures in the presence of the grafting agents. The carbon contents showed no relation to the amount of the 11.3 Å phase.

Table 3.7 Elemental analysis for the n-alkanol-grafted kaolinites.

Compound	C (w%)	H (w%)	S (w%)
K-Pentanol	3.55	2.15	0.93
K-Hexanol	7.69	2.57	0
K-Heptanol	6.22	2.37	0.88
K-Octanol	7.3	2.53	1.06
K-Decanol	6.8	2.49	2.39

3.3.4 Reaction with Thiols

Using the same procedures as described in the previous sections, K-DMSO was reacted with 1,3-propanedithiol and 1-butanethiol in the hope of gaining some insight in the reaction mechanism of kaolinite with alcohols or alcohol like molecules.

In both cases, no new phase was formed, and the XRPD patterns of the products revealed only broadened kaolinite reflections. Aside from the obvious differences between alcohols and thiols, which may be the cause for the lack of reaction, the temperature of the system with thiols was lower than with alcohols, as the boiling point of the thiols is lower. One cannot discard the possibility of reaction when the system is heated to higher temperatures (maybe at an autoclave). However, if the grafting reactions proceed as a traditional esterification (with elimination of the OH group from kaolinite) formation of an Al-S-C linkage is not very probable.

3.4 Conclusion

The inner-surface hydroxyl groups of kaolinite are reactive towards esterification with different types of alcohols, such as n-alkanols, diols, or long-chain glycol mono-ethers. The grafting agents must have easy access to the interlayer space *i.e.*, the grafting reactions proceed only when pre-intercalated kaolinite is used. The grafted derivatives of kaolinite are stable towards exhaustive washing, which would easily affect intercalation compounds. FTIR spectra and thermal behavior of the compounds also indicate the interlayer grafting. The grafted molecules arrange themselves in a monolayer between the kaolinite layers, leading to basal spacings around 11.3 Å.

The derivatives obtained from n-alkanols presented an additional phase with a basal spacing around 10.3 Å. The exact identity of this phase could not be unveiled, but it is likely that it contains intercalated, non-grafted alcohol molecules in addition to grafted alcohol molecules.

CHAPTER 4
RHEOLOGICAL PROPERTIES OF DISPERSIONS OF
GRAFTED KAOLINITES

4.1 Introduction

Rheological studies of kaolinite dispersions hardly presents any novelty, since much was already described, and the main interactions controlling the flow properties of such systems are understood (Jasmund and Lagaly, 1993; Lagaly *et al.*, 1997). On the other hand, the chemical modification of kaolinite by interlayer grafting is a relatively new research field, and the flow behavior of aqueous dispersions of such organoclays was not yet studied.

Rheological measurements of such dispersions could help elucidate the question how the grafted kaolinite particles interact with each other and with the dispersion medium. The possibility of controlling the flow properties of kaolinite dispersions by grafting is another motivation for these studies.

4.2 Experimental

4.2.1 Preparation of the Dispersions

Two different groups of grafted kaolinites were used in the rheological experiments, derivatives obtained by reaction with n-alkanols and with glycol mono-ethers (Table 4.1).

Table 4.1: Grafted kaolinites used in the preparation of aqueous dispersions for rheological measurements.

Type of grafted molecule	Compound
Glycol mono-ether	K-DEGME
	K-EGEE
	K-DEGBE
	K-TPGBE
	K-DEGHE
	K-DEH2EHE
n-Alkanol	K-Pentanol
	K-Hexanol
	K-Heptanol
	K-Octanol
	K-Decanol

For the preparation of aqueous dispersions, 0.5 g the dry grafted kaolinite (or raw kaolinite) were dispersed in 3.5 ml distilled water, agitated vigorously until complete homogenization and immediately measured in the rheometer. The solid content of the dispersions was 12.5 %(w/w).

4.2.2 Rheological Measurements

The rheological properties were studied with a Paar Physica UDS 200 (MP 31 plate-plate system, radius = 25 mm) at 20 °C using 1000 μ l of the dispersions. The shear rate $\dot{\gamma}$ was varied during the experiments in the following sequence (Fig 4.1): First, a shear rate $\dot{\gamma} = 100$

s^{-1} was applied for 10 s in order to homogenize the sample. This step was followed by 20 s resting ($\dot{\gamma} = 0$) so that the probe could rebuild any static aggregation structures. After the pause, the shear rate was linearly increased from $\dot{\gamma} = 0$ to $\dot{\gamma} = 1000 \text{ s}^{-1}$ within 60 s and immediately reduced in the same rate from $\dot{\gamma} = 1000 \text{ s}^{-1}$ to 0. Shear stress values were collected during the last two steps of the process.

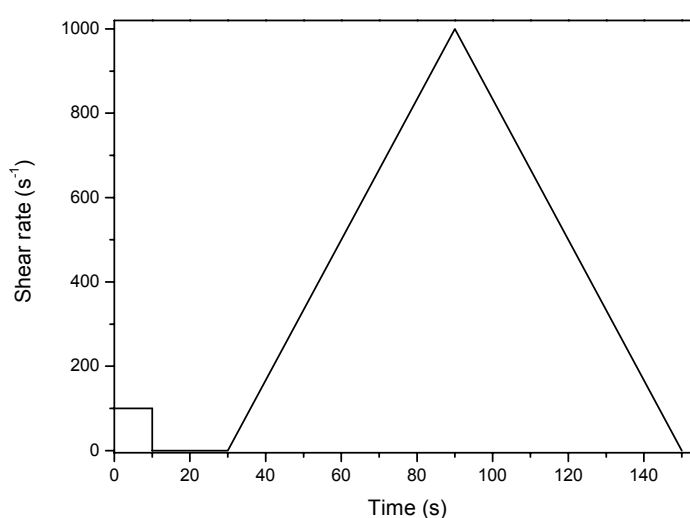


Fig. 4.1: Profile of the shear rate variation during the rheological experiments.

Three parameters derived from the measurements were used in the interpretation of the results: apparent viscosity, yield value and hysteresis area between the increasing and decreasing shear rate curves. The apparent viscosity is the shear stress/shear rate ratio at any shear rate, measured here at $\dot{\gamma} = 1000 \text{ s}^{-1}$ (Permien & Lagaly, 1994). The yield value was obtained by extrapolating the linear (or almost linear) section of the flow curves at the highest shear rates ($\dot{\gamma} \rightarrow 1000 \text{ s}^{-1}$) to $\dot{\gamma} = 0$ (Permien & Lagaly, 1994).

4.3 Results and Discussion

The aqueous dispersions of grafted kaolinite particles presented higher yield values and apparent viscosities than the corresponding dispersion of raw kaolinite (Fig. 4.2, 4.3). Yield values and apparent viscosities for the n-alkanol derivatives increased exponentially with the size of the alkyl chain (Fig. 4.4). The hysteresis area of the flow curves did not increase linearly with the number of carbon atoms of the grafted alkyl chains. The hysteresis area was very small for the pentanol, hexanol and heptanol derivatives and increased to 129 Pa/s and 555 Pa/s for the octanol and decanol derivatives.

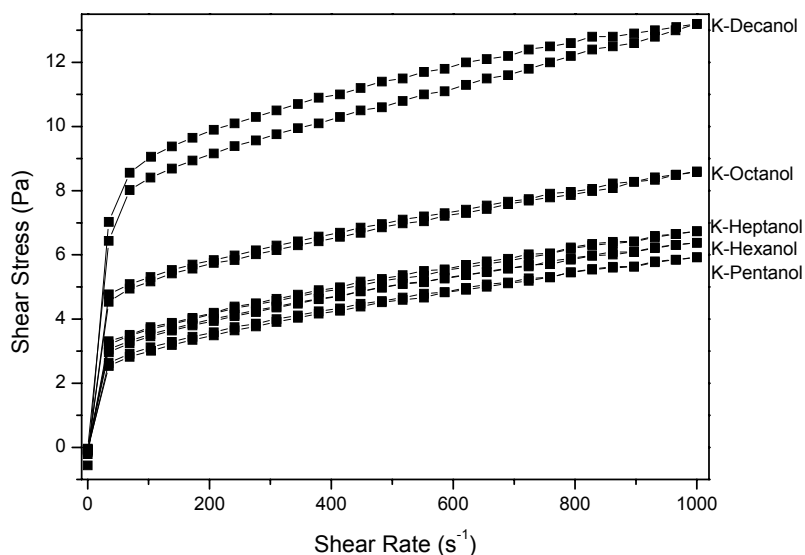


Fig. 4.2: Flow curves of aqueous dispersions of n-alkanol grafted kaolinite particles (solid content = 12.5 % (w/w)).

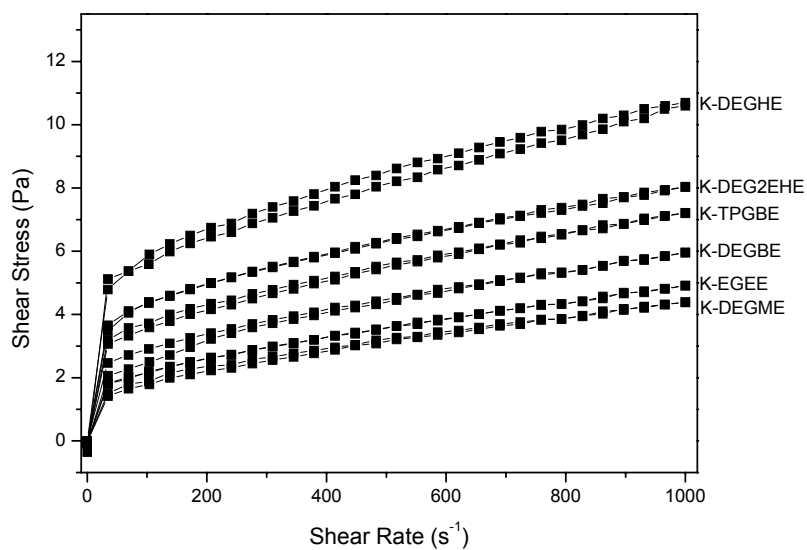


Fig. 4.3: Flow curves of aqueous dispersions of glycol mono ether grafted kaolinite particles (solid content = 12.5 % (w/w)).

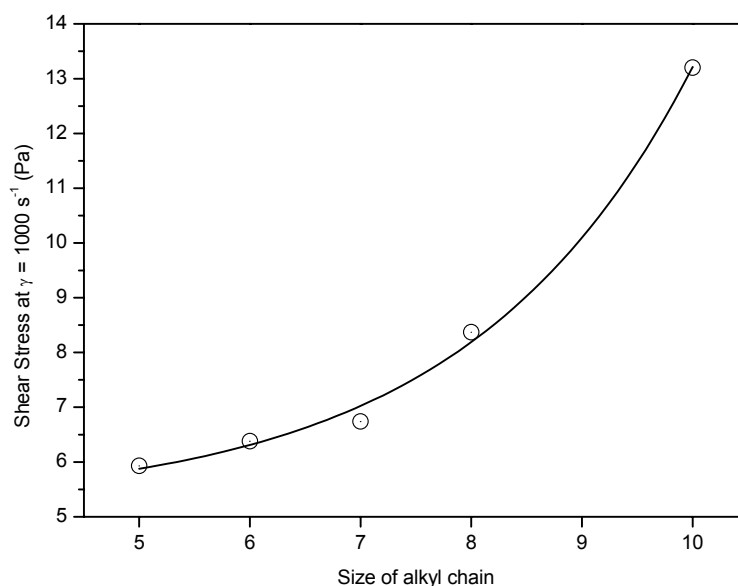


Fig. 4.4: Shear stress at $\dot{\gamma} = 1000 \text{ s}^{-1}$ for aqueous dispersions of kaolinite grafted with n-alkanols as a function of the number of carbon atoms in the alcohol alkyl chain (exponential fit: $R^2 = 0.9966$).

The glycol ether derivatives also showed an exponential increase of the apparent viscosity with the size of the grafted apolar ether rest (Fig. 4.5). The values for the ethylene glycol ethyl ether derivative and for the di(ethylene glycol) ether derivatives are lying on the same curve, leading to the conclusion that the size of the alkyl rest of the ether group is decisive for the interparticle interactions.

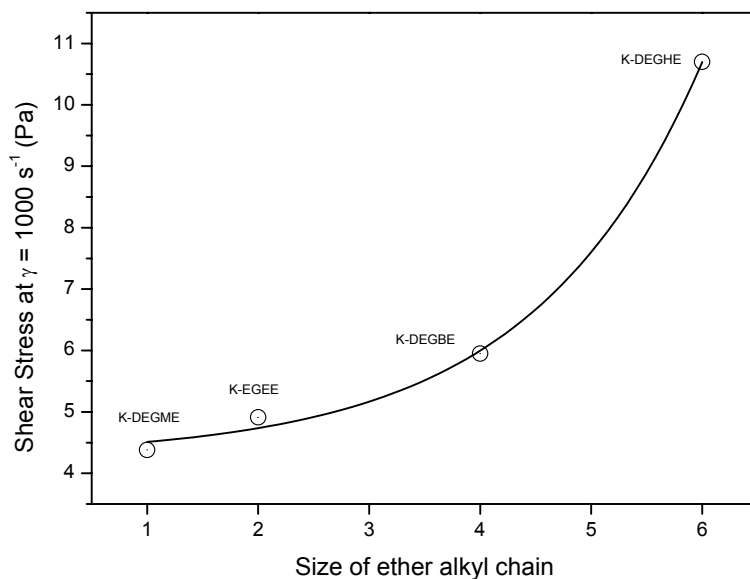


Fig. 4.5: Shear stress at $\dot{\gamma} = 1000 \text{ s}^{-1}$ for aqueous dispersions of kaolinite grafted with ethylene glycol ethyl ether and di(ethylene glycol) mono ethers as a function of the number of carbon atoms in the ether alkyl chain (exponential fit: $R^2 = 0.9979$).

The position of the flow curve of the tri (propylene glycol) butyl ether derivative (K-TPGBE) above the curve for the di(ethylene glycol) butyl ether derivative (K-DEGBE), also supports this assumption. The fact that the di(ethylene glycol) 2-ethylhexyl ether derivative (K-DEG2EHE) presents a lower yield value and apparent viscosity than the di(ethylene glycol) hexyl ether derivative (K-DEGHE) is explained in a similar way. The ethyl group on position 2 changes the linear hexyl chain into a linear butyl chain plus a rest. This configuration reduces the interaction between the particles so that the yield value and apparent viscosity lie between the values for the butyl and hexyl ether derivatives.

The rheology data indicate a close approximation of the kaolinite particles in the dispersion, with the octahedral sheets facing each other. In this arrangement the grafted apolar

chains can interact and are shielded against the polar aqueous medium. The particles must be in close contact since the apolar chains are relatively short. The stability of the dispersions decreased therefore with increasing apolar character of the grafted molecule. When the apolar moiety is too large (higher alkanols or glycol hexyl ethers), the particles aggregate, and the dispersion becomes unstable. The dispersions of ethylene glycol and propanediol-kaolinite were stable for longer periods than the dispersions of raw kaolinite whereas the octanol and decanol-kaolinite particles separated rapidly from the aqueous medium.

The exponential increase of the apparent viscosity with increasing alkyl chain can be viewed as a synergistic effect arising from the increasing interaction between the particles and the increasing apolar character of the kaolinite surface interacting with the aqueous medium.

The slight thixotropic character of the aqueous dispersions of kaolinite grafted with large apolar groups is also a consequence of the interaction between the grafted surfaces of the particles, which enable reversible aggregation/disaggregation processes.

Repeated washing of the grafted derivatives with ethanol, acetone and ethyl ether (beyond the washing steps already described) had no effect on the rheological properties of the dispersions (data not shown). The question arises what will be the effect when the organic molecules are only adsorbed and not grafted to the external particle surface. Raw kaolinite was dispersed in 1-pentanol and di(ethylene glycol) butyl ether for 24 h. The dispersions were washed and dried in the exact same manner as the grafted products. The XRPD of these products showed no changes of the basal spacing of raw kaolinite. The flow curves of aqueous dispersions of these products (Fig. 4.6) indicated that small amounts of alcohol or glycol ether remain adsorbed on kaolinite and contribute to a modest increase of the yield point and apparent viscosity. The values are distinctly smaller than for the dispersions of the grafted products, attesting that adsorption increases only slightly the apparent viscosity.

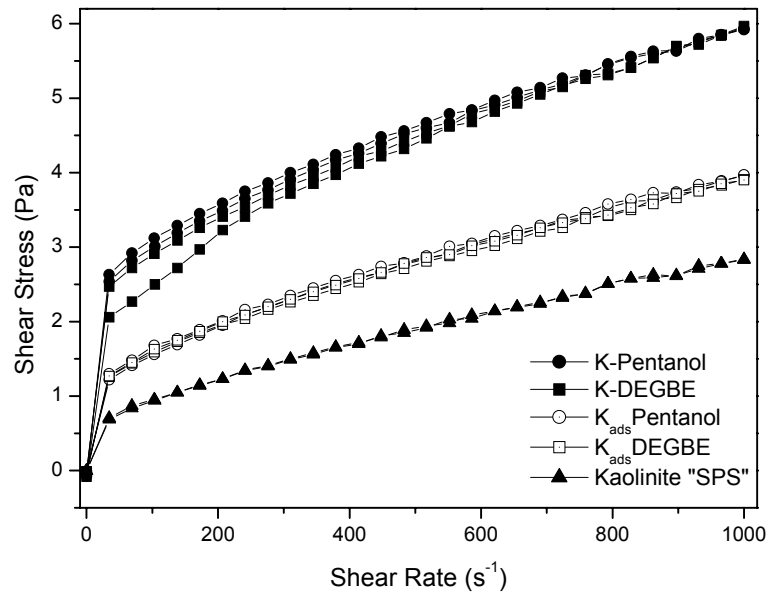


Fig. 4.6: Flow curves of aqueous dispersions of raw kaolinite; kaolinite adsorbed with di(ethylene) glycol butyl ether ($K_{ads}DEGBE$) and with pentanol ($K_{ads}Pentanol$); and of di(ethylene) glycol butyl ether and pentanol grafted kaolinites (solid content = 12.5 % (w/w)).

4.4 Conclusion

The stability of aqueous dispersions of grafted kaolinites decreased with increasing apolar character of the grafting groups. The yield point and apparent viscosity of the aqueous dispersions increased exponentially with the size of the alkyl moiety of the grafted groups. Grafting of organic molecules on kaolinite offers a valuable and interesting ability of controlling the flow properties of aqueous dispersions of the clay mineral.

CHAPTER 5
DELAMINATION OF AMINE-INTERCALATED
KAOLINITES

5.1 Introduction

The best kaolinite exfoliation and delamination methods described to date are not capable of delaminating kaolinite into single layers and a new delamination method is required to achieve this goal.

The method here presented represents a great step forward, since it successfully delaminates kaolinite forming halloysite-like tubes consisting of rolled single layers. The method is based on the intercalation of very large molecules, which take the layers apart by more than seven times their original basal spacing. Subsequently, the layers are definitely separated from each other in solution with the help of ultrasound energy.

It was also the intention of this study to evaluate if and how the interlayer grafting of organic molecules (as described in chapter 3) influences the delamination process: Does grafting evoke any stabilizing effects on the layers, causing them to roll less than pristine kaolinite? Or is it possible to obtain aluminosilicate nanotubes with controllable inner-environment by delaminating grafted kaolinites?

5.2 Intercalation of Primary n-Alkylamines

5.2.1 Intercalation on Non-Grafted Kaolinite

5.2.1.1 Experimental

Kaolinite was intercalated with DMSO (see section 3.2.1) to enable the intercalation of methanol (Raythatha and Lipsicas, 1985; Komori *et al.*, 1998). For this process, ~ 10 g K-DMSO were dispersed in ~ 50 ml methanol and agitated in closed flask at room temperature for periods varying from 1 to 24 h. After this time, the dispersion was centrifuged and the solid was redispersed in fresh methanol. Approximately 15 cycles were performed. The final product (K-MeOH) was either immediately used or kept under methanol for further use.

For the intercalation of n-alkylamines, a procedure adapted from Komori *et al.* (1998, 1999) was used. The freshly prepared K-MeOH (~ 5 g) was dispersed in ~ 50 ml n-hexylamine and agitated in closed flask for 24 h at room temperature. After this period the dispersion was centrifuged and the product redispersed with fresh amine and agitated for another 24 h. The dispersion was centrifuged again and the final product (K-Hexylamine) was either immediately used or kept wet in a closed flask for further use.

n-Octadecylamine and n-docosanamine were intercalated by dispersing ~ 2 g of the freshly prepared K-Hexylamine in ~ 30 ml melted amine (~ 100 °C). The systems were kept under agitation for 24 h in open flasks (to eliminate excess hexylamine and/or water) and afterwards for a further 24 h period with the flasks closed. The dispersions were then centrifuged (while hot) and the products were redispersed in fresh melted amine. After another 24 h agitation period the dispersions were centrifuged and the final products (K-Octadecylamine, K-Docosanamine) were cooled and hand ground to a fine powder.

5.2.1.2 Characterization

The dimethyl sulfoxide-kaolinite (K-DMSO, Fig. 5.1, Table 5.1) showed the typical basal spacing of 11.2 Å (Weiss *et al.*, 1966a; Olejnik *et al.*, 1968). The hexylamine-kaolinite had a basal spacing of 26.6 Å, similar to the values of 26.9 Å (Komori *et al.*, 1999) and 25.3 Å (Weiss *et al.*, 1966a) previously reported. The basal spacing of the octadecylamine-kaolinite (53.2 Å) was slightly smaller than the values of 57.5 Å (Komori *et al.*, 1999) and ~ 58.0 Å (Weiss *et al.*, 1966a) reported before. The basal spacing of 64.2 Å of the intercalation

compound with *n*-docosanamine (not previously described) is, to our best knowledge, the highest spacing so far reported for a kaolinite intercalation compound.

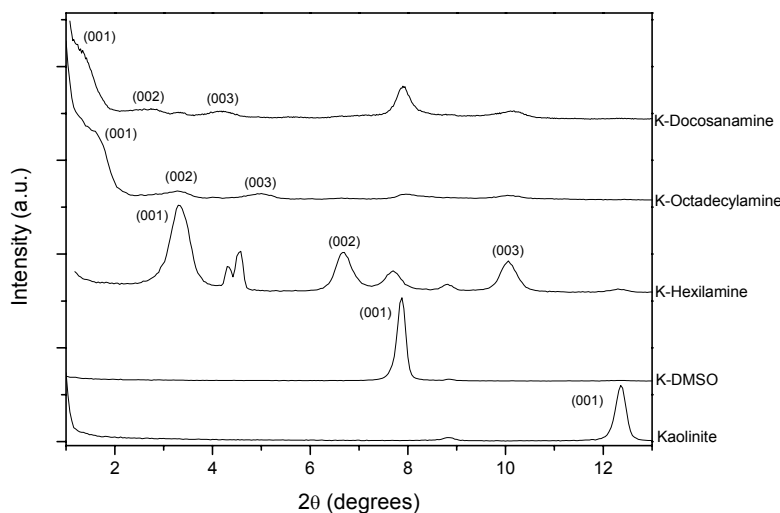


Fig. 5.1: XRPD patterns of the intercalation products obtained from non-grafted kaolinite.

Table 5.1: Basal spacings (d_L) and literature values ($d_L(lit)$) of the intercalation compounds of kaolinite.

Guest molecule	d_L (Å)	$d_L(lit)$ (Å)
DMSO	11.2	11.2 (Weiss <i>et al.</i> , 1966a; Olejnik <i>et al.</i> , 1968)
Hexylamine	26.6	26.9 Å (Komori <i>et al.</i> , 1999) 25.3 Å (Weiss <i>et al.</i> , 1966a)
Octadecylamine	53.2	57.5 Å (Komori <i>et al.</i> , 1999) ~ 58.0 Å (Weiss <i>et al.</i> , 1966a)
Docosanamine	64.2	-

These values indicate that the alkyl chains are fully stretched and perpendicular to the basal plane surface, arranged in a bilayer between the kaolinite layers. The amino groups interact at one side with the interlayer hydroxyl groups, and on the other side with the silica sheet (Weiss *et al.*, 1966a; Komori *et al.*, 1999). The smaller basal spacing obtained with *n*-octadecylamine in comparison to the literature values is probably due to contamination of the amine with *n*-hexadecylamine (Weiss *et al.*, 1966a) and/or formation of kinks (Lagaly, 1976).

5.2.2 Intercalation on Grafted Kaolinites

5.2.2.1 Experimental

Six different grafted kaolinites (K-13BD, K-DEGME, K-DEG2EHE, K-TPGBE, K-Pentanol and K-Heptanol) were intercalated with n-hexylamine by dispersing ~ 5 g grafted kaolinite in ~ 50 ml amine in closed flasks for 24 h. The dispersions were centrifuged, and the sediments redispersed in the same volume of fresh amine. The dispersions were stirred for another 24 h, and then centrifuged. The wet products were kept in closed flasks for further use.

n-Octadecylamine was intercalated by displacement of the previously intercalated hexylamine. Typically, ~ 1 g hexylamine-intercalated grafted kaolinite was added to ~ 20 ml melted amine (100 °C) and kept under stirring for 2 days (1 day with open flask and 1 day with the flask closed). The dispersion was centrifuged (while hot), and the process was repeated with fresh amine. This final product was centrifuged, cooled and triturated for further use.

5.2.2.2 Characterization

Fig. 5.2 presents the XRPD patterns of the grafted kaolinites. The basal spacings of these compounds are listed in Table 5.2. A detailed description of these compounds is presented in chapter 3.

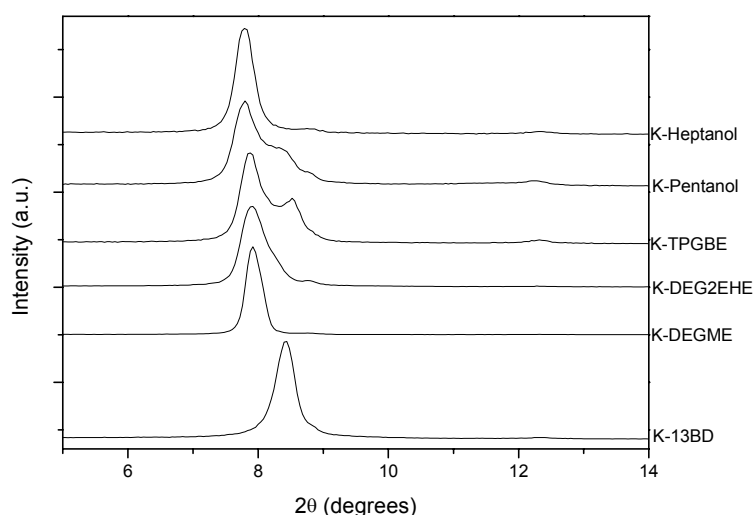


Fig. 5.2: XRPD patterns of the grafted kaolinites used on the amine-intercalation experiments.

Table 5.2: Basal spacings (d_L) of the grafted kaolinites used for amine intercalation.

Grafted Molecule	Product	d_L (Å)
1,3-Butanediol	K-13BD	11.3
Di(ethylene glycol) methyl ether	K-DEGME	11.0
Di(ethylene glycol) 2-ethylhexyl ether	K-DEG2EHE	11.3
Tri(propylene glycol) butyl ether	K-TPGBE	11.3 (70%) 10.3 (30%)
1-Pentanol	K-Pentanol	11.3 (75%) 10.3 (25%)
1-Heptanol	K-Heptanol	11.3

The basal spacings of the grafted kaolinites intercalated with *n*-hexylamine (Fig. 5.3, Table 5.3) are slightly smaller (< 1 Å) than that of raw kaolinite intercalated with the same amine. The compounds intercalated with *n*-octadecylamine (Fig. 5.4, Table 5.3) presented basal spacings larger by 2-3 Å in comparison with the octadecylamine-kaolinite. Considering the uncertainty in the determination of the basal spacings from the broadened reflections in the low- 2θ region, one can assume that the amine molecules in the grafted kaolinites are arranged in such a way that the amino groups interact with the inner-surface hydroxyl groups in a similar way as in the non-grafted kaolinite. During intercalation, the grafted molecules must have changed from an almost parallel orientation to the basal plane surfaces to a perpendicular orientation (Fig. 5.5). In this arrangement, the interaction between the alkyl chains of the grafted molecule and of the amine is optimized and the interlayer expansion needed to accommodate the amine bilayer is kept to a minimum. This explains the very small differences between the basal spacing of amine-intercalated grafted and raw kaolinites.

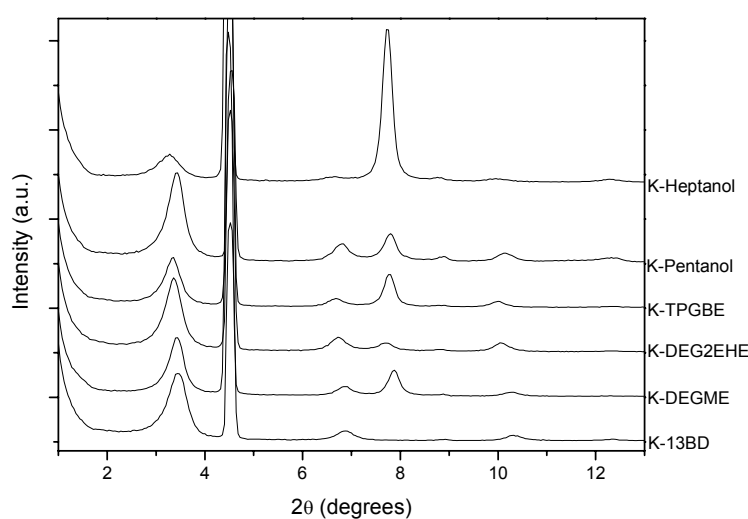


Fig. 5.3: XRPD patterns of grafted kaolinites intercalated with *n*-hexylamine.

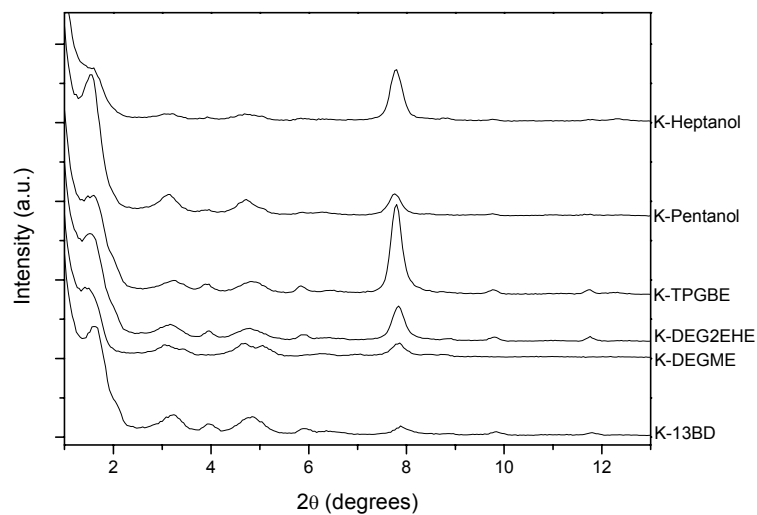


Fig. 5.4: XRPD patterns of grafted kaolinites intercalated with *n*-octadecylamine.

Table 5.3: Basal spacings (d_L) of non-grafted and grafted kaolinites intercalated with *n*-hexyl and *n*-octadecylamine.

Compound	d_L	
	<i>n</i> -Hexylamine (Å)	<i>n</i> -Octadecylamine (Å)
Kaolinite	26.6	53.2
K-13BD	25.7	55.1
K-DEGME	25.7	56.6
K-DEG2EHE	26.2	55.5
K-TPGBE	26.4	54.7
K-Pentanol	26.0	56.1
K-Heptanol	26.5	55.8

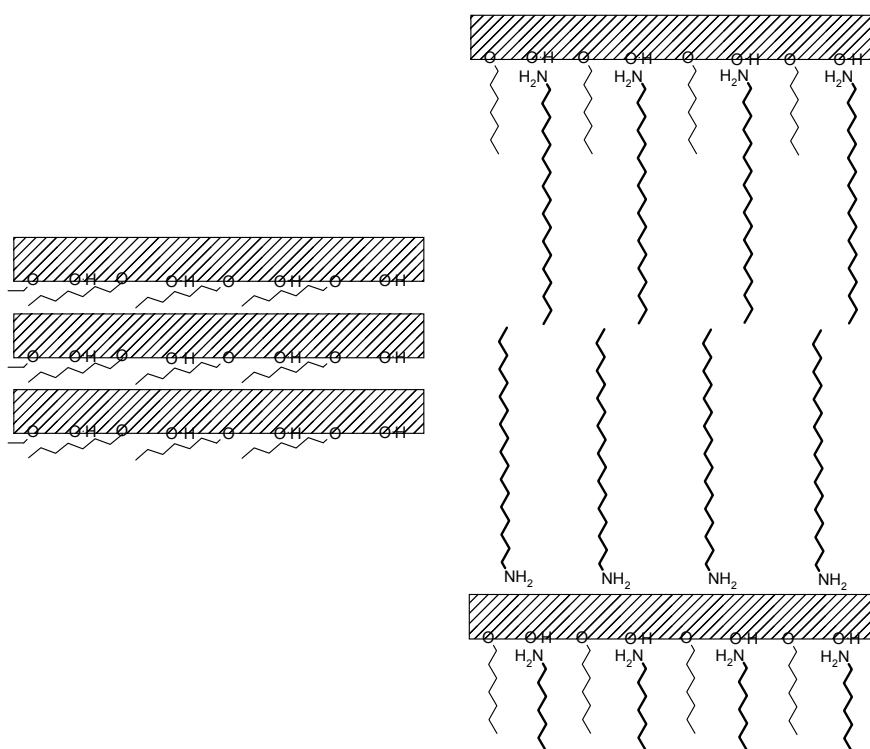


Fig. 5.5: Schematic view of the proposed disposition of the grafted molecules in K-heptanol before and after intercalation with *n*-octadecylamine (not scaled).

As shown by the diffraction patterns (Fig. 5.3), the intercalation reactions did not proceed quantitatively as reflections of the grafted kaolinites are still identifiable. Noteworthy is the fact that the amines are directly intercalated into the grafted kaolinites, but not into raw kaolinite or K-DMSO (Komori *et al.*, 1999). The broadened reflections of the intercalation compounds reveal that the intercalation of the amine bilayer considerably reduces the crystalline order of the kaolinite structure.

5.3 Delamination of Amine-Intercalated Kaolinites

5.3.1 Delamination of Non-Grafted Kaolinite

5.3.1.1 Experimental

Pristine kaolinite intercalated with n-octadecylamine was used for the delamination experiments. A fine powdered (manually ground) sample of this intercalation compound (typically ~ 0.5g) was slowly added to ~ 50 ml toluene in a jacketed beaker, kept under intensive magnetic stirring. The dispersion was sonicated for 2 x 5 min (5 min pause, UP200S equipment, Dr. Hielscher GmbH Germany, frequency 24 kHz, power output 200 W, cylindrical titanium probe with 7 mm diameter). The temperature of the system was kept below 25 °C by circulation of fresh water in the beaker jacket.

After this treatment, the dispersion was centrifuged at 60000 g for 30 min. The separated product was dispersed in 50 ml toluene and kept in agitation for 20 h. This product was centrifuged and washed three more times with 50 ml ethyl ether (~ 20 h each washing step), then dried at 60 °C for 24 h.

5.3.1.2 Characterization

Fig. 5.6 shows the XRPD patterns of the amine-intercalated raw and grafted kaolinites after the toluene treatments. The non-grafted kaolinite is deintercalated almost quantitatively as shown by a very weak broadened reflection at low 2θ values, attributed to remnants of intercalated amine, probably as a highly inhomogeneous interstratified phase. The reflection at $d_L = 8.7 \text{ \AA}$ ($2\theta \sim 10^\circ$) is attributed to the dry kaolinite-methanol intercalation compound (Komori *et al.*, 1998) and the small reflection at $d_L = 11.2 \text{ \AA}$ ($2\theta \sim 7.9^\circ$) is due to the K-DMSO, both phases remnants of the precursor kaolinites. The reflection at $d_L = 10.0 \text{ \AA}$ ($2\theta \sim 8.8^\circ$) comes from the mica present in the original kaolinite sample. Due to the lower crystallinity of the final product, the mica, which is not affected by the process, is now easily recognized.

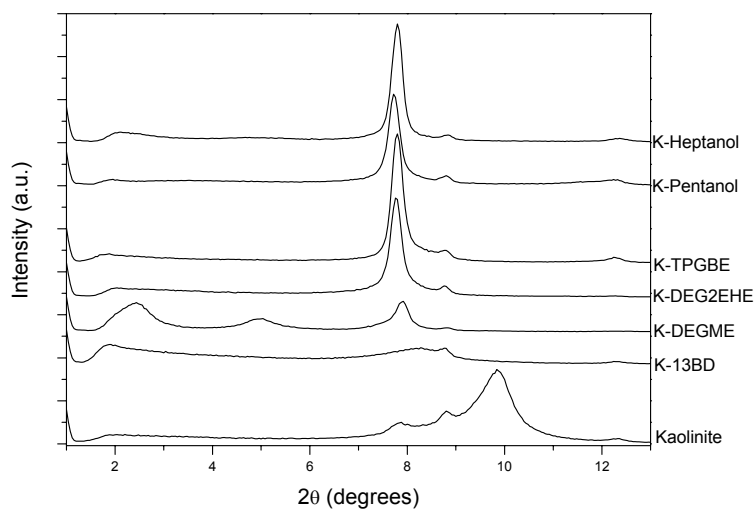


Fig. 5.6: XRPD patterns of kaolinite and grafted derivatives after deintercalation.

Any conclusions about the success of the delamination process must be based on the morphological analysis of the deintercalated products. The raw, untreated kaolinite is composed of platy, euhedral particles with typical pseudo-hexagonal morphology (Fig. 5.7). After the intercalation/deintercalation steps (Fig. 5.8) the sample still presents some thicker particles, but the majority of the sample is composed of thin plates and elongated units. At a higher magnification, the elongated units are recognized as thin kaolinite particles, in form of hollow tubes.

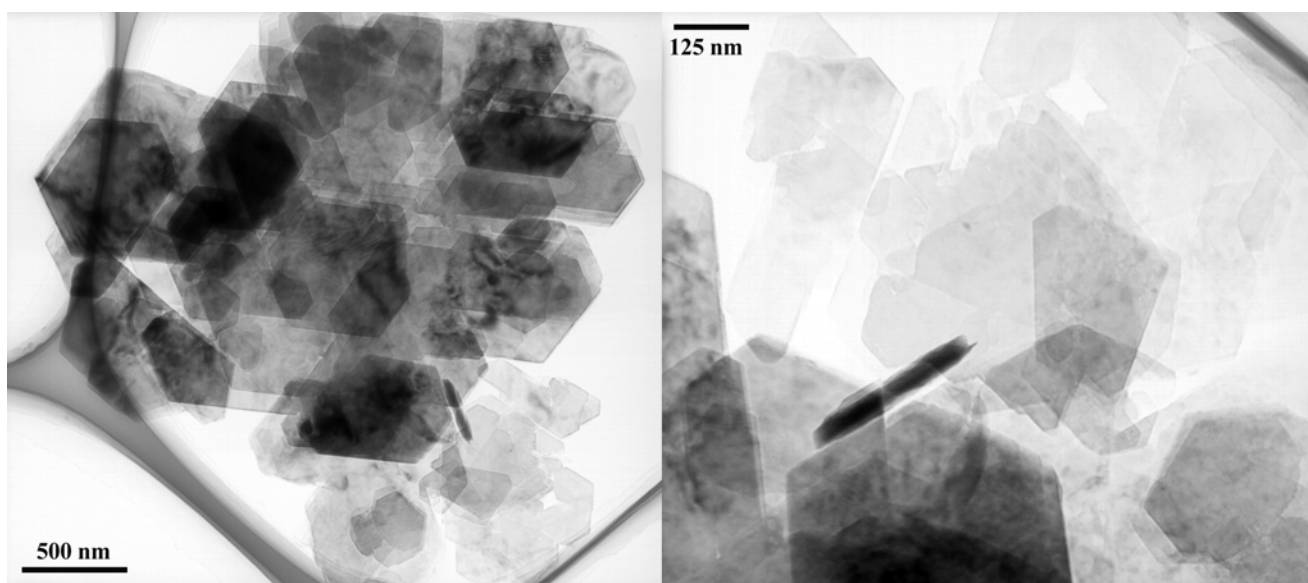


Fig. 5.7: TEM micrographs of raw kaolinite.

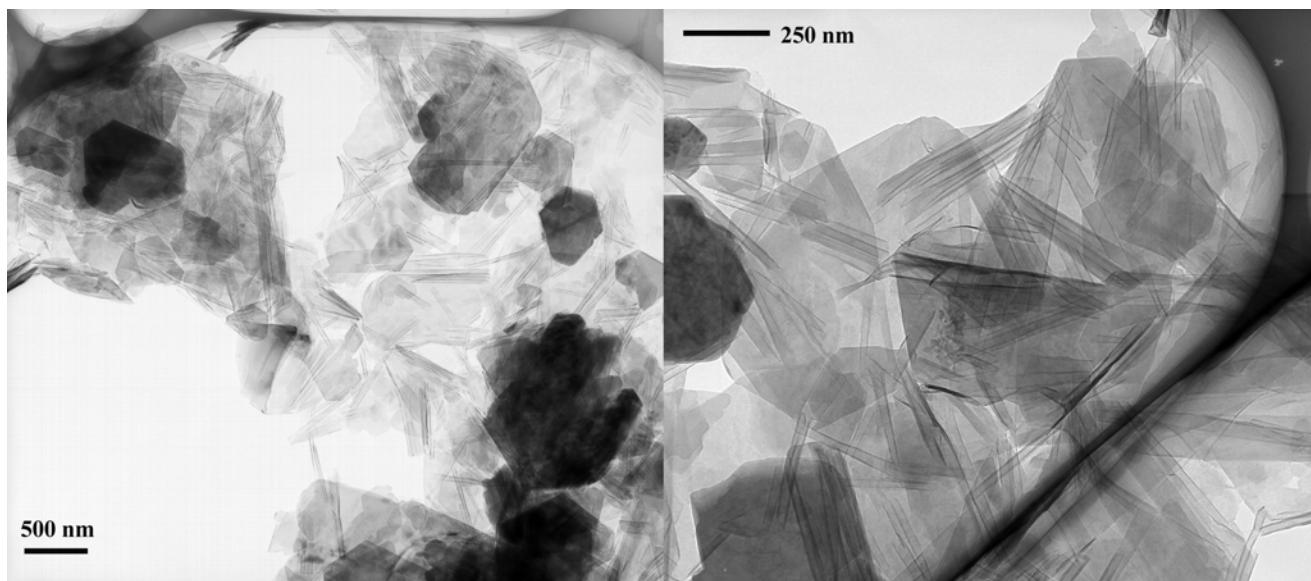


Fig. 5.8: TEM micrographs of the deintercalated kaolinite.

5.3.2 Delamination of Grafted Kaolinites

5.3.2.1 Experimental

The grafted kaolinites intercalated with n-octadecylamine were used for the delamination experiments. Fine powdered (manually ground) samples of these intercalation compounds (typically $\sim 0.5\text{g}$) were slowly added to $\sim 50\text{ ml}$ toluene in a jacketed beaker, kept under intensive magnetic stirring. The dispersions were sonicated for $2 \times 5\text{ min}$ (5 min pause, UP200S equipment, Dr. Hielscher GmbH Germany, frequency 24 kHz, power output 200 W, cylindrical titanium probe with 7 mm diameter). The temperature of the system was kept below $25\text{ }^\circ\text{C}$ by circulation of fresh water in the beaker jacket.

After this treatment, the dispersions were centrifuged at 60000 g for 30 min. The separated products were dispersed in 50 ml toluene and kept in agitation for 20 h. These products were centrifuged and washed three more times with 50 ml ethyl ether ($\sim 20\text{ h}$ each washing step), then dried at $60\text{ }^\circ\text{C}$ for 24 h.

5.3.2.2 Characterization

The X-ray diffraction patterns of the delaminated grafted kaolinites (Fig. 5.6) reveal that the amine molecules are deintercalated, and the original basal spacings of the grafted kaolinites are recovered. At low 2θ values, a weak broadened reflection is seen, attributed to an

interstratified phase, as in the deintercalated raw kaolinite. The derivatives from DEGME and heptanol presented a better resolved reflection at $d_L \sim 40 \text{ \AA}$. It is supposed that the particles remaining intercalated with octadecylamine present a different arrangement for the alkyl chains, probably with the formation of kinks (Lagaly, 1976) or by partially squeezing the alkyl chains out of the interlayer spaces (Poyato-Ferrera *et al.*, 1977).

Deintercalation of the derivative from 1,3-butanediol does not recover the original basal spacing (11.3 \AA), but produced a weak reflection at 10.7 \AA . This compound also shows a much lower crystallinity in comparison to the other deintercalated compounds, possibly indicating an extensive delamination of the sample.

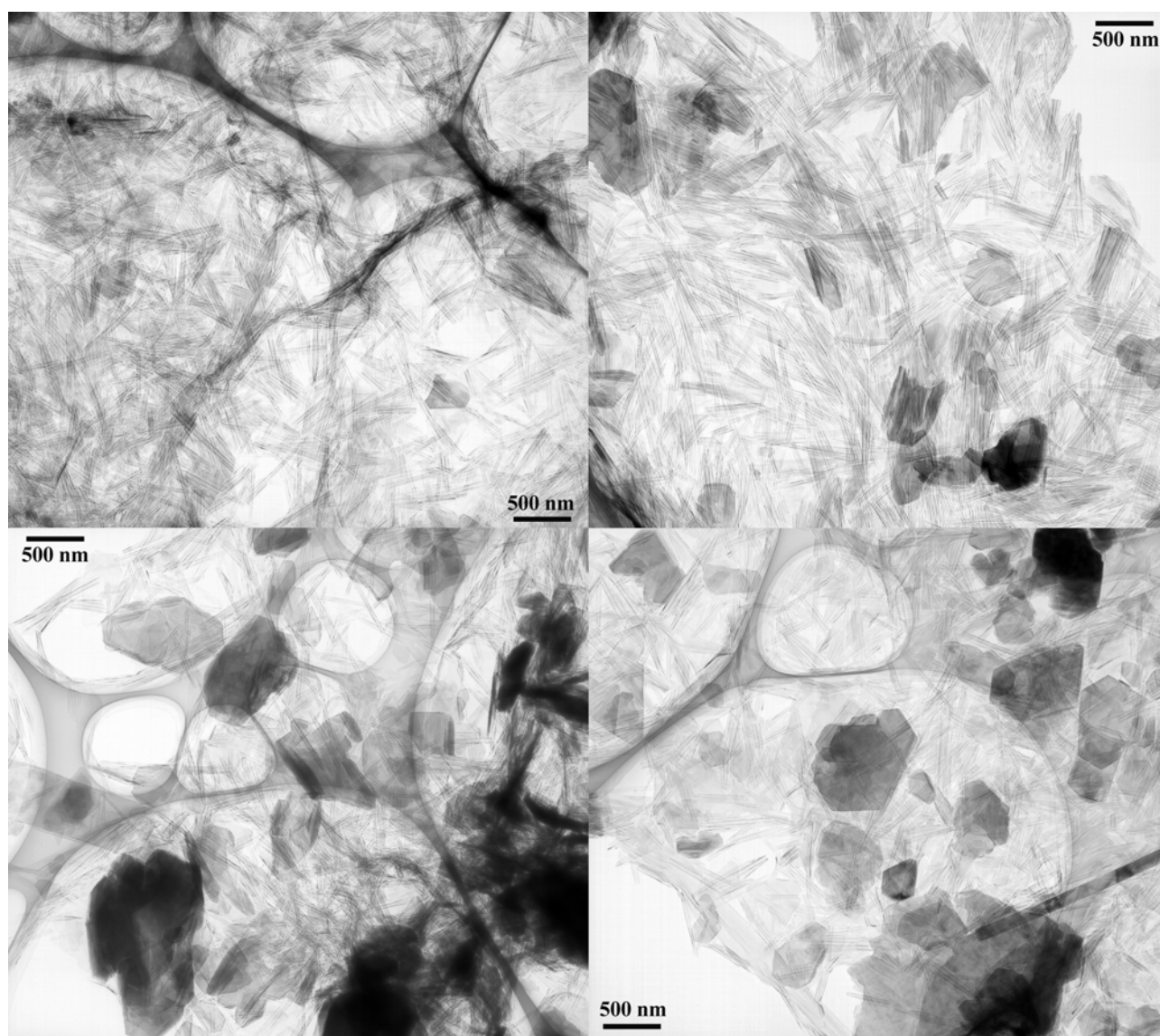


Fig. 5.9: TEM micrographs of the deintercalated kaolinites grafted with 1,3-butanediol, di(ethylene glycol) 2-ethylhexyl ether, tri(propylene glycol) butyl ether and heptanol (from left to right, from top to bottom).

The samples obtained by deintercalation of the grafted kaolinites revealed a higher degree of rolling than the samples derived from raw kaolinite and a large number of tubes. Nevertheless, they also contained some kaolinite particles with recognizable pseudo-hexagonal morphology, some damaged particles and thin plates (Fig. 5.9, 5.10). All tubes formed from the different grafted kaolinites were morphologically similar. The minimum external diameter of the tubes was ~25 nm. The derivative from 1,3-butanediol showed only very small amounts of platey particles, being composed almost exclusively of tubes and some curled thin plates.

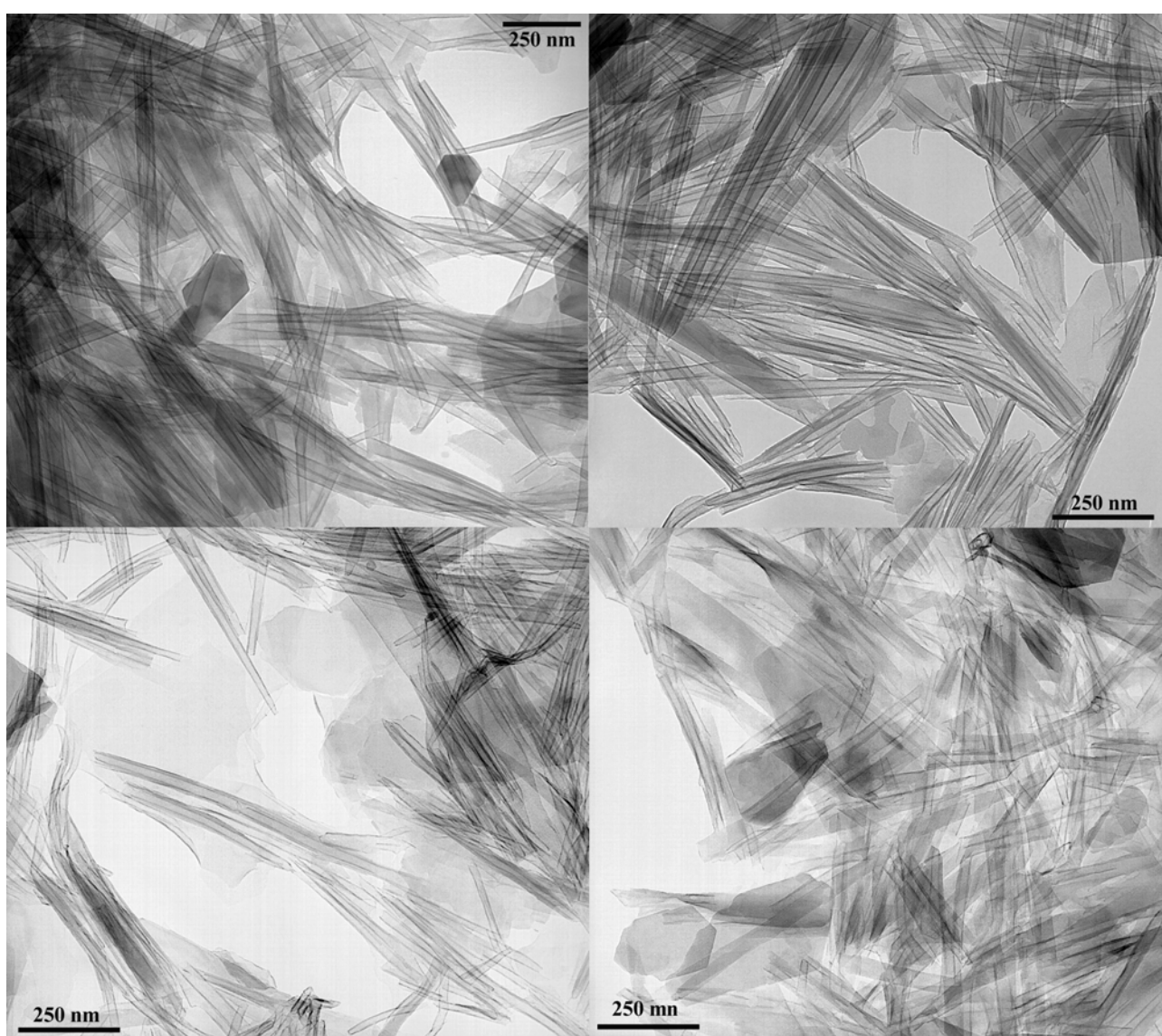


Fig. 5.10: TEM micrographs of the deintercalated kaolinites grafted with 1,3-butanediol, di(ethylene glycol) 2-ethylhexyl ether, pentanol and heptanol (from left to right, from top to bottom).

5.3.3 Discussion

As expected, the deintercalation process separates very thin lamellae from the kaolinite particles. These lamellae curl to form the observed tubes. The smallest tubes in the sample had an external diameter around 25 nm. This value is consistent with the calculated minimum internal diameter for a tube formed by a single kaolinite layer (Bates *et al.*, 1950).

Two essential factors contributed to the higher degree of rolling of the grafted derivatives. The organically modified interlayer surface can interact more efficiently with toluene than the original non-grafted surface. In addition, the intercalation of amines formed products with higher stacking disorder, indicated by the broadened reflections of the XRPD patterns, which is a key parameter needed to separate the layers (Singh & Mackinnon, 1996; Singh, 1996).

It was so far accepted that the hydration of the kaolinite interlayer spaces is an essential requirement to separate and curl the layers because it implies a higher degree of disorder, which is needed to weaken the interlayer hydrogen bonds (Singh, 1996; Singh & Mackinnon, 1996). The present results show that hydration of kaolinite is not a necessary condition to the formation of halloysite-like tubes, as the reactions were carried in organic medium. Rather, the weakening of the interlayer hydrogen bonds is decisive, as proposed by Singh (1996) and proved here by the ease formation of kaolinite tubes when the basal spacing is expanded to more than seven times its original size. In addition, the ultra-sound treatment favored the fast access of the organic solvent to the interlayer spaces and promoted the separation process.

Typical natural halloysite tubes have external diameters between 50 nm and 500 nm (Singh, 1996; Bates *et al.*, 1950). The smallest tubes have a diameter not smaller than 40 nm, what corresponds to a rolled particle composed of ~ 14 layers. Such tubes were obtained by the ammonium or potassium acetate treatment of kaolinite (Weiss & Russow, 1963; Singh & Mackinnon, 1996). The tubes obtained by the process here described show distinctly smaller external diameters. The smallest diameter was ~ 25 nm. Bates *et al.* (1950) calculated that the smallest inner diameter for a rolled single kaolinite layer would be 25.08 nm. Thus, the smallest tubes here prepared are very likely composed of rolled single kaolinite layers. However, we could not prove that these tubes really consisted of monolayers, if not, they contained a few layers only. The maximum degree of delamination of kaolinite was possibly achieved. In further experiments attesting this assumption, the delaminated non-grafted

kaolinite was again submitted to an intercalation/deintercalation process. This yielded a much higher fraction of tubes and much less platey particles (results not shown) but the smallest external diameters remained at ~25 nm. Thinner tubes or different morphologies were not found.

5.4 Conclusion

Grafted derivatives of kaolinite directly intercalate primary n-alkylamines, in contrast to the behavior of raw kaolinite. Deintercalation in toluene with sonication delaminated the particles into very thin lamellae that rolled to form hollow tubes. The highest degree of delamination of kaolinite was possibly achieved. The smallest tubes had external diameters compatible with the value calculated for tubes formed by rolled single kaolinite layers. Interlayer grafting of the kaolinite particles promoted considerably the delamination process.

Delamination of grafted kaolinites yields nanotubes with an external silica-like surface and an inner surface with a hydrophobic/hydrophilic character controlled by the grafted molecules. This tailoring of the tube interior might be of great importance for many applications that are currently envisaged for nanotubes such as in advanced catalysis, sensor/actuator arrays, energy storage/conversion, opto-electronic devices or fixation of bio-active molecules (Dong *et al.*, 2003).

CHAPTER 6
THE REACTION OF KAOLINITE WITH
PHENYLPHOSPHONIC AND SIMILAR ACIDS

6.1 Introduction

The Brazilian research group of F. Wypych described in 1998 a new grafted derivative of kaolinite obtained by the reaction of the raw mineral with phenylphosphonic acid (PPA, see Fig.6.1) (Guimarães *et al.*, 1998).

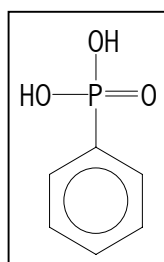


Fig. 6.1: Phenylphosphonic Acid

According to the authors, PPA reacted topotactically with the interlayer hydroxyl groups of kaolinite, establishing an Al-O-P linkage between the clay mineral and the organic molecule, according to the reaction:



The experimental procedure used to obtain the derivative was simple: 2.75 g of PPA were dissolved in an water/acetone mixture (1:1, v/v) and this solution was refluxed with 1.5 g of kaolinite for 20 days at 95 °C. The product was washed with acetone and dried at 60 °C.

The kaolinite phenylphosphonate (K-PPA) thus obtained presented a basal spacing of 15.02 Å, which corresponds to an expansion of 7.86 Å in relation to the unreacted kaolinite. Also described was a phase with basal spacing of 16.45 Å, which was attributed to a hydrated form of the K-PPA derivative.

Different analytical methods were used to characterize the product: XRPD, FTIR, TG/DSC, X-ray fluorescence and elemental analysis (CHN). The authors were convinced of the topotactical grafting of the phenylphosphonate groups onto the aluminol surfaces of kaolinite. To this grafted-kaolinite, the stoichiometry $\text{Al}_2\text{Si}_2\text{O}_5(\text{OH})(\text{HO}_3\text{PPh})_3 \cdot 2 \text{H}_2\text{O}$ was attributed.

In the next year, the same research group reported the intercalation of hexylamine into the K-PPA compound (Guimarães *et al.* 1999). The compound presented a basal spacing of 16.36 Å, which corresponded to an expansion of 1.34 Å in relation to K-PPA. This fact would

imply that the amine molecules were arranged parallel to the basal surfaces of the matrix. The authors also suggested that the nitrogen atoms of the amine would be hydrogen-bound to the hydroxyl groups of the grafted phenylphosphonate groups. This intercalate was investigated by various analytical methods and the following structural formula was proposed: $\text{Al}_2\text{Si}_2\text{O}_5(\text{OH})(\text{HO}_3\text{PPh})_3 \cdot 2 \text{C}_6\text{H}_{13}\text{NH}_2$.

In 2002 Breen *et al.* reported some complementary studies on the K-PPA compound. They also reported that a similar compound could be obtained from the reaction of PPA with halloysite. The authors presented a thermal stability study of the compounds using the TGA technique and some results from VT-DRIFTS which showed the interaction of interlayer water with the kaolinite hydroxyl groups.

At the beginning of this PhD research (2002), the following grafted derivatives of kaolinite were described in the literature:

Table 6.1: Grafted derivatives of kaolinite described until the beginning of 2002.

Derivative	Reference
K-ethylene glycol	Tunney and Detellier, 1993 Tunney and Detellier, 1994a
K-ethylene glycol methyl ether	Tunney and Detellier, 1993
K-di(ethylene glycol) butyl ether	Tunney and Detellier, 1993
K-1,2-propanediol	Tunney and Detellier, 1993
K-1,3-propanediol	Tunney and Detellier, 1993
K-methanol	Tunney and Detellier, 1996a Komori <i>et al.</i> , 2000
K-ethanolamine	Tunney and Detellier, 1997
K-3-amino-1-propanol	Tunney and Detellier, 1997
K-phenylphosphonate	Guimarães <i>et al.</i> , 1998 Guimarães <i>et al.</i> , 1999 Breen <i>et al.</i> , 2002

It was our intention to proceed with the study of these compounds, and to obtain new derivatives. We decided to investigate the possibility of reactions of kaolinite with molecules similar to the ones listed above. From the derivatives listed in Table 6.1, the K-PPA compound immediately steps out of the pattern in two ways:

- All other derivatives were obtained from analogue reactions with similar compounds: diols, glycol mono-ethers and aminoalcohols reacted with the kaolinite interlayer hydroxyl groups in an esterification-like reaction. It should be remembered that PPA is a very strong acid, in comparison with the slight acidic kaolinite hydroxyl groups, which suggests a completely different reaction type for the formation of the K-PPA derivative (at least when comparing to the reactions with alcohol-like molecules).
- PPA reacted directly with non-expanded kaolinite, while all other compounds were obtained only by reaction with the pre-expanded mineral.

We repeated the preparation of K-PPA and, in an analogue way, tested the reaction of kaolinite with phenylphosphonic acid (PPiA, Fig. 6.2a) and 2-nitrophenol-4-arsonic acid (NPAA, Fig. 6.2b)

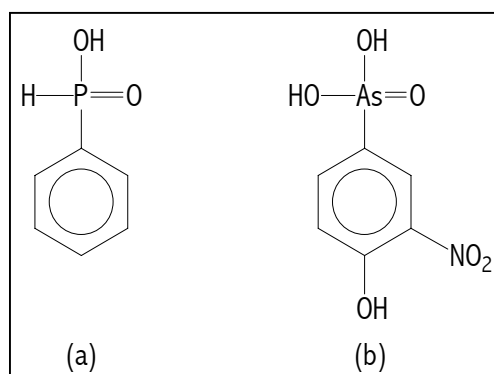


Fig. 6.2: Phenylphosphonic acid (a) and 2-nitrophenol-4-arsonic acid (b)

After characterization of the products by XRPD, some doubts concerning their structure were unveiled. The diffraction patterns of the products from PPiA and NPAA could not be understood in terms of the formation of a grafted kaolinite with layered structure. Strong suspicions also arose about the structure of the formerly described K-PPA compound. In order to elucidate these problems, the same acids were reacted with gibbsite and the products were further analyzed and investigated with TEM/EDX/SAED techniques.

6.2 Preparation of New Compounds

6.2.1 Experimental

6.2.1.1 Preparation of K-PPA

We used the procedure described by Guimarães et al. (1998). An amount of 1.5 g kaolinite was added to 300 ml of a 1:1 water/acetone solution containing 2.75 g PPA (molar ratio kaolinite/acid = 1:3). The dispersion was kept under reflux and constant stirring in an oil-bath at ~ 95 °C for 20 days. The resulting dispersion was washed by centrifugation with acetone (5x) and dried at 50 °C for 24 h.

6.2.1.2 Preparation of K-PPiA and K-NPAA

Approximately 850 mg of the fine sized kaolinite fraction (SPF-K, see Appendix I) were reacted with 100 ml of a 0.1 molar solution of the acid in water. These dispersions were kept under reflux and constant stirring in oil-baths at ~ 80 °C for 1 month and finally washed by centrifugation with water (K-PPiA: 5 times, K-NPAA: 10 times) and dried at 50 °C for 24 h.

6.2.1.3 Preparation of Gi-PPA, Gi-PPiA and Gi-NPAA

An amount of 1 g gibbsite was added to 100 ml of 1:1 water/acetone solutions, containing 6.08 g of PPA, 5.46 g PPiA, or 3.37 g NPAA (corresponding to molar ratios Al/P = 1:3 and Al/As = 1:1). The dispersions were kept under reflux and constant stirring in oil-baths at ~ 80 °C for 1 month, then washed by centrifugation (4000 rpm) with water (1x) and acetone (4x) (Gi-NPAA was washed 10 times with a 1:1 water-acetone mixture and 3 times with acetone). The products were dried at 50 °C for 24 h.

6.2.2 Characterization

6.2.2.1 Kaolinite with PPA, PPiA and NPAA

The diffraction pattern of kaolinite (Fig. 6.3a) revealed a well-crystallized sample (see Appendix I for detailed description of the sample). The basal reflections were observed up to the sixth order, indicating a basal spacing of 7.15 Å, characteristic of this mineral (Santos, 1989; Jasmund and Lagaly, 1993). The diffraction pattern of the fine fraction SPF-K was identical to the original kaolinite (Fig. 6.3b).

The XRPD pattern of K-PPA (Fig. 6.3c), with $d_L = 15.00 \text{ \AA}$ and a reaction ratio $\alpha = 98\%$, is identical to product previously described (Guimarães *et al.*, 1998, 1999; Breen *et al.*, 2002).

The first attempts to obtain the phenylphosphinic and phenylarsonic derivatives of raw kaolinite yielded very low reaction ratios, even after a period of 1 month. Therefore, further attempts were carried with the fine-particle fraction SPF-K (see Appendix I).

The reaction between SPF-K and PPIA yielded a product with the first and by far most intense reflection at 9.73 \AA (calculated from the third order, Fig. 6.3d). Small reflections were observed at 7.33 \AA and at 4.78 \AA . A small quantity of unreacted kaolinite was also identified (Table 6.2).

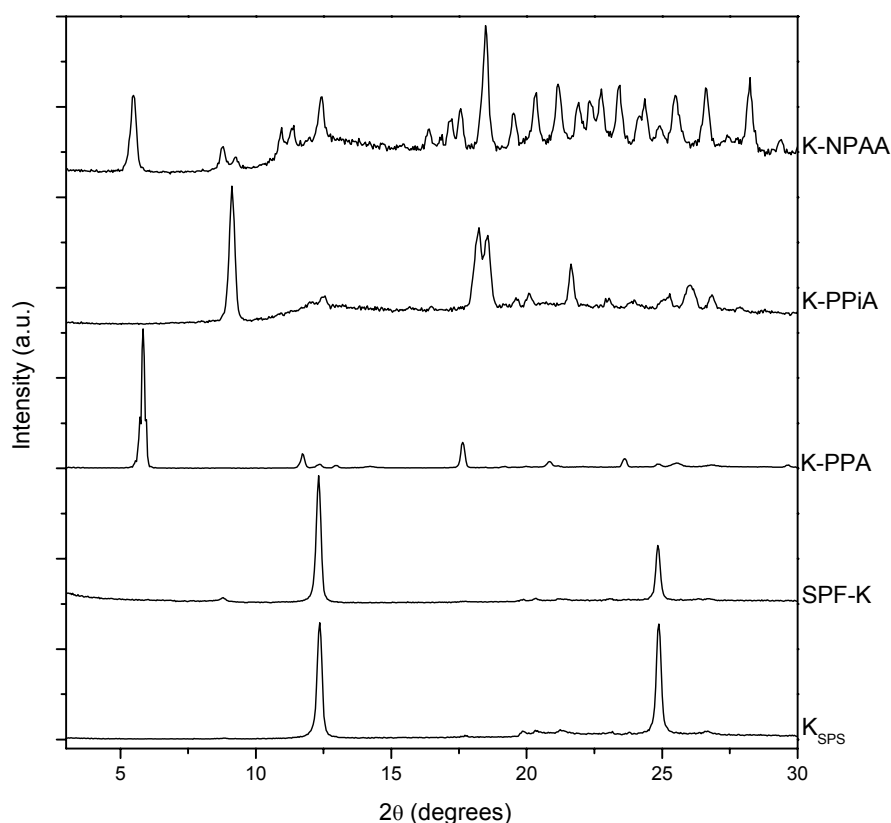


Fig. 6.3: XRPD patterns of raw kaolinite (K_{SPS}), the fine-particle size fraction (SPF-K), and the reaction products with PPA, PPIA and NPAA.

The reaction between NPAA and SPF-K led to a product with an intense reflection at 16.21 \AA followed by four higher-order reflections (Fig. 6.3e). A weak reflection at 10.10 \AA was identified up to the fourth order, and an even weaker reflection at 9.55 \AA up to the third

order. The XRPD pattern also showed many other reflections between 10° and $30^\circ 2\theta$ (Table 6.2), unlike a normal pattern for a layer compound. A considerable amount of kaolinite remained unreacted.

Table 6.2: Values of d_{hkl} , Δd_{hkl} (in relation to unreacted kaolinite) and reaction ratios (α) for raw kaolinite, the fine particle size fraction (SPF-K) and the kaolinite derivatives.

	Kaolinite	K-PPA	K-PPiA			K-NPAA		
d_{hkl} (Å)	7.15	15.00	9.73	7.33	4.78	16.21	10.10	9.55
Δd_{hkl} (Å)	-	7.80	2.58	0.18	-	9.06	2.95	2.40
α (%)	-	98.0	-	-	-	-	-	-

The fine fraction of the kaolinite showed the pseudo-hexagonal morphology of the kaolinite crystals, with well-defined angles and edges (Fig. 6.4). Some beam damage is also seen, due to the higher sensitiveness of the small crystals. The TEM of the PPA derivative of kaolinite revealed a totally new phase, with a morphology distinctly different from the original kaolinite particles (Fig. 6.5). It consisted of very regular and symmetrical crystals, with corner angles of 90° . A few remaining kaolinite crystals were also observed. They were much degraded, with rounded edges and very damaged surfaces.

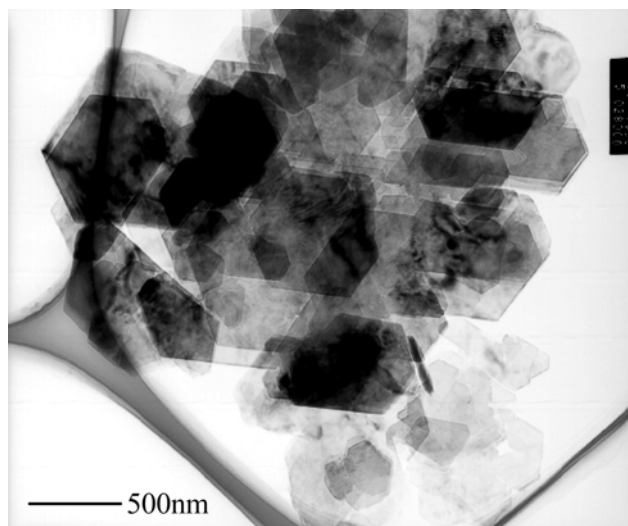


Fig. 6.4: TEM image of the fine-particle size fraction of kaolinite (SPF-K).

When the electron beam was focused to the residual kaolinite crystals, only aluminum and silicon were detected by EDX, in the same proportions as in pure kaolinite. Large

concentration of phosphorus was detected in all crystals of K-PPA, and the silicon content was always very low.

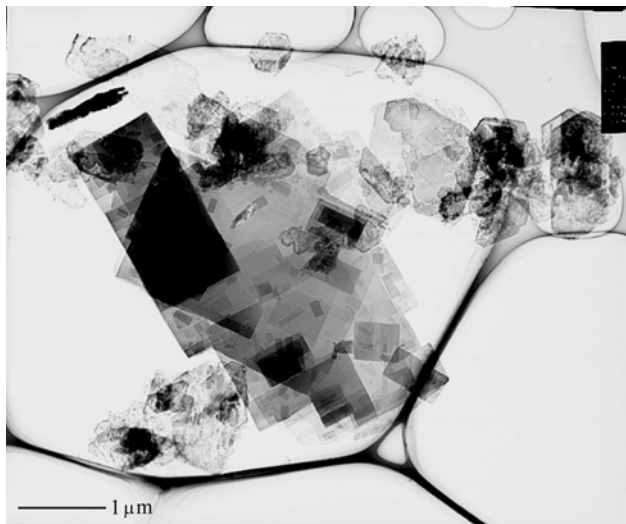


Fig. 6.5: TEM image of K-PPA.

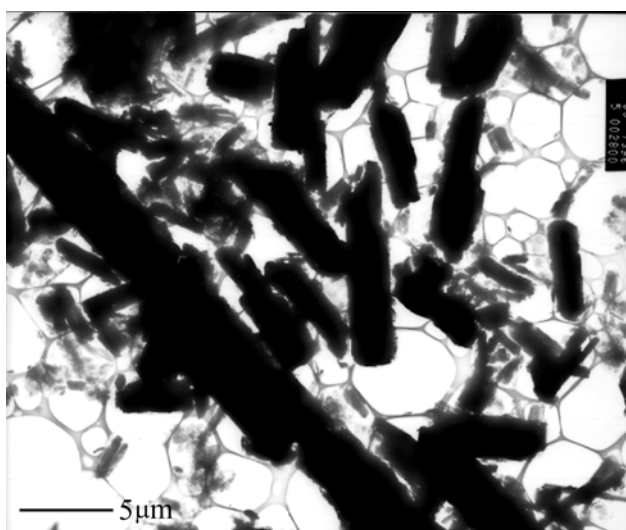


Fig. 6.6: TEM image of K-PPiA

After reaction of kaolinite with PPIA a few much damaged kaolinite crystals were seen. However, the sample mainly consisted of very dense, elongated crystals, with a broad size distribution (Fig. 6.6). The larger crystals were as much as 5 μm in width and more than 15 μm in length; the small ones had dimensions in the order of 0.2 μm x 0.5 μm. The new phase contained phosphorus and aluminum as major constituents, some residual amounts of silicon were also detectable. Phosphorus was completely absent from the residual kaolinite crystals.

Low/medium magnification revealed the needle-like morphology of K-NPAA and some highly damaged kaolinite particles (Fig. 6.7). The new phase contained high concentrations of aluminum and arsenic; silicon was also present in very small concentrations. The residual kaolinite particles contained only silicon and aluminum.

Selected area electron diffraction (SAED) of the K-PPA and the K-PPiA compounds could not be performed due to the extremely fast radiation damage of the crystals. As soon as reached by the beam, the crystals collapsed to an amorphous mass.

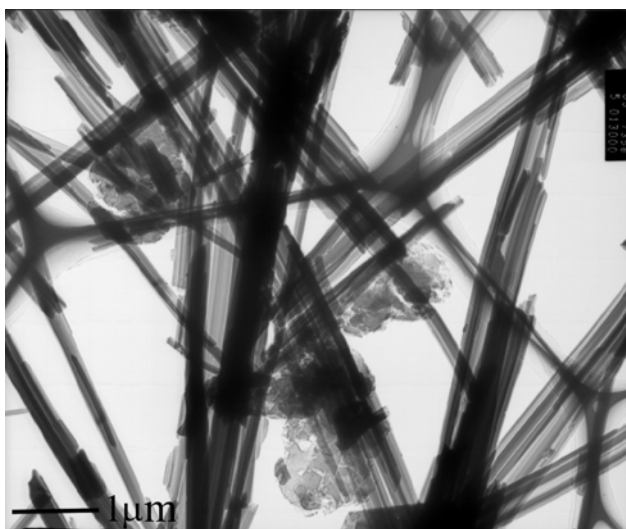


Fig. 6.7: TEM image of K-NPAA

Although the needle-like crystals of K-NPAA were also easily damaged by radiation, SAED patterns in several different orientations could be obtained with extremely low electron-beam intensity (Fig. 6.8). All investigated crystals were twinned on (100). The SAED patterns showed neither systematic extinctions nor obvious symmetry relations. Thus, the new phase had to be described with a triclinic unit cell. The following approximate cell dimensions were derived: $a_0 = 16.70 \text{ \AA}$, $b_0 = 10.60 \text{ \AA}$, $c_0 = 4.85 \text{ \AA}$, $\alpha = 94.4^\circ$, $\beta = 91.9^\circ$ and $\gamma = 103.8^\circ$, assuming the c axis parallel to the needle axis.

Due to the twinning of the crystals on (100), one cannot exclude the possibility (although it is not very likely), that the diffraction patterns were related to monoclinic twins. To exclude this possibility definitely, additional and more intense SAED patterns would be needed, but could not be obtained for the reasons already mentioned.

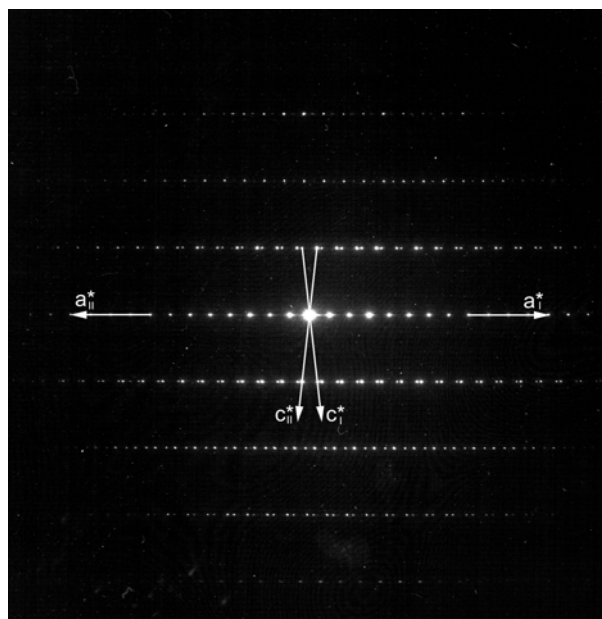


Fig. 6.8: SAED pattern of K-NPAA (parallel to the a^*c^* plane)

The TG/DTA profile of K-PPA (Fig. 6.9) showed a mass loss of 5.1 % up to 230 °C, corresponding to a small endothermic peak centered at 166 °C. A major mass loss occurred between ~ 400 °C and ~ 580 °C, accompanied by a strong exothermic peak at 574 °C. A series of poorly defined endothermic phenomena were observed between 800 °C and 1060 °C. The total mass loss was 38.4 %.

The TG/DTA curves of K-PPiA showed clear differences but also some similarities with K-PPA. A small endothermic event was observed at 235 °C, with no mass change. A very small mass gain (< 0.4 %) occurred between 100 °C and 317 °C, immediately followed by a very strong mass loss up to ~ 370 °C, when a superimposing second stage of mass loss began. The mass changes up to 370 °C were accompanied by two superimposed exothermic phenomena (a shoulder at 340 °C and a sharp and intense peak with maximum at 358 °C). The shoulder can be related to the small mass gain and the subsequent peak to the mass loss. Between 370 °C and 570 °C the mass decreased sharply and then slowly up to ~ 1020 °C. As in K-PPA, an exothermic peak was observed at 580 °C. Between 800 °C and 1060 °C a series of poorly defined endothermic events, with no clear mass changes, were observed. The total mass loss, from 30 °C to 1100 °C, was 39.6 %.

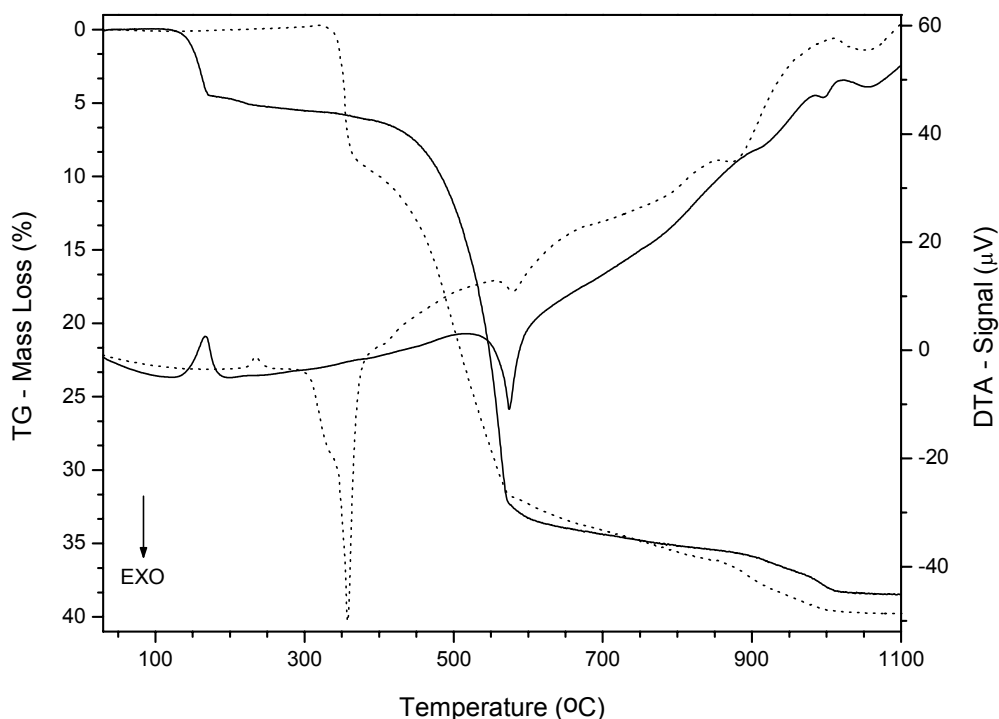


Fig. 6.9: TG/DTA curves of K-PPA (continuous lines) and of K-PPiA (dotted lines)

The thermal profile of K-NPAA could not be measured due to the very strong exothermal, almost explosive decomposition of the nitro groups at ~ 330 °C which expelled the sample out of the crucible.

Fig. 6.10 and 6.11 present the FTIR spectra of raw kaolinite, K-PPA, K-PPiA, and the original acids. To avoid the peaks due to intercalated water in K-PPA, the sample was dried for 1 h at 200 °C (Breen *et al.*, 2002). The XRPD pattern of this dried sample (not shown) was almost identical to the hydrated form and revealed a basal spacing of 14.71 Å. The FTIR spectrum of K-PPA in hydrated form (not shown) was identical to the one described previously (Guimarães *et al.*, 1998). The small bands in the region between 3000 and 2830 cm^{-1} , present in all spectra, were caused by an unidentified external contamination during the preparation of the IR sample.

The spectrum of dried K-PPA showed the four hydroxyl stretching bands of the raw kaolinite (3693, 3668, 3653 and 3619 cm^{-1}) with very small intensities (Olejnik *et al.*, 1968; Frost, 1995; Frost *et al.*, 1997; Balan *et al.*, 2001; Bougeard *et al.* 2000); bands characterizing the P-C₆H₅ bond and the phenyl ring (1436, 1487, 1594 cm^{-1} , four bands in the 3000-3100

cm⁻¹ region); and very intense P-O stretching bands between 1000 and 1300 cm⁻¹ (Thomas and Chittenden, 1970; Cabeza et al., 1998; Haky et al., 1997; Morizzi et al., 2000; Breiting et al., 2001). The Si-O stretching bands (1114, 1102, 1030 and 1009 cm⁻¹) and the Si-O-Al / O-Si-O bending bands (538, 470 and 431 cm⁻¹) (Olejnik et al., 1968; Frost, 1995; Frost et al., 1997; Balan et al., 2001; Bougeard et al. 2000) were largely reduced in intensity or absent. The interpretation of the bands in the region below 1200 cm⁻¹ was difficult because of the overlapping of PPA and kaolinite bands.

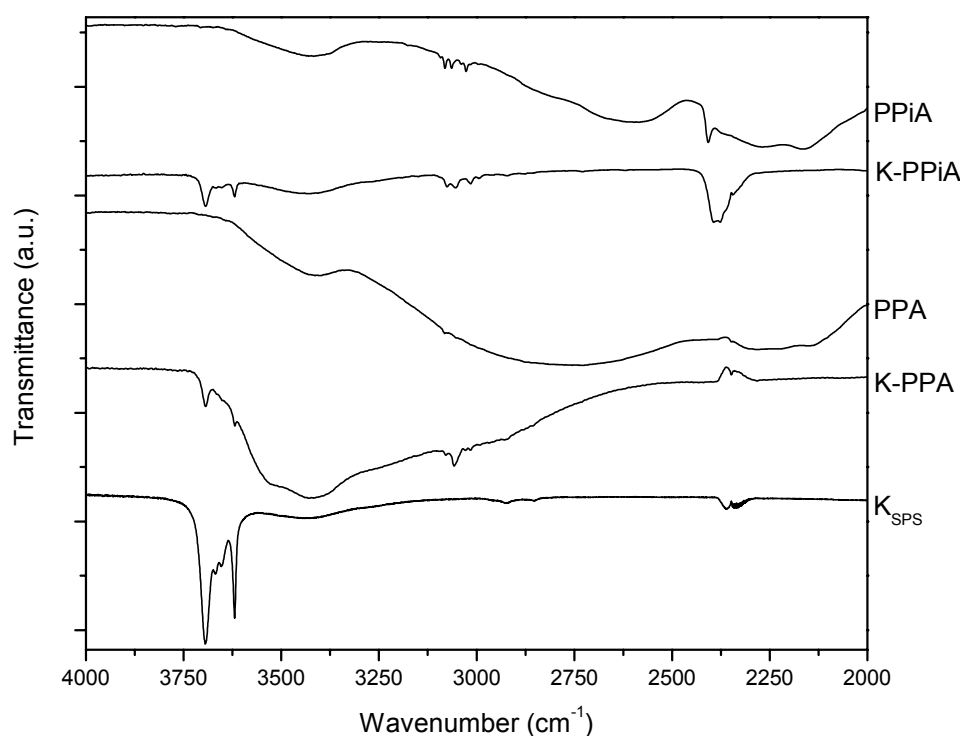


Fig. 6.10: FTIR spectra of raw kaolinite, K-PPA, K-PPiA, and the pure acids (PPA and PPIA), between 4000 and 2000 cm⁻¹.

The FTIR spectrum of K-PPiA showed similarity with that of K-PPA. The major bands were: the four OH stretching bands, again with much reduced intensity; bands of the P-C₆H₅ bond and the phenyl ring (1438, 1483, 1594 cm⁻¹, three bands at 3000-3100 cm⁻¹); an intense P-H stretching band at 2380 cm⁻¹; and the very intense P-O stretching bands between 1000 and 1300 cm⁻¹ (Nakamoto, 1986; Morizzi et al., 2000; Breiting et al., 2001). The interpretation of the spectrum in the region below 1200 cm⁻¹ was even more complicated than for K-PPA due to overlapping of PPIA bands with the Si-O stretching and the Si-O-Al / O-Si-

O bending bands of kaolinite. Nevertheless, it is evident that the intensity of all Si-related bands was strongly reduced.

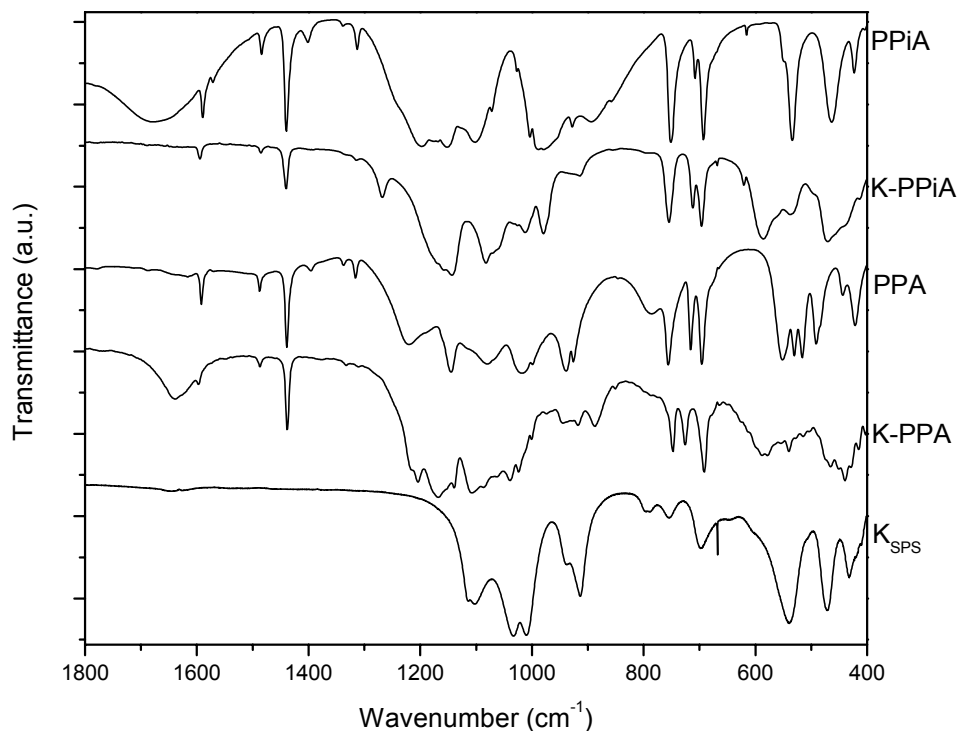


Fig. 6.11: FTIR spectra of raw kaolinite, K-PPA, K-PPiA, and the pure acids (PPA and PPIA), between 1800 and 400 cm^{-1} .

6.2.2.2 Gibbsite with PPA, PPIA and NPAA

The diffraction pattern of gibbsite (Fig. 6.12a) indicated a highly ordered material, with no detectable amounts of bayerite or any other crystalline admixtures (Cesteros *et al.*, 1999; 2001). The third-order basal reflection indicated a basal spacing of 4.83 Å.

The reaction with phenylphosphonic acid formed a new phase showing five orders of basal reflections with a basal spacing of 15.05 Å (Fig. 6.12b). In addition, two weak reflections, indicating spacings of 6.82 Å (only first-order reflection) and 6.21 Å (up to a second-order reflection) could be seen. A considerable amount of unreacted gibbsite was also present. Disregarding the small reflections at of 6.82 Å and 6.21 Å, the reaction ratio was $\alpha = 77\%$ (Table 6.3).

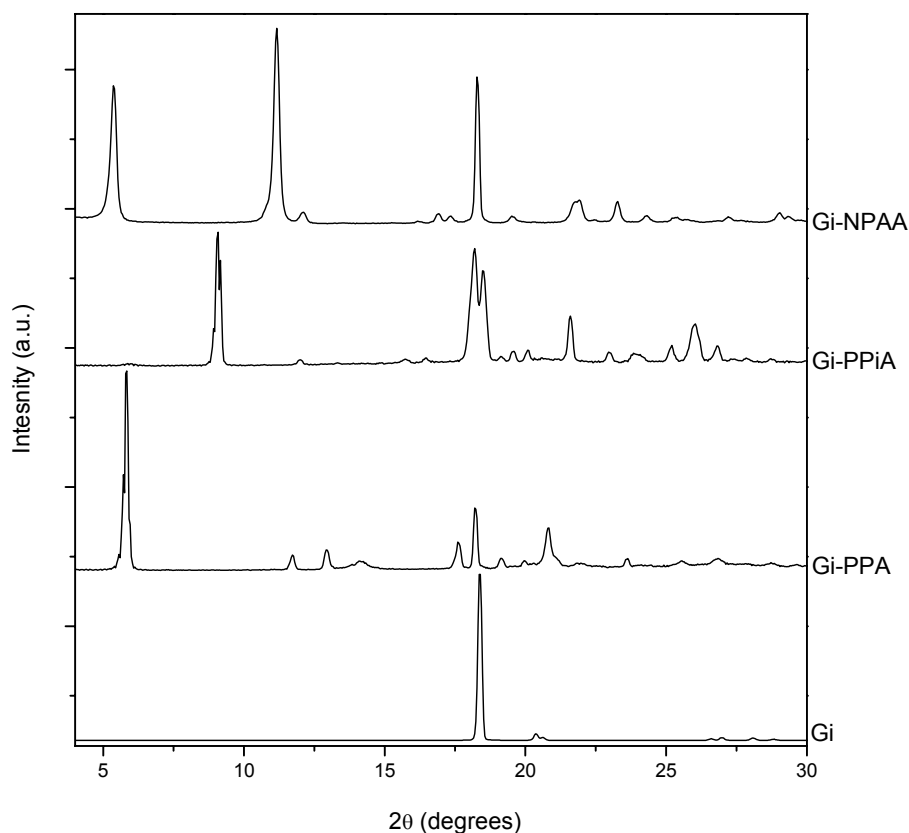


Fig. 6.12: XRPD patterns of gibbsite and the derivatives obtained with PPA, PPiA and NPAA.

Table 6.3: Values of d_{hkl} , Δd_{hkl} (in relation to unreacted gibbsite) and reaction rates (α) for gibbsite and gibbsite derivatives.

	Gibbsite	Gi-PPA			Gi-PPiA				
d_{hkl} (Å)	4.83	15.05	6.82	6.21	9.60	9.75	7.36	5.62	5.38
Δd_{hkl} (Å)	-	10.22	1.99	1.38	4.92	4.77	2.53	0.80	0.55
α (%)	-	77	-	-	-	-	-	-	-
		Gi-NPAA							
d_{hkl} (Å)		16.40	7.91	7.30	5.23	5.11			
Δd_{hkl} (Å)		11.60	3.08	2.47	0.41	0.28			
α (%)		-	-	-	-	-			

In the Gi-PPiA diffraction pattern (Fig. 6.12c) at least five different reflections could be identified in the region between 3° and 20° 2θ : two reflections at 9.60 Å and 9.75 Å (present up to the third-order reflection), and three reflections with low intensities indicating

spacings of 7.36 Å, 5.62 Å and 5.38 Å (only first-order reflections present) (Table 6.3). Unreacted gibbsite was also detected.

The Gi-NPAA compound also showed five different reflections between 3° and 20° 2θ (Fig. 6.12d). The two most intense reflections corresponded to spacings of 16.40 Å and 7.91 Å (seen up to the second and third-order reflections, respectively). One reflection indicating a spacing of 7.30 Å was observed up to the fourth-order, as well as two reflections at 5.23 Å and 5.11 Å (only the first-order reflection present) (Table 6.3). A considerable amount of unreacted gibbsite was also present.

The gibbsite sample consisted of thin platelets with almost hexagonal symmetry and some fragments of these crystals. The particle size ranged from 2 µm to 20 µm diameter. There were also dense, agglomerated lumps with less crystalline appearance (Fig 6.13). EDX analysis indicated only aluminum.

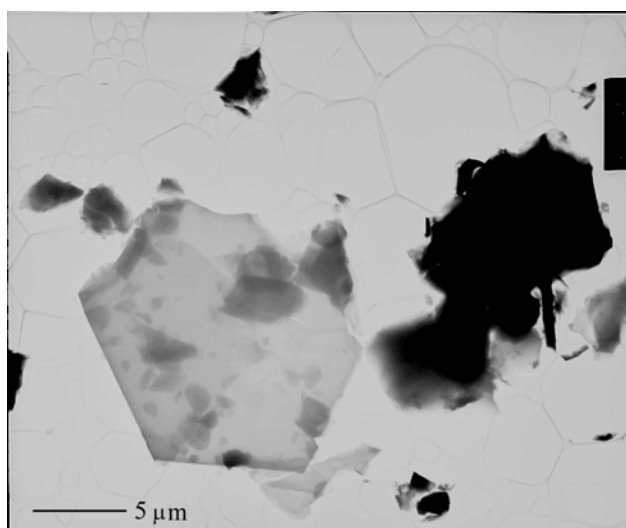


Fig. 6.13: TEM image of gibbsite particles.

Gi-PPA (Fig. 6.14) showed agglomerated crystals, mostly with plate-like morphology. Crystals with edges of $\sim 90^\circ$ were seen as well as some particles with $\sim 60^\circ$ angles. In average, the diameter of these crystals was $\sim 1 - 2$ µm. Larger gibbsite-like platelets, comparable to the original gibbsite, or undefined lumps were not observed. EDX analysis confirmed the presence of aluminum and phosphorus in every spot tested. The reaction product of gibbsite with PPA (Fig. 6.15) was very homogeneous and consisted of elongated crystals, with lengths of $\sim 5 - 10$ µm and $\sim 0,5 - 2$ µm width. The EDX analysis detected only aluminum and phosphorus in all spots. The few residual gibbsite particles showed no detectable traces of phosphorus. Gi-NPAA was composed of long, thin needle-like crystals

like K-NPAA. A few residual gibbsite particles were also observed (Fig. 6.16). Gi-PPA and Gi-PPiA could not be analyzed by SAED, due to the high beam-sensitivity of the crystals. The SAED patterns of the more stable Gi-NPAA compound (not shown) were almost identical with those of K-PPA.

The thermal behaviour of Gi-PPA (Fig. 6.17) was very similar to K-PPA. Two consecutive steps of mass loss were observed (4.7 % up to 175 °C and 2.4 % between 175 °C and 300 °C) with an endothermic peak at 166 °C and two very small endothermic peaks at 225 °C and 276 °C. The mass loss between 400 °C and 845 °C was 33.9 %. An exothermic event was observed at 622 °C. Further 44.8 % of mass were lost between 845 °C and 1100 °C, accompanied by a series of endothermic phenomena between 800 °C and 1080 °C. The total mass loss of 45.9 % was reached at 1100 °C.

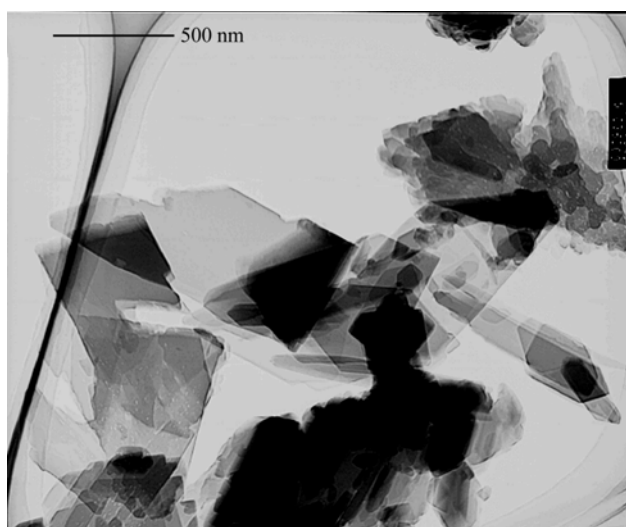


Fig. 6.14: TEM image of Gi-PPA.

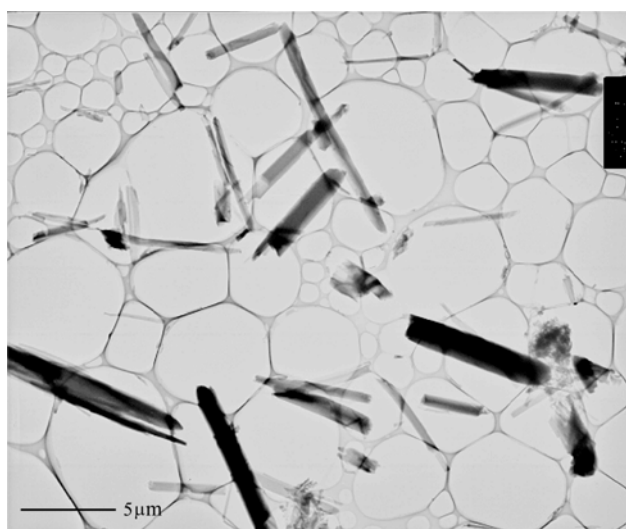


Fig. 6.15: TEM image of Gi-PPiA.

The similarities between the thermal behavior of Gi-PPiA and the kaolinite derivative were not so pronounced. Gi-PPiA showed a mass gain of 0.4 % between 100 °C and 305 °C and a weak endothermic peak at 230 °C. A sequence of five exothermic mass loss processes was observed between 305 °C and 1100 °C. The total mass loss was 47.1 %. An endothermic process was also detected at ~ 1040 °C, without related mass change (Fig. 6.17).

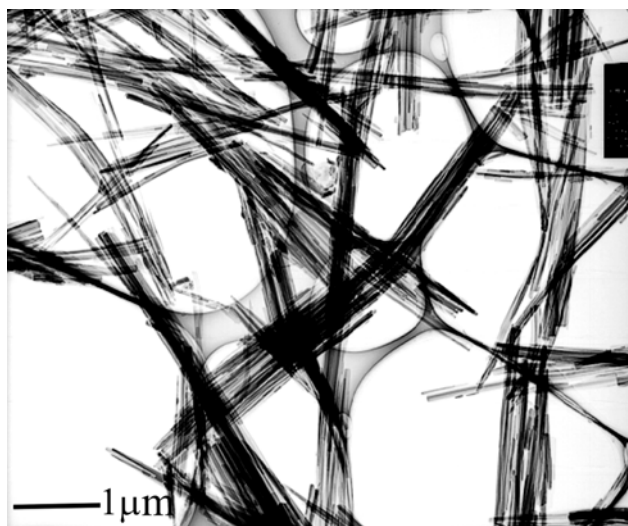


Fig. 6.16: TEM image of Gi-NPAA

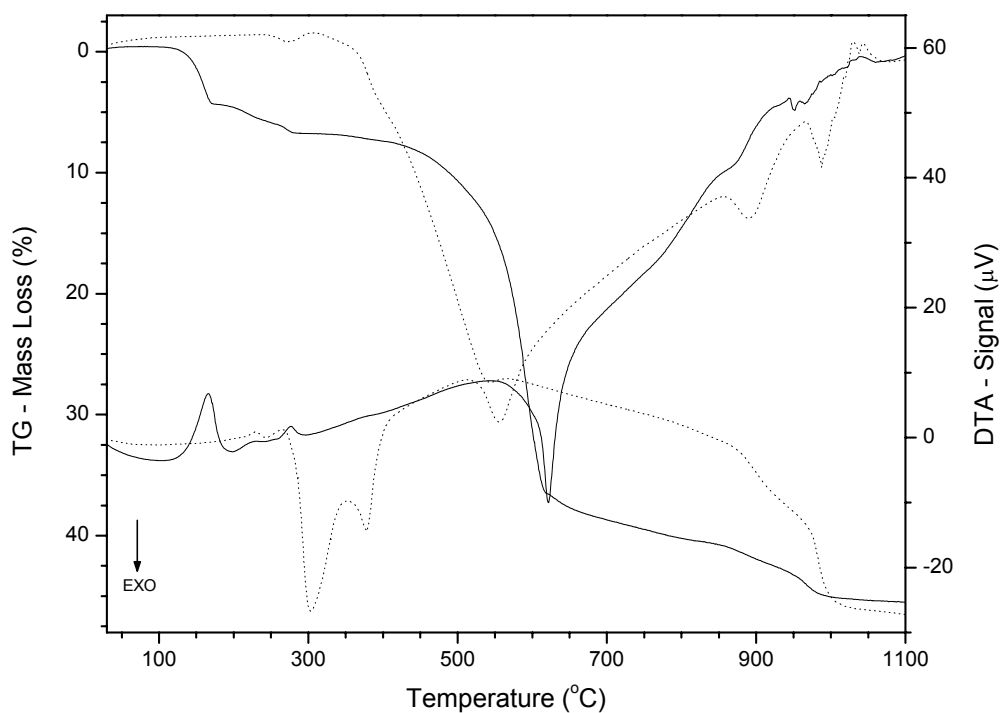


Fig. 6.17: TG/DTA curves of Gi-PPA (continuous lines) and of Gi-PPiA (dotted lines).

The FTIR spectrum of gibbsite (Fig. 6.18a, 6.19a) corresponded to the spectra published before (Frost *et al.*, 1999; Wang and Johnston, 2000 ; Ruan *et al.*, 2001; Kloprogge *et al.*, 2002). The FTIR spectrum of Gi-PPA (Fig. 6.18b, 6.19b) revealed some significant differences in the hydroxyl stretching region (3200-3700 cm^{-1}). In contrast to the original five intense bands of gibbsite, only a small band was observed at 3525 cm^{-1} . Other bands were characteristic of the aromatic ring with attached phosphorus (between 3000 and 3100 cm^{-1} and at 1594, 1486 and 1435 cm^{-1}) and the P-O stretching bands between 1000 and 1300 cm^{-1} (Thomas and Chittenden, 1970; Cabeza *et al.*, 1998; Haky *et al.*, 1997; Morizzi *et al.*, 2000; Breitingner *et al.*, 2001). One notes the strong decrease in intensity of many lower-frequency bands attributed to hydroxyl bending and deformation modes, especially the gibbsite bands at 1018, 966 and 666 cm^{-1} (Frost *et al.*, 1999; Wang and Johnston, 2000 ; Ruan *et al.*, 2001; Kloprogge *et al.*, 2002).

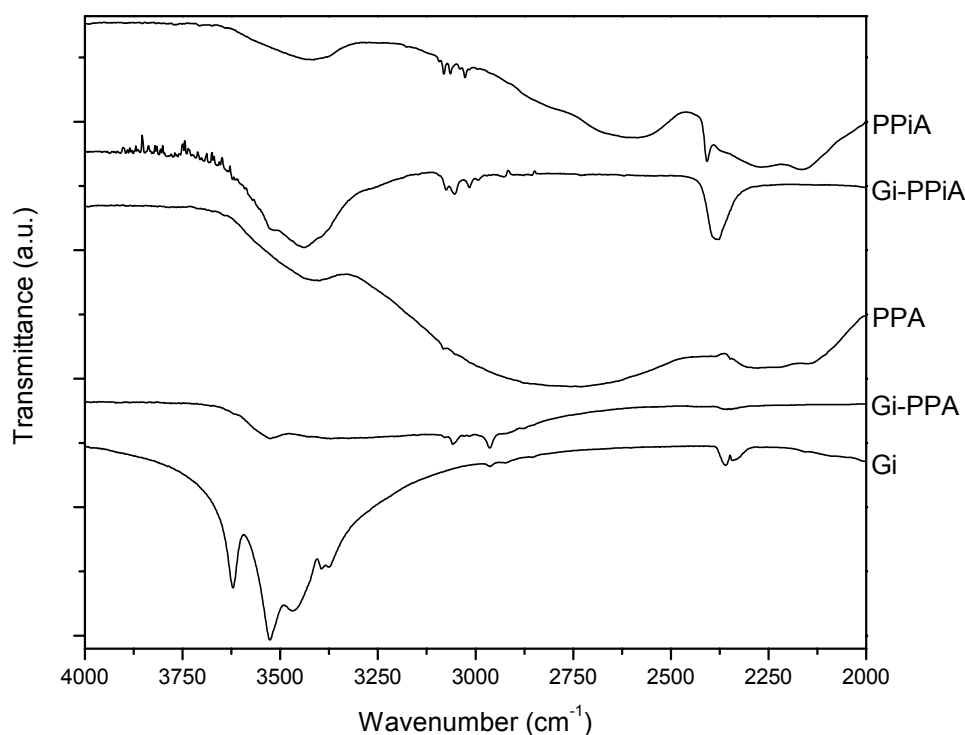


Fig. 6.18: FTIR spectra of gibbsite (Gi), Gi-PPA, Gi-PPiA and the pure acids (PPA and PPiA), between 4000 and 2000 cm^{-1} .

The spectrum of Gi-PPiA (Fig. 6.18d, 6.19d) can be interpreted in a similar way. In the hydroxyl-stretching region, only a broad band with two maxima at 3526 and 3439 cm^{-1}

was seen instead of well-defined bands. The bands related to the aromatic ring with attached phosphorus were also present ($3000\text{--}3100\text{ cm}^{-1}$, 1594 , 1487 and 1436 cm^{-1}) as well as a band of medium intensity in the 2380 cm^{-1} region, attributed to the P-H stretching mode (Nakamoto, 1986; Morizzi *et al.*, 2000; Breitingner *et al.*, 2001). The characteristic P-O stretching bands at the $1000\text{--}1300\text{ cm}^{-1}$ region and the strong intensity decrease of most hydroxyl bending and deformation bands in the lower-frequency region (especially those at 1018 , 795 and 666 cm^{-1} in the gibbsite spectrum) were also seen in this spectrum.

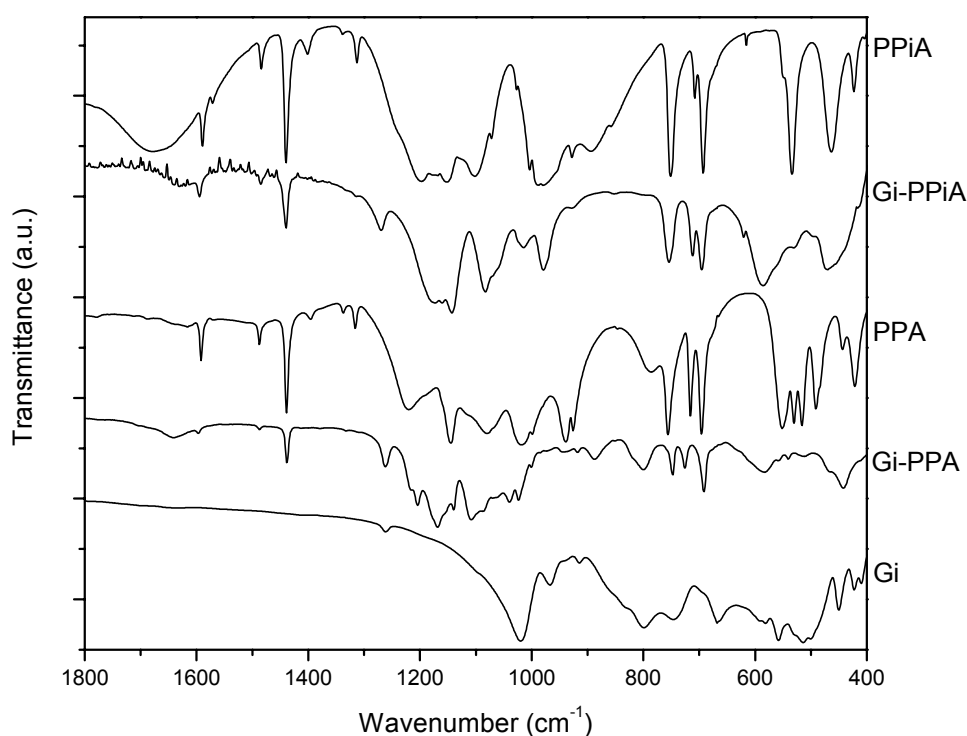


Fig. 6.19: FTIR spectra of gibbsite (Gi), Gi-PPA, Gi-PPiA, and the pure acids (PPA and PPiA), between 1800 and 400 cm^{-1} .

6.2.3 Discussion

The phase K-PPA is, in all analyzed aspects, identical to the phase described previously by Guimarães *et al.* (1998) and by Breen *et al.* (2002). The TEM micrographs and EDX analyses, however, clearly indicate that the reaction product of kaolinite and PPA is no longer related to the original kaolinite structure. The FTIR spectra show the diminished intensities or even the absence of the Si-O stretching bands (1114 , 1102 , 1030 and 1009 cm^{-1}) and the

strong decrease in intensity of the Si-O-Al / O-Si-O bending bands (538, 470 and 431 cm^{-1}). Guimarães *et al.* (1998) also gave some indirect evidence of structural changes: the reported XPS spectra reveals a distinctly lower Si:Al ratio for K-PPA than in the original kaolinite (although the authors did not comment this fact).

As K-PPA and Gi-PPA are characterized by almost identical basal spacings, it is unlikely that the original layer structure of kaolinite is maintained. In addition, these two compounds displayed almost the same morphology, showing particles with many 90° corners, which is totally different from the morphology of the original gibbsite and kaolinite particles. The TG/DTA analyses of these two compounds are also similar. The mass losses cannot be compared because of the presence of unreacted gibbsite in Gi-PPA. The FTIR spectra of Gi-PPA and K-PPA are almost superimposable. All these facts clearly indicate that K-PPA is not kaolinite with grafted phenylphosphonate groups as earlier suggested (Guimarães *et al.*, 1998, 1999; Breen *et al.*, 2002) but rather a lamellar aluminum phenylphosphonate.

Many data on metal phenylphosphonates and similar compounds are available. Raki and Detellier (1996) reacted PPA with bayerite, a metastable monoclinic modification of $\text{Al}(\text{OH})_3$ (Ruan *et al.*, 2001). They obtained an aluminum phenylphosphonate with a basal spacing expansion of 9.64 Å (in relation to the original bayerite) which is only 0.58 Å smaller than for Gi-PPA. The TG profile of their compound is almost identical to the one described here. These authors proposed a layer structure composed of aluminum (hydr)oxide sheets and bilayers of phenyl groups in perpendicular orientation to these sheets. Almost all aluminum phenylphosphonates (or closely related compounds) have lamellar structures, with the organic bilayers between the sheets and intense reflections at $d \sim 15$ Å (Haky *et al.*, 1997; Cabeza *et al.*, 1998; Chaplais *et al.*, 2000; Zakowski *et al.*, 2000). Gi-PPA belongs to this group of compounds, with a structure somewhat different from the described aluminum phenylphosphonates. The reaction conditions, the aluminum source and the Al/P ratio may strongly influence the structure of the final product (Cabeza *et al.*, 1998). A variety of phases may be obtained by varying these conditions.

The structure of K-PPA is certainly closely related to Gi-PPA. The fact that small amounts of silicon were detected by EDX may point toward some isomorphic substitution of Al atoms by Si atoms in K-PPA. Silicon can also be occluded inside the aluminum phosphonate crystals, maybe also in form of a phosphonate. Wypych *et al.* (2003) described a silicon phenylphosphonate which was formed by the reaction of chrysotile with PPA. Amorphous silica could also be adsorbed on the particle surfaces.

In any case, the destruction of the kaolinite structure by phosphates is not new. Weiss *et al.* (1995) described that not only kaolinite but also montmorillonite, sericite and gibbsite are transformed into taranakite ($K_3Al_5H_6(PO_4)_8 \cdot 18H_2O$) and similar layered phosphates by treatment with K_2HPO_4 in acid medium. Formation of $Al(CH_3)_6(PO_4)_3$ from kaolinite and trimethylphosphate (TMP) was also reported (Sánchez-Camazano and Sánchez-Martín, 1994). The authors suggested that “*the compound in question is formed by hydrolysis of TMP, catalyzed by the hydration water of exchange cations of kaolinite, followed by removal of Al from the silicate structure by incompletely hydrolyzed TMP*”. The compound formed had a very strong reflection at 8.84 Å and was identical to the reaction product of Al_2O_3 with TMP.

If K-PPiA were the grafting product of PPiA on kaolinite, a layer separation of 2.58 Å would be too small to accommodate the PPiA molecules. Rather, the TEM images reveal that K-PPiA is not a layered compound. This would also explain the presence of many reflections in the XRPD pattern between 10° and $30^\circ 2\theta$. Due to the EDX analyses, the new phase could be an aluminum phenylphosphinate.

The PPiA derivative of gibbsite displays the same morphological features as K-PPiA, and both compounds are distinctly different from the PPA derivatives. The profiles of the thermal analysis and FTIR spectra of K-PPiA and Gi-PPiA are also comparable and support the assumption that kaolinite reacted with PPiA to form an aluminum phenylphosphinate. The intense reflections at 9.60 – 9.75 Å and 7.36 Å for Gi-PPiA and at 9.73 Å and 7.33 Å for K-PPiA strongly indicate that these two compounds could have the same structure.

Many studies on phosphinate salts of divalent and trivalent transition metal ions were already published (see, for example, Giordano *et al.*, 1969; Colamarino *et al.*, 1976; Cunningham *et al.*, 1979; Shieh *et al.*, 1990; Grohol *et al.*, 1999 or Li and Xiang, 2002). Considering the properties of these compounds, K-PPiA and Gi-PPiA cannot have a layered structure. The structural units of this group of compounds are polymeric linear chains and they are sometimes classified as *Inorganic Coordination Polymers* (Cunningham *et al.*, 1979; Shieh *et al.*, 1990). The phosphinate structures may be contrasted with those of the divalent metal phosphonates. While most metal cations form layered structures with phosphonate groups, the phosphinate salts present a skeletal backbone consisting of metal ions linked by bridging O–P–O groups, thus leading to infinite single chain structures (Cunningham *et al.*, 1979). The dimensionality of these materials seems to be a direct function of the number of oxygen atoms available for coordination to the metal ions (Shieh *et al.*, 1990; Grohol *et al.*, 1999). Grohol *et al.* (1999) stated that, to the best of their knowledge, two- or three-

dimensional metal phosphinates had not yet been prepared, in agreement with the fact that only two oxygen atoms are present in the phosphinate group. However, Morizzi *et al.* (2000) described lamellar phenylphosphinates of gallium(III) and indium(III). Although they cited Grohol *et al.* (1999), they did not report any explanation why layered structures were formed instead of the usual polymeric linear chains. Aluminum phenylphosphinates have not yet been described.

Although the thermal behavior of the two PPIA derivatives show some differences, it does not imply that the compounds could not have similar structures since even small structural differences can produce large differences in the thermal behaviour. The small mass gain observed in both compounds around 200 °C is clearly related to the oxidation of the phosphinate groups.

The FTIR spectra of both compounds clearly confirm the presence of the phenylphosphinate group and the consumption of the OH groups of kaolinite and gibbsite. Though difficult to judge due to band overlapping in the K-PPIA compound, the intensity of the Si-O related bands is also diminished.

The crystalline products obtained from kaolinite and gibbsite with NPAA show almost the same morphology (Fig. 6.7, 6.16). The many X-ray reflections between 10° and 30° 2θ could result from the non-layer structure. The FTIR spectra of K-NPAA and Gi-NPAA (not shown) confirmed the presence of the nitrophenylarsonic groups, and the consumption of the OH groups of kaolinite and gibbsite. Again, the intensity of the Si-related bands in the kaolinite derivative was greatly diminished in comparison with raw kaolinite.

The crystal morphology and the SAED patterns of K-NPAA and Gi-NPAA suggest a chain-like structure with the chains running along the needle axis. These chains most probably consist of [AlO₆] octahedra and [AsO₃Ph] tetrahedra sharing two common oxygens, possibly analogous to structure of the PPIA derivatives. To the best of our knowledge, a one-dimensional metal phenylarsonate was not yet reported. Usually, metal phenylarsonates have lamellar structures similar to the structures of the metal phenylphosphonates (Cunningham *et al.*, 1979; Huan *et al.*, 1990; Morizzi *et al.*, 2000). Nevertheless, a compound can have a lower dimensionality than expected, as already stated by Grohol *et al.* (1999), who described one-dimensional uranyl phenylphosphonates. In these compounds an oxygen atom of the phosphonate group is protonated and cannot coordinate with the uranyl group. Such protonation reactions depend on the pK_a of the starting acid and pH of the reaction medium. Therefore, a lamellar aluminum phenylarsonate may be prepared by choosing appropriate

reaction conditions. On the other hand, a lamellar vanadyl phenylarsonate ($V_2O_4(C_6H_5AsO_3H) \cdot H_2O$) was described, in which the arsonate group contains one unionized hydroxyl group, and a two-dimensional layered structure is formed even with only two oxygen atoms available for coordination (Huan *et al.*, 1990). Such apparent contradictions prove that the structural arrangement of these compounds is not straightforward predictable.

Based on all the collected data, the mechanisms of the reactions here described (and particularly, of the reaction between kaolinite and PPA) are certainly not topotactic, as previously suggested (Guimarães *et al.*, 1998). It is suggested that all these reactions proceed most likely by dissolution of the aluminum-containing matrix (kaolinite or gibbsite) by the acids, with the subsequent new-formation of the insoluble compounds described.

6.3 Conclusion

Reaction of PPA, PPIA and NPAA with kaolinite decomposes the silicate structure by new-formation of aluminum phenyl derivatives. Gibbsite yielded products very similar to these compounds. The aluminum phenylphosphonate forms a layered structure, with $d_{001} = 15.0 \text{ \AA}$ and thin, planar crystallites with square or square-like morphology. The dense, elongated crystals of the aluminum phenylphosphinate very likely contain linear chains as in many other metal phosphinates. The aluminum phenylarsonate displayed a needle-like morphology and is most likely also composed of linear chains of $[\text{AlO}_6]$ octahedra and phenylarsonate groups. No evidence of formation of grafted kaolinite derivatives after the reaction with PPA was found.

CONCLUSION

Conclusion

Various new interlayer-grafted derivatives of kaolinite were obtained. It was shown that the acidic interlayer basal hydroxyl groups and the external basal hydroxyl groups of kaolinite are reactive towards esterification with many n-alkanols, diols and glycol mono-ethers. The Al-O-C covalent bonds formed between the mineral matrix and the grafted organic molecules is very stable towards washing with many solvents. The grafted derivatives also show good thermal stability.

These grafted derivatives of kaolinite formed aqueous dispersions with yield values and apparent viscosities higher than for raw kaolinite. The yield points and apparent viscosities of these dispersions increased exponentially with the size of the alkyl moiety of the grafted molecule. The stability of the dispersions decreased with the apolar character of the grafted molecule. An interesting way to control the flow properties of kaolinite dispersions was achieved by interlayer (and surface) grafting of different organic molecules.

Primary n-alkylamines were able to intercalate directly into interlayer-grafted derivatives of kaolinite. By leaching some n-octadecylamine intercalates with organic solvents, the clay mineral particles could be efficiently delaminated into very thin lamellae. These units very likely consisted of kaolinite monolayers, which curled into halloysite-like morphology, forming nanotubes much smaller in diameter than usual halloysite tubes. This process allows the preparation of nanotubes with a controllable inner surface character, possibly offering new possibilities for many advanced uses.

It was also shown that only alcohol-like molecules could graft to kaolinite hydroxyl groups in an esterification-like reaction. The previously described synthesis of a kaolinite-phenylphosphonate was shown to be misinterpreted. Phenylphosphonic, phenylphosphinic and phenylarsonic acids reacted with kaolinite in non-topotactic reactions, with the dissolution of the mineral structure and new-formation of aluminum derivatives.

The study here reported represents an important contribution to the understanding of kaolinite interlayer reactions. The many new compounds obtained offer new possibilities to the preparation of modified clay mineral/organic polymer nanocomposites with optimized interactions between organic and inorganic phases. Such composite materials should present improved properties in relation to conventional nanocomposites obtained with unmodified inorganic fillers.

The successful delamination of kaolinite into monolayers was also an important achievement, as different approaches to this process were already tried with no success. It was not possible to stabilize the planar layers by grafting, to avoid or minimize the rolling process. Nevertheless, the kaolinite nanotubes with tailored interior should be further investigated, as they may show interesting properties.

Research on kaolinite intercalation compounds, despite the large number of publications already related to this theme, is far away from its downfall. With the possibility to obtain interlayer-grafted derivatives, the investigation of this clay mineral gains a new impulse. Kaolinite is still the most abundant clay mineral, present virtually everywhere, and its industrial and technological uses and importance tend to increase, promoted by the results from basic and applied research.

REFERENCES

REFERENCES

- Andrew R. W., Jackson M. L. and Wada K. (1960) Intersalation as a technique for differentiation of kaolinite from chloritic minerals by X-ray diffraction. *Soil Science Society of America Proceedings*, **24**, 422-424.
- Aparicio P., Pérez-Bernal J. L., Galán E. and Bello M. A. (2004) Kaolin fractal dimensions. Comparison with other properties. *Clay Minerals*, **39**, 75-84.
- Bailey S. W. (1963) Polymorphism of the kaolin minerals. *American Mineralogist*, **48**, 1196-1209.
- Bailey S. W. (1980) Comment – Summary of recommendations of AIPEA nomenclature committee. *Clays and Clay Minerals*, **28**, 73-78.
- Bailey S. W. (1984) Structures of layer silicates. Pp. 1-124 In: *Crystal Structures of Clay Minerals and their X-Ray Identification*. (G. W. Brindley and G Brown, editors). 1st reprint. Mineralogical Society, London, UK.
- Balan E., Saita A. M., Mauri F. and Calas G. (2001) First-principles modeling of the infrared spectrum of kaolinite. *American Mineralogist*, **86**, 1321-1330.
- Basyaruddin M., Rahman A., Tajudin S. M., Hussein M. Z., Rahman R. N. Z. R. A., Salleh A. B. and Basri M. (2005) Application of natural kaolin as support for the immobilization of lipase from *Candida rugosa* as biocatalyst for effective esterification. *Applied Clay Science*, **29**, 111-116.
- Bates T., Hildebrand F. A. and Swineford A. (1950) Morphology and structure of endellite and halloysite. *American Mineralogist*, **35**, 463-484.
- Besra L., Sengupta D. K., Roy S. K. and Ay P. (2002) Flocculation and dewatering of kaolin suspensions in the presence of polyacrylamide and surfactants. *International Journal of Mineral Processing*, **66**, 203-232.
- Bish D. L. (1993) Rietveld refinement of the kaolinite structure at 1.5 K. *Clays and Clay Minerals*, **41**, 738-744.
- Bobos I., Duplay J., Rocha J. and Gomes C. (2001) Kaolinite to halloysite-7 Å transformation in the kaolin deposit of São Vicente de Pereira, Portugal. *Clays and Clay Minerals*, **49**, 596-607.
- Bodenheimer W., Heller L. and Bartura J. (1967) Intersalation of K-acetate in flint clay. *Clay Minerals*, **7**, 237-239.

-
- Bolland M. D. A., Posner A. M. and Quirk J. P. (1980) Surface charge on kaolinites in aqueous suspension. *Australian Journal of Soil Research*, **14**, 197-216.
- Bougeard D., Smirnov K. S. and Geidel E. (2000) Vibrational spectra and structure of kaolinite: a computer simulation study. *Journal of Physical Chemistry B*, **104**, 9210-9217.
- Brady P. V., Randall T. C. and Nagy K. L. (1996) Molecular controls on kaolinite surface charge. *Journal of Colloid and Interface Science*, **183**, 356-364.
- Braggs B., Fornasiero D., Ralston J. and Smart R. S. (1994) The effect of surface modification by an organosilane on the electrochemical properties of kaolinite. *Clays and Clay Minerals*, **42**, 123-136.
- Brandt K. B., Elbokl T. A. and Detellier C. (2003) Intercalation and interlamellar grafting of polyols in layered aluminosilicates. D-Sorbitol and adonitol derivatives of kaolinite. *Journal of Materials Chemistry*, **13**, 2566-2572.
- Breen C., D'Mello N. and Yarwood J. (2002) The thermal stability of mixed phenylphosphonic acid/water intercalates of kaolin and halloysite. A TG-EGA and VT-DRIFTS study. *Journal of Materials Chemistry*, **12**, 273-278.
- Breitinger D. K., Mohr J., Colognesi D., Parker S. F., Schukow H. and Schwab R. G. (2001) Vibrational spectra of augelites $Al_2(OH)_3(XO)_4$ (X = P, As, V). *Journal of Molecular Structure*, **563-564**, 377-382.
- Brindley G. W. (1984) Order-disorder in clay mineral structures. Pp. 125-195 In: *Crystal Structures of Clay Minerals and their X-Ray Identification*. (G. W. Brindley and G Brown, editors). 1st reprint. Mineralogical Society, London, UK.
- Brindley G. W. and Lemaitre J. (1987) Thermal, oxidation and reduction reactions of clay minerals. Pp. 319-370 in: *Chemistry of clays and clay minerals* (A. C. D. Newman, editor). Longman Scientific & Technical, Essex, UK.
- Buggy M., Bradley G. and Sullivan A. (2005) Polymer-filler interactions in kaolin/nylon 6,6 composites containing a silane coupling agent. *Composites Part A – Applied Science and Manufacturing*, **36**, 437-442.
- Cabeza A., Aranda M. A. G., Bruque S., Poojary D. M., Clearfield A. and Sanz J. (1998) Aluminum phenylphosphonates: a fertile family of compounds. *Inorganic Chemistry*, **37**, 4168-4178.
- Cesteros Y., Salagre P., Medina F. and Sueiras J. E. (1999) Several factors affecting faster rates of gibbsite formation. *Chemistry of Materials*, **11**, 123-129.

- Cesteros Y., Salagre P., Medina F. and Sueiras J. E. (2001) A new route to the synthesis of fine-grain gibbsite. *Chemistry of Materials*, **13**, 2595-2600.
- Chaplais G., Bideau J. L., Leclercq D., Mutin H. and Vioux A. (2000) Novel aluminium phenyl, benzyl, and bromobenzylphosphonates: structural characterization and hydration-dehydration reactions. *Journal of Materials Chemistry*, **10**, 1593-1601.
- Chekin S. S. (1992) Preparation of stable suspensions of delaminated kaolinite by combined dimethylsulfoxide-ammonium fluoride treatment: Discussion. *Clays and Clay Minerals*, **40**, 740-741.
- Colamarino P., Orioli P. L., Benzinger W. D. and Gillman H. D. (1976) Synthesis, properties, and structural characterization of lead(II) bis(diphenylphosphinate), $\text{Pb}[\text{OP}(\text{C}_6\text{H}_5)_2\text{O}]_2$. *Inorganic Chemistry*, **15**, 800-804.
- Costa M. L. and Moraes E. L. (1998) Mineralogy, geochemistry and genesis of kaolins from the amazon region. *Mineralium Deposita*, **33**, 283-297.
- Costanzo P. M., Clemency C. V. and Giese R. F. (1980) Low temperature synthesis of a 10-Å hydrate of kaolinite using dimethylsulfoxide and ammonium fluoride. *Clays and Clay Minerals*, **28**, 155-156.
- Costanzo P. M., Giese, R. F., Lipsicas M. and Straley C. (1982) Synthesis of a quasi-stable kaolinite and heat capacity of interlayer water. *Nature*, **296**, 549-551.
- Costanzo P. M., Giese R. F. and Clemency C. V. (1984a) Synthesis of a 10-Å hydrated kaolinite. *Clays and Clay Minerals*, **32**, 29-35.
- Costanzo P. M., Giese, R. F. and Lipsicas M. (1984b) Static and dynamic structure of water in hydrated kaolinite. I. The static structure. *Clays and Clay Minerals*, **32**, 419-428.
- Costanzo P. M. and Giese, R. F. (1985) Dehydration of synthetic hydrated kaolinites: A model for the dehydration of halloysite(10Å). *Clays and Clay Minerals*, **33**, 415-423.
- Cruz M., Jacobs H. and Fripiat J. J. (1973) Interlayer bonding in kaolin minerals. *Proceedings of the International Clay Conference, Madrid*, 25-46.
- Cunningham D., Hennelly P. J. D. and Deeney T. (1979) Divalent metal phenylphosphonates and phenylarsonates. *Inorganica Chimica Acta*, **37**, 95-102.
- Delmon B., Herbillon A. J., Leonard A. J. and Bulens M. (1978) Critical assessment of the joint use of various physico-chemical techniques in the study of the thermal transformation of kaolin. *Proceedings of the International Clay Conference, Oxford*, 639-648.

-
- Deng Y., White G. N. and Dixon J. B. (2002) Effect of structural stress on the intercalation rate of kaolinite. *Journal of Colloid and Interface Science*, **250**, 379-393.
- Dera P., Prewitt C. T., Japel S., Bish D. L. and Johnston C. T., (2003) Pressure-controlled polytypism in hydrous layered materials. *American Mineralogist*, **88**, 1428-1435.
- Domka L., Krysztafkiewicz a. and Kozak M. (2002) Silane modified fillers for reinforcing polymers. *Polymers and Polymer Composites*, **10**, 541-552.
- Domka L. Foltynowicz Z, Jurga S. and Kozak M. (2003) Influence of silane modification of kaolins on physico-mechanical and structural properties of filled PVC composites. *Polymers and Polymer Composites*, **11**, 397-406.
- Dong W., Li W., Yu K., Krishna K., Song L., Wang X., Wang Z., Coppens M. and Feng S. (2003) Synthesis of silica nanotubes from kaolin clay. *Chemical Communications*, 1302-1303.
- El Bokl T. A. and Detellier C. (2005) Kaolinite-based nanohybrid materials. *Book of Abstracts of the 13th International Symposium on Intercalation Compounds, Clermont-Ferrand*, 14 (data also derived from the Oral Contribution presented during the symposium).
- Farmer V. C. (1974) *The infrared spectra of minerals*. Mineralogical Society, London, UK.
- Fedoseev A. D. and Kucharskaja E. V. (1963) Organic derivatives of kaolin. *Proceedings of the International Clay Conference, Stockholm*. **2**, 365-371. Pergamon Press, Oxford, UK.
- Frost R. L. (1988) Hydroxyl deformation in kaolins. *Clays and Clay Minerals*, **46**, 280-289.
- Frost R. L. (1995) Fourier transform Raman spectroscopy of kaolinite, dickite and halloysite. *Clays and Clay Minerals*, **43**, 191-195.
- Frost R. L. and Vassallo A. M. (1996) The dehydroxylation of the kaolinite clay minerals using infrared emission spectroscopy. *Clays and Clay Minerals*, **44**, 635-651.
- Frost R. L., Fredericks P. M. and Bartlett J. R. (1993) Fourier transform Raman spectroscopy of kandite clays. *Spectrochimica Acta*, **49A**, 667-674.
- Frost R. L., Tran T. H. and Kristof J. (1997) The structure of an intercalated ordered kaolinite – a Raman microscopy study. *Clay Minerals*, **32**, 587-596.
- Frost R. L., Kloprogge J. T., Russel S. C. and Szetu J. L. (1999) Vibrational spectroscopy and dehydroxylation of aluminum (oxo)hydroxides: gibbsite. *Applied Spectroscopy*, **53**, 423-434.

- Fukase M., Sakai Y. and Kitajima K. (1996) Synthesis of dioctahedral fluorine mica ceramics by using kaolinite as raw material. *Journal of the Ceramic Society of Japan*, **104**, 764-769.
- Gardolinski J. E. F. C. (2001) *Compostos de intercalação derivados da caulinita*. MSc Dissertation. Universidade Federal do Paraná, Curitiba, Brazil.
- Gardolinski J. E., Peralta-Zamora P. and Wypych F. (1999) Preparation and characterization of a kaolinite-1-methyl-2-pyrrolidone intercalation compound. *Journal of Colloid and Interface Science*, **211**, 137-141.
- Gardolinski J. E., Carrera C. M., Cantão M. P. and Wypych F. (2000) Layered polymer-kaolinite nanocomposites. *Journal of Materials Science*, **35**, 3113-3119.
- Gardolinski J. E., Wypych F. and Cantão M. P. (2001) Esfoliação e hidratação da caulinita após intercalação com uréia. *Química Nova*, **24**, 761-767.
- Gardolinski J. E., Martins Filho H. P. and Wypych F. (2003) Comportamento térmico da caulinita hidratada. *Química Nova*, **26**, 30-35.
- Gardolinski, J. E. F. C., Lagaly G. and Czank M. (2004) On the destruction of kaolinite and gibbsite by phenylphosphonic, phenylphosphinic and phenylarsonic acids: evidence for the formation of new Al compounds. *Clay Minerals*, **39**, 391-404.
- Gastuche M. C., Delvigne J. and Fripiat J. J. (1954) Altération chimique des kaolinites. *Transactions of the 5th International Congress of Soil Science, Leopoldville*, **2**, 439-456.
- Giese R. F. (1991) Kaolin minerals: Structures and stabilities. In: *Hydrous phyllosilicates*. Pp. 29-66. Reviews in Mineralogy, **19** (S. W. Bailey, editor). Mineralogical Society of America, Washington, D. C., USA.
- Giordano F., Randaccio L. and Ripamonti A. (1969) The crystal structures of the monoclinic and orthorhombic forms of a zinc(II) n-buthylphenylphosphinate polymer. *Acta Crystallographica*, **B25**, 1057-1065.
- Gobi (2002) *New forecasts for the international kaolin industry*. Market research report. Gobi International, London, UK [<http://www.gobi.co.uk/press/KaolinPress2002.pdf>].
- Gomes C. F. (1988) *Argilas – O que são e para que servem*. Fundação Calouste Gulbenkian, Lisboa.
- Gonzalez-Garcia S. and Sanchez-Camazano M. (1965) Complejos de adsorción de los minerales de la arcilla con dimetilsulfoxido. *Anales de Edafología y Agrobiología*, **24**, 495-520.
- Grim R. E. (1962) *Applied Clay Mineralogy*, McGraw-Hill Book Company, New York, USA.

- Grim R. E. (1968) *Clay Mineralogy*, 2nd Ed., McGraw-Hill Book Company, New York, USA.
- Grohol D., Gingl F. and Clearfield A. (1999) Syntheses and crystal structures of a linear-chain uranyl phenylphosphinate $\text{UO}_2(\text{O}_2\text{PHC}_6\text{H}_5)_2$ and layered uranyl methylphosphonate $\text{UO}_2(\text{O}_3\text{PCH}_3)$. *Inorganic Chemistry*, **38**, 751-756.
- Gualtieri A., Norby P., Artioli G. and Hanson J. (1997) Kinetics of formation of zeolite Na-A [LTA] from natural kaolinites. *Physics and Chemistry of Minerals*, **24**, 191-199.
- Guggenheim S. and Martin T. (1995) Definition of clay mineral: joint report of the AIPEA and CMS nomenclature committees. *Clay Minerals*, **20**, 257-259.
- Guimarães J. L., Peralta-Zamora P. and Wypych F. (1998) Covalent grafting of phenylphosphonate groups onto the interlamellar aluminol surface of kaolinite. *Journal of Colloid and Interface Science*, 1998, **206**, 281-287.
- Guimarães J. L., Cunha C. J. and Wypych F. (1999) Intercalation of hexylamine into hydrated kaolinite phenylphosphonate. *Journal of Colloid and Interface Science*, 1999, **218**, 211-216.
- Haky J. E., Brady J. B., Dando N. and Weaver D. (1997) Synthesis and structural studies of layered aluminum phenylphosphonate. *Materials Research Bulletin*, **32**, 297-303.
- Heller-Kallai L. and Frenkel M. (1978) Reactions of salts with kaolinite at elevated temperatures – Part 2. *Proceedings of the International Clay Conference, Oxford*, 629-637.
- Heller-Kallai L. and Lapides I. (2003) Thermal reactions of kaolinite with potassium carbonate. *Journal of Thermal Analysis and Calorimetry*, **71**, 689-698.
- Hinckley D. N. (1963) Variability in “crystallinity” values among the kaolin deposits of the coastal plain of Georgia and South Carolina. *Clays and Clay Minerals*, **11**, 229-235.
- Hofmann U. and Frenzel A. (1930) Quellung von Graphit und die Bildung von Graphitsäure. *Berichte der deutschen chemischen Gesellschaft*, **63**, 1248-1262.
- Hofmann U., Endell K. and Wilm D. (1933) Kristallstruktur und Quellung von Montmorillonit (Das Tonmineral der Bentonittone). *Zeitschrift für Kristallographie*, **86**, 340-348.
- Huan G., Johnson J. W., Jacobson A. J. and Merola J. S. (1990) Hydrothermal synthesis and single-crystal structural characterization of $\text{V}_2\text{O}_4(\text{C}_6\text{H}_5\text{AsO}_3\text{H})\cdot\text{H}_2\text{O}$. *Chemistry of Materials*, **2**, 719-723.
- Inoue M., Kondo Y. and Inui T. (1986) The reaction of crystalline aluminum hydroxide in ethylene glycol. *Chemistry Letters*, 1421-1424.

-
- Inoue M., Kondo Y. and Inui T. (1988) An ethylene glycol derivative of boehmite. *Inorganic Chemistry*, **27**, 215-221.
- Inoue M., Tanino H., Kondo Y. and Inui T. (1991a) Formation of organic derivatives of boehmite by the reaction of gibbsite with glycols and aminoalcohols. *Clays and Clay Minerals*, **39**, 151-157.
- Inoue M., Kominami H. and Inui T. (1991b) Reaction of aluminium alkoxides with various glycols and the layer structure of their products. *Journal of the Royal Chemical Society, Dalton Transactions*, 3331-3336.
- Inoue M., Kimura M. and Inui T. (2000) Alkoxyalumoxanes. *Chemistry of Materials*, **12**, 55-61.
- Itagaki T. and Kuroda K. (2003) Organic modification of the interlayer surface of kaolinite with propanediols by transesterification. *Journal of Materials Chemistry*, **13**, 1064-1068.
- Jackson M. L. and Abdel-Kader F. H. (1978) Kaolinite intercalation procedure for all sizes and types with X-ray diffraction spacing distinctive from other phyllosilicates. *Clays and Clay Minerals*, **26**, 81-87.
- Jasmund K. and Lagaly G. (1993) *Tonminerale und Tone: Struktur, Eigenschaften und Einsatz in Industrie und Umwelt*, Steinkopff, Darmstadt, Germany.
- Jeong G. Y. (1998) Formation of vermicular kaolinite from halloysite aggregates in the weathering of plagioclase. *Clays and Clay Minerals*, **46**, 270-279.
- Johansson U., Holmgren A., Forsling W. and Frost R. L. (1998) Isotopic exchange of kaolinite hydroxyl protons: a diffuse reflectance infrared Fourier transform spectroscopy study. *The Analyst*, **123**, 641-645.
- Kloprogge J. T., Ruan H. D. & Frost R. L. (2002) Thermal decomposition of bauxite minerals: infrared emission spectroscopy of gibbsite, boehmite and diaspor. *Journal of Materials Science*, **37**, 1121-1129.
- Komori Y., Sugahara Y. and Kuroda K. (1998) A kaolinite-NMF-methanol intercalation compound as a versatile intermediate for further intercalation reaction of kaolinite. *Journal of Materials Research*, **13**, 930-934.
- Komori Y., Sugahara Y. and Kuroda K. (1999) Intercalation of alkylamines and water into kaolinite with methanol kaolinite as an intermediate. *Applied Clay Science*, **15**, 241-252.
- Komori Y., Enoto H., Takenawa R., Hayashi S., Sugahara Y. and Kuroda K. (2000) Modification of the interlayer surface of kaolinite with methoxy groups. *Langmuir*, **16**, 5506-5508.

-
- Lagaly, G. (1976) Kink-block and gauche-block structures of bimolecular films. *Angewandte Chemie – International Edition*, **15**, 575-586.
- Lagaly G. (1999) Introduction: from clay mineral-polymer interactions to clay mineral-polymer nanocomposites. *Applied Clay Science*, **15**, 1-9.
- Lagaly G. (2001) Introduction: Pesticide-clay interactions and formulations. *Applied Clay Science*, **18**, 205-209.
- Lagaly G., Schulz O. and Zimehl R. (1997) *Dispersionen und Emulsionen - Eine Einführung in die Kolloidik feinverteilter Stoffe einschließlich der Tonminerale*. Steinkopff Verlag, Darmstadt, Germany.
- Lahav N. (1990) Preparation of stable suspensions of delaminated kaolinite by combined dimethylsulfoxide-ammonium fluoride treatment. *Clays and Clay Minerals*, **38**, 219-222.
- LeBaron P., Wang Z. and Pinnavaia T. J. (1999) Polymer-layered silicate nanocomposites: an overview. *Applied Clay Science*, **15**, 11-29.
- Li N. and Xiang S. (2002) Hydrothermal synthesis and crystal structure of two novel aluminophosphites containing infinite Al-O-Al chains. *Journal of Materials Chemistry*, **12**, 1397-1400.
- Loh E. (1973) Optical vibrations in sheet silicates. *Journal of Physics C: Solid State Physics*, **6**, 1091-1104.
- Lombardi K. C., Guimarães J. L., Mangrich A. S., Mattoso N., Abbate M., Schreiner W. H. and Wypych F. (2002) Structural and morphological characterization of the PP-0559 kaolinite from the Brazilian amazon region. *Journal of the Brazilian Chemical Society*, **13**, 270-275.
- Loughnan F. C. and Roberts F. I. (1981) The natural conversion of ordered kaolinite to halloysite (10Å) at burning Mountain near Wingen, New South Wales. *American Mineralogist*, **66**, 997-1005.
- Ma C. and Eggleton R. A. (1999) Cation exchange capacity of kaolinite. *Clays and Clay Minerals*, **47**, 174-180.
- Mai G. (1969) Zur Kenntnis der Kaolinit-Einlagerungsverbindungen. PhD Thesis, Ludwig-Maximilians-Universität, München, Germany.
- van der Marel H. W. and Beutelspacher H. (1976) *Atlas of infrared spectroscopy of clay minerals and their admixtures*. Elsevier, Amsterdam, The Netherlands.
- Mártires R. A. C. (2003) Caulim. In: *Sumário Mineral 2003*, 48-49. Departamento Nacional de Produção Mineral, Brasília [<http://www.dnpm.gov.br/sm2003.html>].

- Mártires R. A. C. (2004) Caulim. In: *Sumário Mineral 2004*, 41-42. Departamento Nacional de Produção Mineral, Brasília [<http://www.dnpm.gov.br/sm2004.html>].
- Maxwell C. B. and Malla P. B. (1999) Chemical delamination of kaolin. *American Ceramic Society Bulletin*, **78**, 57-59.
- Michaelian K. H., Lapidés I., Lahav N., Yariv S. and Brodsky I. (1998) Infrared study of the intercalation of kaolinite by caesium bromide and caesium iodide. *Journal of Colloid and Interface Science*, **204**, 389-393.
- Moore D. M. and Reynolds R. C. (1989) *X-Ray diffraction and the identification and analysis of clay minerals*. Oxford University Press, Oxford.
- Morizzi J., Hobday M. and Rix C (2000) Synthesis and characterization of a series of lamellar gallium and indium phosphonates and related compounds. *Journal of Materials Chemistry*, **10**, 1693-1697.
- Murakami J., Itagaki T. and Kuroda K. (2004) Synthesis of kaolinite-organic nanohybrids with butanediols. *Solid State Ionics*, **172**, 279-282.
- Murat M., Amokrane A., Bastide J. P. and Montanaro L. (1992) Synthesis of zeolites from thermally activated kaolinite – some observations on nucleation and growth. *Clay Minerals*, **27**, 119-130.
- Murray H H. (1991) Kaolin minerals: Their Genesis and Occurrences. Pp. 67-89 In: *Hydrous phyllosilicates*. Reviews in Mineralogy, **19** (S. W. Bailey, editor). Mineralogical Society of America, Washington, D. C., USA.
- Naamen S., Jemai S., Rhaïem H. B. and Amara A. B. H. (2003) Study of the structural evolution of the 10 Å unstable hydrate of kaolinite during dehydration by XRD and SAXS. *Journal of Applied Crystallography*, **36**, 898-905.
- Nakagaki S., Benedito F. L. and Wypych F. (2004) Anionic iron(III) porphyrin immobilized in silanized kaolinite as catalyst for oxidation reactions. *Journal of Molecular Catalysis A: Chemical*, **217**, 121-131.
- Nakamoto K. (1986) *Infrared and Raman Spectra of Inorganic and Coordination Compounds*, 4th. ed., John Willey & Sons, New York.
- Neder R. B., Burghammer M., Grasl T., Schulz H., Bram A. and Fiedler S. (1999) Refinement of the kaolinite structure from single-crystal synchrotron data. *Clays and Clay Minerals*, **47**, 487-494.
- Nemecz E. (1981) *Clay Minerals*. Akadémiai Kiadó, Budapest, Hungary.

-
- Németh J., Rodríguez-Gattorno G., Díaz D., Vázquez-Olmos A. R. and Dékány I. (2004) Synthesis of ZnO nanoparticles on a clay mineral surface in dimethyl sulfoxide medium. *Langmuir*, **20**, 2855-2860.
- Okada K., Watanabe N., Jha K. V., Kameshima Y., Yasumori A. and MacKenzie K. J. D. (2003) *Applied Clay Science*, **23**, 329-336.
- Olejnik S., Aylmore L. A. G., Posner A. M. and Quirk J. P. (1968) Infrared spectra of kaolin mineral-dimethyl sulfoxide complexes. *The Journal of Physical Chemistry*, **72**, 241-249.
- Olejnik S., Posner A. M. and Quirk J. P. (1970) The intercalation of polar organic compounds into kaolinite. *Clay Minerals*, **8**, 421-434.
- van Olphen H. and Deeds C. T. (1963) Short contribution (without title). *Proceedings of the International Clay Conference, Stockholm*, **2**, 380-381. Pergamon Press, Oxford, UK.
- Orth H. (1970) Über Kaolinit-Einlagerungsverbindungen. PhD Thesis, Ludwig-Maximilians-Universität, München, Germany.
- Osmanlioglu A. E. (2002) Immobilization of radioactive waste by cementation with purified kaolin clay. *Waste Management*, **22**, 481-483.
- Paetsch D., Feltkamp K. and Schimmel G. (1963) Ein ungewöhnlicher Kaolinit. *Berichte der Deutscher Keramik Gesellschaft*, **40**, 386-391.
- Papoulis D., Tsolis-Katagas P. and Katagas C. (2004) Progressive stages in the formation of kaolin minerals of different morphologies in the weathering of plagioclase. *Clays and Clay Minerals*, **52**, 275-286.
- Papp S., Szél J., Oszkó A. and Dékány I. (2004) Synthesis of polymer-stabilized nanosized rhodium particles in the interlayer space of layered silicates. *Chemistry of Materials*, **16**, 1674-1685.
- Patakfalvi R., Oszkó A. and Dékány I. (2003) Synthesis and characterization of silver nanoparticle/kaolinite composites. *Colloids and Surfaces A*, **220**, 45-54.
- Permien T. and Lagaly G. (1994) The rheological and colloidal properties of bentonite dispersions in the presence of organic compounds: I. Flow behaviour of sodium-bentonite in water-alcohol. *Clay Minerals*, **29**, 751-760.
- Plaçon A., Giese R. F. and Snyder R. (1988) The Hinckley index for kaolinites. *Clay Minerals*, **23**, 249-260.
- Poyato-Ferrera J., Becker H. O. and Weiss A. (1977) Phase changes in kaolinite-amine-complexes. *Proceedings of the Third European Clay Conference, Oslo*, 148-150.

- Price G. J. and Anari D. M. (2003) An inverse gas chromatography study of calcination and surface modification of kaolinite clays. *Physical Chemistry Chemical Physics*, **5**, 5552-5557.
- Radoslovich E. W. (1963) The cell dimensions and symmetry of layer-lattice silicate. VI. Serpentine and kaolin morphology. *American Mineralogist*, **48**, 368-378.
- Raki L. and Detellier C. (1996) Lamellar organominerals: intercalation of phenylphosphonate into the layers of bayerite. *Chemical Communications*, **21**, 2475-2476.
- Range K. J., Range A. and Weiss A. (1968) Zur Existenz von Kaolinit-Hydraten. *Zeitschrift für Naturforschung*, **23B**, 1144-1147.
- Range K. J., Range A. and Weiss A. (1969) Fire-clay type kaolinite or fire-clay mineral? Experimental classification of kaolinite-halloysite minerals. *Proceedings of the International Clay Conference, Tokyo*, **1**, 3-13. Israel Universities Press, Jerusalem, Israel.
- Rausell-Colom J. A. and Serratosa J. M. (1987) Reactions of clays with organic substances. Pp. 371-422 in: *Chemistry of clays and clay minerals* (A. C. D. Newman, editor). Longman Scientific & Technical, Essex, UK.
- Raythatha R. and Lipsicas M. (1985) Mechanism of synthesis of a 10-Å hydrated kaolinite. *Clays and Clay Minerals*, **33**, 333-339.
- Robertson I. D. M. and Eggleton R. A. (1991) Weathering of granitic muscovite to kaolinite and halloysite and of plagioclase-derived kaolinite to halloysite. *Clays and Clay Minerals*, **39**, 113-126.
- Rocha J., Klinowski J. and Adams J. M. (1991) Synthesis of zeolite Na-A from metakaolinite revisited. *Journal of the Royal Chemical Society, Faraday Transactions*, **87**, 3091-3097.
- Ruan H. D., Frost R. L. and Klopogge J. T. (2001) Comparison of Raman spectra in characterizing gibbsite, bayerite diaspore and boehmite. *Journal of Raman Spectroscopy*, **32**, 745-750.
- Russell J. D., and Fraser A. R. (1994) Infrared methods. Pp. 11-67 In: *Clay Mineralogy: Spectroscopic and chemical determinative methods* (M. J. Wilson, Editor). Chapman & Hall, London, UK.
- Sanchez-Camazano M. and Gonzalez-Garcia S. (1966) Complejos interlaminares de caolinita y haloisita con liquidos polares. *Anales de Edafología y Agrobiología*, **25**, 9-25.
- Sánchez-Camazano M. and Sánchez-Martín M. J. (1994) Trimethyl phosphate induced decomposition of kaolinite. *Clays and Clay Minerals*, **42**, 221-225.

-
- Santos P. S. (1989) *Ciência e Tecnologia de Argilas*, 2nd ed., Edgard Blücher, São Paulo.
- Schroeder P. A. (2004) *Lecture notes for clay mineralogy*, 1-Introduction. On-line lecture notes for the course of clay mineralogy and geochemistry, Department of Geology, University of Georgia, USA [<http://www.gly.uga.edu/schroeder/geol6550/CM01.html>].
- Shieh M., Martin K.J., Squattrito P. J. and Clearfield A. (1990) New low-dimensional zinc compounds containing zinc-oxygen-phosphorus frameworks: two-layered inorganic phosphites and a polymeric organic phosphinate. *Inorganic Chemistry*, **29**, 958-963.
- Shoval S., Yariv S., Michaelian K. H., Lapidis I., Boudeuille M. and Panczer G. (1999) A fifth OH-stretching band in IR spectra of kaolinites. *Journal of Colloid and Interface Science*, **212**, 523-529.
- Singh B. (1996) Why does halloysite roll? – A new model. *Clays and Clay Minerals*, **44**, 191-196.
- Singh B. and Mackinnon I. D. R. (1996) Experimental transformation of kaolinite to halloysite. *Clays and Clay Minerals*, **44**, 825-834.
- Sugahara Y., Satokawa S., Kuroda K. and Kato C. (1988) Evidence for the formation of interlayer polyacrylonitrile in kaolinite. *Clays and Clay Minerals*, **36**, 343-348.
- Sugahara Y., Satokawa S., Kuroda K. and Kato C. (1990) Preparation of a kaolinite-polyacrylamide intercalation compound. *Clays and Clay Minerals*, **38**, 137-143.
- Sugahara Y., Sugiyama T., Nagayama T., Kuroda K. and Kato C. (1992) *Journal of the Ceramic Society of Japan, International Edition*, **100**, 420-423.
- Sutheimer S. H., Maurice P. A. and Zhou Q. (1999) Dissolution of well and poorly crystallized kaolinites: Al speciation and effects of surface characteristics. *American Mineralogist*, **84**, 620-628.
- Takeuchi N., Takahashi H., Ishida S., Horie F. and Wakamatsu M. (2000) Mechanistic study of solid-state reaction between kaolinite and ferrous oxide at high temperatures. *Journal of the Ceramic Society of Japan*, **108**, 876-881.
- Tarasevich Y. I. and Klimova G. M. (2001) Complex-forming adsorbents based on kaolinite, aluminium oxide and polyphosphates for the extraction and concentration of heavy metal ions from water solutions. *Applied Clay Science*, **19**, 95-101.
- Tari G., Fonseca A. T. and Ferreira J. M. F. (1998) Influence of kaolinite delamination on rheological properties and sedimentation behaviour of ceramic suspensions. *British Ceramic Transactions*, **97**, 1-4.

- Thielepape W. (1966) Kaolinit-Einlagerungsverbindungen. PhD Thesis, Ruprecht-Karl-Universität, Heidelberg, Germany.
- Thomas L. C. and Chittenden R. A. (1979) Characteristic infrared absorption frequencies of organophosphorus compounds-VII. Phosphorus ions. *Spectrochimica Acta*, **26A**, 781-800.
- Thompson J. G., Gabbitas N. and Uwins P. J. R. (1993) The intercalation of kaolinite by alkali halides in the solid state: A systematic study of the intercalates and their derivatives. *Clays and Clay Minerals*, **41**, 73-86.
- Triplehorn D. M., Bohor B. F. and Betterton W. J. (2002) Chemical disaggregation of kaolinitic claystones (Tonsteins and flint clays). *Clays and Clay Minerals*, **50**, 766-770.
- Trobajo C., Khainakov S. A., Espina A., García J.R., Salvadó M.A., Pertierra P., García-Granada S., Martín-Izard A. and Bortun A. I. (2001) Synthesis of a mineral-organic hybrid by treatment of phlogopite with phenylphosphonic acid. *Chemistry of Materials*, **13**, 4457-4462.
- Tsunematsu K. and Tateyama H. (1999) Delamination of urea-kaolinite complex by using intercalation procedures. *Journal of the American Ceramic Society*, **82**, 1589-1591.
- Tsunematsu K., Tateyama H., Nishimura S. and Jinnai K. (1992) Delamination of kaolinite by intercalation of urea. *Journal of the Ceramic Society of Japan*, **100**, 178-181.
- Tunney J. J. and Detellier C. (1993) Interlamellar covalent grafting of organic units on kaolinite. *Chemistry of Materials*, **5**, 747-748.
- Tunney J. J. and Detellier C. (1994a) Preparation and characterization of two distinct ethylene glycol derivatives of kaolinite. *Clays and Clay Minerals*, **42**, 552-560.
- Tunney J. J. and Detellier C. (1994b) Preparation and characterization of an 8.4 Å hydrate of kaolinite. *Clays and Clay Minerals*, **42**, 473-476.
- Tunney J. J. and Detellier C. (1996a) Chemically modified kaolinite. Grafting of methoxy groups on the interlamellar aluminol surface of kaolinite. *Journal of Materials Chemistry*, **6**, 1679-1685.
- Tunney J. J. and Detellier C. (1996b) Aluminosilicate nanocomposite materials. Poly(ethylene glycol)-kaolinite intercalates. *Chemistry of Materials*, **8**, 927-935.
- Tunney J. J. and Detellier C. (1997) Interlamellar amino functionalization of kaolinite. *Canadian Journal of Chemistry*, **75**, 1766-1772.
- Wada K. (1961) Lattice expansion of kaolin minerals by treatment with potassium acetate. *American Mineralogist*, **46**, 78-91.

-
- Wada K. (1965) Intercalation of water in kaolin minerals. *American Mineralogist*, **50**, 924-941.
- Wang S. L. and Johnston C. T. (2000) Assignment of the structural OH stretching bands of gibbsite. *American Mineralogist*, **85**, 739-744.
- Weiss A. (1961) Eine Schichteinschlußverbindung von Kaolinit mit Harnstoff. *Angewandte Chemie*, **73**, 736.
- Weiss A. (1963) Ein Geheimnis des chinesischen Porzellans. *Angewandte Chemie*, **75**, 755-762.
- Weiss A. and Russow J. (1963) Über das Einrollen von Kaolinitkristallen zu halloysitähnlichen Röhren und einen Unterschied zwischen Halloysit und röhrenförmigem Kaolinit. *Proceedings of the International Clay Conference, Stockholm*, **2**, 69-73. Pergamon Press, Oxford, UK.
- Weiss A., Thielepape W., Ritter W., Schäfer H. and Göring G. (1963a) Zur Kenntnis von Hydrazin-Kaolinit. *Zeitschrift für anorganische und allgemeine Chemie*, **320**, 183-204.
- Weiss A., Thielepape W., Göring G., Ritter W. and Schäfer H. (1963b) Kaolinit-Einlagerungsverbindungen. *Proceedings of the International Clay Conference, Stockholm*, **1**, 287-305.
- Weiss A., Thielepape W. and Orth H. (1966a) Neue Kaolinit – Einlagerungsverbindungen. *Proceedings of the International Clay Conference, Jerusalem*, **1**, 277-293.
- Weiss A., Thielepape W. and Orth H. Neue Kaolinit – Einlagerungsverbindungen : Discussion (1966b) *Proceedings of the International Clay Conference, Jerusalem*, **2**, 179-181.
- Weiss A., Becker H. O., Orth H., Mai G., Lechner H. and Range K. J. (1969) Particle size effects and reaction mechanism of the intercalation into kaolinite. *Proceedings of the International Clay Conference, Tokyo*, **2**, 180-184. Israel Universities Press, Jerusalem, Israel.
- Weiss A., Gossner U. and Robl C. (1995) Transformation of clay minerals into taranakite and the crystal structure of taranakite. *Proceedings of the International Clay Conference, Adelaide*, 253-259.
- Wiewiora A. and Brindley G. W. (1969) Potassium acetate intercalation in kaolinite and its removal: Effect of material characteristics. *Proceedings of the International Clay Conference, Tokyo*, **1**, 723-733. Israel Universities Press, Jerusalem, Israel.

-
- Wypych F., Schreiner W. H., Mattoso N., Mosca D. H., Marangoni R. and Bento C. A. da S. (2003) Covalent grafting of phenylphosphonate groups onto layered silica derived from in-situ leached chrysotile fibers. *Journal of Materials Chemistry*, **13**, 304-307.
- Zakowski N., Hix G. B. and Morris R. E. (2000) Synthesis of a family of aluminium benzylphosphonates. *Journal of Materials Chemistry*, **10**, 2375-2380.
- Zhou Z. and Gunther W. D. (1992) The nature of the surface charge of kaolinite. *Clays and Clay Minerals*, **40**, 365-368.
- Zvyagin B. B. (1962) Polymorphism of double-layer minerals of the kaolinite type. *Kristallografiya*, **7**, 51-65 (English translation pp. 38-51).

APPENDIX I

Description of materials and analytical methods

1 Materials

All chemicals were used without further treatment (unless otherwise indicated).

Kaolinite

The standard kaolinite used in the experiments was a “SPS” type (Selected Particle Size, used as paper coating kaolin) obtained from the *English Clays Lovering Pochin & Co.* (Cornwall, UK, afterwards renamed to *English China Clays International*, acquired in 1999 by *Imerys* (France)). The specifications from the supplier are [sic]:

Brightness:	85.5 ± 0.7
Yellowness:	4.7 ± 0.5
Particles smaller than 2 µm	80.0 ± 3.0 %
Particles bigger than 10 µm:	0.2 % max.
Viscosity concentration:	69.0 ± 1.0 % solids for 500 cps
Typical chemical analysis:	SiO ₂ : 47.8 %
	Al ₂ O ₃ : 37.0 %
	Fe ₂ O ₃ : 0.58 %
	TiO ₂ : 0.03 %
	CaO: 0.04 %
	MgO: 0.16 %
	K ₂ O: 1.10 %
	Na ₂ O: 0.10 %
	Loss on ignition: 13.1 %

Our XRPD analyses showed that the sample contains < 5 % mica as the only crystalline impurity, observed as a small reflection around 10 Å. The calculated Hinckley crystallinity index was $H_i = 1.25$, indicating an well-ordered material (see section 2.3).

For the reactions with PPIA and NPAA a fine-particle size fraction was used (SPF-K). This fraction was separated from the raw material in a homemade system consisting of a 1 m long tube. A kaolinite slurry was added at the bottom of the tube. The smallest particles were impelled upwards by a counter-flow of water. Water flow of $\sim 1 \text{ l h}^{-1}$ was enough to obtain an

homogeneous dispersion which was collected from a drain at the top of the tube. This dispersion was concentrated by centrifugation and used while still wet.

In some experiments was also used a Brazilian kaolinite from the Capim River basin, at the Amazon region (kindly provided by Prof. Dr. F. Wypych, Dept. of Chemistry, Federal University of Paraná, Brazil). Detailed mineralogical, geochemical and genetic description of similar samples are given by Costa and Moraes, 1998. Lombardi *et al.* (2002) reported a detailed structural and morphological characterization of a similar sample. Our sample did not contain any crystalline impurities detectable by XRPD.

Gibbsite

Pure fine powdered aluminum hydroxide from Merck (hydrargillite) was used.

Specifications from the supplier [sic]:

Chloride	≤ 0.01 %
Sulfate	≤ 0.02 %
Iron	≤ 0.01 %
Sodium	≤ 0.3 %
Particle Size (< 45 μm)	~95 %

Intercalating agents for kaolinite

Material	Purity	Producer
Dimethyl sulfoxide	≥ 99.0 %	Fluka
N-Methylformamide	≥ 99 %	Fluka
Methanol	> 99.8 %	J. T. Baker
Hydrazine monohydrate	≥ 98.0 %	Fluka
Potassium acetate	99.0 – 100.5 %	Merck

Grafting Agents: Alcohols

Material	Purity	Producer
1-Butanol	≥ 99.5 %	Merck
2-Butanol	≥ 99 %	Merck
tert-Butanol	≥ 99 %	Merck
1-Pentanol	≥ 98 %	Fluka
1-Hexanol	98 %	Aldrich
1-Heptanol	> 99.5 %	Fluka
1-Octanol	> 99.5 %	Fluka
1-Decanol	> 97 %	Fluka
1-Tetradecanol	≥ 98 %	Merck
Benzyl alcohol	-	Caesar & Loretz
(±)-1-Phenyl-ethanol	≥ 98 %	Fluka
2-Phenyl-ethanol	> 99 %	Fluka

Grafting Agents: Diols

Material	Purity	Producer
Ethylene glycol	> 99 %	Merck
1,2-Propanediol	≥ 99 %	Merck
1,3-Propanediol	≥ 98 %	Merck
2,2-Dimethyl-1,3-propanediol	≥ 98 %	Fluka
1,2-Butanediol	≥ 98.0 %	Fluka
(±)1,3-Butanediol	≥ 98.0 %	Fluka
1,4-Butanediol	≥ 98.0 %	Fluka
2,3-Butanediol	Mixture of racemic and meso forms ≥ 98.0 %	Fluka
1,6-Hexanediol	> 97 %	Merck
1,8-Octanediol	> 98 %	Merck

Grafting Agents: Glycol mono-ethers

Material	Purity	Producer
Ethylene glycol ethyl ether	> 99 %	Riedel-de Haën
Ethylene glycol hexadecyl ether	> 99 %	Fluka
Di(ethylene glycol) methyl ether	≥ 99.6 %	Aldrich
Di(ethylene glycol) butyl ether	> 98 %	Merck
Di(ethylene glycol) hexyl ether	≥ 98 %	Fluka
Di(ethylene glycol) 2-ethylhexyl ether	98 %	Aldrich
Di(ethylene glycol) decyl ether	≥ 98 %	Fluka
Tri(propylene glycol) butyl ether	Mixture of isomers 95 %	Aldrich
Tetra(ethylene glycol) hexadecyl ether	> 99 %	Fluka
2-Phenoxy-ethanol	≥ 99.0 %	Fluka
1-Phenoxy-2-propanol	93+ %	Aldrich

Amines

Material	Purity	Producer
n-Hexylamine	≥ 98 %	Fluka
n-Decylamine	≥ 98 %	Fluka
n-Octadecylamine	≥ 90 % (hexadecylamine ≤ 10 %)	Fluka
n-Docosanamine	-	Lachat Biochemical Company (Chicago, USA)

Phenylphosphonic and similar Acids

Material	Purity	Producer
Phenylphosphonic acid	≥ 98 %	Fluka
Phenylphosphinic acid	99 %	Aldrich
2-Nitrophenol-4-arsonic acid	≥ 98 %	Fluka

Organic Solvents

Ethanol, acetone, ethyl ether, cyclohexane, dioxane and all other organic solvents used in the experiments were reagent-grade pure chemicals (or equivalent), used without any further treatment.

2 Methods

2.1 X-Ray Powder Diffractometry (XRPD)

X-Ray powder diffraction (XRPD) patterns were recorded on a Philips D5000 diffractometer (Cu-K α radiation, $\lambda = 1.5406 \text{ \AA}$, curved (111) germanium monochromator, count time = 3.5 s, step size = 0.04° , unless otherwise indicated). The basal spacings (d_L) and other interlayer spacings (d_{hkl}) were calculated from the basal reflection of the highest order detectable.

The reaction ratio α (only in systems with one reaction product) was calculated from the reflection intensities:

$$\alpha = I / (I + I_0) \quad (\text{Eq. I.1})$$

with, I = intensity of the (001) reflection of the product and I_0 = intensity of the (001) reflection of the unreacted matrix.

The samples were prepared by dispersing some mg of the product in water or acetone and letting a few drops of this dispersion dry on the surface of a glass plate. Alternatively, the dry powder to be analyzed was directly deposited onto the glass plate that has previously been covered with a thin film of silicone grease.

2.2 Fourier Transform Infrared Absorption Spectroscopy (FTIR)

The FTIR spectra of solids were obtained from KBr discs containing 1% sample material (probe grinded with KBr) in an ATI Mattson Genesis equipment. Liquid samples were measured as a thin film between two KBr blocks. Spectra were recorded from 4000 to 400 cm^{-1} with 2 cm^{-1} resolution, unless otherwise indicated.

2.3 Simultaneous Thermogravimetric – Differential Thermal Analysis (TG/DTA)

Simultaneous thermal analyses (TG/DTA) were made in a Netzsch STA 429 system using a heating rate of 5°C min^{-1} and an air-flow of 100 ml min^{-1} . Approximately 50 mg of the sample were weighed in an alumina crucible. As reference, a crucible with 50 mg powdered alumina was used.

2.4 Transmission Electronic Microscopy (TEM) - Selected Area Electron Diffraction (SAED) - Energy Dispersive X-Ray Spectroscopy (EDX)

The morphological studies, micrographs, selected area electron diffraction (SAED), as well as the EDX measurements were performed in a Philips EM 400T transmission electron microscope operating at 100 kV and equipped with a Kevex EDX module. The EDX equipment was able to detect only elements heavier than sodium but exact quantification of the elements was not possible due to equipment problems.

The samples were prepared by dispersing some mg of the product in ethanol by ultrasound for a few minutes. One drop of this dispersion was added onto a Lacey carbon-film coated copper grid and allowed to dry in air.

2.5 Elemental Analysis (CHNS)

Elemental analyses for carbon, hydrogen, nitrogen and sulfur contents (%(w/w)) were performed in a Eurovector equipment, Model AE 3000 CHNS.

APPENDIX II

**Particle-size study of kaolinite treated after Lahav (1990)
using disc-centrifuge photosedimentometry**

1 Introduction

As discussed in chapter 2, the results presented by Lahav (1990) on the delamination of kaolinite by treatment with DMSO/NH₄F were contested by Chekin in 1992. One of the claims Chekin made was that the product prepared by Lahav showed an insignificant increase of weight percentage of finer particles.

In order to further investigate the effect of the treatment suggested by Lahav, we measured the particle-size distribution of dispersions of kaolinite samples treated by Lahav's method using disc-centrifuge photosedimentometry (DCP). For comparison reasons, control measurements were done with various intercalated kaolinite samples that were washed/deintercalated with water.

2 Experimental and Results

Two 0.50 g aliquots of SPS kaolinite were intercalated with DMSO. Each of the intercalated samples were mixed with 16 ml DMSO (with 9 % (v/v) water) and 0.95 g NH₄F, heated to 60 °C and kept under agitation for 1.5 h. The products were centrifuged at 60000 g for 1 h, washed 4 times with DMSO/water, and the process than was repeated. After another cycle of 4 washing steps with DMSO/water, the resulting product was dispersed in a 0.1 % (w/v) Na₄P₂O₇ solution and the volume was adjusted to 1.000 l (with the pyrophosphate solution).

The intercalation reactions for control measurements were done with hydrazine monohydrate, potassium acetate and DMSO. In each case three 0.50 g SPS kaolinite samples were reacted with an excess of the intercalating agent (pure hydrazine hydrate, saturated solution of potassium acetate and DMSO with 9 % (v/v) water) for the time necessary to reach the maximal intercalation ratio (one of the three systems was used to supply material for XRPD measurements). After intercalation, the dispersions were centrifuged at 60000 g for 1 h, and the products were washed 5 times with water (K-Hydrazine) or 10 times (K-DMSO and K-Acetate). XRPD of the washed probes showed less than 10 % of the intercalated phase remaining (the total time of the washing phase was more than 7 days). The washed products were dispersed in a 0.1 % (w/v) Na₄P₂O₇ solution and the volume was adjusted to 1.000 l.

Another control system was prepared by washing two 0.5 g aliquots of raw SPS kaolinite with water for 8 times and then dispersing them in a 0.1 % (w/v) $\text{Na}_4\text{P}_2\text{O}_7$ solution and adjusting the volume to 1.000 l.

For the DCP measurements 0.00625 % (w/v) dispersions in 0.1 % (w/v) $\text{Na}_4\text{P}_2\text{O}_7$ aqueous solution were prepared from the 0.5 %_{w/v} stock dispersions described above. Two dilutions were prepared from each stock dispersion. Another control system was prepared as a 0.00625 % (w/v) dispersion of raw SPS kaolinite in 0.1 % (w/v) $\text{Na}_4\text{P}_2\text{O}_7$ aqueous solution.

The measurements were performed on a BI-DCP Particle Sizer (Brookhaven Instruments Corporation) at homogeneous mode (HOST analysis). The run parameters were: scan mode: fixed head; disc speed: 2000 rpm; stop time: 50 min; particle density: 2.5600 g/cm³; spin fluid: water, spin fluid volume: 15 ml. The values for density and viscosity for the spin fluid (water) were automatically generated by the equipment software according to the run temperature. The run temperature was the average between the start and stop temperatures collected with the probe above the spin-disk (typical values around 21 °C). A scattering correction file based on the refractive indices of kaolinite and water was generated by the equipment software.

Before injection of the probes, 0.2 ml of ethanol was injected as gradient promoter. Immediately after the injection of the probe, 0.1 ml dodecane was injected in order to hinder evaporation.

Each dilution was measured twice, giving four measurements for each sample, and eight measurements for each compound. The averages of all cumulative mass distributions for a compound were compared, and the results are shown in Fig. II.1. The curves of cumulative mass distribution indicate that the sample from untreated kaolinite presented the largest particles. However, the sample with the smallest particles was the one obtained from simple water washing of the raw kaolinite. All the intercalated/washed samples and the Lahav sample presented cumulative mass distributions between those two. The intercalation/washing was not enough to generate smaller particles than those obtained by the simple mechanical effect of washing. Although partial delamination was already described by intercalation/washing of kaolinite with potassium or ammonium acetates, such effects were only noticed after many cycles (see section 2.8).

Due to the high anisometry of the kaolinite particles, the equivalent Stokes diameter obtained from the DCP measurements is not to be taken with much accuracy. It is clear

however, that in case of a significant alteration of the particle size of the sample, some changes would be noticed in the cumulative mass distributions.

Thus, the results here obtained present convincing arguments for the inefficiency of the delamination method proposed by Lahav, in accordance with the viewpoint presented by Chekin.

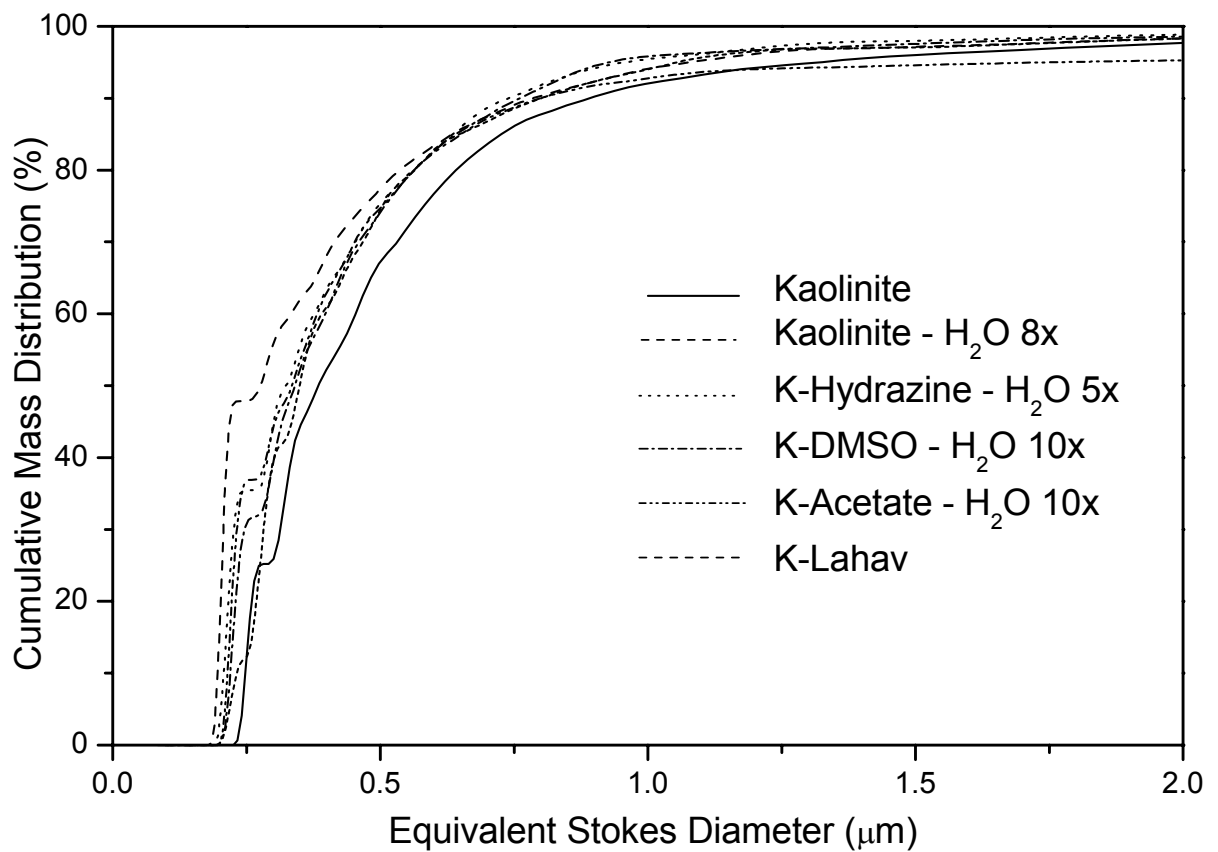


Fig. II.1: Cumulative mass distribution of the dispersions analyzed by disc-centrifuge photosedimentometry.

APPENDIX III

**Investigation of intercalation reactions of kaolinite and
some grafted derivatives in liquid ammonia medium**

1 Introduction

It was one of the objectives of this work to study the intercalation behavior of kaolinite in non-aqueous media. The idea of using liquid ammonia as solvent for intercalation reactions was developed from an analogy with the hydrazine molecule, which is one of the best intercalating agents for kaolinite (see chapter 2). Weiss *et al.* (1966b) commented the fact that ammonia would intercalate in kaolinite at very high pressures. We were unable to intercalate liquid ammonia at atmospheric pressure.

Based on these facts we tried to intercalate various molecules into kaolinite taking advantage of the powerful solvent capacity of liquid ammonia.

2 Experimental and Results

All experiments were performed in a 150 ml jacketed beaker cooled by a flux of isopropanol from a cryostat (Julabo 65). The temperature was kept at $-36\text{ }^{\circ}\text{C}$ to $-34\text{ }^{\circ}\text{C}$, just below the boiling point of ammonia. The contents of the beaker were kept under constant stirring with a magnetic stirrer and the system was closed to avoid the uptake of moisture from the air.

Gaseous ammonia from a gas flask (99.95 %) was first condensed in a trap cooled by liquid nitrogen and then added to the cooled beaker ($\sim 75\text{ ml}$). After the temperature has raised to $\sim -36\text{ }^{\circ}\text{C}$, the intercalating agent was dissolved in the liquid ammonia and kaolinite ($\sim 1\text{ g}$) was added. The amount of intercalating agent used varied from reaction to reaction, as a general rule solids were dissolved almost to the saturation and liquids were added in a rough 1:4 proportion of ammonia to intercalating agent. In the reactions using sulfur, the NH_3/S system was left under agitation for 5-6 hours before the addition of kaolinite, to allow the formation of the complex species from the reaction between the components.

The systems were left under agitation for 1 week at permanent cooling, after which time the agitation was stopped and the liquid phase was discarded after sedimentation. The solid product was hand-ground after reaching room temperature (when needed) and a sample was collected for the XRPD analysis. When using sulfur, the product was quickly washed with CS_2 and another sample for XRPD was collected. Table III.1 shows the substances used in reaction with kaolinite in liquid ammonia.

Table III.1: Substances used in intercalation reactions of kaolinite in liquid ammonia.

Salts	NaN ₃
	KI
	KSCN
	KCH ₃ COO
	NH ₄ CH ₃ COO
	NH ₄ SCN
	NH ₄ NO ₃
	NH ₄ Cl
Organic molecules	Urea
	Acetamide
	Aniline
	Ethylene Glycol
Elements	Sulfur

The XRPD patterns of the products indicated that none were intercalated. Even a saturated solution of ammonium or potassium acetates, which would easily intercalate in aqueous medium, did not react in liquid ammonia.

After these experiments we tried to intercalate KSCN, aniline and sulfur in K-DMSO and K-Potassium Acetate. The results were also disappointing. Either there was no change of the basal spacing or raw kaolinite was recovered.

In the next series of experiments, some grafted-kaolinites were used instead of raw or intercalated kaolinite for the intercalation of sulfur. The following kaolinites were used: K-12PD, K-12BD, K-DEGME, K-PnxEt and K-Heptanol. None of the products showed any change of the basal spacing after the reaction.

The last experiments on intercalation of sulfur from ammonia solutions involved the reaction with the hexylamine intercalates of K-Methanol, K-12PD, K-DEGME and K-Heptanol. The grafted kaolinites did not present any new phases after the reaction, but recovered different amounts of grafted or even raw kaolinite. The K-Methanol-Hexylamine compound showed a different behavior. Fig. III.1 shows the diffraction patterns of the product of the reaction between sulfur and K-Methanol-Hexylamine in liquid ammonia. A reflection at 17.5 Å is seen in the product but disappeared after a 2 day heating at 60 °C. A reflection at 11.3 Å that also disappeared after heating may be attributed to K-Methanol. A reflection at ~ 10 Å was present in both cases, but with smaller intensity after heating. Finally a reflection at

8.7 Å which appeared after heating is attributed to dry K-Methanol. In both cases a small amount of raw kaolinite was also detected. The origin of the 17.5 Å reflection is unclear but one may imagine that it could indicate intercalated sulfur. The phase at 10 Å is also of unclear origin, however, it may be superimposed with the reflection of the mica present in the kaolinite, becoming visible in an effect analogous to what was observed in K-16HD (see section 3.3.1.2).

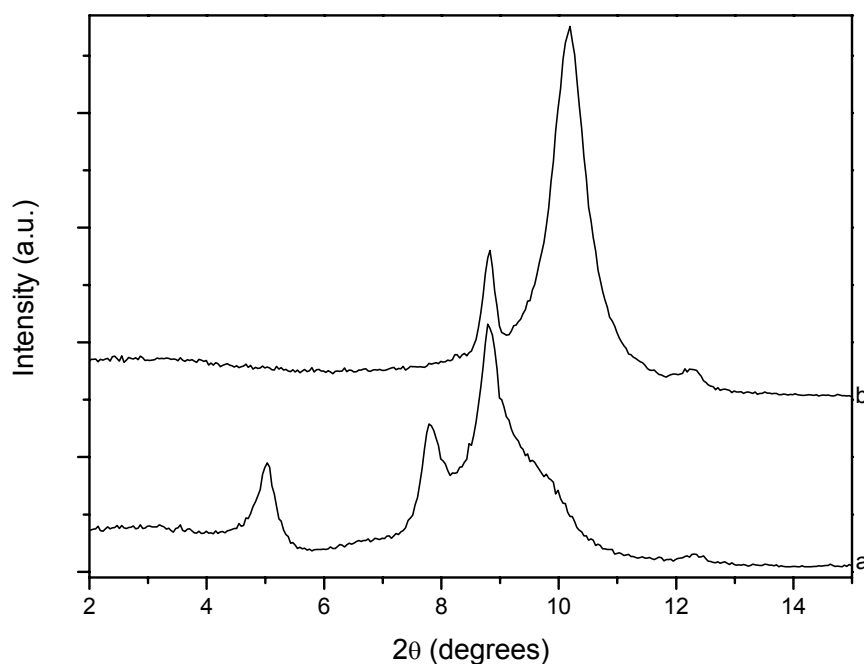


Fig. III.1: XRPD patterns of (a) the reaction product between sulfur ammonia solution and K-Methanol-Hexylamine washed with CS₂ and (b) after heating at 60 °C at air for 2 days.

In a second intercalation reaction attempting to reproduce the results above described and to obtain more product, no new phases were formed, K-Methanol and raw kaolinite were the only phases observed in the diffraction pattern.

As we were unable to reproduce the intercalation, the interpretation of the results of the first reaction remains open.

The possibility of intercalating sulfur in kaolinite, however, is very interesting from the viewpoint of the physicochemical properties of such product and of the structure of the intercalated species. These prospects should encourage further research on this compound.

**“THE END OF MUSIC;
THE END OF THE GENIUS;
THE END OF IT ALL...”**



(Johann Sebastian Bach, Contrapunctus XVIII, Fuga a 3 sogetti (last four bars), *in Die Kunst der Fuge*, BWV1080.)

Curriculum Vitæ

Personal Information

Name: José Eduardo Ferreira da Costa Gardolinski

Birth: 18.11.1977 in Curitiba, Brazil.

Nationality: Brazilian

Marital Status: Married (Helen Caroline Judt Gardolinski)

Higher Education

- 1995-1999: **Bacharel em Química** (Bachelor in Chemistry). Federal University of Paraná, Curitiba, Brazil.
- 2000-2001: **Mestre em Engenharia** (Master in Engineering), Concentration Area: Materials Science & Engineering. Universidade Federal do Paraná, Curitiba, Brazil. Research Lines: Intercalation compounds and nanocomposites derived from lamellar matrixes (especially clay minerals). Dissertation: Compostos de Intercalação Derivados da Caulinita (Intercalation Compounds from Kaolinite). Tutor: Prof. Dr. Fernando Wypych.
- 2002-2005: **Doctor rerum naturalium** (PhD in Natural Sciences). Christian-Albrechts-Universität, Kiel, Germany. Main Subject: Inorganic Chemistry (Colloid Chemistry). Secondary Subjects: Marine Chemistry, Astronomy & Astrophysics. Research Lines: Kaolinite: intercalation chemistry, interlayer grafted derivatives and colloid-chemical studies. Scholarship granted by the German Academic Exchange Service (DAAD). Tutor: Prof. Dr. Dr. h. c. Gerhard Lagaly.

Languages

PORTUGUESE: mother tongue.

ENGLISH: understands, speaks, writes and reads with fluency.

GERMAN: understands, speaks, writes and reads with fluency.

SPANISH: understands and reads at intermediate level, speaks at basic level.

Scientific Publication

Gardolinski J. E., Peralta-Zamora P. and Wypych F. (1999) Preparation and characterization of a kaolinite-1-methyl-2-pyrrolidone intercalation compound. *Journal of Colloid and Interface Science*, **211**, 1, 137-141.

Gardolinski J. E., Ramos L. P., Pinto de Souza G. and Wypych F. (2000) Intercalation of benzamide into kaolinite. *Journal of Colloid and Interface Science*, **221**, 2, 284-290.

Gardolinski J. E., Carrera L. C. M., Cantão M. P. and Wypych F. (2000) Layered Polymer-Kaolinite Nanocomposites. *Journal of Materials Science*, **35**, 3113-3119.

Gardolinski J. E., Wypych F. and Cantão M. P. (2001) Esfoliação e hidratação da caulinita após intercalação com uréia. *Química Nova*, **24**, 6, 761-767.

Gardolinski J. E., Martins Filho H. P. and Wypych F. (2003) Comportamento térmico da caulinita hidratada. *Química Nova*, **26**, 1, 30-35.

Gardolinski J. E. F. C., Lagaly G. & Czank M. (2004) On the destruction of kaolinite and gibbsite by phenylphosphonic, phenylphosphinic and phenylarsonic acids: Evidence for the formation of new Al compounds. *Clay Minerals*, **39**, 391-404.

Wypych F., Arizaga G. G. C. and Gardolinski J. E. F. C. (2005) Intercalation and functionalization of zinc hydroxide nitrate with mono- and dicarboxylic acids. *Journal of Colloid and Interface Science*, **283**, 1, 130-138.

Gardolinski J. E. F. C. and Lagaly G. (2005a) Grafted organic derivatives of kaolinite: I. Synthesis, chemical, and rheological characterization. *Clay Minerals*, IN PRESS.

Gardolinski J. E. F. C. and Lagaly G. (2005b) Grafted organic derivatives of kaolinite: II. Intercalation of primary n-alkylamines and delamination. *Clay Minerals*, IN PRESS.

